Universidad de Concepción
Dirección de Postgrado
Facultad de Ciencias Físicas y Matemáticas
Programa de Doctorado en Ciencias Aplicadas
con Mención en Ingeniería Matemática

MÉTODOS DE GALERKIN DISCONTINUOS PARA PROBLEMAS DE INTERFAZ: APLICACIÓN A PROCESOS DE DESALINIZACIÓN DEL AGUA

DISCONTINUOUS GALERKIN METHODS FOR INTERFACE PROBLEMS: APPLICATION TO WATER DESALINATION PROCESSES

Tesis para optar al grado de Doctor en Ciencias
Aplicadas con mención en Ingeniería Matemática

Isaac Bermúdez Montiel
Concepción-chile
2024

Profesor Guía: Manuel Solano Palma
Departamento de Ingeniería Matemática, Facultad de Ciencias Físicas y Matemáticas
Centro de Investigación en Ingeniería Matemática (CI^2MA)
Universidad de Concepción, Concepción, Chile.

Cotutora: Jessika Pamela Camaño Valenzuela
Departamento de Matemática y Física Aplicadas
Grupo de Investigación en Análisis Numérico y Cálculo Científico ($GIANuC^2$)
Universidad Católica de la Santísima Concepción, Concepción, Chile.
Centro de Investigación en Ingeniería Matemática (CI^2MA)
Universidad de Concepción, Concepción, Chile.

Discontinuous Galerkin Methods for Interface Problems: Application to Water Desalination Processes

Isaac Bermúdez Montiel

Directores de Tesis: Manuel Solano, Universidad de Concepción, Chile.
Jessika Camaño, Universidad Católica de la Santísima Concepción, Chile.

Director de Programa: Raimund Bürger, Universidad de Concepción, Chile.

Comisión examinadora

Prof. Gabriel N. Gatica Pérez, Universidad de Concepción, Concepción, Chile.

Prof. Luis F. Gatica Simpertigue, Universidad Católica de la Santísima Concepción, Concepción, Chile.

Prof. Rommel A. Bustinza Pariona, Universidad de ConcepciónConcepción, Chile.

Calificación: ______________________________

Concepción, Enero de 2025

Evaluadores Externos

Prof. Giordano Tierra, University of North Texas, USA.

Prof. Marco Discacciati, Loughborough University, UK.

Prof. Sander Rhebergen, University of Waterloo, Canada.

Abstract

The aim of this thesis is to develop continuous and discontinuous Galerkin-type discretizations applied to interface problems modelled by systems of partial differential equations (PDEs). The complexity of these problems lies in the unknowns and their associated source terms arising from coupling interfaces, as well as the non-linearity of the equations.

First, we consider a coupled Navier–Stokes/transport system inspired by the modeling of a reverse osmosis effect in water desalination processes when considering feed and permeate channels coupled through a semi-permeate membrane. The variational formulation consists of a set of equations where the velocities and concentrations, along with tensors and vector fields introduced as auxiliary unknowns, and two Lagrange multipliers, are the main unknowns of the system. The latter are introduced to deal with the trace of functions that do not have enough regularity to be restricted to the boundary. In addition, the pressures can be recovered afterwards by a postprocessing formula. As a consequence, we obtain a nonlinear Banach spaces-based mixed formulation, which has a perturbed saddle point structure. We analyze the continuous and discrete solvability of this problem by linearizing the perturbation term and applying the classical Banach fixed point theorem along with the Banach–Nečas–Babuška result. Regarding the discrete scheme, feasible choices of finite element subspaces that can be used include Raviart–Thomas spaces for the auxiliary tensor and vector unknowns, piecewise polynomials for the velocities and concentrations, and continuous polynomial space of lowest order for the traces, yielding stable discrete schemes. An optimal *a priori* error estimate is derived, and numerical results illustrating both, the performance of the scheme confirming the theoretical rates of convergence, and its applicability, are reported.

Once we have established the theoretical foundations to ensure the solvability of the variational scheme, we take advantage of them to numerically address different approaches closely related to reverse osmosis processes by considering coupled Brinkman–Forchheimer/transport equations in addition to Navier–Stokes/transport equations. The cases of a single channel and coupled feed/permeate channels are covered. Thus, through diverse numerical simulations and a variety of configurations, we illustrate the capability of the method to accurately capture the behavior of saline water when passing through membrane-based reverse osmosis desalination channels.

On the other hand, we present and analyze a hybridizable discontinuous Galerkin (HDG) method for coupling Stokes and Darcy equations, whose domains are discretized by two independent triangulations. This causes non-conformity at the intersection of the subdomains or originates a gap (unmeshed region) between them. In order to properly couple the two different discretizations and obtain a high order scheme, we propose suitable transmission conditions based on mass conservation, equilibrium of normal forces, and the Beavers–Joseph–Saffman law. Since the meshes do not necessarily coincide at the interface, we use the Transfer Path Method (TPM) to tie them. We establish the well-posedness of the method and provide error estimates where the influences of the non-conformity and the gap are explicit in the constants. Finally, numerical experiments that illustrate the performance of the method are shown.

Resumen

El objetivo de esta tesis es desarrollar discretizaciones de tipo Galerkin continuo y discontinuo aplicadas a problemas de interfaz modelados por sistemas de ecuaciones en derivadas parciales (EDPs). La complejidad de estos problemas radica en las incógnitas y sus términos fuente asociados, que surgen del acoplamiento en las interfaces, así como en la no linealidad de las ecuaciones.

Primero, consideramos un sistema acoplado Navier–Stokes/transporte inspirado en el modelamiento de un efecto de ósmosis inversa en procesos de desalinización de agua al considerar canales de alimentación y permeado acoplados a través de una membrana semipermeable. La formulación variacional consiste en un conjunto de ecuaciones donde las velocidades y concentraciones, junto con tensores y campos vectoriales introducidos como incógnitas auxiliares, y dos multiplicadores de Lagrange, son las incógnitas principales del sistema. Estos últimos se introducen para tratar con las trazas de funciones que no tienen suficiente regularidad para restringirse en la frontera. Además, las presiones pueden recuperarse posteriormente mediante una fórmula de postprocesamiento. Como consecuencia, obtenemos una formulación mixta no lineal basada en espacios de Banach, que presenta una estructura de punto silla perturbada. Analizamos la solvencia continua y discreta de este problema linearizando el término de perturbación y aplicando el teorema clásico de punto fijo de Banach junto con el resultado de Banach–Nečas–Babuška. En cuanto al esquema discreto, las opciones factibles de subespacios de elementos finitos que pueden utilizarse incluyen espacios Raviart–Thomas para el tensor auxiliar y las incógnitas vectoriales, polinomios a trozos para las velocidades y las concentraciones, y el espacio polinómico continuo de orden inferior para las trazas, lo que da lugar a esquemas discretos estables. Se deriva una estimación óptima del error *a priori* y se presentan resultados numéricos que ilustran tanto el rendimiento del esquema, confirmando las tasas teóricas de convergencia, como su aplicabilidad.

Una vez establecidos los fundamentos teóricos para asegurar la solvencia del esquema variacional, los aprovechamos para abordar numéricamente diferentes enfoques muy relacionados con los procesos de ósmosis inversa considerando las ecuaciones acopladas de Brinkman–Forchheimer/transporte además de las ecuaciones de Navier–Stokes/transporte. Se cubren los casos de un solo canal y de canales acoplados de alimentación/permeado. Así, a través de diversas simulaciones numéricas y una variedad de configuraciones, ilustramos la capacidad del método para capturar con precisión el comportamiento del agua salina cuando pasa a través de canales de desalinización de ósmosis inversa basados en membranas.

Por otro lado, presentamos y analizamos un método discontinuo de Galerkin hibridizable (HDG) para el acoplamiento de las ecuaciones de Stokes y Darcy, cuyos dominios se discretizan mediante dos triangulaciones independientes. Esto provoca no conformidad en la intersección de los subdominios o bien origina un espacio vacío (región no mallada) entre ellos. Para acoplar adecuadamente las dos discretizaciones diferentes y obtener un esquema de alto orden, proponemos condiciones de transmisión adecuadas basadas en la conservación de masa, el equilibrio de fuerzas normales y la ley de Beavers–Joseph–Saffman. Dado que las mallas no coinciden necesariamente en la interfaz, utilizamos el Transfer Path Method (TPM) para unirlas. Establecemos el buen planteamiento del método y proporcionamos estimaciones de error en las que las influencias de la no conformidad y la brecha están explícitas en las constantes. Por último, se muestran experimentos numéricos que ilustran el desempeño del método.

Agradecimientos

Mi más sincero agradecimiento al Dr. Manuel Solano Palma, mi tutor de tesis, por su invaluable orientación, paciencia y excepcional mentoría. Por haber creído en mí, aceptarme como estudiante y dedicarme lo más valioso de la vida: su tiempo. Su pasión por la enseñanza, la investigación y el fútbol ha dejado una huella profunda en mi desarrollo profesional y personal. Además de su guía académica, sus consejos me han sido fundamentales. No solo es un gran profesional, sino también una extraordinaria persona.

Lo anterior también lo extiendo a la Dra. Jessika Camaño, mi co-tutora, de quien me siento muy dichoso de haber recibido la oportunidad de trabajar junto a ella. Ha sido fundamental en todo este proceso, por su calidez humana y su enorme disposición para ayudarme, dedicando su tiempo cada vez que lo necesité. De ambos me siento profundamente agradecido y les aprecio. Sé que no pude haber tenido mejores tutores que ellos.

I thank the Evaluating Committee and the External Reviewers for the time dedicated to revising this thesis and for the comments received. I also thank the members of the Examining Committee for their willingness to serve as jurors for the defense of the thesis.

A la Universidad de Concepción y al cuerpo docente del programa de doctorado. Un reconocimiento especial al Dr. Raimund Bürger, director del programa, por su constante apoyo y disponibilidad ante cada solicitud que realicé como estudiante. Agradezco igualmente al personal administrativo del (CI^{2}MA) y del DIM, quienes me brindaron un trato cálido y amable durante mi tiempo en la universidad. En especial, a la Sra. Lorena, Sra. Paola y la Sra. Cecilia, cuya dedicación hizo que mi experiencia universitaria fuera sumamente agradable. También, a mis compañeros del doctorado, quienes compartieron esta etapa conmigo. Especialmente, quiero agradecer a Yolanda y Juan Paulo, por su amistad, apoyo y los consejos que fueron invaluables en este camino. A Saulo y Paulo, mis amigos extranjeros, por los momentos compartidos durante esta etapa.

Quiero expresar también mi agradecimiento al profesor Gabriel Gatica, por su dedicación en las dos asignaturas que cursé y por invitarme a colaborar con él. Su apoyo fue clave para entender muchos de los conceptos desarrollados en este trabajo y para mi formación como investigador. Al profesor Ricardo Oyarzúa, le agradezco profundamente por su tiempo y colaboración durante esta etapa, y por brindarme, a través del proyecto Dsalt, recursos para mi estadía de investigación en el extranjero. Al profesor Ricardo Ruiz Baier, por recibirme en Australia, por su tiempo dedicado a colaborar conmigo en investigación, y por su calidez humana y generosidad durante nuestra estancia.

Un agradecimiento muy especial a mis profesores de pregrado de la Universidad de Costa Rica, Mario Álvarez y Norman Noguera. Decidir realizar un doctorado fue posible gracias a sus invaluables consejos, su disposición para ayudarme en todo momento y su visión de futuro. No tengo palabras para expresar cuánto les agradezco por todo lo que han hecho por mí. A Bryan Gómez, por su apoyo y consejos fundamentales durante este proceso, mi gratitud es también profunda. A mis queridos amigos de Costa Rica con quienes compartí mis años de pregrado: Nico, Vanessa, Adriana, Alejandra y Ricardo. Su amistad ha sido un regalo en mi vida.

Agradezco a todas las instituciones y programas de becas que han apoyado mi formación, incluyendo los distintos proyectos y fondos de investigación: ANID-Chile a través del Centro de Modelamiento Matemático (FB210005), Anillo de Matemática Computacional para Procesos de Desalinización (ACT210087), Proyectos Fondecyt 1200569, 1240183, y Becas/Doctorado Nacional 21210582.

También quiero expresar mi gratitud a Miranda, por su cariño (que es mutuo) y su apoyo constante hacia nosotros durante este tiempo. Gracias por compartir con nosotros y abrirnos las puertas de su hogar. A Sylvia Palma, por su generosidad al brindarnos un hogar cómodo y acogedor. A ambas, les deseo que Dios las bendiga enormemente. A mis estimadas hermanas en la fe, Solimar y Claudia, por compartir tantas vivencias junto a mi esposa y a mí. De la misma manera, quiero expresar mi gratitud a Mauricio Puentes y su esposa Carime por el cariño recibido de parte de ellos durante nuestra estancia en Chile, y por sus invaluables consejos y oraciones hacia nosotros. Que mi Señor siempre haga resplandecer su rostro sobre ustedes y les colme de bendiciones.

A mis padres, Neftalí y Rosario, y a mis hermanos, Bryan y Lizeth, cuyo amor incondicional y apoyo constante han sido los pilares en mi vida. Su incansable esfuerzo, perseverancia y ejemplo de vida me han inspirado a superar cada obstáculo y alcanzar este logro. A mis suegros William y Marielos, por su generosidad y apoyo en todo momento, por adoptarme como a un hijo y por sus oraciones constantes, tanto hacia mí como a mi esposa. A mi tía Linda, por su cariño y por siempre impulsarme a seguir adelante. Gracias por toda la ayuda que me ha brindado hasta este día y por su apoyo incondicional. A todos ustedes, pido a Dios que me dé la oportunidad de retribuirles todo lo que han hecho por mí. A mi querida abuela Aurora, mi prima Yendry, y mis tíos Santiago y Ligia, quienes, aunque ya no están físicamente, su legado de fe y dedicación a Dios sigue siendo una inspiración para mí.

A mi amada esposa Raquel, quien ha sido el regalo más grande de gracia y amor inagotable de Dios hacia mí. Gracias por ser mi compañera incansable en esta etapa, por su apoyo, amor y por caminar a mi lado como mi socia en la vida. Esta tesis es dedicada a usted. Finalmente, y más importante en mi vida, mi Salvador, Señor y Dios: Yehoshúa. Porque por Él, soy lo que soy; y a pesar de mí, su gracia no ha sido en vano para conmigo.

Isaac Bermúdez Montiel

Contents

Abstract **iii**

Resumen **v**

Agradecimientos **vii**

Contents **ix**

List of Tables **xi**

List of Figures **xii**

Introduction **1**

Introducción **6**

1 A conforming mixed finite element method for a coupled Navier–Stokes/transport system modeling reverse osmosis processes **11**

1.1 Introduction . . . 11

1.1.1 Preliminaries . . . 12

1.1.2 The model problem . . . 14

1.2 The mixed formulation . . . 17

1.3 The continuous solvability analysis . . . 21

1.3.1 The fixed-point strategy . . . 21

1.3.2 Solvability analysis of the fixed-point scheme . . . 27

1.4 The Galerkin scheme . . . 29

1.4.1 Preliminaries . . . 30

1.4.2 Well-definedness of the operators $\widetilde{\mathcal{J}}_h$ and $\widehat{\mathcal{J}}_h$ . . . 31

1.4.3 Discrete solvability analysis 33
1.4.4 *A priori* error analysis 35
1.5 Specific finite element subspaces 37
1.6 Computational results 40
1.7 Appendix 42

2 Further numerical simulations for coupled fluid channels 46
2.1 Introduction 46
2.2 Theoretical description 47
2.2.1 A single channel 47
2.2.2 Coupled feed and permeate channels 53
2.2.3 Comments on the well-posedness of the numerical schemes 56
2.3 Numerical simulations 56
2.3.1 A single feed channel. 57
2.3.2 Coupled feed and permeate channel. 63

3 An HDG method for Stokes/Darcy coupling on dissimilar meshes 69
3.1 Introduction 69
3.2 Preliminaries 71
3.3 The HDG method 75
3.4 Stability analysis 77
3.4.1 An energy argument 81
3.4.2 A duality argument 84
3.4.3 Semi-aligned discrete interfaces 88
3.5 Error Analysis 89
3.6 Numerical results 95

4 Conclusions and future work 101
4.1 Conclusions 101
4.2 Future work 102
4.3 Conclusiones 105
4.4 Trabajo futuro 106

References 108

List of Tables

1.1 Example 1, number of degrees of freedom, meshsizes, iterations, errors, and rates of convergence for the $\mathbb{RT}_0-\mathbf{P}_0-\mathbf{RT}_0-\mathrm{P}_0-\mathrm{P}_1$ approximations of the Navier–Stokes/transport model, and convergence of the P_0-approximation of the postprocessed pressures field. 42

1.2 Simulation conditions [14, 33, 89]. 42

2.1 Physical parameters 56

2.2 Total permeate flow per unit length $\dot{V}/W$ in a single channel for different values of $\mathrm{u_{in}}$ and $\mathit{\Delta}P$, of the three cases (S.1), (S.2) and (S.3). 63

2.3 Increment rate in the value of $\dot{V}/W$ reported in Table 2.2, with respect to the variation of the velocity (first and second rows), hydrostatic transmembrane pressure (third and fourth rows) and configurations (fifth to eight rows). 63

2.4 Coordinates of the center of the circular spacers located inside the feed and permeate channels. 64

2.5 Total permeate flow per unit length $\dot{V}/W$ in coupled channels for $\mathrm{u_{in,f}} = 0.1\,m/s$, $\mathrm{u_{in,p}} = 0.01\,m/s$ and $\mathit{\Delta}P = \mathit{\Delta}P_2$, of the five cases (C.1), (C.2), (C.3), (C.4) and (C.5). 68

2.6 Increment rate in the value of $\dot{V}/W$ reported in Table 2.5, with respect to the variation of configurations. 68

3.1 History of convergence of the HDG method for $\delta = 0$ and without hanging nodes . . . 96

3.2 History of convergence of the HDG method for $\delta = 0$ and with hanging nodes 97

3.3 History of convergence of the HDG method for $\delta = h^{7/4}$ and without hanging nodes . . 98

3.4 History of convergence of the HDG method for $\delta = h^{7/4}$ and with hanging nodes . . . 98

3.5 History of convergence of the HDG method for $\delta = h$ and without hanging nodes . . . 99

List of Figures

1.1 Sketch of the geometry. 14

1.2 Example 2, approximations with `dof` $= 2,616,096$ for the velocity magnitudes of the fluid, pressure fields and concentration levels in the whole domain. 43

2.1 Sketch of a single channel with explicit spacer (left) and implicit spacers (right). 47

2.2 Sketch of the coupled feed and permeate channels. Explicit spacers (left) and implicit spacers (right). 54

2.3 Comparison of exact vs. approximate pressure drop (left) and axial velocity (right) for a single channel. Simulation conditions: $\mathrm{u_{in}} = 0.2\,m/s$, $\Delta P = \Delta P_2$ and clean water, for Poiseuille (impermeable) and Berman (permeable) flows. 57

2.4 Zoom in the region $[5, 10]\,mm \times [0, 0.74]\,mm$. From left to right: axial velocity profiles (left), concentration fields (middle), and pressure drops (right). From top to bottom, cases (S.1), (S.2) and (S.3). Simulation conditions: $\mathrm{u_{in}} = 0.1\,m/s$, $\Delta P = \Delta P_1$. 59

2.5 Salt concentration along the vertical line at $x = 7.7\,mm$, $y \in [0, 0.1]\,mm$ for the three cases (S.1), (S.2) and (S.3). Simulation conditions: $\mathrm{u_{in}}$ equal to $0.1\,m/s$ (top panels) and $0.2\,m/s$ (bottom panels); and ΔP equal to ΔP_1 (left panels) and ΔP_2 (right panels). 60

2.6 Relative pressure drop (top panels), permeate velocity (middle) and concentration level (bottom panels) at the membrane $y = 0\,mm$ without spacers (S.1), with submerged explicit spacers (S.2), and implicit spacers (S.3). Simulation conditions: $\mathrm{u_{in}} = 0.1\,m/s$; and ΔP equal to ΔP_1 (left panels) and ΔP_2 (right panels). 61

2.7 Same as Figure 2.6 but considering $\mathrm{u_{in}} = 0.2\,m/s$. 62

2.8 Axial velocities in the region $[3, 12]\,mm \times [0, 1.48]\,mm$. From top to bottom: cases (C.1), (C.2), (C.3), (C.4) and (C.5). Simulation conditions: $\mathrm{u_{in,f}} = 0.1\,m/s$, $\mathrm{u_{in,p}} = 0.01\,m/s$, $\Delta P = \Delta P_2$. 64

2.9 Pressure drop in the region $[3, 12]\,mm \times [0, 1.48]\,mm$. From top to bottom: cases (C.1), (C.2), (C.3), (C.4) and (C.5). Simulation conditions: $\mathrm{u_{in,f}} = 0.1\,m/s$, $\mathrm{u_{in,p}} = 0.01\,m/s$, $\Delta P = \Delta P_2$. 65

2.10 Salt concentration in the region $[3, 12]\,mm \times [0, 1.48]\,mm$. From top to bottom: cases (C.1), (C.2), (C.3), (C.4) and (C.5). Simulation conditions: $\mathrm{u_{in,f}} = 0.1\,m/s$, $\mathrm{u_{in,p}} = 0.01\,m/s$, $\mathit{\Delta} P = \mathit{\Delta} P_2$. 66

2.11 Salt concentration along the vertical lines at $x = 7.3\,mm$ (left panel) and $x = 7.7\,mm$ (right panel), $y \in [0.74, 1.15]\,mm$ for the five cases (C.1), (C.2), (C.3), (C.4) and (C.5). Simulation conditions: $\mathrm{u_{in,f}} = 0.1\,m/s$, $\mathrm{u_{in,p}} = 0.01\,m/s$, $\mathit{\Delta} P = \mathit{\Delta} P_2$. 66

2.12 Feed channel. Relative pressure drop (top-left panel), permeate velocity (top-right panel) and concentration level (bottom panel) at the membrane ($y = 0.74\,mm$) for all cases (C.1)-(C.5). Simulation conditions: $\mathrm{u_{in,f}} = 0.1\,m/s$, $\mathrm{u_{in,p}} = 0.01\,m/s$, $\mathit{\Delta} P = \mathit{\Delta} P_2$. 67

2.13 Permeate channel. Relative pressure drop (left panel) and concentration level (right panel) at the membrane ($y = 0.74\,mm$) for all cases (C.1)-(C.5). Simulation conditions: $\mathrm{u_{in,f}} = 0.1\,m/s$, $\mathrm{u_{in,p}} = 0.01\,m/s$, $\mathit{\Delta} P = \mathit{\Delta} P_2$. 67

3.1 Left: Example of dissimilar meshes separated by a uniform gap of size δ. Right: A piecewise polygonal interface separating two regions discretized by diferent meshes. . . 73

3.2 Example of *semi-aligned* discrete interfaces separated by a uniform gap of size δ. . . . 88

Introduction

Modeling of a variety of physical phenomena involving the coupling of partial differential equations (PDEs) across an interface has become a very active research area over the years. In general, the types of coupling problems are diverse and can manifest in several forms depending on the underlying physical context. A common scenario involves an interface separating subdomains governed by the same PDE with different coefficients [24]. Another prevalent case occurs when the interface divides subdomains governed by distinct PDEs, such as when an incompressible fluid interacts with a porous medium, where the Stokes/Navier–Stokes equations are coupled with the Darcy equations [11]. Both cases are relevant in science and engineering applications where two systems interact at an interface, leading to the transfer of physical quantities such as stresses and displacements between them. However, the equations describing these models are often difficult to solve analytically, requiring the use of efficient computational methods to obtain approximate solutions. Furthermore, it is of great importance to analyze the conditions under which these systems of equations admit solutions and to determine the stability and convergence properties of the methods employed.

In this context, finite element methods have become a valuable tool for obtaining approximate solutions in finite-dimensional spaces and for developing techniques to simulate these type of problems. This leads to the challenge of specifying, at the continuous level, the conditions under which the problem is well-posed. This includes selecting appropriate function spaces to ensure that both volumetric and boundary/interface terms also make mathematical sense. This can be further complicated in the case of mixed conditions and when non-linear terms appears at the boundary/interface. On the other hand, at the discrete level, additional difficulties arise when discretizing the interface. In this regard, one can proceed in two ways. Rely on a conforming approach, where the mesh is adjusted to the interface and properly aligned to avoid hanging nodes, or mesh each subdomain separately using different meshsizes.

Let us provide a brief discussion regarding these two meshing approaches. The first approach corresponds to the simplest case where the discrete interfaces do not include hanging nodes. This configuration is typical in conforming domain decomposition methods, often relying on classical Lagrange multipliers formulations for interface problems in the context of finite element methods (see, e.g., [61,95,100]). Additionally, using the method described in [106], it is possible to construct discrete interfaces where the nodes on both sides coincide by generating a global mesh covering both subdomains, explicitly designed to align nodes along the continuous interface. However, achieving perfect alignment may become challenging in the presence of complex geometries. In contrast, the second approach allows for the construction of discrete interfaces with hanging nodes. This setup is often referred to in the literature as non-conforming domain decomposition [19]. Within this framework, one of the most widely studied methods is the Mortar method (see, e.g., [12,64,105]), which, under certain conditions, achieves optimal convergence rates. This method relies on a single L^2 projection operator and conserves traction forces. According to [20], the Mortar method leverages the flexibility of subdomains to select discretization techniques that best suit the local behavior of the solution to the PDE. However, implementing this method may involve some complexity due to its reliance on projection techniques. One significant advantage of the Mortar method is its adaptability in handling various types of nonconformities. Recently, in [52], an alternative approach called “Internodes” has been introduced, which the authors suggest may simplify implementation compared to the Mortar method. Unlike the latter, the Internodes approach uses interpolations rather than L^2 projection at interface. However, the choice between these approaches depends on the specific problem configuration, as interpolation-based methods may not always provide the same level of accuracy or stability in certain applications.

Regarding these two perspectives, we point out that the use of the first one can simplify the analysis of the discrete scheme; however, this can be computationally demanding. On the other hand, the use of the second one may complicate the analysis of the discrete scheme, since several situations may arise due to the non-conformity of the meshes. However, this perspective aims to reduce the computational cost related to the meshing of the subdomains.

This thesis focuses on two topics related to interface problems: non-linear transmission conditions in a conforming discretization of the interface and transmission conditions across non-coincident discrete interfaces. To address them, we employ and develop several mathematical and numerical techniques in the context of continuous and discontinuous Galerkin-type discretizations applied to interface problems.

We will briefly comment on the motivation for each of the topics to be considered. The first one is inspired by reverse osmosis (RO) in seawater desalination processes. RO employs semi-permeable membranes to separate solutes, such as salt and organic molecules, from a solvent (typically water). This is achieved by allowing water to pass through the membrane while blocking the solutes, using a working pressure that exceeds the osmotic pressure (i.e., the pressure needed to counteract the natural flow of solvent into a more concentrated solution) [8]. Given that this problem involves a semi-permeable membrane between two channels, where several variables of physical interest are coupled, we aim to study it by treating the membrane as an interface.

Within Galerkin-type discretizations, numerous studies addressing nonlinear boundary conditions can be found in the literature. For example, boundary element methods have been used to solve potential problems [65], while finite element schemes have been applied to Maxwell's equations [99] and the Navier–Stokes equations [21], among others. Furthermore, nonlinear interface conditions closely related to those addressed in this thesis are studied in works such as [30, 31], where discontinuous Galerkin (DG) methods are developed and analyzed. Similar to our approach, these studies on interface problems are motivated by models of solute mass transfer through semipermeable membranes.

In this work, we focus on using mixed finite element methods, as they allow for the introduction of additional unknowns that may be of physical interest or serve as auxiliary variables to facilitate the analysis. In particular, the transmission conditions can be more easily incorporated by employing techniques such as Lagrange multipliers [10, 55, 64, 69]. Moreover, it enables the exact conservation of crucial properties such as momentum and mass (see [25, 27]). In addition, it is worth mentioning that over the last decade, mixed methods have provided significant tools for dealing with non-linear models in multi-physics problems. Regarding this difficulty, various approaches have been proposed. One of them involves an augmentation procedure, offering more flexibility in choosing finite element subspaces, but increasing the complexity and computational cost significantly. Some examples include [4] for a coupled flow-transport problem, [28] and [29] for Navier–Stokes equations, and [49] for Boussinesq equations. Alternatively, one can consider the approach of Banach spaces-based mixed finite element methods to solve perturbed saddle point formulations. We point out that the motivation for employing the latter approach has the advantages of not requiring an augmentation procedure, and the spaces where the unknowns are sought are the natural ones that result from applying the Cauchy–Schwarz and Hölder inequalities to the terms obtained from testing and integrating by parts the equations of the model. Consequently, simpler formulations closely aligned with the original physical model are achieved. Some references include [26] for the convection-diffusion equation, [48] for the Boussinesq problem, and [16, 25] for Navier–Stokes equations.

The second topic is motivated by the convenience of meshing the domains independently. In several applications, the domain of interest $\Omega \subset \mathbb{R}^n$, $n \in \{2, 3\}$, is divided into subdomains where different governing equations are posed. For instance, in the case of solid-fluid interactions, the fluid equations are coupled to the elasticity equations via appropriate transmission conditions across an interface, and it is often desirable to have a finer mesh in the region occupied by the fluid compared to the meshsize used for discretizing the solid. We propose a method to impose the transmission conditions when the discrete interfaces are those induced by meshing separately each subdomain and also can handle curved interfaces, which represents a challenge to develop appropriate numerical methods. Because of the presence of hanging-nodes, we prefer to employ a DG approach that provides flexibility in the construction of meshes and high-order approximation spaces. In particular, we focus on the hybridizable DG (HDG) method.

The HDG method, introduced in [41], discretizes a mixed formulation of the Darcy equation, where the only globally coupled degrees of freedom are those of the numerical traces on the boundaries between elements, while the remaining unknowns are obtained by solving local problems in each element. Specifically, at the continuous level, intra-element variables can be expressed in terms of inter-element unknowns by solving local problems on each element. These problems, referred to as local solvers, can be discretized using a DG method, leading to the family of methods known as HDG methods.

In order to deal with the transmission conditions across discrete interfaces that do not match the true interface, we employ the Transfer Path Method (TPM) [44–46, 94], originally designed for handling boundary value problems in curved domains, but recently employed for coupling dissimilar meshes in the context of a single PDE in the entire domain. In this regard, we mention that our work continues the development of the TPM applied to dissimilar meshes started in [87, 101], and therefore we employ similar techniques. However, in this work, other issues arise due to the fact that two different equations are being coupled. Here, we will consider the coupled Stokes/Darcy equations, where the primal variable of the Stokes system is coupled to the mixed variable of the Darcy equations and vice versa. This adds more difficulties in designing and analyzing the scheme compared to the cases in [87, 101], where a single equation holds in the entire domain.

Keeping in mind the above, we are interested in:

i) To establish the well-posedness of a mixed finite element method for a coupled Navier–Stokes/transport equations with nonlinear transmission conditions, motivated by the modeling of reverse osmosis processes.

ii) Analyzing a hybridizable discontinuous Galerkin (HDG) method for coupling the Stokes and Darcy equations, where the subdomains are discretized by two independent triangulations.

Let us now outline the structure of the thesis according to the sequence of the topics mentioned above.

In Chapter 1, we introduce mixed variational formulations in Banach spaces for the Navier–Stokes and transport models. The variational formulations consist of a set of equations where the velocities and concentrations, along with tensors and vector fields introduced as auxiliary unknowns, together with two Lagrange multipliers, are the main unknowns of the system. Subsequently, we analyze the continuous and discrete solvability of the problem. To do that, the coupled formulation is transformed into an equivalent fixed-point equation, and we apply the classical Banach fixed-point theorem along with the Banach–Nečas–Babuška result. We then construct corresponding Galerkin discretizations based on suitable finite element spaces and derive optimal *a priori* error estimates. This chapter is based on the following paper, which has been published in a WoS journal:

> [15] I. Bermúdez, J. Camaño, R. Oyarzúa and M. Solano. *A conforming mixed finite element method for a coupled Navier–Stokes/transport system modeling reverse osmosis processes*, Comput. Methods Appl. Mech. Engrg., 433 (2025), p. Paper No. 117527.

As a byproduct of i), in Chapter 2, we provide matrix-structured strategies for implementing the proposed Galerkin scheme and perform several numerical simulations motivated by RO modeling to demonstrate the applicability of the mixed method with the Navier-Stokes/transport equations. Furthermore, for specific reasons detailed later in this chapter, we also implement a computational model for a Brinkmann–Forchheimer/transport system using a similar variational formulation. In both cases, reduced models for a single desalination channel are considered. The contents of this chapter are reported in the following preprint:

> [14] I. Bermúdez, V. Burgos, J. Camaño, F. Gajardo, R. Oyarzúa, M. Solano. *Mixed finite element methods for coupled fluid flow problems arising from reverse osmosis modeling*, Preprint 2024-15, Centro de Investigación en Ingeniería Matemática ($\mathrm{CI^2MA}$), Universidad de Concepción, Chile, 2024.

On the other hand, inspired in the results obtained in [87, 101], Chapter 3 focuses on developing an HDG method for the coupled Stokes/Darcy problem with independently discretized subdomains that do not necessarily match. For this, we propose suitable transmission conditions using an appropriate method to tie the discrete interfaces so that allow us to maintain consistency of terms for the case of matching meshes. Subsequently, we establish the unique solvability of the HDG scheme and derive the *a priori* error estimates. The results in this chapter has been accepted for publication in a WoS journal:

> [17] I. Bermúdez, J. Manríquez, and M. Solano, *A hybridizable discontinuous Galerkin method for Stokes/Darcy coupling on dissimilar meshes*, IMA J. Numer. Anal., (2025), doi: `https://doi.org/10.1093/imanum/drae109`.

Finally, we would like to mention that in Chapters 1 and 3, we provide the respective numerical tests that corroborate the developed theory and the accuracy of the numerical schemes. In addition, in

Chapter 2, we simulate different scenarios inspired by reverse osmosis processes. The methods have been implemented in FreeFem++ [73], Matlab [75], and we use Paraview [9] to visualize.

Introducción

La modelación de diversos fenómenos físicos que involucran el acoplamiento de ecuaciones diferenciales parciales (EDPs) a través de una interfaz se ha convertido en un área de investigación muy activa a lo largo de los años. En general, los tipos de problemas de acople son diversos y pueden manifestarse de varias formas dependiendo del contexto físico subyacente. Un escenario común implica una interfaz que separa subdominios gobernados por la misma EDP con diferentes coeficientes [24]. Otro caso frecuente se produce cuando la interfaz divide subdominios gobernados por EDPs distintas, como cuando un fluido incompresible interactúa con un medio poroso, donde las ecuaciones de Stokes/Navier–Stokes se acoplan con las ecuaciones de Darcy [11]. Ambos casos son relevantes en aplicaciones científicas y de ingeniería en las que dos sistemas interactúan en una interfaz, lo que conduce a la transferencia de magnitudes físicas como tensiones y desplazamientos entre ellos. Sin embargo, las ecuaciones que describen estos modelos suelen ser difíciles de resolver analíticamente, requiriendo el uso de métodos computacionales eficientes para obtener soluciones aproximadas. Además, es de gran importancia analizar las condiciones bajo las cuales estos sistemas de ecuaciones admiten soluciones y determinar las propiedades de estabilidad y convergencia de los métodos empleados.

En este contexto, los métodos de elementos finitos se han convertido en una valiosa herramienta para la obtención de soluciones aproximadas en espacios finito-dimensionales y para desarrollar técnicas que simulen este tipo de problemas. Esto conduce al desafío de especificar, a nivel continuo, las condiciones en las que el problema está bien puesto. Esto incluye seleccionar espacios de funciones apropiados para garantizar que tanto los términos volumétricos como los de frontera/interfaz también tengan sentido matemático. Esto puede complicarse aún más en el caso de condiciones mixtas y cuando aparecen términos no lineales en el borde/interfaz. Por otra parte, a nivel discreto, surgen dificultades adicionales cuando se discretiza la interfaz. En este sentido, uno puede proceder de dos maneras. Apoyarse en un enfoque conforme, donde la malla se ajusta a la interfaz y se alinea adecuadamente para evitar nodos colgantes, o mallar cada subdominio por separado utilizando diferentes tamaños de malla.

Discutamos brevemente estos dos enfoques de mallado. El primer enfoque corresponde al caso más sencillo, en el que las interfaces discretas no incluyen nodos colgantes. Esta configuración es típica en los métodos de descomposición de dominios conformes, que a menudo se basan en las formulaciones clásicas de los multiplicadores de Lagrange para los problemas de interfaz en el contexto de los métodos de elementos finitos (véase, por ejemplo, [61, 95, 100]). Además, utilizando el método descrito en [106], es posible construir interfaces discretas en las que los nodos de ambos lados coincidan generando una malla global que cubra ambos subdominios, diseñada explícitamente para alinear los nodos a lo largo de la interfaz continua. Sin embargo, lograr una alineación perfecta puede convertirse en un reto en presencia de geometrías complejas. En contraste, el segundo enfoque permite la construcción de interfaces discretas con nodos colgantes. Esta configuración se conoce a menudo en la literatura como descomposición de dominio no conforme [19]. Dentro de este marco, uno de los métodos más ampliamente estudiados es el método Mortar (véase, por ejemplo, [12, 64, 105]), que, en determinadas condiciones, alcanza tasas de convergencia óptimas. Este método se basa en un único operador de proyección L^2 y conserva las fuerzas de tracción. Según [20], el método Mortar aprovecha la flexibilidad de los subdominios para seleccionar las técnicas de discretización que mejor se adapten al comportamiento local de la solución de la EDP. Sin embargo, la implementación de este método puede implicar cierta complejidad debido a su dependencia de las técnicas de proyección. Una ventaja significativa de el método Mortar es su adaptabilidad en el manejo de diversos tipos de no conformidades. Recientemente, en [52], se ha introducido un enfoque alternativo denominado "Internodes", en el que los autores sugieren que puede simplificar la implementación en comparación con el método Mortar. A diferencia de este último, el enfoque Internodes utiliza interpolaciones en lugar de la proyección L^2 en la interfaz. Sin embargo, la elección entre estos enfoques depende de la configuración específica del problema, ya que los métodos basados en la interpolación no siempre proporcionan el mismo nivel de precisión o estabilidad en determinadas aplicaciones.

En cuanto a estas dos perspectivas, señalamos que el uso de la primera puede simplificar el análisis del esquema discreto; sin embargo, esto puede ser computacionalmente exigente. Por otro lado, el uso de la segunda puede complicar el análisis del esquema discreto, ya que pueden surgir varias situaciones debido a la no conformidad de las mallas. Sin embargo, esta perspectiva pretende reducir el coste computacional relacionado con el mallado de los subdominios.

Esta tesis se enfoca en dos tópicos relacionados con problemas de interfaz: condiciones de transmisión no lineales en una discretización conforme de la interfaz y condiciones de transmisión a través de interfaces discretas no coincidentes. Para abordarlos, empleamos y desarrollamos varias técnicas matemáticas y numéricas en el contexto de discretizaciones continuas y discontinuas de tipo Galerkin aplicadas a problemas de interfaz.

Comentaremos brevemente la motivación de cada uno de los tópicos a considerar. El primero se inspira en la ósmosis inversa (OI) en los procesos de desalinización del agua de mar. La OI emplea membranas semipermeables para separar solutos, como sal y moléculas orgánicas, de un disolvente (normalmente agua). Esto se consigue permitiendo que el agua pase a través de la membrana mientras se bloquean los solutos, utilizando una presión de trabajo que supera la presión osmótica (es decir, la presión necesaria para contrarrestar el flujo natural del disolvente hacia una solución más concentrada) [8]. Dado que este problema involucra una membrana semipermeable entre dos canales, donde se acoplan varias variables de interés físico, pretendemos estudiarlo tratando la membrana como una interfaz.

Dentro de las discretizaciones de tipo Galerkin, se pueden encontrar en la literatura numerosos estudios que abordan condiciones de frontera no lineales. Por ejemplo, los métodos de elementos de frontera se han utilizado para resolver problemas potenciales [65], mientras que los esquemas de elementos finitos se han aplicado a las ecuaciones de Maxwell [99] y a las ecuaciones de Navier-Stokes [21], entre otros. Además, condiciones de interfaz no lineal estrechamente relacionadas con las que se abordan en esta tesis se estudian en trabajos como [30, 31], donde se desarrollan y analizan métodos de Galerkin discontinuo (DG). De forma similar a nuestro enfoque, estos estudios sobre problemas de interfaz están motivados por modelos de transferencia de masa de soluto a través de membranas semipermeables.

En este trabajo, nos centramos en utilizar métodos de elementos finitos mixtos, ya que permiten introducir incógnitas adicionales que pueden ser de interés físico o servir como variables auxiliares para facilitar el análisis. En particular, las condiciones de transmisión pueden incorporarse más fácilmente empleando técnicas como los multiplicadores de Lagrange [10, 55, 64, 69]. Además, permite la conservación exacta de propiedades cruciales como el momento y la masa (véase [25, 27]). Por otro lado, cabe mencionar que en la última década, los métodos mixtos han proporcionado importantes herramientas para tratar con modelos no lineales en problemas multifísicos. En relación con esta dificultad, se han propuesto varios enfoques. Uno de ellos consiste en un procedimiento de aumento, que ofrece más flexibilidad en la elección de subespacios de elementos finitos, pero incrementa significativamente la complejidad y el coste computacional. Algunos ejemplos incluyen [4] para un problema acoplado de flujo-transporte, [28] y [29] para ecuaciones de Navier–Stokes, y [49] para ecuaciones de Boussinesq. Alternativamente, se puede considerar la aproximación de métodos de elementos finitos mixtos basados en espacios de Banach para resolver formulaciones de puntos de silla perturbados. Señalamos que la motivación para emplear este último enfoque tiene las ventajas de no requerir un procedimiento de aumento, y los espacios donde se buscan las incógnitas son los naturales que resultan de aplicar las desigualdades de Cauchy–Schwarz y Hölder a los términos obtenidos de testear e integrar por partes las ecuaciones del modelo. En consecuencia, se consiguen formulaciones más sencillas y cercanas al modelo físico original. Algunas referencias incluyen [26] para la ecuación de convección-difusión, [48] para el problema de Boussinesq, y [16, 25] para las ecuaciones de Navier–Stokes.

El segundo tópico está motivado por la conveniencia de mallar dominios independientemente. En diversas aplicaciones, el dominio de interés $\Omega \subset \mathbb{R}^n$, $n \in \{2, 3\}$, está dividido en subdominios donde se plantean diferentes ecuaciones gobernantes. Por ejemplo, en el caso de las interacciones sólido-fluido, las ecuaciones de fluido se acoplan a las ecuaciones de elasticidad mediante condiciones de transmisión apropiadas a través de una interfaz, y a menudo es deseable tener una malla más fina en la región ocupada por el fluido en comparación con el tamaño de malla utilizado para discretizar el sólido. Proponemos un método para imponer las condiciones de transmisión cuando las interfaces discretas son las inducidas al mallar por separado cada subdominio y también puede manejar interfaces curvas, lo que representa un reto para desarrollar métodos numéricos apropiados. Debido a la presencia de nodos colgantes, preferimos emplear una aproximación DG que proporciona flexibilidad en la construcción de mallas y espacios de aproximación de alto orden. En particular, nos centramos en el método DG hibridizable (HDG).

El método HDG, introducido en [41], discretiza una formulación mixta de la ecuación de Darcy, donde los únicos grados de libertad globalmente acoplados son los de las trazas numéricas en las fronteras entre elementos, mientras que el resto de incógnitas se obtienen resolviendo problemas locales en cada elemento. Específicamente, a nivel continuo, las variables intra-elemento pueden expresarse en términos de incógnitas inter-elemento resolviendo problemas locales en cada elemento. Estos problemas, denominados solvers locales, pueden discretizarse mediante un método DG, dando lugar a la familia de métodos conocidos como métodos HDG.

Con el fin de hacer frente a las condiciones de transmisión a través de interfaces discretas que no coinciden con la verdadera interfaz, empleamos el *Transfer Path Method* (TPM) [44–46, 94], originalmente diseñado para el manejo de problemas de valores de contorno en dominios curvos, pero recientemente empleado para el acoplamiento de mallas disimilares en el contexto de una única EDP en todo el dominio. En este sentido, mencionamos que nuestro trabajo continúa el desarrollo del TPM aplicado a mallas disimilares iniciado en [87, 101], y por tanto empleamos técnicas similares. Sin embargo, en este trabajo surgen otras situaciones debido a que se están acoplando dos ecuaciones diferentes. Aquí consideraremos las ecuaciones acopladas de Stokes/Darcy, donde la variable principal del sistema de Stokes está acoplada a la variable mixta de las ecuaciones de Darcy y viceversa. Esto añade más dificultades en el diseño y análisis del esquema en comparación con los casos de [87, 101], donde una única ecuación se mantiene en todo el dominio.

Teniendo en cuenta lo anterior, nos interesa:

i) Establecer el buen planteamiento de un método de elementos finitos mixto para un acoplamiento de las ecuaciones de Navier–Stokes/transporte con condiciones de transmisión no lineales, motivado por el modelamiento de procesos de ósmosis inversa.

ii) Analizar un método de Galerkin discontinuo hibridizable (HDG) para el acoplamiento de las ecuaciones de Stokes y Darcy, donde los subdominios se discretizan mediante dos triangulaciones independientes.

Esbocemos ahora la estructura de la tesis según la secuencia de los temas antes mencionados.

En el capítulo 1, introducimos formulaciones variacionales mixtas en espacios de Banach para los modelos de Navier–Stokes y de transporte. Las formulaciones variacionales consisten en un conjunto de ecuaciones donde las velocidades y concentraciones, junto con tensores y campos vectoriales introducidos como incógnitas auxiliares, junto con dos multiplicadores de Lagrange, son las principales incógnitas del sistema. Posteriormente, analizamos la solubilidad continua y discreta del problema. Para ello, la formulación acoplada se transforma en una ecuación de punto fijo equivalente, y aplicamos el teorema clásico de punto fijo de Banach junto con el resultado Banach-Nečas-Babuška. A continuación, construimos las discretizaciones Galerkin correspondientes basadas en espacios de elementos finitos adecuados y derivamos estimaciones de error óptimas *a priori*. Este capítulo se basa en el siguiente artículo, publicado en una revista WoS:

[15] I. Bermúdez, J. Camaño, R. Oyarzúa and M. Solano. *A conforming mixed finite element method for a coupled Navier–Stokes/transport system modeling reverse osmosis processes*, Comput. Methods Appl. Mech. Engrg., 433 (2025), p. Paper No. 117527.

Como consecuencia de i), en el capítulo 2, proporcionamos estrategias de estructura matricial para implementar el esquema Galerkin propuesto y realizamos varias simulaciones numéricas motivadas por el modelamiento de OI para demostrar la aplicabilidad del método mixto con las ecuaciones de Navier–Stokes/transporte. Además, por razones específicas que se detallan más adelante en este capítulo, también implementamos un modelo computacional para un sistema de Brinkmann–Forchheimer/transporte utilizando una formulación variacional similar. En ambos casos, se consideran modelos reducidos para un único canal de desalinización. El contenido de este capítulo se recopila en el siguiente preprint:

[14] I. Bermúdez, V. Burgos, J. Camaño, F. Gajardo, R. Oyarzúa, M. Solano. *Mixed finite element methods for coupled fluid flow problems arising from reverse osmosis modeling*, Preprint 2024-15, Centro de Investigación en Ingeniería Matemática (CI^2MA), Universidad de Concepción, Chile, 2024.

Por otro lado, inspirados en los resultados obtenidos en [87, 101], el capítulo 3 se centra en desarrollar un método HDG para el problema acoplado Stokes/Darcy con subdominios discretizados independientemente que no necesariamente coinciden. Para ello, proponemos unas condiciones de transmisión adecuadas utilizando un método apropiado para ligar las interfaces discretas de forma que nos permita mantener la consistencia de los términos para el caso de mallas coincidentes. Posteriormente, establecemos la solvencia única del esquema HDG y derivamos las estimaciones de error *a priori*. Los resultados de este capítulo han sido aceptados para su publicación en una revista WoS:

> [17] I. Bermúdez, J. Manríquez, and M. Solano, *A hybridizable discontinuous Galerkin method for Stokes/Darcy coupling on dissimilar meshes*, IMA J. Numer. Anal., (2025), doi: `https://doi.org/10.1093/imanum/drae109`.

Por último, nos gustaría mencionar que en los Capítulos 1 y 3, proporcionamos las respectivas pruebas numéricas que corroboran la teoría desarrollada y la precisión de los esquemas numéricos. Además, en el Capítulo 2, simulamos diferentes escenarios inspirados en procesos de ósmosis inversa. Los métodos han sido implementados en FreeFem++ [73], Matlab [75], y utilizamos Paraview [9] para visualizar.

CHAPTER 1

A conforming mixed finite element method for a coupled Navier–Stokes/transport system modeling reverse osmosis processes

1.1 Introduction

Membrane-based seawater desalination processes have received special attention during the last decade due to their notable advantages, which include relatively low energy consumption compared to thermal-based techniques like multi-stage flash [98], as well as their capability to use renewable or low-grade energy sources [3,107]. In this regard, the RO process takes a prominent position, being employed in 69% of industrial desalination plants globally [59]. Its mathematical modeling is usually based on the Navier–Stokes and convection-diffusion equations, although the Brinkman equations can also be considered in some scenarios [96]. In particular, for some detailed review of different mathematical models we refer to [77, 85, 104].

As already mentioned, in the reverse osmosis processes water flows at high pressure through a membrane module [98], which consists of several channels separated by semi-permeate membranes. The domain of simulation is a representative rectangular section of these channels. Most of the numerical methods developed in the literature consider only a single desalination channel, due to the high computational cost of simulating several channels. They are usually based on finite differences and finite volumes methods. Regarding the finite element method, most of the simulations are performed using commercial softwares and, to the best of our knowledge, a proper mathematical framework has not been developed. Recently in [33] a finite element method using the Nitsche technique on an RO model was addressed, on which the resulting discrete model is easily implemented since the linearization of the model depends only on the linearization of the flow.

One of the novel aspects of our work is the consideration of two channels coupled by a semi-permeable membrane. To the best of our knowledge, no numerical method has been developed for this setup in the existing literature. Our work proposes and analyzes a mixed variational formulation inspired by the coupling of the Navier–Stokes and transport equations, along with boundary and interface conditions typically used in RO models. In this regard, the consideration of nonlinear transmission conditions on the membrane represents the major difficulty to address the problem, from theoretical and computational points of view, and constitutes another novelty of our work. In the formulation, we introduce two Lagrange multipliers associated to the concentration to deal with the trace of functions that do not have enough regularity to be restricted to the boundary. In this way, the non-linearity at the interface is handled with these new unknowns. Subsequently, an appropriate linearization allows us to overcome this difficulty. Another complexity in analyzing the problem arises from the presence of convective terms in the equations, which as we mentioned in the introduction to the thesis, we will consider the approach of Banach space-based mixed finite element methods.

This chapter is organized as follows. In the rest of this section, we provide an overview of the standard notation and functional spaces that will be utilized throughout the paper, introduce the model problem of interest and define the unknowns to be considered in the variational formulation. Subsequently, in Section 1.2 we identify the saddle point structure of the corresponding variational system. Section 1.3 analyzes the continuous solvability and the equivalent fixed point setting, presenting the well-posedness result under the assumption of sufficiently small data. In Section 1.4, we investigate the associated Galerkin scheme by utilizing a discrete version of the fixed point strategy developed in Section 1.3 for the continuous case. Additionally, we derive the associated *a priori* error estimate in the same section. Furthermore, in Section 1.5 we specify particular choices of discrete subspaces that satisfy the hypotheses from Section 1.4 and show the theoretical behaviour of the errors. Next, in Section 1.6, numerical examples illustrate the performance of the numerical scheme. Conclusions are presented in Chapter 4.

1.1.1 Preliminaries

Sobolev and Banach spaces. Given a Lipschitz-continuous domain $\mathcal{O}$ of $\mathbb{R}^2$ with boundary $\mathit{\Gamma}$, we adopt standard notations for Lebesgue spaces $\mathrm{L}^t(\mathcal{O})$ and Sobolev spaces $\mathrm{W}^{l,t}(\mathcal{O})$, with $l \geq 0$ and $t \in [1, +\infty)$, whose corresponding norms, either for the scalar- and vector-valued case, are denoted by $\|\cdot\|_{0,t;\mathcal{O}}$ and $\|\cdot\|_{l,t;\mathcal{O}}$, respectively. Note that $\mathrm{W}^{0,t}(\mathcal{O}) = \mathrm{L}^t(\mathcal{O})$, and if $t = 2$ we write $\mathrm{H}^l(\mathcal{O})$ instead of $\mathrm{W}^{l,2}(\mathcal{O})$, with the corresponding norm and seminorm denoted by $\|\cdot\|_{l,\mathcal{O}}$ and $|\cdot|_{l,\mathcal{O}}$, respectively. In addition, $\mathrm{H}^{1/2}(\mathit{\Gamma})$ denotes the space of traces of $\mathrm{H}^1(\mathcal{O})$ and $\mathrm{H}^{-1/2}(\mathit{\Gamma})$ its dual space, provided with the duality pairing $\langle\cdot,\cdot\rangle_{\mathit{\Gamma}}$. Also, given $\widetilde{\mathit{\Gamma}} \subseteq \mathit{\Gamma}$, $\mathrm{H}^{1/2}(\widetilde{\mathit{\Gamma}})$ denotes the restriction to $\widetilde{\mathit{\Gamma}}$ of $\mathrm{H}^1(\mathcal{O})$-functions. On the other hand, given any generic scalar functional space M, we let $\mathbf{M}$ and $\mathbb{M}$ be the corresponding vector- and tensor-valued counterparts. Furthermore, as usual, $\mathbb{I}$ stands for the identity tensor in $\mathbb{R}^{2\times 2}$, and $|\cdot|$ denotes the Euclidean norm in $\mathbb{R}^2$. We also introduce some notations to be employed in the forthcoming sections. For any vector fields $\mathbf{v} = (v_1, v_2)^t$ and $\mathbf{w} = (w_1, w_2)^t$ we set the gradient, divergence and tensor product operators, respectively, as

$$\nabla\mathbf{v} := \left(\frac{\partial v_i}{\partial x_j}\right)_{i,j=1,2}, \quad \mathrm{div}(\mathbf{v}) := \sum_{j=1}^{2} \frac{\partial v_j}{\partial x_j}, \quad \text{and} \quad \mathbf{v}\otimes\mathbf{w} := (v_i w_j)_{i,j=1,2}.$$

In addition, for any tensor fields $\boldsymbol{\tau} = (\tau_{ij})_{i,j=1,2}$ and $\boldsymbol{\zeta} = (\zeta_{ij})_{i,j=1,2}$, we let $\mathbf{div}(\boldsymbol{\tau})$ be the divergence operator div acting along the rows of $\boldsymbol{\tau}$, and define the transpose, the trace, the tensor inner product, and the deviatoric tensor, respectively, as

$$\boldsymbol{\tau}^t := (\boldsymbol{\tau}_{ji})_{i,j=1,2}, \quad \mathrm{tr}(\boldsymbol{\tau}) := \sum_{i=1}^{2} \tau_{ii}, \quad \boldsymbol{\tau} : \boldsymbol{\zeta} := \sum_{i,j=1}^{2} \tau_{ij}\zeta_{ij}, \quad \text{and } \boldsymbol{\tau}^{\mathrm{d}} := \boldsymbol{\tau} - \frac{1}{2}\mathrm{tr}(\boldsymbol{\tau})\mathbb{I}. \tag{1.1}$$

On the other hand, given $t \in (1, +\infty)$, we introduce the Banach space

$$\mathbf{H}(\mathrm{div}_t; \mathcal{O}) := \left\{ \mathbf{v} \in \mathbf{L}^2(\mathcal{O}) : \quad \mathrm{div}(\mathbf{v}) \in \mathrm{L}^t(\mathcal{O}) \right\},$$

endowed with the natural norm $\|\mathbf{v}\|_{\mathrm{div}_t;\mathcal{O}} := \|\mathbf{v}\|_{0,\mathcal{O}} + \|\mathrm{div}(\mathbf{v})\|_{0,t;\mathcal{O}}$. The space of matrix-valued functions whose rows belong to $\mathbf{H}(\mathrm{div}_t;\mathcal{O})$ will be denoted by $\mathbb{H}(\mathbf{div}_t;\mathcal{O})$, endowed with the norm $\|\boldsymbol{\tau}\|_{\mathbf{div}_t;\mathcal{O}}$.

We recall some definitions and technical results concerning boundary conditions and extension operators [55, 64, 70]. Let $\widetilde{\Gamma} \subseteq \Gamma$, denote by $\widetilde{\Gamma}^{\mathrm{c}}$ its complement and $\mathbf{n}$ the unit outward normal vector on Γ.

Restriction to $\widetilde{\Gamma}$ of functionals in $\mathrm{H}^{-1/2}(\Gamma)$. Let $E_{0,\widetilde{\Gamma}} : \mathrm{H}^{1/2}(\widetilde{\Gamma}) \to \mathrm{L}^2(\Gamma)$ be the extension operator defined as follows: given $\eta \in \mathrm{H}^{1/2}(\widetilde{\Gamma})$, by $E_{0,\widetilde{\Gamma}}(\eta) = \eta$ on $\widetilde{\Gamma}$, and $E_{0,\widetilde{\Gamma}}(\eta) = 0$, otherwise. We define $\mathrm{H}^{1/2}_{00}(\widetilde{\Gamma}) := \left\{ \eta \in \mathrm{H}^{1/2}(\widetilde{\Gamma}) : E_{0,\widetilde{\Gamma}}(\eta) \in \mathrm{H}^{1/2}(\Gamma) \right\}$, endowed with the norm $\|\eta\|_{1/2,00,\widetilde{\Gamma}} := \|E_{0,\widetilde{\Gamma}}(\eta)\|_{1/2,\Gamma}$, and denote by $\mathrm{H}^{-1/2}_{00}(\widetilde{\Gamma})$ its dual space. Now, given $\mu \in \mathrm{H}^{-1/2}(\Gamma)$, its restriction to $\widetilde{\Gamma}^{\mathrm{c}}$, say $\mu|_{\widetilde{\Gamma}}$, is defined as

$$\langle \mu|_{\widetilde{\Gamma}}, \eta \rangle_{\widetilde{\Gamma}} := \langle \mu, E_{0,\widetilde{\Gamma}}(\eta) \rangle_{\Gamma} \quad \forall\, \eta \in \mathrm{H}^{1/2}_{00}(\widetilde{\Gamma}), \tag{1.2}$$

where $\langle \cdot, \cdot \rangle_{\widetilde{\Gamma}}$ stands for the duality pairing of the spaces $\mathrm{H}^{-1/2}_{00}(\widetilde{\Gamma})$ and $\mathrm{H}^{1/2}_{00}(\widetilde{\Gamma})$ with respect to the $\mathrm{L}^2(\widetilde{\Gamma})$ inner product. Then, it is clear that $\mu|_{\widetilde{\Gamma}} \in \mathrm{H}^{-1/2}_{00}(\widetilde{\Gamma})$. On the other hand, the boundary condition $\mu = 0$ on $\widetilde{\Gamma}$ means

$$\langle \mu, E_{0,\widetilde{\Gamma}}(\eta) \rangle_{\Gamma} = 0 \quad \forall\, \eta \in \mathrm{H}^{1/2}_{00}(\widetilde{\Gamma}). \tag{1.3}$$

A continuous extension of $\mathrm{H}^{1/2}(\widetilde{\Gamma})$-functions. According to [64, Section 2], given $\mu \in \mathrm{H}^{-1/2}(\Gamma)$ such that $\mu = 0$ on $\widetilde{\Gamma}^{\mathrm{c}}$, its restriction to $\widetilde{\Gamma}$ can be identified with an element of $\mathrm{H}^{-1/2}(\widetilde{\Gamma})$, namely

$$\langle \mu, \eta \rangle_{\widetilde{\Gamma}} := \langle \mu, E_{\widetilde{\Gamma}}(\eta) \rangle_{\Gamma} \quad \forall\, \eta \in \mathrm{H}^{1/2}(\widetilde{\Gamma}), \tag{1.4}$$

where $E_{\widetilde{\Gamma}} : \mathrm{H}^{1/2}(\widetilde{\Gamma}) \to \mathrm{H}^{1/2}(\Gamma)$ is any bounded extension operator. In particular, given $\eta \in \mathrm{H}^{1/2}(\widetilde{\Gamma})$, we consider the extension $E_{\widetilde{\Gamma}}(\eta) := z|_{\Gamma}$, where $z \in \mathrm{H}^1(\mathcal{O})$ is the unique solution to the boundary value problem

$$\triangle z = 0 \quad \text{in} \quad \mathcal{O}, \quad z = \eta \quad \text{on} \quad \widetilde{\Gamma}, \quad \text{and} \quad \nabla z \cdot \mathbf{n} = 0 \quad \text{on} \quad \widetilde{\Gamma}^{\mathrm{c}}, \tag{1.5}$$

satisfying $\|z\|_{1,\mathcal{O}} \leq C \|\eta\|_{1/2,\widetilde{\Gamma}}$, where C is a positive constant. The latter implies $\|E_{\widetilde{\Gamma}}(\eta)\|_{1/2,\Gamma} \leq C \|\eta\|_{1/2,\widetilde{\Gamma}}$.

Decomposition of $\mathrm{H}^{1/2}(\Gamma)$-functions. Given $\zeta \in \mathrm{H}^{1/2}(\Gamma)$, it is not difficult to prove (see, [64, Lemma 2.2]) that there exist unique elements $\zeta_{\widetilde{\Gamma}} \in \mathrm{H}^{1/2}(\widetilde{\Gamma})$ and $\zeta_{\widetilde{\Gamma}^{\mathrm{c}}} \in \mathrm{H}^{1/2}_{00}(\widetilde{\Gamma}^{\mathrm{c}})$ such that $\zeta =$

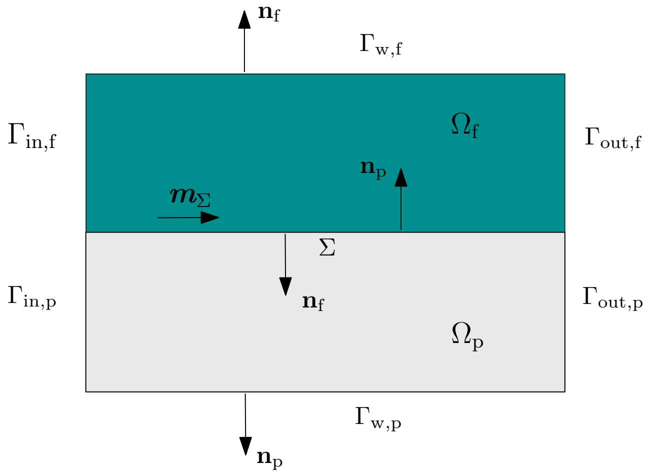

Figure 1.1: *Sketch of the geometry.*

$E_{\widetilde{\Gamma}}(\zeta_{\widetilde{\Gamma}}) + E_{0,\widetilde{\Gamma}^{\rm c}}(\zeta_{\widetilde{\Gamma}^{\rm c}})$, and hence

$$\langle \mu, \zeta\rangle_\Gamma := \langle \mu, E_{\widetilde{\Gamma}}(\zeta_{\widetilde{\Gamma}})\rangle_\Gamma + \langle \mu, E_{0,\widetilde{\Gamma}^{\rm c}}(\zeta_{\widetilde{\Gamma}^{\rm c}})\rangle_\Gamma \quad \forall\, \mu \in \mathrm{H}^{-1/2}(\Gamma). \tag{1.6}$$

Remark 1.1. We denote by $\boldsymbol{E}_{\widetilde{\Gamma}}$ and $\boldsymbol{E}_{0,\widetilde{\Gamma}^{\rm c}}$ the extension operators acting on vector-valued functions, and (1.6) also holds in this case. They are defined as the element-wise application of the extension operator specified above.

1.1.2 The model problem

In order to describe the geometry, we let $\Omega_{\rm f}$ and $\Omega_{\rm p}$ be two open bounded and simply connected polygonal domains in $\mathbb{R}^2$ such that $\partial\Omega_{\rm f} \cap \partial\Omega_{\rm p} = \Sigma \neq \emptyset$ and $\Omega_{\rm f} \cap \Omega_{\rm p} = \emptyset$, and set $\Omega := \Omega_{\rm f} \cup \Sigma \cup \Omega_{\rm p}$. In turn, for each $\star \in \{{\rm f},{\rm p}\}$, $\partial\Omega_\star \setminus \overline{\Sigma}$ is divided in three parts: $\Gamma_{{\rm in},\star}$ (inlet), $\Gamma_{{\rm out},\star}$ (outlet) and $\Gamma_{{\rm w},\star}$ (wall), such that $\partial\Omega_\star \setminus \overline{\Sigma} = \Gamma_{{\rm in},\star} \cup \overline{\Gamma}_{{\rm w},\star} \cup \Gamma_{{\rm out},\star}$ as depicted in Figure 1.1. The unit normal vector, $\mathbf{n}_\star$, is chosen pointing outward from $\Omega_\star$, thus $\mathbf{n}_{\rm f} = -\mathbf{n}_{\rm p}$ on the interior points of Σ. We also consider a unit tangent vector $\boldsymbol{m}_\Sigma$ on Σ as drawn Figure 1.1. We are interested in the Navier–Stokes/transport coupled problem, which is formulated in what follows in terms of the fluid velocity $\mathbf{u}_\star$, the fluid relative pressure $p_\star$, and the salt concentration $\widetilde{\phi}_\star$ occupying the region $\Omega_\star$, for each $\star \in \{{\rm f},{\rm p}\}$. More precisely, the corresponding system of equations is given by

$$\begin{gathered}
-\nu\,\triangle\mathbf{u}_\star + \rho\,\mathbf{div}(\mathbf{u}_\star\otimes\mathbf{u}_\star) + \nabla p_\star \,=\, \mathbf{0} \quad \text{in} \quad \Omega_\star, \quad \operatorname{div}(\mathbf{u}_\star) \,=\, 0 \quad \text{in} \quad \Omega_\star,\\
\mathbf{u}_\star \,=\, \mathbf{u}_{{\rm in},\star} \quad \text{on} \quad \Gamma_{{\rm in},\star}, \quad \mathbf{u}_\star = \mathbf{0} \quad \text{on} \quad \Gamma_{{\rm w},\star}, \quad (\nu\nabla\mathbf{u}_\star - p_\star\mathbb{I})\mathbf{n}_\star = \mathbf{0} \quad \text{on} \quad \Gamma_{{\rm out},\star},\\
-\kappa\,\triangle\widetilde{\phi}_\star + \mathbf{u}_\star\cdot\nabla\widetilde{\phi}_\star = 0 \quad \text{in} \quad \Omega_\star,\\
\widetilde{\phi}_\star = \widetilde{\phi}_{{\rm in},\star} \quad \text{on} \quad \Gamma_{{\rm in},\star}, \quad \kappa\,\nabla\widetilde{\phi}_\star\cdot\mathbf{n}_\star = 0 \quad \text{on} \quad \Gamma_{{\rm w},\star}\cup\Gamma_{{\rm out},\star},
\end{gathered} \tag{1.7}$$

where ν is the fluid dynamic viscosity, ρ is the fluid density and κ is the solute diffusivity through the solvent. All these parameters are assumed to be positive constants. In addition, for each $\star \in \{{\rm f},{\rm p}\}$,

$\mathbf{u}_{\mathrm{in},\star} \in \mathbf{H}^{1/2}(\Gamma_{\mathrm{in},\star})$ is a given inlet velocity profile, and $\widetilde{\phi}_{\mathrm{in},\star} \in \mathbb{R}$. The corresponding transmission conditions are given by

$$\begin{aligned} \mathbf{u}_\star \cdot \boldsymbol{m}_\Sigma = 0, \quad \mathbf{u}_\mathrm{f} \cdot \mathbf{n}_\mathrm{f} \;=\; -\mathbf{u}_\mathrm{p} \cdot \mathbf{n}_\mathrm{p}, \quad \mathbf{u}_\mathrm{f} \cdot \mathbf{n}_\mathrm{f} \;=\; A\Delta P - AiRT(\widetilde{\phi}_\mathrm{f} - \widetilde{\phi}_\mathrm{p}) \quad \text{on} \quad \Sigma, \\ (\widetilde{\phi}_\mathrm{f}\mathbf{u}_\mathrm{f} - \kappa\,\nabla\widetilde{\phi}_\mathrm{f}) \cdot \mathbf{n}_\mathrm{f} \;=\; -(\widetilde{\phi}_\mathrm{p}\mathbf{u}_\mathrm{p} - \kappa\,\nabla\widetilde{\phi}_\mathrm{p}) \cdot \mathbf{n}_\mathrm{p}, \quad (\widetilde{\phi}_\mathrm{f}\mathbf{u}_\mathrm{f} - \kappa\,\nabla\widetilde{\phi}_\mathrm{f}) \cdot \mathbf{n}_\mathrm{f} \;=\; B(\widetilde{\phi}_\mathrm{f} - \widetilde{\phi}_\mathrm{p}) \quad \text{on} \quad \Sigma. \end{aligned} \tag{1.8}$$

Here, A, i, R, T and B are physical parameters assumed to be positive constants. Specific values of the parameters can be found in Table 1.2. On the other hand, the transmembrane pressure ΔP represents the differences in pressure across a membrane, i.e., $\Delta P(\boldsymbol{x}) = \lim_{\varepsilon \to 0^+} p_\mathrm{f}^\mathrm{A}(\boldsymbol{x} - \varepsilon\boldsymbol{n}_\mathrm{f}) - \lim_{\varepsilon \to 0^+} p_\mathrm{p}^\mathrm{A}(\boldsymbol{x} - \varepsilon\boldsymbol{n}_\mathrm{p})$, for $\boldsymbol{x} \in \Sigma$, where p_f^A and p_p^A are the total pressures on the feed and permeate channels. This term causes nontrivial difficulties in the mathematical framework, and in the literature it is common to consider a simplified model that represents a small piece Ω of the entire reverse osmosis module [6, 33, 76, 84, 85]. In fact, let us define the feed and permeate operating pressures P_f^in and P_p^in, respectively, which are the pressures at which the system operates. We can then write the pressures relative to these operational pressures as $p_\mathrm{f} := p_\mathrm{f}^\mathrm{A} - P_\mathrm{f}^\mathrm{in}$ and $p_\mathrm{p} := p_\mathrm{p}^\mathrm{A} - P_\mathrm{p}^\mathrm{in}$. Therefore, $\Delta P = (p_\mathrm{f} - p_\mathrm{p}) + (P_\mathrm{f}^\mathrm{in} - P_\mathrm{p}^\mathrm{in})$ and an order of magnitude analysis shows that the difference $(p_\mathrm{f} - p_\mathrm{p})$ is negligible compared to the order of magnitude of $(P_\mathrm{f}^\mathrm{in} - P_\mathrm{p}^\mathrm{in})$. For instance, the former can be about 10^6 Pa for a reverse osmosis module, whereas the latter can be around 10^1 Pa for a short open channel such as the one considered in this study. This means that it is possible to approximate $\Delta P \approx (P_\mathrm{f}^\mathrm{in} - P_\mathrm{p}^\mathrm{in})$. Operating values of ΔP can be found in Section 2.2 of [80], whereas simulations values for the approximation of ΔP can be found in [6, 33, 76, 84, 85]. Even though this simplified model, it is still useful to determine quantities of interest in reverse osmosis, since it provides an accurate representation of the fluid flow, pressure drop and concentration polarization phenomena in membrane channels and can be applied in areas of study such as membrane spacer geometry optimization [90].

Now, denoting $a_0 := A\Delta P$, $a_1 := AiRT$ and $a_2 := B$, we realize that they are also positive constants satisfying the following conditions:

$$2a_1\widetilde{\phi}_{\mathrm{in,f}} + a_2 \;\geq\; a_0 + a_1\widetilde{\phi}_{\mathrm{in,p}}, \quad \text{and} \quad 2a_1\widetilde{\phi}_{\mathrm{in,p}} + a_0 + a_2 \;\geq\; a_1\widetilde{\phi}_{\mathrm{in,f}}. \tag{1.9}$$

Moreover, for the sake of the subsequent analysis, we consider the change of variable

$$\phi_\star := \widetilde{\phi}_\star - \widetilde{\phi}_{\mathrm{in},\star} \quad \text{in} \quad \Omega_\star, \tag{1.10}$$

which defines a new concentration variable $\phi_\star$ that satisfies a homogeneous Dirichlet boundary condition at the inlet, i.e., $\phi_\star = 0$ on $\Gamma_{\mathrm{in},\star}$. Instead of directly seeking $\widetilde{\phi}_\star$, we now focus on $\phi_\star$. As we will see in Section 1.2, this will allow us to look for the Lagrange multiplier associated to $\phi_\star$ in the space $\mathrm{H}_{00}^{1/2}(\Gamma_{\mathrm{in},\star}^\mathrm{c})$. Moreover, because $\widetilde{\phi}_{\mathrm{in},\star}$ is constant, we realize that $\nabla\phi_\star = \nabla\widetilde{\phi}_\star$ in $\Omega_\star$. Thus, the third equation of the first row of (1.8) can be rewritten as

$$\mathbf{u}_\mathrm{f} \cdot \mathbf{n}_\mathrm{f} = \widetilde{a}_0 - a_1(\phi_\mathrm{f} - \phi_\mathrm{p}) \quad \text{on} \quad \Sigma, \;\; \text{where } \widetilde{a}_0 = a_0 - a_1(\widetilde{\phi}_{\mathrm{in,f}} - \widetilde{\phi}_{\mathrm{in,p}}), \tag{1.11}$$

whereas the second row of (1.8), becomes

$$\begin{aligned} (\{\phi_\mathrm{f} + \widetilde{\phi}_{\mathrm{in,f}}\}\mathbf{u}_\mathrm{f} - \kappa\,\nabla\phi_\mathrm{f}) \cdot \mathbf{n}_\mathrm{f} \;&=\; -(\{\phi_\mathrm{p} + \widetilde{\phi}_{\mathrm{in,p}}\}\mathbf{u}_\mathrm{p} - \kappa\,\nabla\phi_\mathrm{p}) \cdot \mathbf{n}_\mathrm{p} \quad \text{on} \quad \Sigma, \\ (\{\phi_\mathrm{f} + \widetilde{\phi}_{\mathrm{in,f}}\}\mathbf{u}_\mathrm{f} - \kappa\,\nabla\phi_\mathrm{f}) \cdot \mathbf{n}_\mathrm{f} \;&=\; a_2(\phi_\mathrm{f} - \phi_\mathrm{p} + \widetilde{\phi}_{\mathrm{in,f}} - \widetilde{\phi}_{\mathrm{in,p}}) \quad \text{on} \quad \Sigma. \end{aligned} \tag{1.12}$$

Next, since we are interested in a mixed variational formulation, and in order to employ the integration by parts formula typically required by this approach, motivated by the Neumann-type boundary conditions, we introduce the auxiliary unknowns:

$$\boldsymbol{\sigma}_\star := \nu\nabla\mathbf{u}_\star - p_\star\mathbb{I} \quad \text{and} \quad \mathbf{t}_\star := \kappa\,\nabla\phi_\star \quad \text{in} \quad \Omega_\star. \tag{1.13}$$

In turn, it is straightforward to see, taking matrix trace, that the first equation of (1.13) together with the incompressibility condition $\mathrm{div}(\mathbf{u}_\star) = 0$, are equivalent to the pair

$$\frac{1}{\nu}\boldsymbol{\sigma}_\star^{\mathrm{d}} = \nabla\mathbf{u}_\star \quad \text{in} \quad \Omega_\star, \quad \text{and} \quad p_\star = -\frac{1}{2}\mathrm{tr}(\boldsymbol{\sigma}_\star) \quad \text{in} \quad \Omega_\star. \tag{1.14}$$

In this way, thanks to the fact that $\mathrm{div}(\mathbf{u}_\star) = 0$ in $\Omega_\star$, we note that $\mathbf{div}(\mathbf{u}_\star\otimes\mathbf{u}_\star) = (\nabla\mathbf{u}_\star)\mathbf{u}_\star = \dfrac{1}{\nu}\boldsymbol{\sigma}_\star^{\mathrm{d}}\mathbf{u}_\star$, and find that the first equation of (1.7) can be rewritten as $\mathbf{div}(\boldsymbol{\sigma}_\star) = \dfrac{\rho}{\nu}\boldsymbol{\sigma}_\star^{\mathrm{d}}\mathbf{u}_\star$, whereas the third row of (1.7) becomes $\kappa\,\mathrm{div}(\mathbf{t}_\star) = \mathbf{u}_\star\cdot\mathbf{t}_\star$.

Remark 1.2. We anticipate that we will look for $\mathbf{u}_\star$ in $\mathbf{L}^4(\Omega_\star)$ (cf. Section 1.2). Then, we write $\mathbf{div}(\boldsymbol{\sigma}_\star) = \dfrac{\rho}{\nu}\boldsymbol{\sigma}_\star^{\mathrm{d}}\mathbf{u}_\star$ instead of $\mathbf{div}(\boldsymbol{\sigma}_\star) = \rho(\nabla\mathbf{u}_\star)\mathbf{u}_\star$, to avoid the presence of the term $\nabla\mathbf{u}_\star$. Otherwise, we will need to look for $\mathbf{u}_\star$ in $\mathbf{H}^1(\Omega_\star)$ and therefore its discrete approximation will be sought in a $\mathbf{P}_1$-conforming space. This implies more computational effort compared to the use of a $\mathbf{P}_0$ space. Similarly, this motivates writing $\kappa\mathrm{div}(\mathbf{t}_\star) = \mathbf{u}_\star\cdot\mathbf{t}_\star$ instead of $\kappa\mathrm{div}(\mathbf{t}_\star) = \mathbf{u}_\star\cdot\kappa\nabla\phi_\star$.

On the other hand, by (1.12) and the second equation of (1.13), we observe that

$$\begin{aligned}
(\{\phi_{\mathrm{f}} + \widetilde{\phi}_{\mathrm{in,f}}\}\mathbf{u}_{\mathrm{f}} - \mathbf{t}_{\mathrm{f}})\cdot\mathbf{n}_{\mathrm{f}} &= -(\{\phi_{\mathrm{p}} + \widetilde{\phi}_{\mathrm{in,p}}\}\mathbf{u}_{\mathrm{p}} - \mathbf{t}_{\mathrm{p}})\cdot\mathbf{n}_{\mathrm{p}} \quad \text{on} \quad \Sigma,\\
(\{\phi_{\mathrm{f}} + \widetilde{\phi}_{\mathrm{in,f}}\}\mathbf{u}_{\mathrm{f}} - \mathbf{t}_{\mathrm{f}})\cdot\mathbf{n}_{\mathrm{f}} &= a_2(\phi_{\mathrm{f}} - \phi_{\mathrm{p}} + \widetilde{\phi}_{\mathrm{in,f}} - \widetilde{\phi}_{\mathrm{in,p}}) \quad \text{on} \quad \Sigma.
\end{aligned} \tag{1.15}$$

In this way, replacing (1.11) back into (1.15) and utilizing the second equation of the first row of (1.8), some algebraic manipulations allow us to arrive at the following system of equations:

$$\begin{gathered}
\frac{1}{\nu}\boldsymbol{\sigma}_\star^{\mathrm{d}} = \nabla\mathbf{u}_\star \quad \text{in} \quad \Omega_\star, \quad \mathbf{div}(\boldsymbol{\sigma}_\star) = \frac{\rho}{\nu}\boldsymbol{\sigma}_\star^{\mathrm{d}}\mathbf{u}_\star \quad \text{in} \quad \Omega_\star,\\
\mathbf{u}_\star = \mathbf{u}_{\mathrm{in},\star} \quad \text{on} \quad \Gamma_{\mathrm{in},\star}, \quad \mathbf{u}_\star = \mathbf{0} \quad \text{on} \quad \Gamma_{\mathrm{w},\star}, \quad \boldsymbol{\sigma}_\star\mathbf{n}_\star = \mathbf{0} \quad \text{on} \quad \Gamma_{\mathrm{out},\star},\\
\mathbf{t}_\star = \kappa\,\nabla\phi_\star \quad \text{in} \quad \Omega_\star, \quad \kappa\,\mathrm{div}(\mathbf{t}_\star) = \mathbf{u}_\star\cdot\mathbf{t}_\star \quad \text{in} \quad \Omega_\star,\\
\phi_\star = 0 \quad \text{on} \quad \Gamma_{\mathrm{in},\star}, \quad \text{and} \quad \mathbf{t}_\star\cdot\mathbf{n}_\star = 0 \quad \text{on} \quad \Gamma_{\mathrm{out},\star}\cup\Gamma_{\mathrm{w},\star},
\end{gathered} \tag{1.16}$$

with transmission conditions

$$\begin{aligned}
\mathbf{u}_\star\cdot\boldsymbol{m}_\Sigma = 0, \quad \mathbf{u}_{\mathrm{f}}\cdot\mathbf{n}_{\mathrm{f}} = -\mathbf{u}_{\mathrm{p}}\cdot\mathbf{n}_{\mathrm{p}}, \quad \mathbf{u}_{\mathrm{f}}\cdot\mathbf{n}_{\mathrm{f}} &= -a_1(\phi_{\mathrm{f}} - \phi_{\mathrm{p}}) + \widetilde{a}_0 \quad \text{on} \quad \Sigma,\\
\mathbf{t}_{\mathrm{f}}\cdot\mathbf{n}_{\mathrm{f}} = -a_1(\phi_{\mathrm{f}} - \phi_{\mathrm{p}})\phi_{\mathrm{f}} - (\widetilde{a}_{1,\mathrm{f}} - \widetilde{a}_0)\phi_{\mathrm{f}} &+ \widetilde{a}_{1,\mathrm{f}}\phi_{\mathrm{p}} + \widetilde{a}_{2,\mathrm{f}} \quad \text{on} \quad \Sigma, \quad \text{and}\\
\mathbf{t}_{\mathrm{p}}\cdot\mathbf{n}_{\mathrm{p}} = a_1(\phi_{\mathrm{f}} - \phi_{\mathrm{p}})\phi_{\mathrm{p}} - (\widetilde{a}_0 + \widetilde{a}_{1,\mathrm{p}})\phi_{\mathrm{p}} &+ \widetilde{a}_{1,\mathrm{p}}\phi_{\mathrm{f}} - \widetilde{a}_{2,\mathrm{p}} \quad \text{on} \quad \Sigma,
\end{aligned} \tag{1.17}$$

where $\widetilde{a}_0 = a_0 - a_1(\widetilde{\phi}_{\mathrm{in,f}} - \widetilde{\phi}_{\mathrm{in,p}})$, $\quad \widetilde{a}_{1,\star} = a_1\widetilde{\phi}_{\mathrm{in},\star} + a_2$ and $\widetilde{a}_{2,\star} = \widetilde{a}_0\widetilde{\phi}_{\mathrm{in},\star} - a_2(\widetilde{\phi}_{\mathrm{in,f}} - \widetilde{\phi}_{\mathrm{in,p}})$.

Remark 1.3. The set of transmission conditions in (1.8) can be arranged in several ways and the functional framework must be set accordingly. We find convenient to write the second row of (1.8) in terms of only two variables, the concentration $\phi_\star$ and its gradient $\mathbf{t}_\star$, and thus avoid the presence of $\mathbf{u}_\star$. Otherwise, in agreement with Remark 1.2, if $\mathbf{u}_\star$ appears explicitly on the interface, and we look for $\mathbf{u}_\star$ in $\mathbf{L}^4(\Omega_\star)$, we would need to introduce a Lagrange multiplier to handle the restriction of $\mathbf{u}_\star$ to the interface.

Note that the pressure has been eliminated from the system, but can be recovered by (1.14). Also, we observe that, thanks to the above change of variable, condition (1.9) becomes:

$$\widetilde{a}_{1,\mathrm{f}} - \widetilde{a}_0 \,\geq\, 0 \quad \text{and} \quad \widetilde{a}_{1,\mathrm{p}} + \widetilde{a}_0 \,\geq\, 0. \tag{1.18}$$

It is important to highlight that the algebraic manipulations performed in (1.17) along with the change of variable (1.10) naturally lead to the establishment of (1.18). These conditions will be used to ensure the result in (1.47). In this sense, if we take the values from Table 1.2, one can readily verify that

$$\widetilde{a}_{1,\mathrm{f}} - \widetilde{a}_0 = 8.76417 \times 10^{-7}\, m\, s^{-1} \quad \text{and} \quad \widetilde{a}_{1,\mathrm{p}} + \widetilde{a}_0 = 6.68063 \times 10^{-6}\, m\, s^{-1},$$

both quantities strictly positive, as required.

1.2 The mixed formulation

Given $\star \in \{\mathrm{f}, \mathrm{p}\}$, we first set $\Gamma^{\mathrm{c}}_{\mathrm{in},\star} := \partial\Omega_\star \setminus \Gamma_{\mathrm{in},\star}$ and $\Gamma^{\mathrm{c}}_{\mathrm{out},\star} := \partial\Omega_\star \setminus \Gamma_{\mathrm{out},\star}$. We begin by testing the first equations of the first and third rows of (1.16) against tensor- and vector-valued functions $\boldsymbol{\tau}_\star$ and $\mathbf{s}_\star$, yielding

$$\frac{1}{\nu}\int_{\Omega_\star} \boldsymbol{\sigma}^{\mathrm{d}}_\star : \boldsymbol{\tau}_\star - \int_{\Omega_\star} \nabla\mathbf{u}_\star : \boldsymbol{\tau}_\star = 0 \quad \text{and} \quad \frac{1}{\kappa}\int_{\Omega_\star} \mathbf{t}_\star \cdot \mathbf{s}_\star - \int_{\Omega_\star} \nabla\phi_\star \cdot \mathbf{s}_\star = 0, \tag{1.19}$$

respectively. It is clear that the first terms in (1.19) are well-defined if $\boldsymbol{\sigma}_\star, \boldsymbol{\tau}_\star \in \mathbb{L}^2(\Omega_\star)$ and $\mathbf{t}_\star, \mathbf{s}_\star \in \mathbf{L}^2(\Omega_\star)$. In turn, multiplying the second equations of the first and third rows of (1.16) by a vector- and scalar-valued functions $\mathbf{v}_\star$ and $\psi_\star$, respectively, we notice that

$$\int_{\Omega_\star} \mathbf{v}_\star \cdot \mathbf{div}(\boldsymbol{\sigma}_\star) - \frac{\rho}{\nu}\int_{\Omega_\star} \boldsymbol{\sigma}^{\mathrm{d}}_\star \mathbf{u}_\star \cdot \mathbf{v}_\star \;=\; 0 \quad \text{and} \quad \int_{\Omega_\star} \mathrm{div}(\mathbf{t}_\star)\psi_\star - \frac{1}{\kappa}\int_{\Omega_\star} \mathbf{u}_\star \cdot \mathbf{t}_\star \psi_\star \;=\; 0. \tag{1.20}$$

Then, knowing that $\boldsymbol{\sigma}_\star$ and $\mathbf{t}_\star$ are L^2-functions, using the Cauchy–Schwarz and Hölder inequalities, we find that for all $s, t \in (1, +\infty)$, such that $\frac{1}{s} + \frac{1}{t} = 1$, there hold

$$\left|\int_{\Omega_\star} \boldsymbol{\sigma}^{\mathrm{d}}_\star \mathbf{u}_\star \cdot \mathbf{v}_\star\right| \leq \|\boldsymbol{\sigma}_\star\|_{0;\Omega_\star} \|\mathbf{u}_\star\|_{0,2s;\Omega_\star} \|\mathbf{v}_\star\|_{0,2t;\Omega_\star}, \quad \text{and}$$

$$\left|\int_{\Omega_\star} \mathbf{u}_\star \cdot \mathbf{t}_\star \psi_\star\right| \leq \|\mathbf{u}_\star\|_{0,2s;\Omega_\star} \|\mathbf{t}_\star\|_{0,\Omega_\star} \|\psi_\star\|_{0,2t;\Omega_\star},$$

which show that the second terms of the left-hand sides in the equations of (1.20) make sense for $\mathbf{u}_\star \in \mathbf{L}^{2s}(\Omega_\star)$, $\mathbf{v}_\star \in \mathbf{L}^{2t}(\Omega_\star)$ and $\psi_\star \in \mathrm{L}^{2t}(\Omega_\star)$. Thus, forcing their first terms to require that $\mathbf{div}(\boldsymbol{\sigma}_\star) \in \mathbf{L}^{(2t)'}(\Omega_\star)$, and $\mathrm{div}(\mathbf{t}_\star) \in \mathrm{L}^{(2t)'}(\Omega_\star)$, where $(2t)' := \frac{2t}{2t-1}$ is the conjugate of $2t$.

Now, we go back to the second equation of (1.19) to deal with the second term. After applying the integration by parts formula and considering the test function $\mathbf{s}_\star$ in the same space of $\mathbf{t}_\star$, we realize that the volumetric terms are well defined if $\mathrm{div}(\mathbf{s}_\star) \in \mathrm{L}^{(2t)'}(\Omega_\star)$ and $\phi_\star \in \mathrm{L}^{2t}(\Omega_\star)$. Since traces of $\mathrm{L}^{2t}(\Omega_\star)$-functions are not defined, we introduce a Lagrange multiplier $\xi_\star := -\phi_\star|_{\Gamma^{\mathrm{c}}_{\mathrm{in},\star}} \in \mathrm{H}^{1/2}_{00}(\Gamma^{\mathrm{c}}_{\mathrm{in},\star})$, and realize that the second equation of (1.19), becomes

$$\frac{1}{\kappa}\int_{\Omega_\star} \mathbf{t}_\star \cdot \mathbf{s}_\star + \int_{\Omega_\star} \phi_\star \mathrm{div}(\mathbf{s}_\star) + \langle \mathbf{s}_\star \cdot \mathbf{n}_\star, \xi_\star \rangle_{\Gamma^{\mathrm{c}}_{\mathrm{in},\star}} \;=\; 0.$$

Here, we have used the facts that $\phi_\star = 0$ on $\Gamma_{\mathrm{in},\star}$ and $\mathbf{s}_\star \cdot \mathbf{n}_\star$ is well defined if $\mathrm{H}^1(\Omega_\star)$ is continuously embedded in $\mathrm{L}^{2t}(\Omega_\star)$ (see [48, Section 3.1] for details). The latter is guaranteed in two dimensions for $2t \in [1, +\infty)$.

Similarly, to apply the integration by parts formula to the first equation of (1.19) and obtain

$$\frac{1}{\nu}\int_{\Omega_\star} \boldsymbol{\sigma}^{\mathrm{d}}_\star : \boldsymbol{\tau}_\star + \int_{\Omega_\star} \mathbf{u}_\star \cdot \mathbf{div}(\boldsymbol{\tau}_\star) \;=\; \langle \boldsymbol{\tau}_\star \mathbf{n}_\star,\, \mathbf{u}_\star \rangle_{\partial\Omega_\star}, \tag{1.21}$$

it suffices to assume that $\mathbf{div}(\boldsymbol{\tau}_\star) \in \mathbf{L}^{(2s)'}(\Omega_\star)$, and that $\mathbf{H}^1(\Omega_\star)$ is continuously embedded in $\mathbf{L}^{2s}(\Omega_\star)$, where $(2s)' := \frac{2s}{2s-1}$ is the conjugate of $2s$, so that $\boldsymbol{\tau}_\star \mathbf{n}_\star$ is well defined. This is guaranteed in two dimensions for $2s \in [1, +\infty)$. It remains to properly handle the term $\langle \boldsymbol{\tau}_\star \mathbf{n}_\star, \mathbf{u}_\star \rangle_{\partial\Omega_\star}$ since, *a priori*, the trace of $\mathbf{u}_\star$ is not in $\mathbf{H}^{1/2}(\partial\Omega_\star)$. To that end, we will make use of the boundary and transmission conditions specified in (1.16) and (1.17). More precisely, let $\star \in \{\mathrm{f}, \mathrm{p}\}$ and for the sake of convenience we define the following auxiliary functions

$$\mathbf{g}_\star := \begin{cases} \mathbf{0} & \text{on} \quad \Gamma_{\mathrm{w},\star}, \\ \mathbf{u}_{\mathrm{in},\star} & \text{on} \quad \Gamma_{\mathrm{in},\star}, \\ \widetilde{a}_0 \mathbf{n}_{\mathrm{f}} & \text{on} \quad \Sigma, \end{cases} \quad \text{and} \quad \mathbf{g}^{\xi}_\star := \begin{cases} \mathbf{0} & \text{on} \quad \Gamma_{\mathrm{w},\star}, \\ \mathbf{0} & \text{on} \quad \Gamma_{\mathrm{in},\star}, \\ a_1(\xi_{\mathrm{f}} - \xi_{\mathrm{p}})\mathbf{n}_{\mathrm{f}} & \text{on} \quad \Sigma. \end{cases} \tag{1.22}$$

We observe that $\mathbf{g}_\star \in \mathbf{H}^{1/2}(\Gamma^{\mathrm{c}}_{\mathrm{out},\star})$ if $\mathbf{u}_{\mathrm{in},\star}$ fulfills the following compatibility conditions:

$$\begin{aligned} \mathbf{u}_{\mathrm{in,f}} &= \mathbf{0} && \text{on} \quad \overline{\Gamma}_{\mathrm{in,f}} \cap \overline{\Gamma}_{\mathrm{w,f}}, & \mathbf{u}_{\mathrm{in,p}} &= \mathbf{0} && \text{on} \quad \overline{\Gamma}_{\mathrm{in,p}} \cap \overline{\Gamma}_{\mathrm{w,p}}, \\ \mathbf{u}_{\mathrm{in,f}} &= \widetilde{a}_0 \mathbf{n}_{\mathrm{f}} && \text{on} \quad \overline{\Gamma}_{\mathrm{in,f}} \cap \overline{\Sigma}, & \mathbf{u}_{\mathrm{in,p}} &= -\widetilde{a}_0 \mathbf{n}_{\mathrm{p}} && \text{on} \quad \overline{\Gamma}_{\mathrm{in,p}} \cap \overline{\Sigma}, \end{aligned} \tag{1.23}$$

where, for $\boldsymbol{x} \in \overline{\Gamma}_{\mathrm{in},\star} \cap \overline{\Sigma}$, $\mathbf{n}_\star(\boldsymbol{x})$ is taking as $\mathbf{n}_\star(\boldsymbol{x}) = \lim\limits_{\varepsilon \to 0^+} \mathbf{n}_\star(\boldsymbol{x} - \varepsilon \boldsymbol{m}_\Sigma)$. Moreover $\mathbf{g}^{\xi}_\star$ is also in $\mathbf{H}^{1/2}(\Gamma^{\mathrm{c}}_{\mathrm{out},\star})$ since we recall that $\xi_\star \in \mathrm{H}^{1/2}_{00}(\Gamma^{\mathrm{c}}_{\mathrm{in},\star})$. In this way, bearing in mind the boundary and transmission conditions (1.16) and (1.17), and considering the test function $\boldsymbol{\tau}_\star$ in the space $\mathbb{H}_{\Gamma_{\mathrm{out}}}(\mathbf{div}_{(2s)'};\Omega_\star) := \Big\{ \boldsymbol{\tau}_\star \in \mathbb{H}(\mathbf{div}_{(2s)'};\Omega_\star) : \boldsymbol{\tau}_\star \mathbf{n}_\star = \mathbf{0} \text{ on } \Gamma_{\mathrm{out},\star} \Big\}$, where $\boldsymbol{\tau}_\star \mathbf{n}_\star = \mathbf{0}$ on $\Gamma_{\mathrm{out},\star}$ is understood in the sense of (1.3), from (1.21) we find that

$$\frac{1}{\nu}\int_{\Omega_\star} \boldsymbol{\sigma}^{\mathrm{d}}_\star : \boldsymbol{\tau}_\star + \int_{\Omega_\star} \mathbf{u}_\star \cdot \mathbf{div}(\boldsymbol{\tau}_\star) \;=\; \langle \boldsymbol{\tau}_\star \mathbf{n}_\star,\, \mathbf{g}_\star + \mathbf{g}^{\xi}_\star \rangle_{\Gamma^{\mathrm{c}}_{\mathrm{out},\star}} \quad \forall\, \boldsymbol{\tau}_\star \in \mathbb{H}_{\Gamma_{\mathrm{out}}}(\mathbf{div}_{(2s)'};\Omega_\star).$$

If we would also like to seek $\boldsymbol{\sigma}_\star$ and $\boldsymbol{\tau}_\star$ in the same function space, it follows immediately that $s = t = 2$ and $(2s)' = (2t)' = 4/3$, which we will be considered from now on.

Remark 1.4. The compatibility conditions (1.23) are satisfied, for example, if we consider a domain $\Omega = \Omega_{\rm f} \cup \Omega_{\rm p} \cup \Sigma$, where

$$\Omega_{\rm f} = (0,L)\times(d,2d), \quad \Omega_{\rm p} = (0,L)\times(0,d), \quad \text{and} \quad \Sigma = (0,L)\times\{d\},$$

with the following inlet velocities:

$$\mathbf{u}_{\rm in,f} := \begin{pmatrix} 6\mathrm{u}_{\rm in,f}\Big(1-\frac{y}{d}\Big)\left(\frac{y}{d}-2\right) \\ \widetilde{a}_0\Big(\frac{y}{d}-2\Big) \end{pmatrix}, \quad y\in[d,2d], \quad \text{and} \quad \mathbf{u}_{\rm in,p} := \begin{pmatrix} 6\mathrm{u}_{\rm in,p}\frac{y}{d}\Big(1-\frac{y}{d}\Big) \\ -\widetilde{a}_0\frac{y}{d} \end{pmatrix}, \quad y\in[0,d],$$

where $\mathrm{u}_{\rm in,f}$ and $\mathrm{u}_{\rm in,p}$ stand for the inlet mean feed and permeate fluid velocities, respectively. We observe that, when the second component of any of the above velocities is zero, the first component is similar to that of the Poiseuille flux, which is a parabolic profile with unit mean velocity. On the other hand, when the second component of the inlet velocity does not vanish, the profile is similar to the Berman flow. The latter is commonly used to model a constant permeate flux through a membrane as shown in [14, 18, 33, 77, 104] to name a few references.

In turn, thanks to the last equation in (1.16), the last two equations of (1.17), and the fact that $\xi_\star \in \mathrm{H}^{1/2}_{00}(\Gamma^{\rm c}_{\rm in,\star})$, we deduce that

$$\begin{aligned} \langle \mathbf{t}_{\rm f}\cdot\mathbf{n}_{\rm f}\,,\,\eta_{\rm f}\rangle_{\Gamma^{\rm c}_{\rm in,f}} &= a_1\int_\Sigma(\xi_{\rm p}-\xi_{\rm f})\,\xi_{\rm f}\,\eta_{\rm f} + \big(\widetilde{a}_{1,\rm f}-\widetilde{a}_0\big)\int_\Sigma \xi_{\rm f}\,\eta_{\rm f} - \widetilde{a}_{1,\rm f}\int_\Sigma \xi_{\rm p}\eta_{\rm f} + \widetilde{a}_{2,\rm f}\int_\Sigma \eta_{\rm f}, \\ \langle \mathbf{t}_{\rm p}\cdot\mathbf{n}_{\rm p}\,,\,\eta_{\rm p}\rangle_{\Gamma^{\rm c}_{\rm in,p}} &= -\,a_1\int_\Sigma(\xi_{\rm p}-\xi_{\rm f})\,\xi_{\rm p}\,\eta_{\rm p} + \big(\widetilde{a}_{1,\rm p}+\widetilde{a}_0\big)\int_\Sigma \xi_{\rm p}\,\eta_{\rm p} - \widetilde{a}_{1,\rm p}\int_\Sigma \xi_{\rm f}\eta_{\rm p} - \widetilde{a}_{2,\rm p}\int_\Sigma \eta_{\rm p} \end{aligned}$$

for all $\eta_\star \in \mathrm{H}^{1/2}_{00}(\Gamma^{\rm c}_{\rm in,\star})$, with $\star\in\{\rm f,p\}$. Consequently, introducing the spaces

$$\begin{aligned} &\mathbb{H}^\star_{\rm S} := \mathbb{H}_{\Gamma_{\rm out}}(\mathbf{div}_{4/3};\Omega_\star), && \mathbf{H}^\star_{\rm T} := \mathbf{H}(\mathrm{div}_{4/3};\Omega_\star), && \mathrm{M}^\star_{\rm T} := \mathrm{H}^{1/2}_{00}(\Gamma^{\rm c}_{\rm in,\star}), \\ &\mathbf{Q}^\star_{\rm S} := \mathbf{L}^4(\Omega_\star), && \mathrm{X}^\star_{\rm T} := \mathrm{L}^4(\Omega_\star), && \end{aligned}$$

defining the global spaces

$$\begin{aligned} &\mathbb{H} := \mathbb{H}^{\rm f}_{\rm S}\times\mathbb{H}^{\rm p}_{\rm S}, && \mathbf{H} := \mathbf{H}^{\rm f}_{\rm T}\times\mathbf{H}^{\rm p}_{\rm T}, && \mathrm{M} := \mathrm{M}^{\rm f}_{\rm T}\times\mathrm{M}^{\rm p}_{\rm T}, \\ &\mathbf{Q} := \mathbf{Q}^{\rm f}_{\rm S}\times\mathbf{Q}^{\rm p}_{\rm S}, && \mathrm{X} := \mathrm{X}^{\rm f}_{\rm T}\times\mathrm{X}^{\rm p}_{\rm T}, && \mathrm{Q} := \mathrm{X}\times\mathrm{M}, \end{aligned}$$

setting the notation

$$\begin{aligned} &\vec{\boldsymbol{\tau}} := (\boldsymbol{\tau}_{\rm f},\boldsymbol{\tau}_{\rm p})\in\mathbb{H}, && \vec{\mathbf{s}} := (\mathbf{s}_{\rm f},\mathbf{s}_{\rm p})\in\mathbf{H}, && \vec{\eta} := (\eta_{\rm f},\eta_{\rm p})\in\mathrm{M}, \\ &\vec{\mathbf{w}} := (\mathbf{w}_{\rm f},\mathbf{w}_{\rm p})\in\mathbf{Q}, && \vec{\psi} := (\psi_{\rm f},\psi_{\rm p})\in\mathrm{X}, && (\vec{\psi},\vec{\eta}) := (\psi_{\rm f},\psi_{\rm p},\eta_{\rm f},\eta_{\rm p})\in\mathrm{Q}, \end{aligned}$$

and equipping the above global spaces with the norms

$$\begin{aligned} &\|\vec{\boldsymbol{\tau}}\|_{\mathbb{H}} := \|\boldsymbol{\tau}_{\rm f}\|_{\mathbf{div}_{4/3};\Omega_{\rm f}} + \|\boldsymbol{\tau}_{\rm p}\|_{\mathbf{div}_{4/3};\Omega_{\rm p}} && \forall\,\vec{\boldsymbol{\tau}} := (\boldsymbol{\tau}_{\rm f},\boldsymbol{\tau}_{\rm p})\in\mathbb{H}, \\ &\|\vec{\mathbf{w}}\|_{\mathbf{Q}} := \|\mathbf{w}_{\rm f}\|_{0,4;\Omega_{\rm f}} + \|\mathbf{w}_{\rm p}\|_{0,4;\Omega_{\rm p}} && \forall\,\vec{\mathbf{w}} := (\mathbf{w}_{\rm f},\mathbf{w}_{\rm p})\in\mathbf{Q}, \end{aligned}$$

$$
\begin{aligned}
\|\vec{\mathbf{s}}\|_{\mathbf{H}} &:= \|\mathbf{s}_{\mathrm{f}}\|_{\mathrm{div}_{4/3};\Omega_{\mathrm{f}}} + \|\mathbf{s}_{\mathrm{p}}\|_{\mathrm{div}_{4/3};\Omega_{\mathrm{p}}} && \forall\, \vec{\mathbf{s}} := (\mathbf{s}_{\mathrm{f}}, \mathbf{s}_{\mathrm{p}}) \in \mathbf{H},\\
\|\vec{\psi}\|_{\mathrm{X}} &:= \|\psi_{\mathrm{f}}\|_{0,4;\Omega_{\mathrm{f}}} + \|\psi_{\mathrm{p}}\|_{0,4;\Omega_{\mathrm{p}}} && \forall\, \vec{\psi} := (\psi_{\mathrm{f}}, \psi_{\mathrm{p}}) \in \mathrm{X},\\
\|\vec{\eta}\|_{\mathrm{M}} &:= \|\eta_{\mathrm{f}}\|_{1/2,00,\Gamma^{\mathrm{c}}_{\mathrm{in,f}}} + \|\eta_{\mathrm{p}}\|_{1/2,00,\Gamma^{\mathrm{c}}_{\mathrm{in,p}}} && \forall\, \vec{\eta} := (\eta_{\mathrm{f}}, \eta_{\mathrm{p}}) \in \mathrm{M},\\
\|(\vec{\psi},\vec{\eta})\|_{\mathrm{Q}} &:= \|\vec{\psi}\|_{\mathrm{X}} + \|\vec{\eta}\|_{\mathrm{M}} && \forall\, (\vec{\psi},\vec{\eta}) := (\psi_{\mathrm{f}}, \psi_{\mathrm{p}}, \eta_{\mathrm{f}}, \eta_{\mathrm{p}}) \in \mathrm{Q},
\end{aligned}
$$

we arrive at the following variational formulation of (1.16): Find $\big(\vec{\boldsymbol{\sigma}}, \vec{\mathbf{u}}\big) \in \mathbb{H}\times\mathbf{Q}$ and $\big(\vec{\mathbf{t}}, (\vec{\phi},\vec{\xi})\big) \in \mathbf{H}\times\mathrm{Q}$ such that

$$
\begin{aligned}
\mathbf{a}_{\mathrm{S}}(\vec{\boldsymbol{\sigma}},\vec{\boldsymbol{\tau}}) \quad &+ \mathbf{b}_{\mathrm{S}}(\vec{\boldsymbol{\tau}},\vec{\mathbf{u}}) && && = \mathbf{F}_{\vec{\xi}}(\vec{\boldsymbol{\tau}}),\\
\mathbf{b}_{\mathrm{S}}(\vec{\boldsymbol{\sigma}},\vec{\mathbf{v}}) \quad & && - \mathbf{O}_{\mathrm{S}}(\vec{\mathbf{u}};\vec{\boldsymbol{\sigma}},\vec{\mathbf{v}}) && = 0,\\
\mathbf{a}_{\mathrm{T}}(\vec{\mathbf{t}},\vec{\mathbf{s}}) \quad &+ \mathbf{b}_{\mathrm{T}}(\vec{\mathbf{s}},(\vec{\phi},\vec{\xi})) && && = 0,\\
\mathbf{b}_{\mathrm{T}}(\vec{\mathbf{t}},(\vec{\psi},\vec{\eta})) \quad &- \mathbf{d}_{\mathrm{T}}((\vec{\phi},\vec{\xi}),(\vec{\psi},\vec{\eta})) && - \mathbf{O}_{\mathrm{T}}(\vec{\mathbf{u}};\vec{\mathbf{t}},\vec{\psi}) \,-\, \mathbf{C}_{\mathrm{T}}(\vec{\xi};\vec{\xi},\vec{\eta}) && = \mathcal{F}_{\vec{\xi}}(\vec{\psi},\vec{\eta}),
\end{aligned}
\tag{1.24}
$$

for all $(\vec{\boldsymbol{\tau}},\vec{\mathbf{v}}) \in \mathbb{H}\times\mathbf{Q}$ and $(\vec{\mathbf{s}},(\vec{\psi},\vec{\eta})) \in \mathbf{H}\times\mathrm{Q}$, where, $\mathbf{a}_{\mathrm{S}} : \mathbb{H}\times\mathbb{H} \to \mathbb{R}$, $\mathbf{a}_{\mathrm{T}} : \mathbf{H}\times\mathbf{H} \to \mathbb{R}$, $\mathbf{b}_{\mathrm{S}} : \mathbb{H}\times\mathbf{Q} \to \mathbb{R}$, $\mathbf{b}_{\mathrm{T}} : \mathbf{H}\times\mathrm{Q} \to \mathbb{R}$, and $\mathbf{d}_{\mathrm{T}} : \mathrm{Q}\times\mathrm{Q} \to \mathbb{R}$, are the bilinear forms defined by

$$
\mathbf{a}_{\mathrm{S}}(\vec{\boldsymbol{\sigma}},\,\vec{\boldsymbol{\tau}}) := \frac{1}{\nu}\sum_{\star\in\{\mathrm{f,p}\}}\int_{\Omega_\star} \boldsymbol{\sigma}^{\mathrm{d}}_\star : \boldsymbol{\tau}^{\mathrm{d}}_\star \qquad \forall\,(\vec{\boldsymbol{\sigma}},\vec{\boldsymbol{\tau}}) \in \mathbb{H}\times\mathbb{H}, \tag{1.25a}
$$

$$
\mathbf{a}_{\mathrm{T}}(\vec{\mathbf{t}},\,\vec{\mathbf{s}}) := \frac{1}{\kappa}\sum_{\star\in\{\mathrm{f,p}\}}\int_{\Omega_\star} \mathbf{t}_\star\cdot\mathbf{s}_\star \qquad \forall\,(\vec{\mathbf{t}},\vec{\mathbf{s}}) \in \mathbf{H}\times\mathbf{H}, \tag{1.25b}
$$

$$
\mathbf{b}_{\mathrm{S}}(\vec{\boldsymbol{\tau}},\vec{\mathbf{v}}) := \sum_{\star\in\{\mathrm{f,p}\}}\int_{\Omega_\star} \mathbf{v}_\star\cdot\mathbf{div}(\boldsymbol{\tau}_\star) \qquad \forall\,(\vec{\boldsymbol{\tau}},\vec{\mathbf{v}}) \in \mathbb{H}\times\mathbf{Q}, \tag{1.25c}
$$

$$
\mathbf{b}_{\mathrm{T}}(\vec{\mathbf{s}},(\vec{\psi},\vec{\eta})) := \sum_{\star\in\{\mathrm{f,p}\}}\left\{\int_{\Omega_\star}\psi_\star\mathrm{div}(\mathbf{s}_\star) + \langle\mathbf{s}_\star\cdot\mathbf{n}_\star,\,\eta_\star\rangle_{\Gamma^{\mathrm{c}}_{\mathrm{in},\star}}\right\} \quad \forall\,(\vec{\mathbf{s}},(\vec{\psi},\vec{\eta})) \in \mathbf{H}\times\mathrm{Q}, \tag{1.25d}
$$

$$
\mathbf{d}_{\mathrm{T}}((\vec{\phi},\vec{\xi}),(\vec{\psi},\vec{\eta})) := (\widetilde{a}_{1,\mathrm{f}} - \widetilde{a}_0)\int_\Sigma \xi_{\mathrm{f}}\eta_{\mathrm{f}} + \big(\widetilde{a}_{1,\mathrm{p}} + \widetilde{a}_0\big)\int_\Sigma \xi_{\mathrm{p}}\,\eta_{\mathrm{p}} \qquad \forall\,((\vec{\phi},\vec{\xi}),(\vec{\psi},\vec{\eta})) \in \mathrm{Q}\times\mathrm{Q}, \tag{1.25e}
$$

whereas for each $(\vec{\mathbf{w}},\vec{\chi}) \in \mathbf{Q}\times\mathrm{M}$, $\mathbf{O}_{\mathrm{S}}(\vec{\mathbf{w}};\cdot,\cdot) : \mathbb{H}\times\mathbf{Q} \to \mathbb{R}$, $\mathbf{O}_{\mathrm{T}}(\vec{\mathbf{w}};\cdot,\cdot) : \mathbf{H}\times\mathrm{X} \to \mathbb{R}$, and $\mathbf{C}_{\mathrm{T}}(\vec{\chi};\cdot,\cdot) : \mathrm{M}\times\mathrm{Q} \to \mathbb{R}$ are the bilinear forms given by

$$
\begin{aligned}
\mathbf{O}_{\mathrm{S}}(\vec{\mathbf{w}};\vec{\boldsymbol{\sigma}},\vec{\mathbf{v}}) &:= \frac{\rho}{\nu}\sum_{\star\in\{\mathrm{f,p}\}}\int_{\Omega_\star}\boldsymbol{\sigma}^{\mathrm{d}}_\star\mathbf{w}_\star\cdot\mathbf{v}_\star && \forall\,(\vec{\boldsymbol{\sigma}},\vec{\mathbf{v}}) \in \mathbb{H}\times\mathbf{Q},\\
\mathbf{O}_{\mathrm{T}}(\vec{\mathbf{w}};\vec{\mathbf{t}},\vec{\psi}) &:= \frac{1}{\kappa}\sum_{\star\in\{\mathrm{f,p}\}}\int_{\Omega_\star}\mathbf{w}_\star\cdot\mathbf{t}_\star\psi_\star && \forall\,(\vec{\mathbf{t}},\vec{\psi}) \in \mathbf{H}\times\mathrm{X},\\
\mathbf{C}_{\mathrm{T}}(\vec{\chi};\vec{\xi},\vec{\eta}) &:= a_1\int_\Sigma\xi_{\mathrm{f}}(\chi_{\mathrm{p}}-\chi_{\mathrm{f}})\eta_{\mathrm{f}} - a_1\int_\Sigma\xi_{\mathrm{p}}(\chi_{\mathrm{p}}-\chi_{\mathrm{f}})\eta_{\mathrm{p}} && \forall\,(\vec{\xi},\vec{\eta}) \in \mathrm{M}\times\mathrm{M}.
\end{aligned}
\tag{1.26}
$$

Finally, $\mathbf{F}_{\vec{\chi}} \in \mathbb{H}'$ and $\mathcal{F}_{\vec{\chi}} \in \mathrm{Q}'$ are the functionals defined by

$$
\begin{aligned}
\mathbf{F}_{\vec{\chi}}(\vec{\boldsymbol{\tau}}) &:= \langle\boldsymbol{\tau}_{\mathrm{f}}\,\mathbf{n}_{\mathrm{f}},\,\mathbf{g}_{\mathrm{f}}+\mathbf{g}^{\chi}_{\mathrm{f}}\rangle_{\Gamma^{\mathrm{c}}_{\mathrm{out,f}}} + \langle\boldsymbol{\tau}_{\mathrm{p}}\,\mathbf{n}_{\mathrm{p}},\,\mathbf{g}_{\mathrm{p}}+\mathbf{g}^{\chi}_{\mathrm{p}}\rangle_{\Gamma^{\mathrm{c}}_{\mathrm{out,p}}} && \forall\,\vec{\boldsymbol{\tau}} \in \mathbb{H},\\
\mathcal{F}_{\vec{\chi}}(\vec{\psi},\vec{\eta}) &:= -\widetilde{a}_{1,\mathrm{f}}\int_\Sigma\chi_{\mathrm{p}}\eta_{\mathrm{f}} - \widetilde{a}_{1,\mathrm{p}}\int_\Sigma\chi_{\mathrm{f}}\eta_{\mathrm{p}} + \widetilde{a}_{2,\mathrm{f}}\int_\Sigma\eta_{\mathrm{f}} - \widetilde{a}_{2,\mathrm{p}}\int_\Sigma\eta_{\mathrm{p}} && \forall\,(\vec{\psi},\vec{\eta}) \in \mathrm{Q}.
\end{aligned}
\tag{1.27}
$$

1.3 The continuous solvability analysis

We analyze the solvability of (1.24) by applying the results provided by [60, Theorem 2.34] and [50, Theorem 3.4], along with the Banach–Nečas–Babuška Theorem (cf. [60, Theorem 2.6]).

1.3.1 The fixed-point strategy

We begin by rewriting (1.24) as an equivalent fixed point equation. Indeed, we first let $\widetilde{\mathcal{J}} : \mathbf{Q}\times \mathrm{M} \to \mathbb{H}\times\mathbf{Q}$ be the operator defined for each $\vec{\mathbf{w}} := (\mathbf{w}_{\mathrm{f}}, \mathbf{w}_{\mathrm{p}})$ and $\vec{\chi} := (\chi_{\mathrm{f}}, \chi_{\mathrm{p}})$, with $(\vec{\mathbf{w}}, \vec{\chi}) \in \mathbf{Q}\times\mathrm{M}$ as

$$\widetilde{\mathcal{J}}(\vec{\mathbf{w}}, \vec{\chi}) \,=\, \big(\widetilde{\mathcal{J}}_1(\vec{\mathbf{w}}, \vec{\chi}), \widetilde{\mathcal{J}}_2(\vec{\mathbf{w}}, \vec{\chi})\big) := (\vec{\boldsymbol{\sigma}}, \vec{\mathbf{u}}), \tag{1.28}$$

where $(\vec{\boldsymbol{\sigma}}, \vec{\mathbf{u}}) \in \mathbb{H}\times\mathbf{Q}$ is the unique solution (to be confirmed in Theorem 1.1) of the following problem:

$$\begin{array}{llll} \mathbf{a}_{\mathrm{S}}(\vec{\boldsymbol{\sigma}}, \vec{\boldsymbol{\tau}}) + \mathbf{b}_{\mathrm{S}}(\vec{\boldsymbol{\tau}}, \vec{\mathbf{u}}) & = & \mathbf{F}_{\vec{\chi}}(\vec{\boldsymbol{\tau}}) & \forall\, \vec{\boldsymbol{\tau}} \in \mathbb{H}, \\ \mathbf{b}_{\mathrm{S}}(\vec{\boldsymbol{\sigma}}, \vec{\mathbf{v}}) - \mathbf{O}_{\mathrm{S}}(\vec{\mathbf{w}}; \vec{\boldsymbol{\sigma}}, \vec{\mathbf{v}}) & = & 0 & \forall\, \vec{\mathbf{v}} \in \mathbf{Q}. \end{array} \tag{1.29}$$

In turn, we let $\widehat{\mathcal{J}} : \mathbf{Q}\times\mathrm{M} \to \mathbf{H}\times\mathrm{Q}$ be the operator given by

$$\widehat{\mathcal{J}}(\vec{\mathbf{w}}, \vec{\chi}) \,=\, \big(\widehat{\mathcal{J}}_1(\vec{\mathbf{w}}, \vec{\chi}), (\widehat{\mathcal{J}}_2(\vec{\mathbf{w}}, \vec{\chi}), \widehat{\mathcal{J}}_3(\vec{\mathbf{w}}, \vec{\chi}))\big) := (\vec{\mathbf{t}}, (\vec{\phi}, \vec{\xi})) \quad \forall\, (\vec{\mathbf{w}}, \vec{\chi}) \in \mathbf{Q}\times\mathrm{M}, \tag{1.30}$$

where $(\vec{\mathbf{t}}, (\vec{\phi}, \vec{\xi})) \in \mathbf{H}\times\mathrm{Q}$ is the unique solution (to be confirmed in Theorem 1.2) of the following system of equations:

$$\begin{array}{llll} \mathbf{a}_{\mathrm{T}}(\vec{\mathbf{t}}, \vec{\mathbf{s}}) + \mathbf{b}_{\mathrm{T}}(\vec{\mathbf{s}}, (\vec{\phi}, \vec{\xi})) & = & 0 & \forall\, \vec{\mathbf{s}} \in \mathbf{H}, \\ \mathbf{b}_{\mathrm{T}}(\vec{\mathbf{t}}, (\vec{\psi}, \vec{\eta})) - \mathbf{d}_{\mathrm{T}}((\vec{\phi}, \vec{\xi}), (\vec{\psi}, \vec{\eta})) - \mathbf{O}_{\mathrm{T}}(\vec{\mathbf{w}}; \vec{\mathbf{t}}, \vec{\psi}) - \mathbf{C}_{\mathrm{T}}\big(\vec{\chi}; \vec{\xi}, \vec{\eta}\big) & = & \mathcal{F}_{\vec{\chi}}(\vec{\psi}, \vec{\eta}) & \forall\, (\vec{\psi}, \vec{\eta}) \in \mathrm{Q}. \end{array} \tag{1.31}$$

Finally, defining the operator $\mathcal{J} : \mathbf{Q}\times\mathrm{M} \to \mathbf{Q}\times\mathrm{M}$ as

$$\mathcal{J}(\vec{\mathbf{w}}, \vec{\chi}) \,=\, \big(\widetilde{\mathcal{J}}_2(\vec{\mathbf{w}}, \vec{\chi}), \widehat{\mathcal{J}}_3(\vec{\mathbf{w}}, \vec{\chi})\big) = (\vec{\mathbf{u}}, \vec{\xi}) \quad \forall\, (\vec{\mathbf{w}}, \vec{\chi}) \in \mathbf{Q}\times\mathrm{M}, \tag{1.32}$$

we observe that solving (1.24) is equivalent to seeking a fixed point of $\mathcal{J}$, that is: Find $(\vec{\mathbf{u}}, \vec{\xi}) \in \mathbf{Q}\times\mathrm{M}$ such that $\mathcal{J}(\vec{\mathbf{u}}, \vec{\xi}) = (\vec{\mathbf{u}}, \vec{\xi})$.

We now aim to prove that the operator $\mathcal{J}$ is well-defined. To do that we first state the boundedness of all the variational forms involved (cf. (1.25), (1.26) and (1.27)). First, it is easy to see through a direct application of Hölder's inequality that

$$\begin{array}{rcll} |\mathbf{a}_{\mathrm{S}}(\vec{\boldsymbol{\sigma}}, \vec{\boldsymbol{\tau}})| & \leq & \|\mathbf{a}_{\mathrm{S}}\| \|\vec{\boldsymbol{\sigma}}\|_{\mathbb{H}} \|\vec{\boldsymbol{\tau}}\|_{\mathbb{H}} & \forall\, \vec{\boldsymbol{\sigma}}, \vec{\boldsymbol{\tau}} \in \mathbb{H}, \\ |\mathbf{b}_{\mathrm{S}}(\vec{\boldsymbol{\tau}}, \vec{\mathbf{v}})| & \leq & \|\mathbf{b}_{\mathrm{S}}\| \|\vec{\boldsymbol{\tau}}\|_{\mathbb{H}} \|\vec{\mathbf{v}}\|_{\mathbf{Q}} & \forall\, \big(\vec{\boldsymbol{\tau}}, \vec{\mathbf{v}}\big) \in \mathbb{H}\times\mathbf{Q}, \\ |\mathbf{a}_{\mathrm{T}}(\vec{\mathbf{t}}, \vec{\mathbf{s}})| & \leq & \|\mathbf{a}_{\mathrm{T}}\| \|\vec{\mathbf{t}}\|_{\mathbf{H}} \|\vec{\mathbf{s}}\|_{\mathbf{H}} & \forall\, \vec{\mathbf{t}}, \vec{\mathbf{s}} \in \mathbf{H}, \end{array} \tag{1.33}$$

with $\|\mathbf{a}_{\mathrm{S}}\| := \nu^{-1}$, $\|\mathbf{b}_{\mathrm{S}}\| := 1$ and $\|\mathbf{a}_{\mathrm{T}}\| := \kappa^{-1}$. In turn, employing again the Cauchy–Schwarz and

Hölder inequalities, we find that for each $\vec{\mathbf{w}} \in \mathbf{Q}$, there hold

$$|\mathbf{O}_{\mathrm{S}}(\vec{\mathbf{w}};\vec{\boldsymbol{\zeta}},\vec{\mathbf{v}})| \leq \frac{\rho}{\nu}\,\|\vec{\mathbf{w}}\|_{\mathbf{Q}}\,\|\vec{\boldsymbol{\zeta}}\|_{\mathbb{H}}\,\|\vec{\mathbf{v}}\|_{\mathbf{Q}} \qquad \forall\,(\vec{\boldsymbol{\zeta}},\vec{\mathbf{v}}) \in \mathbb{H}\times\mathbf{Q}, \tag{1.34a}$$

$$|\mathbf{O}_{\mathrm{T}}(\vec{\mathbf{w}};\vec{\mathbf{r}},\vec{\psi})| \leq \frac{1}{\kappa}\,\|\vec{\mathbf{w}}\|_{\mathbf{Q}}\,\|\vec{\mathbf{r}}\|_{\mathbf{H}}\,\|\vec{\psi}\|_{\mathrm{X}} \qquad \forall\,(\vec{\mathbf{r}},\vec{\psi}) \in \mathbf{H}\times\mathrm{X}. \tag{1.34b}$$

On the other hand, the following bounds for $\mathbf{b}_{\mathrm{T}}$ and $\mathbf{d}_{\mathrm{T}}$ will be proved in Appendix 1.7:

$$|\mathbf{b}_{\mathrm{T}}(\vec{\mathbf{s}},(\vec{\psi},\vec{\eta}))| \leq \|\mathbf{b}_{\mathrm{T}}\|\,\|\vec{\mathbf{s}}\|_{\mathbf{H}}\,\|(\vec{\psi},\vec{\eta})\|_{\mathrm{Q}} \qquad \forall\,\big(\vec{\mathbf{s}},(\vec{\psi},\vec{\eta})\big) \in \mathbf{H}\times\mathrm{Q}, \tag{1.35a}$$

$$|\mathbf{d}_{\mathrm{T}}((\vec{\phi},\vec{\xi}),(\vec{\psi},\vec{\eta}))| \leq \|\mathbf{d}_{\mathrm{T}}\|\,\|(\vec{\phi},\vec{\xi})\|_{\mathrm{Q}}\,\|(\vec{\psi},\vec{\eta})\|_{\mathrm{Q}} \qquad \forall\,(\vec{\phi},\vec{\xi}),\,(\vec{\psi},\vec{\eta}) \in \mathrm{Q}, \tag{1.35b}$$

where $\|\mathbf{b}_{\mathrm{T}}\| := \max\big\{1,\|i_4^{\mathrm{f}}\|,\|i_4^{\mathrm{p}}\|\big\}$, $\|\mathbf{d}_{\mathrm{T}}\| := (\widetilde{a}_{1,\mathrm{f}}+\widetilde{a}_{1,\mathrm{p}})\max\big\{(c_2^{\mathrm{f}})^2,(c_2^{\mathrm{p}})^2\big\}$, $i_4^\star$ is the continuous injection from $\mathrm{H}^1(\Omega_\star)$ to $\mathrm{L}^4(\Omega_\star)$ and $c_2^\star$ the Sobolev constant defined in (1.100). In turn, denoting $\vec{\mathbf{g}} := (\mathbf{g}_{\mathrm{f}},\mathbf{g}_{\mathrm{p}})$ with $\mathbf{g}_\star$ as in (1.22), in Appendix 1.7 we will show that given $\vec{\chi} \in \mathrm{M}$, we have

$$|\mathbf{F}_{\vec{\chi}}(\vec{\boldsymbol{\tau}})| \,\leq\, C_{\mathbf{F}}\big\{\|\vec{\mathbf{g}}\|_{1/2,\Gamma_{\mathrm{out}}^{\mathrm{c}}} + a_1\|\vec{\chi}\|_{\mathrm{M}}\big\}\,\|\vec{\boldsymbol{\tau}}\|_{\mathbb{H}} \qquad \forall\,\vec{\boldsymbol{\tau}} \in \mathbb{H}, \tag{1.36}$$

where

$$\|\vec{\mathbf{g}}\|_{1/2,\Gamma_{\mathrm{out}}^{\mathrm{c}}} := \|\mathbf{g}_{\mathrm{f}}\|_{1/2,\Gamma_{\mathrm{out,f}}^{\mathrm{c}}} + \|\mathbf{g}_{\mathrm{p}}\|_{1/2,\Gamma_{\mathrm{out,p}}^{\mathrm{c}}}, \quad C_{\mathbf{F}} := \max\big\{1,\|\mathbf{i}_4^{\mathrm{f}}\|,\|\mathbf{i}_4^{\mathrm{p}}\|\big\}\,\max\big\{C_{\mathrm{f}},C_{\Sigma,\mathrm{f}},C_{\mathrm{p}},C_{\Sigma,\mathrm{p}},1\big\},$$

and $\mathbf{i}_4^\star$ is the vector-valued version of $i_4^\star$. Finally, employing the same tools to bound $\mathbf{d}_{\mathrm{T}}$, given $\vec{\chi} \in \mathrm{M}$, it readily follows that

$$\begin{aligned} |\mathbf{C}_{\mathrm{T}}(\vec{\chi};\vec{\xi},\vec{\eta})| \,&\leq\, \widetilde{a}_1\,\|\vec{\chi}\|_{\mathrm{M}}\,\|\vec{\xi}\|_{\mathrm{M}}\,\|\vec{\eta}\|_{\mathrm{M}} \qquad && \forall\,(\vec{\xi},\,\vec{\eta}) \in \mathrm{M}\times\mathrm{M}, \quad \text{and} \\ |\mathcal{F}_{\vec{\chi}}(\vec{\psi},\vec{\eta})| \,&\leq\, \widetilde{a}_3\,(1+\|\vec{\chi}\|_{\mathrm{M}})\|(\vec{\psi},\vec{\eta})\|_{\mathrm{Q}} \qquad && \forall\,(\vec{\psi},\vec{\eta}) \in \mathrm{Q}, \end{aligned} \tag{1.37}$$

with

$$\begin{aligned} &\widetilde{a}_1 := a_1\max\big\{(c_3^{\mathrm{f}})^2,(c_3^{\mathrm{p}})^2\big\}\max\big\{c_3^{\mathrm{f}},c_3^{\mathrm{p}}\big\}, \quad \text{and} \\ &\widetilde{a}_3 := \max\{|\widetilde{a}_{1,\mathrm{f}}|,|\widetilde{a}_{1,\mathrm{p}}|,|\widetilde{a}_{2,\mathrm{f}}|,|\widetilde{a}_{2,\mathrm{p}}|\}\max\big\{c_2^{\mathrm{f}}c_2^{\mathrm{p}},c_2^{\mathrm{f}},c_2^{\mathrm{p}}\big\}. \end{aligned} \tag{1.38}$$

Further details of the previous bounds and the involved constants can be found in Appendix 1.7.

Well-definedness of the operator $\widetilde{\mathcal{J}}$

We will show that (1.29) is well-posed and therefore the operator $\widetilde{\mathcal{J}}$ (cf. (1.28)) is well-defined. For that, given $\star \in \{\mathrm{f},\mathrm{p}\}$, we prove that $\mathbf{a}_{\mathrm{S}}$ and $\mathbf{b}_{\mathrm{S}}$ satisfy the corresponding hypotheses from [60, Theorem 2.34]. Let

$$\mathcal{K}_{\mathrm{S}} = \big\{\vec{\boldsymbol{\tau}} := (\boldsymbol{\tau}_{\mathrm{f}},\,\boldsymbol{\tau}_{\mathrm{p}}) \in \mathbb{H}: \quad \mathbf{div}(\boldsymbol{\tau}_\star) = \mathbf{0} \text{ in } \Omega_\star\big\},$$

which corresponds to the kernel of the operator induced by the bilinear form $\mathbf{b}_{\mathrm{S}}$ (cf. (1.25c)). We proceed in a similar way to [66, Section 2.2] to show that $\mathbf{a}_{\mathrm{S}}$ is $\mathcal{K}_{\mathrm{S}}$-elliptic. To do that, it suffices to consider the decomposition

$$\mathbb{H}(\mathbf{div}_{4/3};\Omega_\star) = \mathbb{H}_0(\mathbf{div}_{4/3};\Omega_\star)\,\oplus\,\mathbb{R}\,\mathbb{I},$$

where

$$\mathbb{H}_0(\mathbf{div}_{4/3};\Omega_\star) := \left\{ \boldsymbol{\tau}_\star \in \mathbb{H}(\mathbf{div}_{4/3};\Omega_\star) : \quad \int_{\Omega_\star} \mathrm{tr}(\boldsymbol{\tau}_\star) \,=\, 0 \right\},$$

and recall two useful estimates. First, by suitably modifying the proof of [67, Lemma 2.3], it can be shown (see, e.g. [25, Lemma 3.1]) that there exists a positive constant $c_{1,\star}$, depending only on $\Omega_\star$, such that

$$c_{1,\star}\,\|\boldsymbol{\tau}_\star\|_{0,\Omega_\star} \,\leq\, \|\boldsymbol{\tau}_\star^{\mathrm{d}}\|_{0,\Omega_\star} + \|\mathbf{div}(\boldsymbol{\tau}_\star)\|_{0,4/3;\Omega_\star} \quad \forall\,\boldsymbol{\tau}_\star \in \mathbb{H}_0(\mathbf{div}_{4/3};\Omega_\star). \tag{1.39}$$

Similarly, following the proof of [66, Lemma 2.2] (see also [67, Lemma 2.5]), one can show that there exists a positive constant $c_{2,\star}$, depending only on $\Gamma_{\mathrm{out},\star}$ and $\Omega_\star$, such that

$$c_{2,\star}\,\|\boldsymbol{\tau}_\star\|_{\mathbf{div}_{4/3};\Omega_\star} \,\leq\, \|\boldsymbol{\tau}_{\star,0}\|_{\mathbf{div}_{4/3};\Omega_\star} \quad \forall\,\boldsymbol{\tau}_\star := \boldsymbol{\tau}_{\star,0} + d_\star\mathbb{I} \in \mathbb{H}_{\Gamma_{\mathrm{out}}}(\mathbf{div}_{4/3};\Omega_\star), \tag{1.40}$$

with $\boldsymbol{\tau}_{\star,0} \in \mathbb{H}_0(\mathbf{div}_{4/3};\Omega_\star)$ and $d_\star \in \mathbb{R}$.

Lemma 1.1. *There exists $\alpha_{\mathbf{s}} > 0$ such that $\mathbf{a}_{\mathrm{S}}(\vec{\boldsymbol{\tau}},\vec{\boldsymbol{\tau}}) \,\geq\, \alpha_{\mathrm{S}}\,\|\vec{\boldsymbol{\tau}}\|^2_{\mathbb{H}} \quad \forall\,\vec{\boldsymbol{\tau}} \in \mathcal{K}_{\mathrm{S}}$.*

Proof. Given $\vec{\boldsymbol{\tau}} = (\boldsymbol{\tau}_{\mathrm{f}},\boldsymbol{\tau}_{\mathrm{p}}) \in \mathcal{K}_{\mathrm{S}}$, applying (1.39) and (1.40), it is straightforward to see from the definition of $\mathbf{a}_{\mathrm{S}}$ (cf. (1.25a)), that

$$\mathbf{a}_{\mathrm{S}}(\vec{\boldsymbol{\tau}},\vec{\boldsymbol{\tau}}) \,\geq\, \alpha_{\mathbf{s}}\|\vec{\boldsymbol{\tau}}\|^2_{\mathbb{H}},$$

with constant $\alpha_{\mathbf{s}} = \dfrac{1}{2\nu}\min\{c_{1,\mathrm{f}}c_{2,\mathrm{f}},\, c_{1,\mathrm{p}}c_{2,\mathrm{p}}\}^2$, depending only on $\Gamma_{\mathrm{out},\star}$ and $\Omega_\star$, with $\star \in \{\mathrm{f},\mathrm{p}\}$. ■

We now establish the continuous inf-sup condition for the bilinear form $\mathbf{b}_{\mathrm{S}}$, whose proof is an adaptation of [25, Lemma 3.3] to our context.

Lemma 1.2. *There exists a positive constant β_{S} such that*

$$\sup_{\substack{\vec{\boldsymbol{\tau}}\in\mathbb{H}\\ \vec{\boldsymbol{\tau}}\neq\mathbf{0}}} \frac{\mathbf{b}_{\mathrm{S}}(\vec{\boldsymbol{\tau}},\vec{\mathbf{v}})}{\|\vec{\boldsymbol{\tau}}\|_{\mathbb{H}}} \,\geq\, \beta_{\mathrm{S}}\,\|\vec{\mathbf{v}}\|_{\mathbf{Q}} \qquad \forall\,\vec{\mathbf{v}} \in \mathbf{Q}. \tag{1.41}$$

Proof. Given $\vec{\mathbf{v}} = (\mathbf{v}_{\mathrm{f}},\mathbf{v}_{\mathrm{p}}) \in \mathbf{Q}$, we set $\widetilde{\mathbf{v}}_\star := |\mathbf{v}_\star|^2\mathbf{v}_\star$ with $\star \in \{\mathrm{f},\mathrm{p}\}$ and let $\mathbf{z}_\star \in \mathbf{H}^1(\Omega_\star)$ be the unique solution to the boundary value problem

$$-\triangle\mathbf{z}_\star \,=\, \widetilde{\mathbf{v}}_\star \quad \text{in} \quad \Omega_\star, \quad \mathbf{z}_\star \,=\, \mathbf{0} \quad \text{on} \quad \Gamma^{\mathrm{c}}_{\mathrm{out},\star}, \quad \text{and} \qquad \nabla\mathbf{z}_\star\mathbf{n}_\star \,=\, \mathbf{0} \quad \text{on} \quad \Gamma_{\mathrm{out},\star}.$$

Thus, defining $\widetilde{\boldsymbol{\tau}}_\star := -\nabla\mathbf{z}_\star \in \mathbb{L}^2(\Omega_\star)$, noticing that $\widetilde{\boldsymbol{\tau}}_\star \in \mathbb{H}^\star_{\mathrm{S}}$ and proceeding similarly to the proof of [25, Lemma 3.3], it follows that

$$\sup_{\substack{\vec{\boldsymbol{\tau}}\in\mathbb{H}\\ \vec{\boldsymbol{\tau}}\neq\mathbf{0}}} \frac{\mathbf{b}_{\mathrm{S}}(\vec{\boldsymbol{\tau}},\vec{\mathbf{v}})}{\|\vec{\boldsymbol{\tau}}\|_{\mathbb{H}}} \,\geq \beta_{\mathrm{S},\star}\|\mathbf{v}_\star\|_{0,4;\Omega_\star},$$

where $\beta_{\mathrm{S},\star} \,=\, (c_{\mathrm{p},\star}\|\mathbf{i}_4^\star\| + 1)^{-1}$, $c_{\mathrm{p},\star}$ is a Poincaré's constant depending only on $|\Omega_\star|$ and $\mathbf{i}_4^\star$ is the continuous injection of $\mathbf{H}^1(\Omega_\star)$ into $\mathbf{L}^4(\Omega_\star)$. Thus, (1.41) is satisfied with $\beta_{\mathrm{S}} \,=\, \dfrac{1}{2}\min\left\{\beta_{\mathrm{S,f}},\, \beta_{\mathrm{S,p}}\right\}$. ■

Letting now $\mathbf{A} : (\mathbb{H}\times\mathbf{Q})\times(\mathbb{H}\times\mathbf{Q}) \to \mathbb{R}$ be the bilinear form given by

$$\mathbf{A}\big((\vec{\boldsymbol{\zeta}},\vec{\mathbf{z}}),(\vec{\boldsymbol{\tau}},\vec{\mathbf{v}})\big) := \mathbf{a}_{\mathrm{S}}(\vec{\boldsymbol{\zeta}},\vec{\boldsymbol{\tau}}) + \mathbf{b}_{\mathrm{S}}(\vec{\boldsymbol{\tau}},\vec{\mathbf{z}}) + \mathbf{b}_{\mathrm{S}}(\vec{\boldsymbol{\zeta}},\vec{\mathbf{v}}) \qquad \forall\,(\vec{\boldsymbol{\zeta}},\vec{\mathbf{z}}),(\vec{\boldsymbol{\tau}},\vec{\mathbf{v}}) \in \mathbb{H}\times\mathbf{Q},$$

we deduce that (1.29), can be stated, equivalently as: Find $(\vec{\boldsymbol{\sigma}},\vec{\mathbf{u}}) \in \mathbb{H}\times\mathbf{Q}$ such that

$$\mathbf{A}_{\vec{\mathbf{w}}}\big((\vec{\boldsymbol{\sigma}},\vec{\mathbf{u}}),(\vec{\boldsymbol{\tau}},\vec{\mathbf{v}})\big) := \mathbf{A}\left((\vec{\boldsymbol{\sigma}},\vec{\mathbf{u}}),(\vec{\boldsymbol{\tau}},\vec{\mathbf{v}})\right) - \mathbf{O}_{\mathrm{S}}(\vec{\mathbf{w}};\vec{\boldsymbol{\sigma}},\vec{\mathbf{v}}) \;=\; \mathbf{F}_{\vec{\chi}}(\vec{\boldsymbol{\tau}}) \qquad \forall\,(\vec{\boldsymbol{\tau}},\vec{\mathbf{v}}) \in \mathbb{H}\times\mathbf{Q}. \tag{1.42}$$

Consequently, knowing from Lemmas 1.1 and 1.2 that $\mathbf{a}_{\mathrm{S}}$ and $\mathbf{b}_{\mathrm{S}}$ satisfy the hypotheses of [60, Theorem 2.34], a direct application of this result yields the existence of a positive constant $\alpha_{\mathbf{A}}$, depending on $\|\mathbf{a}_{\mathrm{S}}\|$, α_{S}, and β_{S}, such that

$$\sup_{\substack{(\vec{\boldsymbol{\tau}},\vec{\mathbf{v}})\in\mathbb{H}\times\mathbf{Q}\\ (\vec{\boldsymbol{\tau}},\vec{\mathbf{v}})\neq\mathbf{0}}} \frac{\mathbf{A}\big((\vec{\boldsymbol{\zeta}},\vec{\mathbf{z}}),(\vec{\boldsymbol{\tau}},\vec{\mathbf{v}})\big)}{\|(\vec{\boldsymbol{\tau}},\vec{\mathbf{v}})\|_{\mathbb{H}\times\mathbf{Q}}} \;\geq\; \alpha_{\mathbf{A}}\,\|(\vec{\boldsymbol{\zeta}},\vec{\mathbf{z}})\|_{\mathbb{H}\times\mathbf{Q}} \qquad \forall\,(\vec{\boldsymbol{\zeta}},\vec{\mathbf{z}}) \in \mathbb{H}\times\mathbf{Q}. \tag{1.43}$$

Then, it follows from (1.34a), (1.42) and (1.43) that

$$\sup_{\substack{(\vec{\boldsymbol{\tau}},\vec{\mathbf{v}})\in\mathbb{H}\times\mathbf{Q}\\ (\vec{\boldsymbol{\tau}},\vec{\mathbf{v}})\neq\mathbf{0}}} \frac{\mathbf{A}_{\vec{\mathbf{w}}}\big((\vec{\boldsymbol{\zeta}},\vec{\mathbf{z}}),(\vec{\boldsymbol{\tau}},\vec{\mathbf{v}})\big)}{\|(\vec{\boldsymbol{\tau}},\vec{\mathbf{v}})\|_{\mathbb{H}\times\mathbf{Q}}} \;\geq\; \Big\{\alpha_{\mathbf{A}} - \frac{\rho}{\nu}\|\vec{\mathbf{w}}\|_{\mathbf{Q}}\Big\}\,\|(\vec{\boldsymbol{\zeta}},\vec{\mathbf{z}})\|_{\mathbb{H}\times\mathbf{Q}} \qquad \forall\,(\vec{\boldsymbol{\zeta}},\vec{\mathbf{z}}) \in \mathbb{H}\times\mathbf{Q}.$$

Hence, assuming that $\|\vec{\mathbf{w}}\|_{\mathbf{Q}} \leq \dfrac{\nu\,\alpha_{\mathbf{A}}}{2\,\rho}$, we arrive at

$$\sup_{\substack{(\vec{\boldsymbol{\tau}},\vec{\mathbf{v}})\in\mathbb{H}\times\mathbf{Q}\\ (\vec{\boldsymbol{\tau}},\vec{\mathbf{v}})\neq\mathbf{0}}} \frac{\mathbf{A}_{\vec{\mathbf{w}}}\big((\vec{\boldsymbol{\zeta}},\vec{\mathbf{z}}),(\vec{\boldsymbol{\tau}},\vec{\mathbf{v}})\big)}{\|(\vec{\boldsymbol{\tau}},\vec{\mathbf{v}})\|_{\mathbb{H}\times\mathbf{Q}}} \;\geq\; \frac{\alpha_{\mathbf{A}}}{2}\,\|(\vec{\boldsymbol{\zeta}},\vec{\mathbf{z}})\|_{\mathbb{H}\times\mathbf{Q}} \qquad \forall\,(\vec{\boldsymbol{\zeta}},\vec{\mathbf{z}}) \in \mathbb{H}\times\mathbf{Q}. \tag{1.44}$$

Similarly, noting that $\mathbf{A}$ is symmetric, employing (1.34a) and (1.43), and assuming again that $\|\vec{\mathbf{w}}\|_{\mathbf{Q}} \leq \dfrac{\nu\,\alpha_{\mathbf{A}}}{2\,\rho}$, we obtain

$$\sup_{\substack{(\vec{\boldsymbol{\zeta}},\vec{\mathbf{z}})\in\mathbb{H}\times\mathbf{Q}\\ (\vec{\boldsymbol{\zeta}},\vec{\mathbf{z}})\neq\mathbf{0}}} \frac{\mathbf{A}_{\vec{\mathbf{w}}}\big((\vec{\boldsymbol{\zeta}},\vec{\mathbf{z}}),(\vec{\boldsymbol{\tau}},\vec{\mathbf{v}})\big)}{\|(\vec{\boldsymbol{\zeta}},\vec{\mathbf{z}})\|_{\mathbb{H}\times\mathbf{Q}}} \;\geq\; \frac{\alpha_{\mathbf{A}}}{2}\,\|(\vec{\boldsymbol{\tau}},\vec{\mathbf{v}})\|_{\mathbb{H}\times\mathbf{Q}} \;>\; 0 \qquad \forall\,(\vec{\boldsymbol{\tau}},\vec{\mathbf{v}}) \in \mathbb{H}\times\mathbf{Q},\ (\vec{\boldsymbol{\tau}},\vec{\mathbf{v}}) \neq \mathbf{0}. \tag{1.45}$$

Then, we are now in position to prove that the operator $\widetilde{\mathcal{J}}$ (cf. (1.28)) is well-defined.

Theorem 1.1. *For each $\vec{\chi} \in \mathrm{M}$ and $\vec{\mathbf{w}} \in \mathbf{Q}$ such that $\|\vec{\mathbf{w}}\|_{\mathbf{Q}} \leq \dfrac{\nu\,\alpha_{\mathbf{A}}}{2\,\rho}$, there exists a unique $(\vec{\boldsymbol{\sigma}},\vec{\mathbf{u}}) \in \mathbb{H}\times\mathbf{Q}$ solution to (1.29) (equivalently (1.42)). Moreover, there holds*

$$\|\widetilde{\mathcal{J}}(\vec{\mathbf{w}},\vec{\chi})\|_{\mathbb{H}\times\mathbf{Q}} \;=\; \|(\vec{\boldsymbol{\sigma}},\vec{\mathbf{u}})\|_{\mathbb{H}\times\mathbf{Q}} \;\leq\; \frac{2C_{\mathbf{F}}}{\alpha_{\mathbf{A}}}\Big\{\|\vec{\mathbf{g}}\|_{1/2,\Gamma_{\mathrm{out}}^{\mathrm{c}}} + a_1\|\vec{\chi}\|_{\mathrm{M}}\Big\}. \tag{1.46}$$

Proof. We first recall from (1.44) and (1.45), that $\mathbf{A}_{\vec{\mathbf{w}}}$ satisfies the hypotheses of the Banach–Nečas–Babuška Theorem [60, Theorem 2.6], which allows us to conclude the well-posedness of (1.42). In turn, the estimate (1.46) is a direct consequence of (1.44), (1.42) and (1.36). ∎

Well-definedness of the operator $\widehat{\mathcal{J}}$

We will prove now that (1.31) is well-posed, equivalently, that $\widehat{\mathcal{J}}$ is well-defined. Indeed, it is clear that $\mathbf{a}_{\mathrm{T}}$ and $\mathbf{d}_{\mathrm{T}}$ are symmetric, and the former is positive semidefinite. In addition, thanks to (1.18), it follows that $\mathbf{d}_{\mathrm{T}}$ (cf. (1.25e)), satisfies

$$\mathbf{d}_{\mathrm{T}}((\vec{\psi},\vec{\eta}),(\vec{\psi},\vec{\eta})) \,=\, (\widetilde{a}_{1,\mathrm{f}}-\widetilde{a}_0)\|\eta_{\mathrm{f}}\|^2_{0,\Sigma}+(\widetilde{a}_{1,\mathrm{p}}+\widetilde{a}_0)\|\eta_{\mathrm{p}}\|^2_{0,\Sigma} \geq 0 \qquad \forall\,(\vec{\psi},\vec{\eta})\in \mathrm{Q}, \tag{1.47}$$

which confirm hypothesis **i**) of [50, Theorem 3.4]). On the other hand, given $\star\in\{\mathrm{f},\mathrm{p}\}$, we let $\mathcal{K}_{\mathrm{T}}$ be the kernel of the operator induced by the bilinear form $\mathbf{b}_{\mathrm{T}}$ (cf. (1.25d)), that is

$$\mathcal{K}_{\mathrm{T}} := \Big\{\vec{\mathbf{s}}:=(\mathbf{s}_{\mathrm{f}},\mathbf{s}_{\mathrm{p}})\in\mathbf{H}: \quad \mathrm{div}(\mathbf{s}_\star) \,=\, 0 \quad \text{in} \quad \Omega_\star \quad \text{and} \quad \mathbf{s}_\star\cdot\mathbf{n}_\star \,=\, 0 \quad \text{on} \quad \Gamma^{\mathrm{c}}_{\mathrm{in},\star}\Big\}.$$

Then, it is straightforward to see from the definition of $\mathbf{a}_{\mathrm{T}}$ (cf. (1.25b)), that for each $\vec{\mathbf{s}}:=(\mathbf{s}_{\mathrm{f}},\mathbf{s}_{\mathrm{p}})\in\mathcal{K}_{\mathrm{T}}$, there holds

$$\mathbf{a}_{\mathrm{T}}(\vec{\mathbf{s}},\vec{\mathbf{s}}) \,\geq\, \frac{1}{2\kappa}\,\|\vec{\mathbf{s}}\|^2_{\mathbf{H}} \qquad \forall\,\vec{\mathbf{s}}\in\mathcal{K}_{\mathrm{T}}, \tag{1.48}$$

which proves that $\mathbf{a}_{\mathrm{T}}$ is $\mathcal{K}_{\mathrm{T}}$-elliptic with constant $\alpha_{\mathrm{T}}=\dfrac{1}{2\kappa}$, and hence that $\mathbf{a}_{\mathrm{S}}$ verify the continuous inf-sup condition required by the hypothesis **ii)** of [50, Theorem 3.4]. Now, we provide the corresponding inf-sup condition of the bilinear form $\mathbf{b}_{\mathrm{T}}$ (cf. (1.25d)) and its proof is basically an adaptation of the version in [10, Theorem 2.1].

Lemma 1.3. *There exists a positive constant β_{T} such that*

$$\sup_{\substack{\vec{\mathbf{s}}\in\mathbf{H}\\ \vec{\mathbf{s}}\neq\mathbf{0}}}\frac{\mathbf{b}_{\mathrm{T}}(\vec{\mathbf{s}},(\vec{\psi},\vec{\eta}))}{\|\vec{\mathbf{s}}\|_{\mathbf{H}}} \,\geq\, \beta_{\mathrm{T}}\,\|(\vec{\psi},\vec{\eta})\|_{\mathrm{Q}} \qquad \forall\,(\vec{\psi},\vec{\eta})\in\mathrm{Q}. \tag{1.49}$$

Proof. Let $(\vec{\psi},\vec{\eta})\in\mathrm{Q}$. Then, similarly as done in Lemma 1.2, we deduce that

$$\sup_{\substack{\vec{\mathbf{s}}\in\mathbf{H}\\ \vec{\mathbf{s}}\neq\mathbf{0}}}\frac{\mathbf{b}_{\mathrm{T}}(\vec{\mathbf{s}},(\vec{\psi},\vec{\eta}))}{\|\vec{\mathbf{s}}\|_{\mathbf{H}}} \,\geq\, \widetilde{\beta}_{\mathrm{T}}\|\vec{\psi}\|_{\mathrm{X}}, \tag{1.50}$$

with $\widetilde{\beta}_{\mathrm{T}}\,=\,\dfrac{1}{2}\min\Big\{\,\big(c_{\mathrm{p,f}}\|i^{\mathrm{f}}_4\|+1\big)^{-1},\,(c_{\mathrm{p,p}}\|i^{\mathrm{p}}_4\|+1)^{-1}\,\Big\}$, where $i^\star_4$ is the continuous injection of $\mathrm{H}^1(\Omega_\star)$ into $\mathrm{L}^4(\Omega_\star)$ and $c_{\mathrm{p},\star}$ is the Poincare's constant, for each $\star\in\{\mathrm{f},\mathrm{p}\}$. On the other hand, given $\mu_\star\in\mathrm{H}^{-1/2}_{00}(\Gamma^{\mathrm{c}}_{\mathrm{in},\star})$, we let $\widehat{z}_\star\in\mathrm{H}^1(\Omega_\star)$ be the solution to

$$\triangle\widehat{z}_\star \,=\, 0 \quad \text{in} \quad \Omega_\star, \quad \widehat{z}_\star \,=\, 0 \quad \text{on} \quad \Gamma_{\mathrm{in},\star}, \quad \text{and} \quad \nabla\widehat{z}_\star\cdot\mathbf{n}_\star \,=\, \mu_\star \quad \text{on} \quad \Gamma^{\mathrm{c}}_{\mathrm{in},\star},$$

and set $\widehat{\mathbf{s}}_\star:=\nabla\widehat{z}_\star\in\mathbf{L}^2(\Omega_\star)$. Noticing that $\widehat{\mathbf{s}}_\star\in\mathbf{H}^\star_{\mathrm{T}}$, proceeding analogously to the proof of [10, Theorem 2.1], we conclude that there exists a constant $\widehat{\beta}_{\mathrm{T},\star} > 0$ such that

$$\sup_{\substack{\vec{\mathbf{s}}\in\mathbf{H}\\ \vec{\mathbf{s}}\neq\mathbf{0}}} \frac{\mathbf{b}_{\mathrm{T}}(\vec{\mathbf{s}},(\vec{\psi},\vec{\eta}))}{\|\vec{\mathbf{s}}\|_{\mathbf{H}}} \;\geq\; \widehat{\beta}_{\mathrm{T},\star}\|\eta_\star\|_{1/2,00,\Gamma^{\mathrm{c}}_{\mathrm{in},\star}}.$$

The above, along with (1.50), yields (1.49) with $\beta_{\mathrm{T}} \;=\; \dfrac{1}{2}\min\Big\{\widetilde{\beta}_{\mathrm{T}}, \dfrac{1}{2}\min\big\{\widehat{\beta}_{\mathrm{T,f}}, \widehat{\beta}_{\mathrm{T,p}}\big\}\Big\}$. ■

Now, we let $\mathcal{A} : (\mathbf{H}\times\mathrm{Q})\times(\mathbf{H}\times\mathrm{Q}) \to \mathbb{R}$ be the bounded bilinear form defined by

$$\mathcal{A}\big((\vec{\mathbf{r}},(\vec{\varphi},\vec{\lambda})),(\vec{\mathbf{s}},(\vec{\psi},\vec{\eta}))\big) := \mathbf{a}_{\mathrm{T}}\big(\vec{\mathbf{r}},\vec{\mathbf{s}}\big) + \mathbf{b}_{\mathrm{T}}\big(\vec{\mathbf{s}},(\vec{\varphi},\vec{\lambda})\big) + \mathbf{b}_{\mathrm{T}}\big(\vec{\mathbf{r}},(\vec{\psi},\vec{\eta})\big) - \mathbf{d}_{\mathrm{T}}\big((\vec{\varphi},\vec{\lambda}),(\vec{\psi},\vec{\eta})\big) \tag{1.51}$$

for all $(\vec{\mathbf{r}},(\vec{\varphi},\vec{\lambda}))$, $(\vec{\mathbf{s}},(\vec{\psi},\vec{\eta})) \in \mathbf{H}\times\mathrm{Q}$. Next, letting now $\mathcal{A}_{\vec{\mathbf{w}},\vec{\chi}} : (\mathbf{H}\times\mathrm{Q})\times(\mathbf{H}\times\mathrm{Q}) \to \mathbb{R}$ be the bilinear form such that

$$\mathcal{A}_{\vec{\mathbf{w}},\vec{\chi}}\big((\vec{\mathbf{r}},(\vec{\varphi},\vec{\lambda})),(\vec{\mathbf{s}},(\vec{\psi},\vec{\eta}))\big) := \mathcal{A}\big((\vec{\mathbf{r}},(\vec{\varphi},\vec{\lambda})),(\vec{\mathbf{s}},(\vec{\psi},\vec{\eta}))\big) - \mathbf{O}_{\mathrm{T}}(\vec{\mathbf{w}};\vec{\mathbf{r}},\vec{\psi}) - \mathbf{C}_{\mathrm{T}}(\vec{\chi};\vec{\lambda},\vec{\eta}) \tag{1.52}$$

for all $(\vec{\mathbf{r}},(\vec{\varphi},\vec{\lambda}))$, $(\vec{\mathbf{s}},(\vec{\psi},\vec{\eta})) \in \mathbf{H}\times\mathrm{Q}$. We realize that (1.31) can be rewritten, equivalently, as: Find $(\vec{\mathbf{t}},(\vec{\phi},\vec{\xi})) \in \mathbf{H}\times\mathrm{Q}$ such that

$$\mathcal{A}_{\vec{\mathbf{w}},\vec{\chi}}\big((\vec{\mathbf{t}},(\vec{\phi},\vec{\xi})),(\vec{\mathbf{s}},(\vec{\psi},\vec{\eta}))\big) \;=\; \mathcal{F}_{\vec{\chi}}(\vec{\psi},\vec{\eta}) \qquad \forall\,(\vec{\mathbf{s}},(\vec{\psi},\vec{\eta})) \in \mathbf{H}\times\mathrm{Q}. \tag{1.53}$$

Then, thanks to (1.48), (1.47) and (1.49), the hypotheses of [50, Theorem 3.4] are satisfied, and hence the *a priori* estimates given by [50, Theorem 3.4, eq. (3.51)] imply the existence of a positive constant $\alpha_{\mathcal{A}}$, depending on $\|\mathbf{a}_{\mathrm{T}}\|$, α_{T}, $\|\mathbf{d}_{\mathrm{T}}\|$, and β_{T}, such that

$$\sup_{\substack{(\vec{\mathbf{s}},(\vec{\psi},\vec{\eta}))\in\mathbf{H}\times\mathrm{Q}\\ (\vec{\mathbf{s}},(\vec{\psi},\vec{\eta}))\neq\mathbf{0}}} \frac{\mathcal{A}\big((\vec{\mathbf{r}},(\vec{\varphi},\vec{\lambda})),(\vec{\mathbf{s}},(\vec{\psi},\vec{\eta}))\big)}{\|(\vec{\mathbf{s}},(\vec{\psi},\vec{\eta}))\|_{\mathbf{H}\times\mathrm{Q}}} \;\geq\; \alpha_{\mathcal{A}}\,\|(\vec{\mathbf{r}},(\vec{\varphi},\vec{\lambda}))\|_{\mathbf{H}\times\mathrm{Q}} \qquad \forall\,(\vec{\mathbf{r}},(\vec{\varphi},\vec{\lambda})) \in \mathbf{H}\times\mathrm{Q}. \tag{1.54}$$

Thus, from (1.52), (1.34b), (1.37) and (1.54), it follows that

$$\sup_{\substack{(\vec{\mathbf{s}},(\vec{\psi},\vec{\eta}))\in\mathbf{H}\times\mathrm{Q}\\ (\vec{\mathbf{s}},(\vec{\psi},\vec{\eta}))\neq\mathbf{0}}} \frac{\mathcal{A}_{\vec{\mathbf{w}},\vec{\chi}}\big((\vec{\mathbf{r}},(\vec{\varphi},\vec{\lambda})),(\vec{\mathbf{s}},(\vec{\psi},\vec{\eta}))\big)}{\|(\vec{\mathbf{s}},(\vec{\psi},\vec{\eta}))\|_{\mathbf{H}\times\mathrm{Q}}} \;\geq\; \Big\{\alpha_{\mathcal{A}} - \widetilde{a}_1\|\vec{\chi}\|_{\mathrm{M}} - \kappa^{-1}\|\vec{\mathbf{w}}\|_{\mathbf{Q}}\Big\}\,\|(\vec{\mathbf{r}},(\vec{\varphi},\vec{\lambda}))\|_{\mathbf{H}\times\mathrm{Q}}$$

for all $(\vec{\mathbf{r}},(\vec{\varphi},\vec{\lambda})) \in \mathbf{H}\times\mathrm{Q}$. Hence, under the assumption $\|(\vec{\mathbf{w}},\vec{\chi})\|_{\mathbf{Q}\times\mathrm{M}} \leq \dfrac{\kappa\alpha_{\mathcal{A}}}{2(1+\kappa\widetilde{a}_1)}$, we arrive at

$$\sup_{\substack{(\vec{\mathbf{s}},(\vec{\psi},\vec{\eta}))\in\mathbf{H}\times\mathrm{Q}\\ (\vec{\mathbf{s}},(\vec{\psi},\vec{\eta}))\neq\mathbf{0}}} \frac{\mathcal{A}_{\vec{\mathbf{w}},\vec{\chi}}\big((\vec{\mathbf{r}},(\vec{\varphi},\vec{\lambda})),(\vec{\mathbf{s}},(\vec{\psi},\vec{\eta}))\big)}{\|(\vec{\mathbf{s}},(\vec{\psi},\vec{\eta}))\|_{\mathbf{H}\times\mathrm{Q}}} \;\geq\; \frac{\alpha_{\mathcal{A}}}{2}\,\|(\vec{\mathbf{r}},(\vec{\varphi},\vec{\lambda}))\|_{\mathbf{H}\times\mathrm{Q}} \qquad \forall\,(\vec{\mathbf{r}},(\vec{\varphi},\vec{\lambda})) \in \mathbf{H}\times\mathrm{Q}. \tag{1.55}$$

Similarly, using the fact that $\mathcal{A}$ is symmetric, employing the same boundedness estimates for $\mathbf{O}_{\mathrm{T}}$ (cf. (1.34b)) and $\mathbf{C}_{\mathrm{T}}$ (cf. (1.37)), and assuming again that $\|(\vec{\mathbf{w}},\vec{\chi})\|_{\mathbf{Q}\times\mathrm{M}} \leq \dfrac{\kappa\alpha_{\mathcal{A}}}{2(1+\kappa\widetilde{a}_1)}$, we are able to prove the companion inf-sup condition to (1.55), that is

$$\sup_{\substack{(\vec{\mathbf{r}},(\vec{\varphi},\vec{\lambda}))\in\mathbf{H}\times\mathrm{Q}\\(\vec{\mathbf{r}},(\vec{\varphi},\vec{\lambda}))\neq\mathbf{0}}} \frac{\mathcal{A}_{\vec{\mathbf{w}},\vec{\chi}}\big((\vec{\mathbf{r}},(\vec{\varphi},\vec{\lambda})),(\vec{\mathbf{s}},(\vec{\psi},\vec{\eta}))\big)}{\|(\vec{\mathbf{r}},(\vec{\varphi},\vec{\lambda}))\|_{\mathbf{H}\times\mathrm{Q}}} \geq \frac{\alpha_{\mathcal{A}}}{2}\,\|(\vec{\mathbf{s}},(\vec{\psi},\vec{\eta}))\|_{\mathbf{H}\times\mathrm{Q}} > 0$$

for all $(\vec{\mathbf{s}},(\vec{\psi},\vec{\eta}))\in\mathbf{H}\times\mathrm{Q}$, $(\vec{\mathbf{s}},(\vec{\psi},\vec{\eta}))\neq\mathbf{0}$. As a consequence, we are in position to establish that $\widehat{\mathcal{J}}$ (cf. (1.30)) is well defined.

Theorem 1.2. *For each $(\vec{\mathbf{w}},\vec{\chi})\in\mathbf{Q}\times\mathrm{M}$ such that $\|(\vec{\mathbf{w}},\vec{\chi})\|_{\mathbf{Q}\times\mathrm{M}} \leq \dfrac{\kappa\alpha_{\mathcal{A}}}{2(1+\kappa\widetilde{a}_1)}$, there exists a unique $(\vec{\mathbf{t}},(\vec{\phi},\vec{\xi})) = \widehat{\mathcal{J}}(\vec{\mathbf{w}},\vec{\chi})\in\mathbf{H}\times\mathrm{Q}$ solution to (1.31) (equivalently (1.53)). Moreover, there holds*

$$\|\widehat{\mathcal{J}}(\vec{\mathbf{w}},\vec{\chi})\|_{\mathbf{H}\times\mathrm{Q}} = \|(\vec{\mathbf{t}},(\vec{\phi},\vec{\xi}))\|_{\mathbf{H}\times\mathrm{Q}} \leq \frac{2}{\alpha_{\mathcal{A}}}\widetilde{a}_3\big(1+\|\vec{\chi}\|_{\mathrm{M}}\big), \tag{1.56}$$

where $\widetilde{a}_1$ and $\widetilde{a}_3$ have been defined in (1.38).

Proof. It follows from a straightforward application of [60, Theorem 2.6]. In particular, the *a priori* estimate (1.56) follows from (1.55) and the fact that, according to (1.37), there holds $\|\mathcal{F}_{\vec{\chi}}\| \leq \widetilde{a}_3\,\big(1+\|\vec{\chi}\|_{\mathrm{M}}\big)$. ∎

1.3.2 Solvability analysis of the fixed-point scheme

Knowing from the previous sections that the operators $\widetilde{\mathcal{J}}$, $\widehat{\mathcal{J}}$, and hence $\mathcal{J}$ are well-defined, we now focus on the solvability of the fixed-point equation (1.32). To this end, in what follows we first derive sufficient conditions on $\mathcal{J}$ to map a closed ball of $\mathbf{Q}\times\mathrm{M}$ into itself. Indeed, from now on setting $\delta := \min\left\{\dfrac{\nu\,\alpha_{\mathbf{A}}}{2\,\rho}, \dfrac{\kappa\alpha_{\mathcal{A}}}{2(1+\kappa\widetilde{a}_1)}\right\}$, we let

$$\mathrm{W}(\delta) := \Big\{(\vec{\mathbf{w}},\vec{\chi})\in\mathbf{Q}\times\mathrm{M}:\quad \|(\vec{\mathbf{w}},\vec{\chi})\|_{\mathbf{Q}\times\mathrm{M}} \leq \delta\Big\}. \tag{1.57}$$

Lemma 1.4. *If*

$$C_{\mathbf{F}}\Big\{\|\vec{\mathbf{g}}\|_{1/2,\Gamma_{\mathrm{out}}^{\mathrm{c}}} + a_1\delta\Big\} \leq \frac{\alpha_{\mathbf{A}}}{4}\delta, \quad \text{and} \quad \widetilde{a}_3(1+\delta) \leq \frac{\alpha_{\mathcal{A}}}{4}\delta, \tag{1.58}$$

then $\mathcal{J}\big(\mathrm{W}(\delta)\big) \subseteq \mathrm{W}(\delta)$.

Proof. Given $(\vec{\mathbf{w}},\vec{\chi})\in\mathrm{W}(\delta)$, we first recall from (1.32) that $\mathcal{J}(\vec{\mathbf{w}},\vec{\chi}) = \big(\widetilde{\mathcal{J}}_2(\vec{\mathbf{w}},\vec{\chi}),\widehat{\mathcal{J}}_3(\vec{\mathbf{w}},\vec{\chi})\big)$. In this way, the choice of δ along with assumption (1.58) allows to conclude from (1.46) and (1.56) that $\|\widetilde{\mathcal{J}}_2(\vec{\mathbf{w}},\vec{\chi})\|_{\mathbf{Q}}$ and $\|\widehat{\mathcal{J}}_3(\vec{\mathbf{w}},\vec{\chi})\|_{\mathrm{M}}$ are bounded each by $\delta/2$, which implies that $\|\mathcal{J}(\vec{\mathbf{w}},\vec{\chi})\|_{\mathbf{Q}\times\mathrm{M}} \leq \delta$, and hence $\mathcal{J}\big(\mathrm{W}(\delta)\big) \subseteq \mathrm{W}(\delta)$. ∎

We continue the analysis with the Lipschitz-continuity properties of $\widetilde{\mathcal{J}}$ and $\widehat{\mathcal{J}}$.

Lemma 1.5. *There exist positive constants* $\mathrm{L}_{\mathrm{S},1}$ *and* $\mathrm{L}_{\mathrm{S},2}$*, depending only on* ν*,* ρ*,* $\alpha_{\mathbf{A}}$*,* a_1*, and* $C_{\mathbf{F}}$ *such that*

$$\|\widetilde{\mathcal{J}}(\vec{\mathbf{w}},\vec{\chi}) - \widetilde{\mathcal{J}}(\vec{\mathbf{w}}_0,\vec{\chi}_0)\|_{\mathbb{H}\times\mathbf{Q}} \le \Big\{\mathrm{L}_{\mathrm{S},1}\big(\|\vec{\mathbf{g}}\|_{1/2,\Gamma_{\mathrm{out}}^{\mathrm{c}}} + a_1\delta\big) + \mathrm{L}_{\mathrm{S},2}\Big\}\|(\vec{\mathbf{w}},\vec{\chi}) - (\vec{\mathbf{w}}_0,\vec{\chi}_0)\|_{\mathbf{Q}\times\mathrm{M}} \tag{1.59}$$

for all $(\vec{\mathbf{w}},\vec{\chi}), (\vec{\mathbf{w}}_0,\vec{\chi}_0) \in \mathrm{W}(\delta)$.

Proof. Given $(\vec{\mathbf{w}},\vec{\chi})$, $(\vec{\mathbf{w}}_0,\vec{\chi}_0) \in \mathrm{W}(\delta)$, we set $\widetilde{\mathcal{J}}(\vec{\mathbf{w}},\vec{\chi}) = (\vec{\boldsymbol{\sigma}},\vec{\mathbf{u}}) \in \mathbb{H}\times\mathbf{Q}$ and $\widetilde{\mathcal{J}}(\vec{\mathbf{w}}_0,\vec{\chi}_0) = (\vec{\boldsymbol{\sigma}}_0,\vec{\mathbf{u}}_0) \in \mathbb{H}\times\mathbf{Q}$ as the unique solutions of the formulations (1.29) (equivalently (1.42)), that is

$$\mathbf{A}_{\vec{\mathbf{w}}}\big((\vec{\boldsymbol{\sigma}},\vec{\mathbf{u}}),(\vec{\boldsymbol{\tau}},\vec{\mathbf{v}})\big) = \mathbf{F}_{\vec{\chi}}(\vec{\boldsymbol{\tau}}) \quad \text{and} \quad \mathbf{A}_{\vec{\mathbf{w}}_0}\big((\vec{\boldsymbol{\sigma}}_0,\vec{\mathbf{u}}_0),(\vec{\boldsymbol{\tau}},\vec{\mathbf{v}})\big) = \mathbf{F}_{\vec{\chi}_0}(\vec{\boldsymbol{\tau}}),$$

respectively, both for all $(\vec{\boldsymbol{\tau}},\vec{\mathbf{v}}) \in \mathbb{H}\times\mathbf{Q}$. Then, applying the global inf-sup condition (1.44) to $(\vec{\boldsymbol{\zeta}},\vec{\mathbf{z}}) := \big(\vec{\boldsymbol{\sigma}}-\vec{\boldsymbol{\sigma}}_0,\vec{\mathbf{u}}-\vec{\mathbf{u}}_0\big)$, using the above identities, (1.42), (1.34a) and (1.27), we find that

$$\begin{aligned}\frac{\alpha_{\mathbf{A}}}{2}\,\|\big(\vec{\boldsymbol{\sigma}}-\vec{\boldsymbol{\sigma}}_0,\vec{\mathbf{u}}-\vec{\mathbf{u}}_0\big)\|_{\mathbb{H}\times\mathbf{Q}} &\le \sup_{\substack{(\vec{\boldsymbol{\tau}},\vec{\mathbf{v}})\in\mathbb{H}\times\mathbf{Q}\\(\vec{\boldsymbol{\tau}},\vec{\mathbf{v}})\neq\mathbf{0}}} \frac{\mathbf{A}_{\vec{\mathbf{w}}}\big((\vec{\boldsymbol{\sigma}}-\vec{\boldsymbol{\sigma}}_0,\vec{\mathbf{u}}-\vec{\mathbf{u}}_0),(\vec{\boldsymbol{\tau}},\vec{\mathbf{v}})\big)}{\|(\vec{\boldsymbol{\tau}},\vec{\mathbf{v}})\|_{\mathbb{H}\times\mathbf{Q}}}\\
&= \sup_{\substack{(\vec{\boldsymbol{\tau}},\vec{\mathbf{v}})\in\mathbb{H}\times\mathbf{Q}\\(\vec{\boldsymbol{\tau}},\vec{\mathbf{v}})\neq\mathbf{0}}} \frac{\mathbf{O}_{\mathrm{S}}(\vec{\mathbf{w}}-\vec{\mathbf{w}}_0;\vec{\boldsymbol{\sigma}}_0,\vec{\mathbf{v}}) + \big(\mathbf{F}_{\vec{\chi}}-\mathbf{F}_{\vec{\chi}_0}\big)(\vec{\boldsymbol{\tau}})}{\|(\vec{\boldsymbol{\tau}},\vec{\mathbf{v}})\|_{\mathbb{H}\times\mathbf{Q}}} \le \frac{\rho}{\nu}\|\vec{\mathbf{w}}-\vec{\mathbf{w}}_0\|_{\mathbf{Q}}\|\vec{\boldsymbol{\sigma}}_0\|_{\mathbb{H}} + a_1 C_{\mathbf{F}}\,\|\vec{\chi}-\vec{\chi}_0\|_{\mathrm{M}},\end{aligned}$$

which, along with the fact that $\|\widetilde{\mathcal{J}}(\vec{\mathbf{w}},\vec{\chi}) - \widetilde{\mathcal{J}}(\vec{\mathbf{w}}_0,\vec{\chi}_0)\|_{\mathbb{H}\times\mathbf{Q}} = \|(\vec{\boldsymbol{\sigma}},\vec{\mathbf{u}}) - (\vec{\boldsymbol{\sigma}}_0,\vec{\mathbf{u}}_0)\|_{\mathbb{H}\times\mathbf{Q}}$ and (1.46), yields (1.59), with $\mathrm{L}_{\mathrm{S},1} := \dfrac{4\rho\, C_{\mathbf{F}}}{\nu\alpha_{\mathbf{A}}^2}$ and $\mathrm{L}_{\mathrm{S},2} := \dfrac{2a_1 C_{\mathbf{F}}}{\alpha_{\mathbf{A}}}$, thus completing the proof. ∎

Lemma 1.6. *There exists a positive constant* L_{T}*, depending only on* $\alpha_{\mathcal{A}}$*,* $\widetilde{a}_1$*,* $\widetilde{a}_3$ *and* κ*, such that*

$$\|\widehat{\mathcal{J}}(\vec{\mathbf{w}},\vec{\chi}) - \widehat{\mathcal{J}}(\vec{\mathbf{w}}_0,\vec{\chi}_0)\|_{\mathbf{H}\times\mathrm{Q}} \le \mathrm{L}_{\mathrm{T}}\,\big(1+\delta\big)\,\|(\vec{\mathbf{w}},\vec{\chi}) - (\vec{\mathbf{w}}_0,\vec{\chi}_0)\|_{\mathbf{Q}\times\mathrm{M}} \tag{1.60}$$

for all $(\vec{\mathbf{w}},\vec{\chi})$*,* $(\vec{\mathbf{w}}_0,\vec{\chi}_0) \in \mathrm{W}(\delta)$.

Proof. Given $(\vec{\mathbf{w}},\vec{\chi})$, $(\vec{\mathbf{w}}_0,\vec{\chi}_0) \in \mathrm{W}(\delta)$, we let $\widehat{\mathcal{J}}(\vec{\mathbf{w}},\vec{\chi}) = (\vec{\mathbf{t}},(\vec{\phi},\vec{\xi})) \in \mathbf{H}\times\mathrm{Q}$ and $\widehat{\mathcal{J}}(\vec{\mathbf{w}}_0,\vec{\chi}_0) = (\vec{\mathbf{t}}_0,(\vec{\phi}_0,\vec{\xi}_0)) \in \mathbf{H}\times\mathrm{Q}$ as the unique solutions of (1.31), Then, subtracting both systems and rearranging the terms appropriately, we find that

$$\begin{aligned}\mathcal{A}_{\vec{\mathbf{w}},\vec{\chi}}\big((\vec{\mathbf{t}}-\vec{\mathbf{t}}_0,(\vec{\phi}-\vec{\phi}_0,\vec{\xi}-\vec{\xi}_0)),(\vec{\mathbf{s}},(\vec{\psi},\vec{\eta}))\big) &= \mathbf{O}_{\mathrm{T}}(\vec{\mathbf{w}}-\vec{\mathbf{w}}_0;\vec{\mathbf{t}}_0,\vec{\psi}) + \mathbf{C}_{\mathrm{T}}(\vec{\chi}-\vec{\chi}_0;\vec{\xi}_0,\vec{\eta})\\
&\quad + \big(\mathcal{F}_{\vec{\chi}}-\mathcal{F}_{\vec{\chi}_0}\big)(\vec{\psi},\vec{\eta})\end{aligned}$$

for all $(\vec{\mathbf{s}},(\vec{\psi},\vec{\eta})) \in \mathbf{H}\times\mathrm{Q}$. In this way, applying the global inf-sup condition (1.55) to $(\vec{\mathbf{r}},(\vec{\varphi},\vec{\lambda})) := (\vec{\mathbf{t}},(\vec{\phi},\vec{\xi})) - (\vec{\mathbf{t}}_0,(\vec{\phi}_0,\vec{\xi}_0))$, and then employing the foregoing identity along with (1.34b) and (1.37), we obtain

$$\begin{aligned}\frac{\alpha_{\mathcal{A}}}{2}\,\|(\vec{\mathbf{t}},(\vec{\phi},\vec{\xi})) - (\vec{\mathbf{t}}_0,(\vec{\phi}_0,\vec{\xi}_0))\|_{\mathbf{H}\times\mathrm{Q}} &\le \sup_{\substack{(\vec{\mathbf{s}},(\vec{\psi},\vec{\eta}))\in\mathbf{H}\times\mathrm{Q}\\(\vec{\mathbf{s}},(\vec{\psi},\vec{\eta}))\neq\mathbf{0}}} \frac{\mathcal{A}_{\vec{\mathbf{w}},\vec{\chi}}\big((\vec{\mathbf{t}},(\vec{\phi},\vec{\xi})) - (\vec{\mathbf{t}}_0,(\vec{\phi}_0,\vec{\xi}_0)),(\vec{\mathbf{s}},(\vec{\psi},\vec{\eta}))\big)}{\|(\vec{\mathbf{s}},(\vec{\psi},\vec{\eta}))\|_{\mathbf{H}\times\mathrm{Q}}}\\
&\le \kappa^{-1}\|\vec{\mathbf{w}}-\vec{\mathbf{w}}_0\|_{\mathbf{Q}}\,\|\vec{\mathbf{t}}_0\|_{\mathbf{H}} + \widetilde{a}_1\|\vec{\chi}-\vec{\chi}_0\|_{\mathrm{M}}\|\,\|\vec{\xi}_0\|_{\mathrm{M}} + \widetilde{a}_3\|\vec{\chi}-\vec{\chi}_0\|_{\mathrm{M}},\end{aligned}$$

from which, using the bounds for $\|\vec{\mathbf{t}}_0\|_{\mathbf{H}} = \|\widehat{\mathscr{J}}_1(\vec{\mathbf{w}},\vec{\chi})\|_{\mathbf{H}}$ and $\|\vec{\xi}_0\|_{\mathrm{M}} = \|\widehat{\mathscr{J}}_3(\vec{\mathbf{w}}_0,\vec{\chi}_0)\|_{\mathrm{M}}$ provided by (1.56), we arrive at (1.60) with $\mathrm{L_T} := \dfrac{2}{\alpha_{\mathcal{A}}}\widetilde{a}_3 \max\left\{\dfrac{2}{\alpha_{\mathcal{A}}}\big(\kappa^{-1}+\widetilde{a}_1\big), 1\right\}$. ■

Having proved Lemmas 1.5 and 1.6, we are able to establish now the Lipschitz-continuity of our fixed point operator $\mathscr{J}$ in the closed ball $\mathrm{W}(\delta)$.

Lemma 1.7. *Let* $\mathrm{L_{S,1}}$, $\mathrm{L_{S,2}}$ *and* $\mathrm{L_T}$ *be the constants provided by Lemmas 1.5 and 1.6. There holds*

$$\|\mathscr{J}(\vec{\mathbf{w}},\vec{\chi}) - \mathscr{J}(\vec{\mathbf{w}}_0,\vec{\chi}_0)\|_{\mathbf{Q}\times\mathrm{M}} \leq \Big\{\mathrm{L_{S,1}}\left(\|\vec{\mathbf{g}}\|_{1/2,\Gamma_{\mathrm{out}}^{\mathrm{c}}} + a_1\delta\right) + \mathrm{L_{S,2}} + \mathrm{L_T}\left(1+\delta\right)\Big\}\, \|(\vec{\mathbf{w}},\vec{\chi}) - (\vec{\mathbf{w}}_0,\vec{\chi}_0)\|_{\mathbf{Q}\times\mathrm{M}}$$

for all $(\vec{\mathbf{w}},\vec{\chi}), (\vec{\mathbf{w}}_0,\vec{\chi}_0) \in \mathrm{W}(\delta)$.

Proof. It follows from the definition of $\mathscr{J}$ (cf. (1.32)) and the estimates (1.59) and (1.60). ■

Owing to the above analysis, we now establish the main result of this section.

Theorem 1.3. *Let us assume that the given data are sufficiently small to satisfy* (1.58)*, and*

$$\mathrm{L_{S,1}}\left(\|\vec{\mathbf{g}}\|_{1/2,\Gamma_{\mathrm{out}}^{\mathrm{c}}} + a_1\delta\right) + \mathrm{L_{S,2}} + \mathrm{L_T}\big(1+\delta\big) < 1. \tag{1.61}$$

The problem (1.24) *has a unique solution* $(\vec{\boldsymbol{\sigma}},\vec{\mathbf{u}}) \in \mathbb{H}\times\mathbf{Q}$ *and* $\big(\vec{\mathbf{t}},(\vec{\phi},\vec{\xi})\big) \in \mathbf{H}\times\mathrm{Q}$ *with* $(\vec{\mathbf{u}},\vec{\xi}) \in \mathrm{W}(\delta)$. *Moreover, there hold*

$$\|(\vec{\boldsymbol{\sigma}},\vec{\mathbf{u}})\|_{\mathbb{H}\times\mathbf{Q}} \leq \frac{2C_{\mathbf{F}}}{\alpha_{\mathbf{A}}}\Big\{\|\vec{\mathbf{g}}\|_{1/2,\Gamma_{\mathrm{out}}^{\mathrm{c}}} + a_1\delta\Big\}, \quad \textit{and} \tag{1.62}$$

$$\|(\vec{\mathbf{t}},(\vec{\phi},\vec{\xi}))\|_{\mathbf{H}\times\mathrm{Q}} \leq \frac{2}{\alpha_{\mathcal{A}}}\widetilde{a}_3\big(1+\delta\big). \tag{1.63}$$

Proof. We first recall that the choice of δ and the assumptions of Lemma 1.4 guarantee that $\mathscr{J}$ maps $\mathrm{W}(\delta)$ into itself. Then, bearing in mind the Lipschitz-continuity of $\mathscr{J} : \mathrm{W}(\delta) \to \mathrm{W}(\delta)$ given by Lemma 1.7 and the hypotheses (1.61), a straightforward application of the classical Banach fixed-point Theorem yields the existence of a unique fixed point $(\vec{\mathbf{u}},\vec{\xi}) \in \mathrm{W}(\delta)$ of this operator, and hence a unique solution of (1.24). In addition, the *a priori* estimates provided by (1.46) and (1.56), yield (1.62) and (1.63), which completes the proof. ■

1.4 The Galerkin scheme

In order to approximate the solution of our mixed variational formulation (1.24), we now introduce the associated Galerkin scheme, analyze its solvability by applying a discrete version of the fixed-point approach adopted in the previous section, and derive the corresponding *a priori* error estimate.

1.4.1 Preliminaries

Let $\mathcal{T}_h^{\mathrm{f}}$ and $\mathcal{T}_h^{\mathrm{p}}$ be the respective triangulations of the domains Ω_{f} and Ω_{p} formed by shape-regular triangles of diameter h_K and denote by h_{f} and h_{p} their corresponding meshsizes. Assume that they match on Σ so that $\mathcal{T}_h := \mathcal{T}_h^{\mathrm{f}} \cup \mathcal{T}_h^{\mathrm{p}}$ is a conforming triangulation of $\Omega := \Omega_{\mathrm{f}} \cup \Sigma \cup \Omega_{\mathrm{p}}$. Hereafter, $h := \max\{h_{\mathrm{f}},\, h_{\mathrm{p}}\}$. Now, for each $\star \in \{\mathrm{f},\mathrm{p}\}$, letting $\widetilde{\mathbb{H}}_h^{\boldsymbol{\sigma}_\star} \subseteq \mathbb{H}(\mathbf{div}_{4/3};\Omega_\star)$, selecting a set of arbitrary discrete spaces, namely

$$
\begin{array}{lll}
\mathbb{H}_h^{\boldsymbol{\sigma}_\star} := \widetilde{\mathbb{H}}_h^{\boldsymbol{\sigma}_\star} \cap \mathbb{H}_{\Gamma_{\mathrm{out}}}(\mathbf{div}_{4/3};\Omega_\star), & \mathbf{H}_h^{\mathbf{t}_\star} \subseteq \mathbf{H}(\mathrm{div}_{4/3};\Omega_\star), & \mathrm{M}_h^{\xi_\star} \subseteq \mathrm{H}_{00}^{1/2}(\Gamma_{\mathrm{in},\star}^{\mathrm{c}}), \\
\mathbf{Q}_h^{\mathbf{u}_\star} \subseteq \mathbf{L}^4(\Omega_\star), & \mathrm{X}_h^{\phi_\star} \subseteq \mathrm{L}^4(\Omega_\star), &
\end{array}
\tag{1.64}
$$

defining the global spaces

$$
\begin{array}{lll}
\mathbb{H}_h := \mathbb{H}_h^{\boldsymbol{\sigma}_{\mathrm{f}}} \times \mathbb{H}_h^{\boldsymbol{\sigma}_{\mathrm{p}}}, & \mathbf{H}_h := \mathbf{H}_h^{\mathbf{t}_{\mathrm{f}}} \times \mathbf{H}_h^{\mathbf{t}_{\mathrm{p}}}, & \mathrm{M}_h := \mathrm{M}_h^{\xi_{\mathrm{f}}} \times \mathrm{M}_h^{\xi_{\mathrm{p}}}, \\
\mathbf{Q}_h := \mathbf{Q}_h^{\mathbf{u}_{\mathrm{f}}} \times \mathbf{Q}_h^{\mathbf{u}_{\mathrm{p}}}, & \mathrm{X}_h := \mathrm{X}_h^{\phi_{\mathrm{f}}} \times \mathrm{X}_h^{\phi_{\mathrm{p}}}, & \mathrm{Q}_h := \mathrm{X}_h \times \mathrm{M}_h,
\end{array}
$$

and setting the notation

$$
\begin{array}{lll}
\vec{\boldsymbol{\tau}}_h := (\boldsymbol{\tau}_h^{\mathrm{f}}, \boldsymbol{\tau}_h^{\mathrm{p}}) \in \mathbb{H}_h, & \vec{\mathbf{s}}_h := (\mathbf{s}_h^{\mathrm{f}}, \mathbf{s}_h^{\mathrm{p}}) \in \mathbf{H}_h, & \vec{\xi}_h := (\xi_h^{\mathrm{f}}, \xi_h^{\mathrm{p}}) \in \mathrm{M}_h, \\
\vec{\mathbf{w}}_h := (\mathbf{w}_h^{\mathrm{f}}, \mathbf{w}_h^{\mathrm{p}}) \in \mathbf{Q}_h, & \vec{\psi}_h := (\psi_h^{\mathrm{f}}, \psi_h^{\mathrm{p}}) \in \mathrm{X}_h, & (\vec{\phi}_h, \vec{\xi}_h) := (\phi_h^{\mathrm{f}}, \phi_h^{\mathrm{p}}, \xi_h^{\mathrm{f}}, \xi_h^{\mathrm{p}}) \in \mathrm{Q}_h,
\end{array}
$$

the Galerkin scheme associated to (1.24) reads: Find $\big(\vec{\boldsymbol{\sigma}}_h, \vec{\mathbf{u}}_h\big) \in \mathbb{H}_h \times \mathbf{Q}_h$ and $\big(\vec{\mathbf{t}}_h, (\vec{\phi}_h, \vec{\xi}_h)\big) \in \mathbf{H}_h \times \mathrm{Q}_h$ such that

$$
\begin{array}{rlll}
\mathbf{a}_{\mathrm{S}}(\vec{\boldsymbol{\sigma}}_h, \vec{\boldsymbol{\tau}}_h) & + \mathbf{b}_{\mathrm{S}}(\vec{\boldsymbol{\tau}}_h, \vec{\mathbf{u}}_h) & & = \mathbf{F}_{\vec{\xi}_h}(\vec{\boldsymbol{\tau}}_h), \\
\mathbf{b}_{\mathrm{S}}(\vec{\boldsymbol{\sigma}}_h, \vec{\mathbf{v}}_h) & & -\mathbf{O}_{\mathrm{S}}(\vec{\mathbf{u}}_h; \vec{\boldsymbol{\sigma}}_h, \vec{\mathbf{v}}_h) & = 0, \\
\mathbf{a}_{\mathrm{T}}(\vec{\mathbf{t}}_h, \vec{\mathbf{s}}_h) & + \mathbf{b}_{\mathrm{T}}(\vec{\mathbf{s}}_h, (\vec{\phi}_h, \vec{\xi}_h)) & & = 0, \\
\mathbf{b}_{\mathrm{T}}(\vec{\mathbf{t}}_h, (\vec{\psi}_h, \vec{\eta}_h)) & -\mathbf{d}_{\mathrm{T}}((\vec{\phi}_h, \vec{\xi}_h), (\vec{\psi}_h, \vec{\eta}_h)) & -\mathbf{O}_{\mathrm{T}}(\vec{\mathbf{u}}_h; \vec{\mathbf{t}}_h, \vec{\psi}_h) - \mathbf{C}_{\mathrm{T}}(\vec{\xi}_h; \vec{\xi}_h, \vec{\eta}_h) & = \mathcal{F}_{\vec{\xi}_h}(\vec{\psi}_h, \vec{\eta}_h),
\end{array}
\tag{1.65}
$$

for all $(\vec{\boldsymbol{\tau}}_h, \vec{\mathbf{v}}_h) \in \mathbb{H}_h \times \mathbf{Q}_h$ and $(\vec{\mathbf{s}}_h, (\vec{\psi}_h, \vec{\eta}_h)) \in \mathbf{H}_h \times \mathrm{Q}_h$.

Then, we adopt the discrete version of the strategy employed in Section 1.3.1 to analyze the solvability of (1.65). To this end, we let $\widetilde{\mathcal{J}}_h : \mathbf{Q}_h \times \mathrm{M}_h \to \mathbb{H}_h \times \mathbf{Q}_h$ be the discrete operator defined by

$$
\widetilde{\mathcal{J}}_h(\vec{\mathbf{w}}_h, \vec{\chi}_h) = \big(\widetilde{\mathcal{J}}_{1,h}(\vec{\mathbf{w}}_h, \vec{\chi}_h), \widetilde{\mathcal{J}}_{2,h}(\vec{\mathbf{w}}_h, \vec{\chi}_h)\big) := (\vec{\boldsymbol{\sigma}}_h, \vec{\mathbf{u}}_h)
$$

for all $(\vec{\mathbf{w}}_h, \vec{\chi}_h) \in \mathbf{Q}_h \times \mathrm{M}_h$, where $(\vec{\boldsymbol{\sigma}}_h, \vec{\mathbf{u}}_h) \in \mathbb{H}_h \times \mathbf{Q}_h$ is the unique solution (to be confirmed in Theorem 1.4) of the following problem:

$$
\begin{array}{lll}
\mathbf{a}_{\mathrm{S}}(\vec{\boldsymbol{\sigma}}_h, \vec{\boldsymbol{\tau}}_h) + \mathbf{b}_{\mathrm{S}}(\vec{\boldsymbol{\tau}}_h, \vec{\mathbf{u}}_h) & & = \mathbf{F}_{\vec{\chi}_h}(\vec{\boldsymbol{\tau}}_h), \\
\mathbf{b}_{\mathrm{S}}(\vec{\boldsymbol{\sigma}}_h, \vec{\mathbf{v}}_h) & - \mathbf{O}_{\mathrm{S}}(\vec{\mathbf{w}}_h; \vec{\boldsymbol{\sigma}}_h, \vec{\mathbf{v}}_h) & = 0,
\end{array}
\tag{1.66}
$$

for all $(\vec{\boldsymbol{\tau}}_h, \vec{\mathbf{v}}_h) \in \mathbb{H}_h \times \mathbf{Q}_h$. In addition, we also let $\widehat{\mathcal{J}}_h : \mathbf{Q}_h \times \mathrm{M}_h \to \mathbf{H}_h \times \mathrm{Q}_h$ be the discrete operator given by

$$\widehat{\mathcal{J}}_h(\vec{\mathbf{w}}_h, \vec{\chi}_h) \;=\; \big(\widehat{\mathcal{J}}_{1,h}(\vec{\mathbf{w}}_h, \vec{\chi}_h), (\widehat{\mathcal{J}}_{2,h}(\vec{\mathbf{w}}_h, \vec{\chi}_h), \widehat{\mathcal{J}}_{3,h}(\vec{\mathbf{w}}_h, \vec{\chi}_h))\big) := (\vec{\mathbf{t}}_h, (\vec{\phi}_h, \vec{\xi}_h))$$

for all $(\vec{\mathbf{w}}_h, \vec{\chi}_h) \in \mathbf{Q}_h \times \mathrm{M}_h$, where $(\vec{\mathbf{t}}_h, (\vec{\phi}_h, \vec{\xi}_h)) \in \mathbf{H}_h \times \mathrm{Q}_h$ is the unique solution (to be confirmed in Theorem 1.5) of the following system of equations:

$$\begin{aligned} &\mathbf{a}_{\mathrm{T}}(\vec{\mathbf{t}}_h, \vec{\mathbf{s}}_h) \,+\, \mathbf{b}_{\mathrm{T}}(\vec{\mathbf{s}}_h, (\vec{\phi}_h, \vec{\xi}_h)) && = 0, \\ &\mathbf{b}_{\mathrm{T}}(\vec{\mathbf{t}}_h, (\vec{\psi}_h, \vec{\eta}_h)) - \mathbf{d}_{\mathrm{T}}((\vec{\phi}_h, \vec{\xi}_h), (\vec{\psi}_h, \vec{\eta}_h)) \,-\, \mathbf{O}_{\mathrm{T}}(\vec{\mathbf{w}}_h; \vec{\mathbf{t}}_h, \vec{\psi}_h) - \mathbf{C}_{\mathrm{T}}\big(\vec{\chi}_h; \vec{\xi}_h, \vec{\eta}_h\big) && = \mathcal{F}_{\vec{\chi}_h}(\vec{\psi}_h, \vec{\eta}_h), \end{aligned} \tag{1.67}$$

for all $(\vec{\mathbf{s}}_h, (\vec{\psi}_h, \vec{\eta}_h)) \in \mathrm{Q}_h \times \mathbf{H}_h$.

Finally, we define the operator $\mathcal{J}_h : \mathbf{Q}_h \times \mathrm{M}_h \to \mathbf{Q}_h \times \mathrm{M}_h$ as

$$\mathcal{J}_h(\vec{\mathbf{w}}_h, \vec{\chi}_h) \;=\; \big(\widetilde{\mathcal{J}}_{2,h}(\vec{\mathbf{w}}_h, \vec{\chi}_h), \widehat{\mathcal{J}}_{3,h}(\vec{\mathbf{w}}_h, \vec{\chi}_h)\big) = (\vec{\mathbf{u}}_h, \vec{\xi}_h) \quad \forall\, (\vec{\mathbf{w}}_h, \vec{\chi}_h) \in \mathbf{Q}_h \times \mathrm{M}_h, \tag{1.68}$$

and notice that solving (1.65) is equivalent to seeking a unique fixed point of $\mathcal{J}_h$, that is $(\vec{\mathbf{u}}_h, \vec{\xi}_h) \in \mathbf{Q}_h \times \mathrm{M}_h$ such that $\mathcal{J}_h(\vec{\mathbf{u}}_h, \vec{\xi}_h) = (\vec{\mathbf{u}}_h, \vec{\xi}_h)$.

1.4.2 Well-definedness of the operators $\widetilde{\mathcal{J}}_h$ and $\widehat{\mathcal{J}}_h$

In this section we proceed analogously to Sections 1.3.1 and 1.3.1 and establish the well-posedness of the discrete systems (1.66) and (1.67), equivalently that the discrete operators $\widetilde{\mathcal{J}}_h$ and $\widehat{\mathcal{J}}_h$ are well-defined. To this end, given $\star \in \{\mathrm{f}, \mathrm{p}\}$, we introduce certain hypotheses on the finite element subspaces defined above, and the discrete kernels associated with the bilinear forms $\mathbf{b}_{\mathrm{S}}$, and $\mathbf{b}_{\mathrm{T}}$, respectively, that is

$$\begin{aligned} \mathcal{K}_{\mathrm{S},h} &:= \Big\{ \vec{\boldsymbol{\tau}}_h \in \mathbb{H}_h : \quad \int_{\Omega_\star} \mathbf{v}_h^\star \cdot \mathbf{div}(\boldsymbol{\tau}_h^\star) \;=\; 0 \quad \forall\, \mathbf{v}_h^\star \in \mathbf{Q}_h^{\mathbf{u}_\star} \Big\}, \\ \mathcal{K}_{\mathrm{T},h} &:= \Big\{ \vec{\mathbf{s}}_h \in \mathbf{H}_h : \quad \int_{\Omega_\star} \psi_h^\star \mathrm{div}(\mathbf{s}_h^\star) \;=\; 0 \quad \forall\, \psi_h^\star \in \mathrm{X}_h^{\phi_\star} \quad \text{and} \quad \langle \mathbf{s}_h^\star \cdot \mathbf{n}_\star, \eta_h^\star \rangle_{\Gamma^{\mathrm{c}}_{\mathrm{in},\star}} \;=\; 0 \quad \forall\, \eta_h^\star \in \mathrm{M}_h^{\xi_\star} \Big\}. \end{aligned}$$

More precisely, from now on we assume that

(H.1) $\widetilde{\mathbb{H}}_h^{\boldsymbol{\sigma}_\star}$ contains the multiplies of the identity tensor $\mathbb{I}$,

(H.2) $\mathbf{div}(\mathbb{H}_h^{\boldsymbol{\sigma}_\star}) \;\subseteq\; \mathbf{Q}_h^{\mathbf{u}_\star}$,

(H.3) there exists a positive constant $\beta_{\mathrm{S},\mathbf{d}}$, independent of h, such that

$$\sup_{\substack{\vec{\boldsymbol{\tau}}_h \in \mathbb{H}_h \\ \vec{\boldsymbol{\tau}}_h \neq \mathbf{0}}} \frac{\mathbf{b}_{\mathrm{S}}(\vec{\boldsymbol{\tau}}_h, \vec{\mathbf{v}}_h)}{\|\vec{\boldsymbol{\tau}}_h\|_{\mathbb{H}}} \;\geq\; \beta_{\mathrm{S},\mathbf{d}}\, \|\vec{\mathbf{v}}_h\|_{\mathbf{Q}} \quad \forall\, \vec{\mathbf{v}}_h \in \mathbf{Q}_h, \tag{1.69}$$

(H.4) $\mathrm{div}(\mathbf{H}_h^{\mathbf{t}_\star}) \;\subseteq\; \mathrm{X}_h^{\phi_\star}$,

(H.5) there exists a positive constant $\beta_{\mathrm{T},\mathbf{d}}$, independent of h, such that

$$\sup_{\substack{\vec{\mathbf{s}}_h\in\mathbf{H}_h\\ \vec{\mathbf{s}}_h\neq\mathbf{0}}} \frac{\mathbf{b}_{\mathrm{T}}(\vec{\mathbf{s}}_h,(\vec{\psi}_h,\vec{\eta}_h))}{\|\vec{\mathbf{s}}_h\|_{\mathbf{H}}} \,\geq\, \beta_{\mathrm{T},\mathbf{d}}\,\|(\vec{\psi}_h,\vec{\eta}_h)\|_{\mathrm{Q}} \quad \forall\,(\vec{\psi}_h,\vec{\eta}_h)\in \mathrm{Q}_h. \tag{1.70}$$

Then, bearing in mind the assumption **(H.2)**, we find that

$$\mathcal{K}_{\mathrm{S},h} := \Big\{ \vec{\boldsymbol{\tau}}_h\in\mathbb{H}_h : \quad \mathbf{div}(\boldsymbol{\tau}_h^{\star}) = \mathbf{0} \quad \text{in} \quad \Omega_\star \Big\}.$$

In this regard, it is worth noting that the $\mathcal{K}_{\mathrm{S}}$-ellipticity of the bilinear form $\mathbf{a}_{\mathrm{S}}$, as shown in Lemma 1.1, relies solely on the divergence-free property of the tensors in $\mathcal{K}_{\mathrm{S}}$ along with the estimate (1.40). Therefore, by selecting our discrete space $\mathbb{H}_h^{\boldsymbol{\sigma}_\star} := \widetilde{\mathbb{H}}_h^{\boldsymbol{\sigma}_\star}\cap\mathbb{H}_{\Gamma_{\mathrm{out}}}(\mathbf{div}_{4/3};\Omega_\star)$, it follows that $\mathbf{a}_{\mathrm{S}}$ is also $\mathcal{K}_{\mathrm{S},h}$-elliptic with the same positive constant α_{S}, that is

$$\mathbf{a}_{\mathrm{S}}(\vec{\boldsymbol{\tau}}_h,\vec{\boldsymbol{\tau}}_h) \,\geq\, \alpha_{\mathbf{s}}\,\|\vec{\boldsymbol{\tau}}_h\|^2_{\mathbb{H}} \qquad \forall\,\vec{\boldsymbol{\tau}}_h\in\mathcal{K}_{\mathrm{S},h}. \tag{1.71}$$

In this way, **(H.3)** and (1.71), guarantee, thanks to [60, Proposition 2.42], the discrete global inf-sup condition for $\mathbf{A}$ (cf. (1.43)) with a positive constant $\alpha_{\mathbf{A},\mathbf{d}}$, depending only on α_{S}, $\beta_{\mathrm{S},\mathbf{d}}$, and $\|\mathbf{a}_{\mathrm{S}}\|$, and hence independent of h, that is

$$\sup_{\substack{(\vec{\boldsymbol{\tau}}_h,\vec{\mathbf{v}}_h)\in\mathbb{H}_h\times\mathbf{Q}_h\\ (\vec{\boldsymbol{\tau}}_h,\vec{\mathbf{v}}_h)\neq\mathbf{0}}} \frac{\mathbf{A}\big((\vec{\boldsymbol{\zeta}}_h,\vec{\mathbf{z}}_h),(\vec{\boldsymbol{\tau}}_h,\vec{\mathbf{v}}_h)\big)}{\|(\vec{\boldsymbol{\tau}}_h,\vec{\mathbf{v}}_h)\|_{\mathbb{H}\times\mathbf{Q}}} \,\geq\, \alpha_{\mathbf{A},\mathbf{d}}\,\|(\vec{\boldsymbol{\zeta}}_h,\vec{\mathbf{z}}_h)\|_{\mathbb{H}\times\mathbf{Q}} \qquad \forall\,(\vec{\boldsymbol{\zeta}}_h,\vec{\mathbf{z}}_h)\in\mathbb{H}_h\times\mathbf{Q}_h, \tag{1.72}$$

so that, for each $\vec{\mathbf{w}}_h\in\mathbf{Q}_h$ such that $\|\vec{\mathbf{w}}_h\|_{\mathbf{Q}} \leq \dfrac{\nu\,\alpha_{\mathbf{A},\mathbf{d}}}{2\,\rho}$, there holds

$$\sup_{\substack{(\vec{\boldsymbol{\tau}}_h,\vec{\mathbf{v}}_h)\in\mathbb{H}_h\times\mathbf{Q}_h\\ (\vec{\boldsymbol{\tau}}_h,\vec{\mathbf{v}}_h)\neq\mathbf{0}}} \frac{\mathbf{A}_{\vec{\mathbf{w}}_h}\big((\vec{\boldsymbol{\zeta}}_h,\vec{\mathbf{z}}_h),(\vec{\boldsymbol{\tau}}_h,\vec{\mathbf{v}}_h)\big)}{\|(\vec{\boldsymbol{\tau}}_h,\vec{\mathbf{v}}_h)\|_{\mathbb{H}\times\mathbf{Q}}} \,\geq\, \frac{\alpha_{\mathbf{A},\mathbf{d}}}{2}\,\|(\vec{\boldsymbol{\zeta}}_h,\vec{\mathbf{z}}_h)\|_{\mathbb{H}\times\mathbf{Q}} \qquad \forall\,(\vec{\boldsymbol{\zeta}}_h,\vec{\mathbf{z}}_h)\in\mathbb{H}_h\times\mathbf{Q}_h. \tag{1.73}$$

Consequently, we are now in position to establish the discrete analogue of Theorem 1.1.

Theorem 1.4. *For each $\vec{\mathbf{w}}_h\in\mathbf{Q}_h$, and $\vec{\chi}_h\in\mathrm{M}_h$ such that $\|\vec{\mathbf{w}}_h\|_{\mathbf{Q}} \leq \dfrac{\nu\,\alpha_{\mathbf{A},\mathbf{d}}}{2\,\rho}$, there exists a unique $(\vec{\boldsymbol{\sigma}}_h,\vec{\mathbf{u}}_h)\in\mathbb{H}_h\times\mathbf{Q}_h$ solution to (1.66), equivalently*

$$\mathbf{A}_{\vec{\mathbf{w}}_h}\big((\vec{\boldsymbol{\sigma}}_h,\vec{\mathbf{u}}_h),(\vec{\boldsymbol{\tau}}_h,\vec{\mathbf{v}}_h)\big) \,=\, \mathbf{F}_{\vec{\chi}_h}(\vec{\boldsymbol{\tau}}_h) \qquad \forall\,(\vec{\boldsymbol{\tau}}_h,\vec{\mathbf{v}}_h)\in\mathbb{H}_h\times\mathbf{Q}_h. \tag{1.74}$$

Moreover, there holds

$$\|\widetilde{\mathcal{J}}_h(\vec{\mathbf{w}}_h,\,\vec{\chi}_h)\|_{\mathbb{H}\times\mathbf{Q}} \,=\, \|(\vec{\boldsymbol{\sigma}}_h,\vec{\mathbf{u}}_h)\|_{\mathbb{H}\times\mathbf{Q}} \,\leq\, \frac{2C_{\mathbf{F}}}{\alpha_{\mathbf{A},\mathbf{d}}}\Big\{\|\vec{\mathbf{g}}\|_{1/2,\Gamma^{\mathrm{c}}_{\mathrm{out}}} + a_1\|\vec{\chi}_h\|_{\mathrm{M}}\Big\}. \tag{1.75}$$

Proof. Let $(\vec{\mathbf{w}}_h,\vec{\chi}_h)\in\mathbf{Q}_h\times\mathrm{M}_h$, such that $\|\vec{\mathbf{w}}_h\|_{\mathbf{Q}} \leq \dfrac{\nu\,\alpha_{\mathbf{A},\mathbf{d}}}{2\,\rho}$. Analogously to the continuous case, we find that $\mathbf{A}_{\vec{\mathbf{w}}_h}$ (cf. (1.73)) satisfies the hypotheses of the discrete Banach–Nečas–Babuška theorem [60, Theorem 2.22], and then we conclude the existence of a unique $(\vec{\boldsymbol{\sigma}}_h,\vec{\mathbf{u}}_h)\in\mathbb{H}_h\times\mathbf{Q}_h$ solution to (1.74).

In addition, the *a priori* error estimates (1.75) is consequence of (1.74), (1.73) and the boundedness of $\mathbf{F}_{\vec{\chi}_h}$ (cf. (1.36)). ■

Similarly, thanks to **(H.4)**, it is easy to see that $\mathcal{K}_{\mathrm{T},h}$ can be characterized as

$$\mathcal{K}_{\mathrm{T},h} := \left\{ \vec{\mathbf{s}}_h := (\mathbf{s}_h^{\mathrm{f}}, \mathbf{s}_h^{\mathrm{p}}) \in \mathbf{H}_h : \quad \operatorname{div}(\mathbf{s}_h^{\star}) = 0 \quad \text{in} \quad \Omega_{\star} \quad \text{and} \quad \langle \mathbf{s}_h^{\star} \cdot \mathbf{n}_{\star}, \eta_h^{\star} \rangle_{\Gamma_{\mathrm{in},\star}^{\mathrm{c}}} = 0 \quad \forall\, \eta_h^{\star} \in \mathrm{M}_h^{\xi_\star} \right\},$$

and hence $\mathbf{a}_{\mathrm{T}}(\vec{\mathbf{s}}_h, \vec{\mathbf{s}}_h) \geq \frac{1}{2\kappa} \|\vec{\mathbf{s}}_h\|_{\mathbf{H}}^2$ for all $\vec{\mathbf{s}}_h \in \mathcal{K}_{\mathrm{T},h}$. In turn, knowing from the continuous analysis that $\mathbf{d}_{\mathrm{T}}$ is positive semi-definite in Q (cf. (1.47)), this property is also true in Q_h. Hence, bearing in mind **(H.5)**, a straightforward application of [50, Theorem 3.5] implies the discrete global inf-sup condition for $\mathcal{A}$ (cf. (1.51)) with a positive constant $\alpha_{\mathcal{A},\mathbf{d}}$, depending on $\|\mathbf{a}_{\mathrm{T}}\|$, α_{T}, $\|\mathbf{d}_{\mathrm{T}}\|$, and $\beta_{\mathrm{T},\mathbf{d}}$, and thus the same property is shared by $\mathcal{A}_{\vec{\mathbf{w}}_h,\vec{\chi}_h}$ (cf. (1.52)) for each $(\vec{\mathbf{w}}_h, \vec{\chi}_h) \in \mathbf{Q}_h \times \mathrm{M}_h$ such that $\|(\vec{\mathbf{w}}_h, \vec{\chi}_h)\|_{\mathbf{Q}\times\mathrm{M}} \leq \dfrac{\kappa\alpha_{\mathcal{A},\mathbf{d}}}{2(1+\kappa\widetilde{a}_1)}$, that is

$$\sup_{\substack{(\vec{\mathbf{s}}_h,(\vec{\psi}_h,\vec{\eta}_h))\in\mathbf{H}_h\times\mathrm{Q}_h \\ (\vec{\mathbf{s}}_h,(\vec{\psi}_h,\vec{\eta}_h))\neq\mathbf{0}}} \frac{\mathcal{A}_{\vec{\mathbf{w}}_h,\vec{\chi}_h}\big((\vec{\mathbf{r}}_h,(\vec{\varphi}_h,\vec{\lambda}_h)),(\vec{\mathbf{s}}_h,(\vec{\psi}_h,\vec{\eta}_h))\big)}{\|(\vec{\mathbf{s}}_h,(\vec{\psi}_h,\vec{\eta}_h))\|_{\mathbf{H}\times\mathrm{Q}}} \geq \frac{\alpha_{\mathcal{A},\mathbf{d}}}{2} \|(\vec{\mathbf{r}}_h,(\vec{\varphi}_h,\vec{\lambda}_h))\|_{\mathbf{H}\times\mathrm{Q}} \tag{1.76}$$

for all $(\vec{\mathbf{r}}_h,(\vec{\varphi}_h,\vec{\lambda}_h)) \in \mathbf{H}_h \times \mathrm{Q}_h$.

In this way, we are now in a position to establish the discrete analogue of Theorem 1.2.

Theorem 1.5. *For each $(\vec{\mathbf{w}}_h, \vec{\chi}_h) \in \mathbf{Q}_h \times \mathrm{M}_h$ such that $\|(\vec{\mathbf{w}}_h, \vec{\chi}_h)\|_{\mathbf{Q}\times\mathrm{M}} \leq \dfrac{\kappa\alpha_{\mathcal{A},\mathbf{d}}}{2(1+\kappa\widetilde{a}_1)}$, there exists a unique $(\vec{\mathbf{t}}_h,(\vec{\phi}_h,\vec{\xi}_h)) = \widehat{\mathcal{J}}_h(\vec{\mathbf{w}}_h,\vec{\chi}_h) \in \mathbf{H}_h \times \mathrm{Q}_h$ solution to (1.67). Moreover, there holds*

$$\|\widehat{\mathcal{J}}_h(\vec{\mathbf{w}}_h,\vec{\chi}_h)\|_{\mathbf{H}\times\mathrm{Q}} = \|(\vec{\mathbf{t}}_h,(\vec{\phi}_h,\vec{\xi}_h))\|_{\mathbf{H}\times\mathrm{Q}} \leq \frac{2}{\alpha_{\mathcal{A},\mathbf{d}}}\widetilde{a}_3\big(1+\|\vec{\chi}_h\|_{\mathrm{M}}\big). \tag{1.77}$$

Proof. It reduces to a direct application of [60, Theorem 2.22]. In particular, the *a priori* estimate (1.77) follows from (1.76) and the fact that, according to (1.37), there holds $\|\mathcal{F}_{\vec{\chi}_h}\| \leq \widetilde{a}_3\left(1+\|\vec{\chi}_h\|_{\mathrm{M}}\right)$. ■

1.4.3 Discrete solvability analysis

Having established that the discrete operators $\widetilde{\mathcal{J}}_h$, $\widehat{\mathcal{J}}_h$, and hence $\mathcal{J}_h$ are well defined, we now address the solvability of the fixed-point equation (1.68). For that, we set $\delta_{\mathbf{d}} := \min\left\{ \dfrac{\nu\alpha_{\mathbf{A},\mathbf{d}}}{2\,\rho}, \dfrac{\kappa\alpha_{\mathcal{A},\mathbf{d}}}{2(1+\kappa\widetilde{a}_1)} \right\}$, and define

$$\mathrm{W}(\delta_{\mathbf{d}}) := \Big\{ (\vec{\mathbf{w}}_h,\vec{\chi}_h) \in \mathbf{Q}_h \times \mathrm{M}_h : \quad \|(\vec{\mathbf{w}}_h,\vec{\chi}_h)\|_{\mathbf{Q}\times\mathrm{M}} \leq \delta_{\mathbf{d}} \Big\}, \tag{1.78}$$

to provide sufficient conditions under which $\mathcal{J}_h$ maps $\mathrm{W}(\delta_{\mathbf{d}})$ into itself. More precisely, we have the following result.

Lemma 1.8. *If*

$$C_{\mathbf{F}}\Big\{ \|\vec{\mathbf{g}}\|_{1/2,\Gamma_{\mathrm{out}}^{\mathrm{c}}} + a_1\delta_{\mathbf{d}} \Big\} \leq \frac{\alpha_{\mathbf{A},\mathbf{d}}}{4}\delta_{\mathbf{d}}, \quad \text{and} \quad \widetilde{a}_3\big(1+\delta_{\mathbf{d}}\big) \leq \frac{\alpha_{\mathcal{A},\mathbf{d}}}{4}\delta_{\mathbf{d}}, \tag{1.79}$$

then $\mathcal{J}_h\big(\mathrm{W}(\delta_{\mathbf{d}})\big) \subseteq \mathrm{W}(\delta_{\mathbf{d}})$.

Proof. It follows analogously to the proof of Lemma 1.4, but now using the well-posedness and associated *a priori* estimates of $\widetilde{\mathcal{J}}_h$ and $\widehat{\mathcal{J}}_h$ provided by Theorems 1.4 and 1.5, respectively. ∎

Next, we establish the Lipschitz-continuity properties of $\widetilde{\mathcal{J}}_h$ and $\widehat{\mathcal{J}}_h$.

Lemma 1.9. *There exist positive constants* $\mathrm{L}^1_{\mathrm{S},\mathbf{d}}$ *and* $\mathrm{L}^2_{\mathrm{S},\mathbf{d}}$ *depending only on* ν, ρ, $\alpha_{\mathbf{A},\mathbf{d}}$, a_1, *and* $C_{\mathbf{F}}$ *such that*

$$\|\widetilde{\mathcal{J}}_h(\vec{\mathbf{w}}_h,\vec{\chi}_h) - \widetilde{\mathcal{J}}_h(\vec{\mathbf{w}}_{0,h},\vec{\chi}_{0,h})\|_{\mathbb{H}\times\mathbf{Q}} \le \Big\{\mathrm{L}^1_{\mathrm{S},\mathbf{d}}\left(\|\vec{\mathbf{g}}\|_{1/2,\Gamma^{\mathrm{c}}_{\mathrm{out}}} + a_1\delta_{\mathbf{d}}\right) + \mathrm{L}^2_{\mathrm{S},\mathbf{d}}\Big\}\, \|(\vec{\mathbf{w}}_h,\vec{\chi}_h) - (\vec{\mathbf{w}}_{0,h},\vec{\chi}_{0,h})\|_{\mathbf{Q}\times\mathrm{M}}$$

for all $(\vec{\mathbf{w}}_h,\vec{\chi}_h), (\vec{\mathbf{w}}_{0,h},\vec{\chi}_{0,h}) \in \mathrm{W}(\delta_{\mathbf{d}})$.

Proof. It follows analogously to the proof of Lemma 1.5, using now the discrete inf-sup condition satisfied by $\mathbf{A}_{\vec{\mathbf{w}}_h}$ (cf. (1.73)) with constant $\dfrac{\alpha_{\mathbf{A},\mathbf{d}}}{2}$. ∎

Lemma 1.10. *There exists a positive constant* $\mathrm{L}_{\mathrm{T},\mathbf{d}}$, *depending only on* $\alpha_{\mathcal{A},\mathbf{d}}$, $\widetilde{a}_1$, $\widetilde{a}_3$ *and* κ, *such that*

$$\|\widehat{\mathcal{J}}_h(\vec{\mathbf{w}}_h,\vec{\chi}_h) - \widehat{\mathcal{J}}_h(\vec{\mathbf{w}}_{0,h},\vec{\chi}_{0,h})\|_{\mathbf{H}\times\mathrm{Q}} \,\le\, \mathrm{L}_{\mathrm{T},\mathbf{d}}\left(1+\delta_{\mathbf{d}}\right)\|(\vec{\mathbf{w}}_h,\vec{\chi}_h) - (\vec{\mathbf{w}}_{0,h},\vec{\chi}_{0,h})\|_{\mathbf{Q}\times\mathrm{M}}$$

for all $(\vec{\mathbf{w}}_h,\vec{\chi}_h), (\vec{\mathbf{w}}_{0,h},\vec{\chi}_{0,h}) \in \mathrm{W}(\delta_{\mathbf{d}})$.

Proof. It follows very closely to the arguments from the proof of Lemma 1.6, employing now the discrete inf-sup condition satisfied by $\mathcal{A}_{\vec{\mathbf{w}}_h,\vec{\chi}_h}$ (cf. (1.76)) with constant $\dfrac{\alpha_{\mathcal{A},\mathbf{d}}}{2}$. ∎

As a consequence, we are able to establish the Lipschitz-continuity of the operator $\mathcal{J}_h$.

Lemma 1.11. *Let* $\mathrm{L}^1_{\mathrm{S},\mathbf{d}}$, $\mathrm{L}^2_{\mathrm{S},\mathbf{d}}$ *and* $\mathrm{L}_{\mathrm{T},\mathbf{d}}$ *be the constants provided by Lemmas 1.9 and 1.10. There holds*

$$\begin{aligned}&\|\mathcal{J}_h(\vec{\mathbf{w}}_h,\vec{\chi}_h) - \mathcal{J}_h(\vec{\mathbf{w}}_{0,h},\vec{\chi}_{0,h})\|_{\mathbf{Q}\times\mathrm{M}}\\ &\quad\le \Big\{\mathrm{L}^1_{\mathrm{S},\mathbf{d}}\big(\|\vec{\mathbf{g}}\|_{1/2,\Gamma^{\mathrm{c}}_{\mathrm{out}}} + a_1\delta_{\mathbf{d}}\big) + \mathrm{L}^2_{\mathrm{S},\mathbf{d}} + \mathrm{L}_{\mathrm{T},\mathbf{d}}\big(1+\delta_{\mathbf{d}}\big)\Big\}\|(\vec{\mathbf{w}}_h,\vec{\chi}_h) - (\vec{\mathbf{w}}_{0,h},\vec{\chi}_{0,h})\|_{\mathbf{Q}\times\mathrm{M}}\end{aligned} \tag{1.80}$$

for all $(\vec{\mathbf{w}}_h,\vec{\chi}_h), (\vec{\mathbf{w}}_{0,h},\vec{\chi}_{0,h}) \in \mathrm{W}(\delta_{\mathbf{d}})$.

Proof. Given $(\vec{\mathbf{w}}_h,\vec{\chi}_h), (\vec{\mathbf{w}}_{0,h},\vec{\chi}_{0,h}) \in \mathrm{W}(\delta_{\mathbf{d}})$, it suffices to employ the definition of $\mathcal{J}_h$ (cf. (1.68)), and the upper bounds of Lemmas 1.9 and 1.10. ∎

According to the above, the main result of this section is establish as follows.

Theorem 1.6. *If the given data are sufficiently small to satisfy* (1.79), *then the problem* (1.65) *has at least one solution* $(\vec{\boldsymbol{\sigma}}_h,\vec{\mathbf{u}}_h) \in \mathbb{H}_h \times \mathbf{Q}_h$ *and* $(\vec{\mathbf{t}}_h,(\vec{\phi}_h,\vec{\xi}_h)) \in \mathbf{H}_h \times \mathrm{Q}_h$ *with* $(\vec{\mathbf{u}}_h,\vec{\xi}_h) \in \mathrm{W}(\delta_{\mathbf{d}})$. *Moreover, under the further assumption*

$$\mathrm{L}^1_{\mathrm{S},\mathbf{d}}\left(\|\vec{\mathbf{g}}\|_{1/2,\Gamma^{\mathrm{c}}_{\mathrm{out}}} + a_1\delta_{\mathbf{d}}\right) + \mathrm{L}^2_{\mathrm{S},\mathbf{d}} + \mathrm{L}_{\mathrm{T},\mathbf{d}}\left(1+\delta_{\mathbf{d}}\right) \,<\, 1, \tag{1.81}$$

this solution is unique. In addition, in both cases there hold

$$\|(\vec{\boldsymbol{\sigma}}_h, \vec{\mathbf{u}}_h)\|_{\mathbb{H}\times\mathbf{Q}} \leq \frac{2C_{\mathbf{F}}}{\alpha_{\mathbf{A},\mathbf{d}}}\Big\{\|\vec{\mathbf{g}}\|_{1/2,\Gamma_{\rm out}^{\rm c}} + a_1\delta_{\mathbf{d}}\Big\}, \quad \textit{and} \tag{1.82}$$

$$\|(\vec{\mathbf{t}}_h, (\vec{\phi}_h, \vec{\xi}_h))\|_{\mathbf{H}\times\mathrm{Q}} \leq \frac{2}{\alpha_{\mathcal{A},\mathbf{d}}}\widetilde{a}_3\big(1+\delta_{\mathbf{d}}\big). \tag{1.83}$$

Proof. We first notice that the assumptions of Lemma 1.8 guarantee that $\mathcal{J}_h$ maps $\mathrm{W}(\delta_{\mathbf{d}})$ into itself. Then, the continuity of $\mathcal{J}_h : \mathrm{W}(\delta_{\mathbf{d}}) \to \mathrm{W}(\delta_{\mathbf{d}})$ (cf. (1.80)) and a straightforward application of the Brouwer Theorem (cf. [40, Theorem 9.9-2]) implies the existence of at least one solution $(\vec{\mathbf{u}}_h, \vec{\xi}_h) \in \mathrm{W}(\delta_{\mathbf{d}})$ to (1.65). Next, the uniqueness of solution is a consequence of the Banach fixed-point Theorem and assumption (1.81). Finally, thanks to the *a priori* estimates (1.75) and (1.77), we obtain (1.82) and (1.83). ■

1.4.4 *A priori* error analysis

We consider finite element subspaces satisfying the assumptions specified in Section 1.4.2, and derive the Céa estimate for the Galerkin error $\mathtt{E} := \mathtt{E}_{\rm S} + \mathtt{E}_{\rm T}$, where

$$\mathtt{E}_{\rm S} := \|(\vec{\boldsymbol{\sigma}}, \vec{\mathbf{u}}) - (\vec{\boldsymbol{\sigma}}_h, \vec{\mathbf{u}}_h)\|_{\mathbb{H}\times\mathbf{Q}} \quad \text{and} \quad \mathtt{E}_{\rm T} := \|(\vec{\mathbf{t}}, (\vec{\phi}, \vec{\xi})) - (\vec{\mathbf{t}}_h, (\vec{\phi}_h, \vec{\xi}_h))\|_{\mathbf{H}\times\mathrm{Q}},$$

and $(\vec{\boldsymbol{\sigma}}, \vec{\mathbf{u}}) \in \mathbb{H}\times\mathbf{Q}$, $(\vec{\mathbf{t}}, (\vec{\phi}, \vec{\xi})) \in \mathbf{H}\times\mathrm{Q}$ and $(\vec{\boldsymbol{\sigma}}_h, \vec{\mathbf{u}}_h) \in \mathbb{H}_h\times\mathbf{Q}_h$, $(\vec{\mathbf{t}}_h, (\vec{\phi}_h, \vec{\xi}_h)) \in \mathbf{H}_h\times\mathrm{Q}_h$ are the unique solutions to (1.24) and (1.65), respectively, with $(\vec{\mathbf{u}}, \vec{\xi}) \in \mathrm{W}(\delta)$ (cf. (1.57)) and $(\vec{\mathbf{u}}_h, \vec{\xi}_h) \in \mathrm{W}(\delta_{\mathbf{d}})$ (cf. (1.78)). In what follows, given a subspace Z_h of an arbitrary Banach space $\big(Z, \|\cdot\|_Z\big)$, we set

$$\mathrm{dist}\big(z, Z_h\big) := \inf_{z_h\in Z_h}\|z - z_h\|_Z \qquad \forall\, z \in Z.$$

Now, using (1.42) and (1.53), we observe that (1.24) and (1.65) can be rewritten as the following pairs of continuous formulations and their associated discrete counterparts

$$\begin{aligned}\mathbf{A}\big((\vec{\boldsymbol{\sigma}}, \vec{\mathbf{u}}), (\vec{\boldsymbol{\tau}}, \vec{\mathbf{v}})\big) &= \mathbf{O}_{\rm S}(\vec{\mathbf{u}}; \vec{\boldsymbol{\sigma}}, \vec{\mathbf{v}}) + \mathbf{F}_{\vec{\xi}}(\vec{\boldsymbol{\tau}}),\\ \mathbf{A}\big((\vec{\boldsymbol{\sigma}}_h, \vec{\mathbf{u}}_h), (\vec{\boldsymbol{\tau}}_h, \vec{\mathbf{v}}_h)\big) &= \mathbf{O}_{\rm S}(\vec{\mathbf{u}}_h; \vec{\boldsymbol{\sigma}}_h, \vec{\mathbf{v}}_h) + \mathbf{F}_{\vec{\xi}_h}(\vec{\boldsymbol{\tau}}_h)\end{aligned} \tag{1.84}$$

for all $(\vec{\boldsymbol{\tau}}, \vec{\mathbf{v}}) \in \mathbb{H}\times\mathbf{Q}$ and $(\vec{\boldsymbol{\tau}}_h, \vec{\mathbf{v}}_h) \in \mathbb{H}_h\times\mathbf{Q}_h$, and

$$\begin{aligned}\mathcal{A}\big((\vec{\mathbf{t}}, (\vec{\phi}, \vec{\xi})), (\vec{\mathbf{s}}, (\vec{\psi}, \vec{\eta}))\big) &= \mathbf{O}_{\rm T}(\vec{\mathbf{u}}; \vec{\mathbf{t}}, \vec{\psi}) + \mathbf{C}_{\rm T}(\vec{\xi}; \vec{\xi}, \vec{\eta}) + \mathcal{F}_{\vec{\xi}}(\vec{\psi}, \vec{\eta}),\\ \mathcal{A}\big((\vec{\mathbf{t}}_h, (\vec{\phi}_h, \vec{\xi}_h)), (\vec{\mathbf{s}}_h, (\vec{\psi}_h, \vec{\eta}_h))\big) &= \mathbf{O}_{\rm T}(\vec{\mathbf{u}}_h; \vec{\mathbf{t}}_h, \vec{\psi}_h) + \mathbf{C}_{\rm T}(\vec{\xi}_h; \vec{\xi}_h, \vec{\eta}_h) + \mathcal{F}_{\vec{\xi}_h}(\vec{\psi}_h, \vec{\eta}_h)\end{aligned} \tag{1.85}$$

for all $(\vec{\mathbf{s}}, (\vec{\psi}, \vec{\eta})) \in \mathbf{H}\times\mathrm{Q}$ and $(\vec{\mathbf{s}}_h, (\vec{\psi}_h, \vec{\eta}_h)) \in \mathbf{H}_h\times\mathrm{Q}_h$.

Then, from (1.84), it is easy to see that for each $(\vec{\boldsymbol{\tau}}_h, \vec{\mathbf{v}}_h) \in \mathbb{H}_h\times\mathbf{Q}_h$, there holds

$$\mathbf{A}\left((\vec{\boldsymbol{\sigma}}, \vec{\mathbf{u}}) - (\vec{\boldsymbol{\sigma}}_h, \vec{\mathbf{u}}_h), (\vec{\boldsymbol{\tau}}_h, \vec{\mathbf{v}}_h)\right) = \mathbf{O}_{\rm S}(\vec{\mathbf{u}}; \vec{\boldsymbol{\sigma}}, \vec{\mathbf{v}}_h) - \mathbf{O}_{\rm S}(\vec{\mathbf{u}}_h; \vec{\boldsymbol{\sigma}}_h, \vec{\mathbf{v}}_h) + \big(\mathbf{F}_{\vec{\xi}} - \mathbf{F}_{\vec{\xi}_h}\big)(\vec{\boldsymbol{\tau}}_h),$$

whence, subtracting and adding $\vec{\boldsymbol{\sigma}}_h$ in the second component of the first term, invoking the boundedness properties of $\mathbf{O}_{\rm S}$ (cf. (1.34a)), $\mathbf{F}_{\vec{\xi}} - \mathbf{F}_{\vec{\xi}_h}$ (cf. (1.36)), and the *a priori* estimates (cf. (1.62) and (1.82)) for $\|\vec{\mathbf{u}}\|_{\mathbf{Q}}$ and $\|\vec{\boldsymbol{\sigma}}_h\|_{\mathbb{H}}$, respectively, we obtain for each $(\vec{\boldsymbol{\tau}}_h, \vec{\mathbf{v}}_h) \in \mathbb{H}_h \times \mathbf{Q}_h$

$$\begin{aligned} &\mathbf{A}\left((\vec{\boldsymbol{\sigma}}, \vec{\mathbf{u}}) - (\vec{\boldsymbol{\sigma}}_h, \vec{\mathbf{u}}_h), (\vec{\boldsymbol{\tau}}_h, \vec{\mathbf{v}}_h)\right) \\ &\quad \leq \left\{\frac{\rho}{\nu}\|\vec{\mathbf{u}}\|_{\mathbf{Q}}\|\vec{\boldsymbol{\sigma}} - \vec{\boldsymbol{\sigma}}_h\|_{\mathbb{H}} + \frac{\rho}{\nu}\|\vec{\boldsymbol{\sigma}}\|_{\mathbb{H}}\|\vec{\mathbf{u}} - \vec{\mathbf{u}}_h\|_{\mathbf{Q}} + a_1 C_{\mathbf{F}}\|\vec{\xi} - \vec{\xi}_h\|_{\mathrm{M}}\right\}\|(\vec{\boldsymbol{\tau}}_h, \vec{\mathbf{v}}_h)\|_{\mathbb{H}\times\mathbf{Q}}. \end{aligned} \tag{1.86}$$

Now, the triangle inequality gives for each $(\vec{\boldsymbol{\zeta}}_h, \vec{\mathbf{z}}_h) \in \mathbb{H}_h \times \mathbf{Q}_h$

$$\mathtt{E}_{\mathrm{S}} \leq \|(\vec{\boldsymbol{\sigma}}, \vec{\mathbf{u}}) - (\vec{\boldsymbol{\zeta}}_h, \vec{\mathbf{z}}_h)\|_{\mathbb{H}\times\mathbf{Q}} + \|(\vec{\boldsymbol{\zeta}}_h, \vec{\mathbf{z}}_h) - (\vec{\boldsymbol{\sigma}}_h, \vec{\mathbf{u}}_h)\|_{\mathbb{H}\times\mathbf{Q}}, \tag{1.87}$$

and then, applying (1.72), subtracting and adding $(\vec{\boldsymbol{\sigma}}, \vec{\mathbf{u}})$ in the first component of $\mathbf{A}$, and using the boundedness of $\mathbf{A}$ with constant $\|\mathbf{A}\|$, which depends on $\|\mathbf{a}_{\mathrm{S}}\|$, and $\|\mathbf{b}_{\mathrm{S}}\|$ (cf. (1.33)), we find that

$$\begin{aligned} \alpha_{\mathbf{A},\mathbf{d}}\|(\vec{\boldsymbol{\zeta}}_h, \vec{\mathbf{z}}_h) - (\vec{\boldsymbol{\sigma}}_h, \vec{\mathbf{u}}_h)\|_{\mathbb{H}\times\mathbf{Q}} &\leq \sup_{\substack{(\vec{\boldsymbol{\tau}}_h, \vec{\mathbf{v}}_h) \in \mathbb{H}_h \times \mathbf{Q}_h \\ (\vec{\boldsymbol{\tau}}_h, \vec{\mathbf{v}}_h) \neq \mathbf{0}}} \frac{\mathbf{A}\big((\vec{\boldsymbol{\zeta}}_h, \vec{\mathbf{z}}_h) - (\vec{\boldsymbol{\sigma}}_h, \vec{\mathbf{u}}_h), (\vec{\boldsymbol{\tau}}_h, \vec{\mathbf{v}}_h)\big)}{\|(\vec{\boldsymbol{\tau}}_h, \vec{\mathbf{v}}_h)\|_{\mathbb{H}\times\mathbf{Q}}} \\ &\leq \|\mathbf{A}\|\|(\vec{\boldsymbol{\sigma}}, \vec{\mathbf{u}}) - (\vec{\boldsymbol{\zeta}}_h, \vec{\mathbf{z}}_h)\|_{\mathbb{H}\times\mathbf{Q}} + \sup_{\substack{(\vec{\boldsymbol{\tau}}_h, \vec{\mathbf{v}}_h) \in \mathbb{H}_h \times \mathbf{Q}_h \\ (\vec{\boldsymbol{\tau}}_h, \vec{\mathbf{v}}_h) \neq \mathbf{0}}} \frac{\mathbf{A}\big((\vec{\boldsymbol{\sigma}}, \vec{\mathbf{u}}) - (\vec{\boldsymbol{\sigma}}_h, \vec{\mathbf{u}}_h), (\vec{\boldsymbol{\tau}}_h, \vec{\mathbf{v}}_h)\big)}{\|(\vec{\boldsymbol{\tau}}_h, \vec{\mathbf{v}}_h)\|_{\mathbb{H}\times\mathbf{Q}}}. \end{aligned}$$

In this way, inserting (1.86) into the supremum and replacing the resulting estimate in (1.87), and the fact that $(\vec{\boldsymbol{\zeta}}_h, \vec{\mathbf{z}}_h)$ is arbitrary, we conclude that there exists a positive constant $C_{\mathtt{ST}}$ depending only on ρ, ν, $\alpha_{\mathbf{A},\mathbf{d}}$, and hence independent of h, such that

$$\mathtt{E}_{\mathrm{S}} \leq C_{\mathtt{ST}}\Big\{\mathrm{dist}\big((\vec{\boldsymbol{\sigma}}, \vec{\mathbf{u}}), \mathbb{H}_h \times \mathbf{Q}_h\big) + \|\vec{\mathbf{u}}\|_{\mathbf{Q}}\|\vec{\boldsymbol{\sigma}} - \vec{\boldsymbol{\sigma}}_h\|_{\mathbb{H}} + \|\vec{\boldsymbol{\sigma}}\|_{\mathbb{H}}\|\vec{\mathbf{u}} - \vec{\mathbf{u}}_h\|_{\mathbf{Q}} + a_1 C_{\mathbf{F}}\|\vec{\xi} - \vec{\xi}_h\|_{\mathrm{M}}\Big\}. \tag{1.88}$$

Similarly, for each $(\vec{\mathbf{s}}_h, (\vec{\psi}_h, \vec{\eta}_h)) \in \mathbf{H}_h \times \mathrm{Q}_h$, from (1.85), we deduce that

$$\begin{aligned} &\mathcal{A}\big((\vec{\mathbf{t}}, (\vec{\phi}, \vec{\xi})) - (\vec{\mathbf{t}}_h, (\vec{\phi}_h, \vec{\xi}_h)), (\vec{\mathbf{s}}_h, (\vec{\psi}_h, \vec{\eta}_h))\big) \\ &\quad = \mathbf{O}_{\mathrm{T}}(\vec{\mathbf{u}}; \vec{\mathbf{t}}, \vec{\psi}_h) + \mathbf{C}_{\mathrm{T}}(\vec{\xi}; \vec{\xi}, \vec{\eta}_h) - \mathbf{O}_{\mathrm{T}}(\vec{\mathbf{u}}_h; \vec{\mathbf{t}}_h, \vec{\psi}_h) - \mathbf{C}_{\mathrm{T}}(\vec{\xi}_h; \vec{\xi}_h, \vec{\eta}_h) + \big(\mathcal{F}_{\vec{\xi}} - \mathcal{F}_{\vec{\xi}_h}\big)(\vec{\psi}_h, \vec{\eta}_h), \end{aligned}$$

from which, subtracting and adding $\vec{\mathbf{t}}_h$ and $\vec{\xi}_h$ in the second component of the first and second terms, respectively, invoking the boundedness properties of $\mathbf{O}_{\mathrm{T}}$, $\mathbf{C}_{\mathrm{T}}$, and $\mathcal{F}_{\vec{\xi}} - \mathcal{F}_{\vec{\xi}_h}$, the a priori estimates (cf. (1.63) and (1.82)), we proceed exactly as in the previous case for $\mathtt{E}_{\mathrm{S}}$, and realize that there exists a positive constant $C_{\mathtt{TT}}$, depending only on $\|\mathcal{A}\|$, $\alpha_{\mathcal{A},\mathbf{d}}$, $\widetilde{a}_1$ and κ, and hence independent of h, such that

$$\begin{aligned} \mathtt{E}_{\mathrm{T}} \leq C_{\mathtt{TT}}\Big\{&\mathrm{dist}\big((\vec{\mathbf{t}}, \vec{\phi}, \vec{\xi}), \mathbf{H}_h \times \mathrm{Q}_h\big) + \|\vec{\mathbf{t}}_h\|_{\mathbf{H}}\|\vec{\mathbf{u}} - \vec{\mathbf{u}}_h\|_{\mathbf{Q}} + \|\vec{\mathbf{t}} - \mathbf{t}_h\|_{\mathbf{H}}\|\vec{\mathbf{u}}\|_{\mathbf{Q}} \\ &+ \big(\|\xi\|_{\mathrm{M}} + \|\xi_h\|_{\mathrm{M}} + \widetilde{a}_3\big)\|\vec{\xi} - \vec{\xi}_h\|_{\mathrm{M}}\Big\}. \end{aligned} \tag{1.89}$$

Consequently, we are in position to establish the announced Céa estimate.

Theorem 1.7. *In addition to the hypotheses of Theorems 1.3 and 1.6, assume that*

$$\begin{aligned} \frac{2C_{\mathbf{F}}}{\alpha_{\mathbf{A}}}\Big\{\|\vec{\mathbf{g}}\|_{1/2,\Gamma_{\mathrm{out}}^{\mathrm{c}}}+a_1\delta\Big\}+\frac{2}{\alpha_{\mathcal{A},\mathbf{d}}}\widetilde{a}_3(1+\delta_{\mathbf{d}}) &\leq \frac{1}{2C_{\mathtt{ST}}}, \quad \text{and} \\ \frac{2C_{\mathbf{F}}}{\alpha_{\mathbf{A}}}\Big\{\|\vec{\mathbf{g}}\|_{1/2,\Gamma_{\mathrm{out}}^{\mathrm{c}}}+a_1\delta\Big\}+\frac{4}{\widehat{\alpha}_{\mathcal{A}}}\widetilde{a}_3(1+\widehat{\delta})+\widetilde{a}_3+a_1C_{\mathbf{F}} &\leq \frac{1}{2C_{\mathtt{TT}}}, \end{aligned} \tag{1.90}$$

where $\widehat{\alpha}_{\mathcal{A}} := \min\big\{\alpha_{\mathcal{A}},\alpha_{\mathcal{A},\mathbf{d}}\big\}$, *and* $\widehat{\delta} := \max\big\{\delta,\delta_{\mathbf{d}}\big\}$. *There exists a positive constant* $C_{\mathtt{e}}$, *independent of* h, *such that*

$$\begin{aligned} &\|(\vec{\boldsymbol{\sigma}},\vec{\mathbf{u}})-(\vec{\boldsymbol{\sigma}}_h,\vec{\mathbf{u}}_h)\|_{\mathbb{H}\times\mathbf{Q}}+\|(\vec{\mathbf{t}},(\vec{\phi},\vec{\xi}))-(\vec{\mathbf{t}}_h,(\vec{\phi}_h,\vec{\xi}_h))\|_{\mathbf{H}\times\mathrm{Q}} \\ &\quad\leq\; 2C_{\mathtt{e}}\Big\{\mathrm{dist}\big((\vec{\boldsymbol{\sigma}},\vec{\mathbf{u}}),\mathbb{H}_h\times\mathbf{Q}_h\big)+\mathrm{dist}\big((\vec{\mathbf{t}},(\vec{\phi},\vec{\xi})),\mathbf{H}_h\times\mathrm{Q}_h\big)\Big\}. \end{aligned} \tag{1.91}$$

Proof. By combining (1.88) and (1.89), it suffices to use the bounds given by Theorems 1.3 and 1.6 along with (1.90), which yield (1.91). ∎

We end this section by remarking that (1.14) suggests the following postprocessed approximation for the pressure $p_\star$

$$p_h^\star \;=\; -\frac{1}{n}\mathrm{tr}(\boldsymbol{\sigma}_h^\star) \quad \text{in} \quad \Omega_\star, \tag{1.92}$$

so that, it is easy to show that

$$\|p_\star-p_h^\star\|_{0,\Omega_\star} \;\leq\; \frac{1}{\sqrt{n}}\|\boldsymbol{\sigma}_\star-\boldsymbol{\sigma}_h^\star\|_{0,\Omega_\star}. \tag{1.93}$$

Thus, combining (1.91) and (1.93), we conclude the existence of $\widehat{C}_{\mathtt{e}} \geq 0$, independent of h, such that

$$\begin{aligned} &\|(\vec{\boldsymbol{\sigma}},\vec{\mathbf{u}})-(\vec{\boldsymbol{\sigma}}_h,\vec{\mathbf{u}}_h)\|_{\mathbb{H}\times\mathbf{Q}}+\|(\vec{\mathbf{t}},(\vec{\phi},\vec{\xi}))-(\vec{\mathbf{t}}_h,(\vec{\phi}_h,\vec{\xi}_h))\|_{\mathbf{H}\times\mathrm{Q}}+\sum_{\star\in\{\mathrm{f},\mathrm{p}\}}\|p_\star-p_h^\star\|_{0,\Omega_\star} \\ &\quad\leq\widehat{C}_{\mathtt{e}}\Big\{\mathrm{dist}\big((\vec{\boldsymbol{\sigma}},\vec{\mathbf{u}}),\mathbb{H}_h\times\mathbf{Q}_h\big)+\mathrm{dist}((\vec{\mathbf{t}},(\vec{\phi},\vec{\xi})),\mathbf{H}_h\times\mathrm{Q}_h)\Big\}. \end{aligned} \tag{1.94}$$

1.5 Specific finite element subspaces

In what follows, given $K \in \mathcal{T}_h^\star$, with $\star \in \{\mathrm{f},\mathrm{p}\}$, we let $\mathrm{P}_0(K)$ be the space of polynomials of degree 0 defined on K, whose vector version is denoted by $\mathbf{P}_0(K) := [\mathrm{P}_0(K)]^2$. Next, we define the corresponding local Raviart–Thomas spaces of order 0 as (see [67, Chapter 3] for further details) $\mathbf{RT}_0(K) := \mathbf{P}_0(K) \oplus \mathrm{P}_0(K)\boldsymbol{x}$, where $\boldsymbol{x} := (x_1,x_2)^t$ is a generic vector in $\mathbb{R}^2$. Then, we introduce, respectively, the following finite element spaces for the variables $\mathbf{t}_\star$, $\boldsymbol{\sigma}_\star$, $\phi_\star$ and $\mathbf{u}_\star$:

$$\begin{aligned} &\mathbf{H}_h^{\mathbf{t}_\star} := \Big\{\mathbf{s}_h^\star \in \mathbf{H}(\mathrm{div};\Omega_\star): \quad \mathbf{s}_h^\star|_K \in \mathbf{RT}_0(K) \quad \forall\, K \in \mathcal{T}_h^\star\Big\}, \quad \mathbb{H}_h^{\boldsymbol{\sigma}_\star} := \mathbb{H}_{\Gamma_{\mathrm{out}}}(\mathbf{div}_{4/3};\Omega_\star)\cap\widetilde{\mathbb{H}}_h^\star, \text{ with} \\ &\widetilde{\mathbb{H}}_h^\star := \Big\{\boldsymbol{\tau}_h^\star \in \mathbb{H}(\mathbf{div};\Omega_\star): \quad \boldsymbol{\tau}_{h,i}^\star|_K \in \mathbf{RT}_0(K), \quad \forall\, i\in\{1,2\}, \quad \forall\, K \in \mathcal{T}_h^\star\Big\}, \\ &\mathrm{X}_h^{\phi_\star} := \Big\{\psi_h^\star \in \mathrm{L}^2(\Omega_\star): \quad \psi_h^\star|_K \in \mathrm{P}_0(K) \quad \forall\, K \in \mathcal{T}_h^\star\Big\}, \quad \text{and} \end{aligned}$$

$$\mathbf{Q}_h^{\mathbf{u}_\star} := \Big\{ \mathbf{v}_h^\star \in \mathbf{L}^2(\Omega_\star) : \quad \mathbf{v}_h^\star|_K \in \mathbf{P}_0(K) \quad \forall\, K \in \mathcal{T}_h^\star \Big\},$$

where $\boldsymbol{\tau}_{h,i}^\star$ denotes the ith-row of $\boldsymbol{\tau}_h^\star$. It remains to introduce the finite element space for the variable $\xi_\star$. To that aim, we proceed similarly to [69] and denote by $\Gamma_{\mathrm{in},\star,h}^{\mathrm{c}}$ the partition of $\Gamma_{\mathrm{in},\star}^{\mathrm{c}}$ inherited from $\mathcal{T}_h^\star$. Let us assume, without loss of generality, that the number of edges of $\Gamma_{\mathrm{in},\star,h}^{\mathrm{c}}$ is even. Then, we let $\Gamma_{\mathrm{in},\star,2h}^{\mathrm{c}}$ be the partition of $\Gamma_{\mathrm{in},\star}^{\mathrm{c}}$ arising by joining pairs of adjacent edges of $\Gamma_{\mathrm{in},\star,h}^{\mathrm{c}}$. If the number of edges of $\Gamma_{\mathrm{in},\star,h}^{\mathrm{c}}$ is odd, we simply reduce it to the even case by adding one node to the discretization of the boundary $\Gamma_{\mathrm{in},\star}^{\mathrm{c}}$ and locally modify the triangulation to keep the mesh conformity and regularity. In this way, denoting by $\boldsymbol{x}_0$ and $\boldsymbol{x}_N$ the extreme points of $\overline{\Gamma}_{\mathrm{in},\star}^{\mathrm{c}}$, we define the following finite element space:

$$\mathrm{M}_h^{\xi_\star} := \left\{ \eta_h^\star \in \mathcal{C}(\Gamma_{\mathrm{in},\star}^{\mathrm{c}}) : \quad \eta_h^\star|_e \in \mathrm{P}_1(e) \quad \forall \text{ edge } e \in \Gamma_{\mathrm{in},\star,2h}^{\mathrm{c}}, \quad \eta_h^\star(\boldsymbol{x}_0) = \eta_h^\star(\boldsymbol{x}_N) = 0 \right\}.$$

We stress here that the above particular subspaces satisfy the inclusions (1.64). We now verify that these subspaces satisfy the hypotheses **(H.1)**-**(H.5)**.

First, it is easy to show (see, [25, Section 4.2] for details) that $\widetilde{\mathbb{H}}_h^\star$ satisfy **(H.1)** and **(H.2)**. Next, in order to check **(H.3)**, we require the following result.

Lemma 1.12. *Assume that there exists a polygonal convex domain $\widehat{B}_\star$ such that $\Omega_\star \subseteq \widehat{B}_\star$ and $\Gamma_{\mathrm{out},\star} \subseteq \partial\widehat{B}_\star$. There exists a positive constant $\beta_{\mathrm{S},\mathbf{d}}^\star$, independent of h, such that*

$$\sup_{\substack{\boldsymbol{\tau}_h^\star \in \mathbb{H}_h^{\boldsymbol{\sigma}_\star} \\ \boldsymbol{\tau}_h^\star \neq \mathbf{0}}} \frac{\displaystyle\int_{\Omega_\star} \mathbf{v}_h^\star \cdot \mathbf{div}(\boldsymbol{\tau}_h^\star)}{\|\boldsymbol{\tau}_h^\star\|_{\mathbf{div}_{4/3};\Omega_\star}} \,\geq\, \beta_{\mathrm{S},\mathbf{d}}^\star \|\mathbf{v}_h^\star\|_{0,4;\Omega_\star} \quad \forall\, \mathbf{v}_h^\star \in \mathbf{Q}_h^{\mathbf{u}_\star}.$$

Proof. We proceed similarly to the proof of [25, Lemma 4.3], employing the arguments utilized in [34, Lemma 4.1]. ∎

In this way, since for each $\star \in \{\mathrm{f}, \mathrm{p}\}$ we have

$$\sup_{\substack{\vec{\boldsymbol{\tau}}_h \in \mathbb{H}_h \\ \vec{\boldsymbol{\tau}}_h \neq \mathbf{0}}} \frac{\mathbf{b}_{\mathrm{S}}(\vec{\boldsymbol{\tau}}_h, \vec{\mathbf{v}}_h)}{\|\vec{\boldsymbol{\tau}}_h\|_{\mathbb{H}}} \geq \sup_{\substack{\boldsymbol{\tau}_h^\star \in \mathbb{H}_h^{\boldsymbol{\sigma}_\star} \\ \boldsymbol{\tau}_h^\star \neq \mathbf{0}}} \frac{\displaystyle\int_{\Omega_\star} \mathbf{v}_h^\star \cdot \mathbf{div}(\boldsymbol{\tau}_h^\star)}{\|\boldsymbol{\tau}_h^\star\|_{\mathbf{div}_{4/3};\Omega_\star}} \,\geq\, \beta_{\mathrm{S},\mathbf{d}}^\star \|\mathbf{v}_h^\star\|_{0,4;\Omega_\star} \quad \forall\, \mathbf{v}_h^\star \in \mathbf{Q}_h^{\mathbf{u}_\star}, \tag{1.95}$$

it is straightforward to see that $\mathbb{H}_h$ and $\mathbf{Q}_h$, satisfy **(H.3)** (cf. (1.69)) with a positive constant $\beta_{\mathrm{S},\mathbf{d}}$, independent of h.

On the other hand, we observe that **(H.4)** holds according to [67, Lemma 3.7]. It only remains to verify **(H.5)**. To that aim, we follow the simplest approach suggested in [70]. More precisely, for each $\star \in \{\mathrm{f}, \mathrm{p}\}$, we recall (cf. [70, Lemma 5.2]) that there exists a positive constant $\beta^\star$, independent of h, such that

$$\sup_{\substack{\mathbf{s}_h^\star \in \mathbf{H}_h^{\mathbf{t}_\star} \\ \mathbf{s}_h^\star \neq \mathbf{0}}} \frac{\displaystyle\int_{\Omega_\star} \psi_h^\star \mathrm{div}(\mathbf{s}_h^\star) + \langle \mathbf{s}_h^\star \cdot \mathbf{n}_\star, \eta_h^\star \rangle_{\Gamma_{\mathrm{in},\star}^{\mathrm{c}}}}{\|\mathbf{s}_h^\star\|_{\mathrm{div};\Omega_\star}} \geq \beta^\star \left\{ \|\psi_h^\star\|_{0;\Omega_\star} + \|\eta_h^\star\|_{1/2,00,\Gamma_{\mathrm{in},\star}^{\mathrm{c}}} \right\} \tag{1.96}$$

for all $(\psi_h^\star, \eta_h^\star) \in \mathrm{X}_h^{\phi_\star} \times \mathrm{M}_h^{\xi_\star}$. Then, proceeding similarly to [68, Section 4.4.1], we use the fact that there exists a positive constant $c(\Omega_\star)$, depending only on $|\Omega_\star|$, such that $\|\mathbf{s}_\star\|_{\mathrm{div}_{4/3};\Omega_\star} \leq c(\Omega_\star)\, \|\mathbf{s}_\star\|_{\mathrm{div};\Omega_\star}$ for all $\mathbf{s}_\star \in \mathbf{H}(\mathrm{div};\Omega_\star)$, along with (1.96), to deduce that

$$\sup_{\substack{\mathbf{s}_h^\star \in \mathbf{H}_h^{\mathbf{t}_\star} \\ \mathbf{s}_h^\star \neq \mathbf{0}}} \frac{\displaystyle\int_{\Omega_\star} \psi_h^\star \mathrm{div}(\mathbf{s}_h^\star) + \langle \mathbf{s}_h^\star \cdot \mathbf{n}_\star, \eta_h^\star \rangle_{\Gamma_{\mathrm{in},\star}^{\mathrm{c}}}}{\|\mathbf{s}_h^\star\|_{\mathrm{div}_{4/3};\Omega_\star}} \geq \frac{\beta^\star}{c(\Omega_\star)} \|\eta_h^\star\|_{1/2,00,\Gamma_{\mathrm{in},\star}^{\mathrm{c}}} \quad \forall\, (\psi_h^\star, \eta_h^\star) \in \mathrm{X}_h^{\phi_\star} \times \mathrm{M}_h^{\xi_\star}. \tag{1.97}$$

In addition, we have the following result.

Lemma 1.13. *Assume that there exists a polygonal convex domain $\widetilde{B}_\star$ such that $\Omega_\star \subseteq \widetilde{B}_\star$ and $\Gamma_{\mathrm{in},\star}^{\mathrm{c}} \subseteq \partial\widetilde{B}_\star$. Then there exists a positive constant $\widetilde{\beta}_{\mathrm{T},\mathbf{d}}^\star$, independent of h, such that*

$$\sup_{\substack{\mathbf{s}_h^\star \in \mathbf{RT}_0(\mathcal{T}_h^\star) \\ \mathbf{s}_h^\star \neq \mathbf{0}}} \frac{\displaystyle\int_{\Omega_\star} \psi_h^\star \mathrm{div}(\mathbf{s}_h^\star) + \langle \mathbf{s}_h^\star \cdot \mathbf{n}_\star, \eta_h^\star \rangle_{\Gamma_{\mathrm{in},\star}^{\mathrm{c}}}}{\|\mathbf{s}_h^\star\|_{\mathrm{div}_{4/3};\Omega_\star}} \geq \widetilde{\beta}_{\mathrm{T},\mathbf{d}}^\star \|\psi_h^\star\|_{0,4;\Omega_\star} \quad \forall\, (\psi_h^\star, \eta_h^\star) \in \mathrm{X}_h^{\phi_\star} \times \mathrm{M}_h^{\xi_\star}. \tag{1.98}$$

Proof. Similarly as in Lemma 1.12, the result follows directly from [34, Lemma 4.1]. ■

Hence, a straightforward linear combination of (1.97) and (1.98) implies that

$$\sup_{\substack{\mathbf{s}_h^\star \in \mathbf{H}_h^{\mathbf{t}_\star} \\ \mathbf{s}_h^\star \neq \mathbf{0}}} \frac{\displaystyle\int_{\Omega_\star} \psi_h^\star \mathrm{div}(\mathbf{s}_h^\star) + \langle \mathbf{s}_h^\star \cdot \mathbf{n}_\star, \eta_h^\star \rangle_{\Gamma_{\mathrm{in},\star}^{\mathrm{c}}}}{\|\mathbf{s}_h^\star\|_{\mathrm{div}_{4/3};\Omega_\star}} \geq \widehat{\beta}_{\mathrm{T},\mathbf{d}}^\star \left\{ \|\psi_h^\star\|_{0,4;\Omega_\star} + \|\eta_h^\star\|_{1/2,00,\Gamma_{\mathrm{in},\star}^{\mathrm{c}}} \right\} \quad \forall\, (\psi_h^\star, \eta_h^\star) \in \mathrm{X}_h^{\phi_\star} \times \mathrm{M}_h^{\xi_\star},$$

where $\widehat{\beta}_{\mathrm{T},\mathbf{d}}^\star$ is a positive constant depending only on $\beta^\star$, $\widetilde{\beta}_{\mathrm{T},\mathbf{d}}^\star$ and $c(\Omega_\star)$.

Finally, proceeding in the same way as we did in (1.95), we deduce that $\mathbf{H}_h$ and Q_h, satisfy **(H.5)** (cf. (1.70)) with a positive constant $\beta_{\mathrm{T},\mathbf{d}}$, independent of h.

We end this section by providing the rates of convergence of the Galerkin scheme (1.65) with the specific finite element subspaces introduced in Section 1.5. More precisely, we can state the following main theorem.

Theorem 1.8. *Let us consider the hypothesis of Theorem 1.7. In addition, let $p_\star$ and $p_h^\star$ be the exact and approximate pressures defined by (1.14) and (1.92), respectively. Assume that $\boldsymbol{\sigma}_\star \in \mathbb{H}^1(\Omega_\star) \cap \mathbb{H}_{\Gamma_{\mathrm{out}}}(\mathbf{div}_{4/3};\Omega_\star)$, $\mathbf{div}(\boldsymbol{\sigma}_\star) \in \mathbf{W}^{1,4/3}(\Omega_\star)$, $\mathbf{t}_\star \in \mathbf{H}^1(\Omega_\star)$, $\mathrm{div}(\mathbf{t}_\star) \in \mathrm{W}^{1,4/3}(\Omega_\star)$, $\mathbf{u}_\star \in \mathbf{W}^{1,4}(\Omega_\star)$,*

$\phi_\star \in \mathrm{W}^{1,4}(\Omega_\star)$ *and* $\xi_\star \in \mathrm{H}^{3/2}_{00}(\Gamma^{\mathrm{c}}_{\mathrm{in},\star})$. *Then, there exists a constant* $C > 0$, *independent of* h, *such that*

$$\begin{aligned}&\|(\vec{\boldsymbol{\sigma}},\vec{\mathbf{u}}) - (\vec{\boldsymbol{\sigma}}_h,\vec{\mathbf{u}}_h)\|_{\mathbb{H}\times\mathbf{Q}} + \|(\vec{\mathbf{t}},(\vec{\phi},\vec{\xi})) - (\vec{\mathbf{t}}_h,(\vec{\phi}_h,\vec{\xi}_h))\|_{\mathbf{H}\times\mathrm{Q}} + \sum_{\star\in\{\mathrm{f},\mathrm{p}\}} \|p_\star - p^\star_h\|_{0,\Omega_\star}\\ &\leq C\sum_{\star\in\{\mathrm{f},\mathrm{p}\}} h\Big\{\|\boldsymbol{\sigma}_\star\|_{1,\Omega_\star} + \|\mathbf{div}(\boldsymbol{\sigma}_\star)\|_{1,4/3;\Omega_\star} + \|\mathbf{u}_\star\|_{1,4;\Omega} + \|\mathbf{t}_\star\|_{1,\Omega_\star} + \|\mathrm{div}(\mathbf{t}_\star)\|_{1,4/3;\Omega_\star} + \|\phi_\star\|_{1,4;\Omega_\star}\\ &\quad + \|\xi_\star\|_{3/2,00,\Gamma^{\mathrm{c}}_{\mathrm{in},\star}}\Big\}.\end{aligned}$$

Proof. The proof follows from the corresponding Céa estimate (1.94), the approximation properties of the subspaces involved. In particular, for $\mathbb{H}^{\boldsymbol{\sigma}_\star}_h$ and $\mathbf{H}^{\mathbf{t}_\star}_h$ we refer, respectively, to [25, eq. (4.7)] and [26, eq. (3.8)], which in turn are consequences of [60, Lemma B.67, Lemma 1.101] and [67, Section 3.4.4]. For $\mathbf{Q}^{\mathbf{u}_\star}_h$ and $\mathrm{X}^{\phi_\star}_h$ we refer to [60, Proposition 1.135, Section 1.6.3], whereas for $\mathrm{M}^{\xi_\star}_h$ we refer to [69, Section 5.4, **(AP3)**]. ∎

1.6 Computational results

To illustrate the performance of the method, we present two computational simulations. The first one consists of a manufactured solution to verify numerically the rates of convergence anticipated by Theorem 1.8. The second one represents a scenario inspired by conditions typically found in reverse osmosis processes, with no analytical solution available. The implementation is done in `FreeFem++` (cf. [73]). The iterative method arises directly from the uncoupling strategy presented in Section 1.4.1. In both numerical experiments, we use Picard iteration and the following stopping criteria. Let us denote by **coeff** the vector that contains all the degrees of freedom associates to $\vec{\boldsymbol{\sigma}}_h, \vec{\mathbf{u}}_h, \vec{\mathbf{t}}_h, \vec{\phi}_h$ and $\vec{\xi}_h$. Given a tolerance `tol`, we stop the fixed point iteration when the relative error between two consecutive iterations (m and $m+1$), satisfies

$$\frac{\|\mathbf{coeff}^{m+1} - \mathbf{coeff}^{m}\|_{l^2}}{\|\mathbf{coeff}^{m+1}\|_{l^2}} \leq \texttt{tol}. \tag{1.99}$$

Here, $\|\cdot\|_{l^2}$ stands for the usual Euclidean norm in $\mathbb{R}^{\texttt{dof}}$ and `dof` denoting the total number of degrees of freedom. Subsequently, errors are defined as follows:

$$\begin{aligned}&e(\boldsymbol{\sigma}_\star) = \|\boldsymbol{\sigma}_\star - \boldsymbol{\sigma}^\star_h\|_{\mathbf{div}_{4/3};\Omega_\star}, \quad && e(\mathbf{u}_\star) = \|\mathbf{u}_\star - \mathbf{u}^\star_h\|_{0,4;\Omega_\star}, \quad && e(p_\star) = \|p_\star - p^\star_h\|_{0,\Omega_\star},\\ &e(\mathbf{t}_\star) = \|\mathbf{t}_\star - \mathbf{t}^\star_h\|_{\mathrm{div}_{4/3};\Omega_\star}, && e(\phi_\star) = \|\phi_\star - \phi^\star_h\|_{0,4;\Omega_\star}, && e(\xi_\star) = \|\xi_\star - \xi^\star_h\|_{1/2,00,\Gamma^{\mathrm{c}}_{\mathrm{in},\star}}.\end{aligned}$$

Here, for practical computation, due to the fact that $\mathrm{H}^{1/2}_{00}(\Gamma^{\mathrm{c}}_{\mathrm{in},\star})$ is the interpolation space (see, e.g. [1, Chapter 5], [88, Appendix B]) with index 1/2 between $\mathrm{L}^2(\Gamma^{\mathrm{c}}_{\mathrm{in},\star})$ and $\mathrm{H}^1(\Gamma^{\mathrm{c}}_{\mathrm{in},\star})$, the norm $\|\xi_\star - \xi^\star_h\|_{1/2,00,\Gamma^{\mathrm{c}}_{\mathrm{in},\star}}$ will be estimated by $\|\xi_\star - \xi^\star_h\|_{(0,1),\Gamma^{\mathrm{c}}_{\mathrm{in},\star}}$, where

$$\|\chi_\star\|_{(0,1),\Gamma^{\mathrm{c}}_{\mathrm{in},\star}} := \|\chi_\star\|^{1/2}_{0,\Gamma^{\mathrm{c}}_{\mathrm{in},\star}}\,\|\chi_\star\|^{1/2}_{1,\Gamma^{\mathrm{c}}_{\mathrm{in},\star}} \quad \forall \chi_\star \in \mathrm{H}^1(\Gamma^{\mathrm{c}}_{\mathrm{in},\star}).$$

In turn, the experimental order of convergence, is set as

$$r(*) = \frac{\log(e(*)/e'(*))}{\log(h/h')} \qquad \forall * \in \left\{\boldsymbol{\sigma}_\star, \mathbf{u}_\star, p_\star, \mathbf{t}_\star, \phi_\star, \xi_\star\right\},$$

where e and e' denote the errors computed on two consecutive meshes of sizes h and h'. In addition, we refer to the number of iterations as `iter`. Next, in our two examples, we consider the computational domain $\Omega = \Omega_\mathrm{f} \cup \Omega_\mathrm{p} \cup \Sigma$, where $\Omega_\mathrm{f} = (0, L) \times (d, 2d)$, $\Omega_\mathrm{p} = (0, L) \times (0, d)$, and $\Sigma = (0, L) \times \{d\}$.

Example 1: A manufactured smooth solution. In our first numerical test, we consider the computational domain Ω with $L = 1$ and $d = 0.5$, and set the parameters $\nu = 2$, $\rho = 0.1$, $\kappa = 1.6$, $a_0 = 10^{-8}$, $a_1 = 0.01$ and $a_2 = 2.5 \times 10^{-6}$. In addition, we define the manufactured solution:

$$p_\star = \cos(\pi x)\exp{(y)}, \quad \mathbf{u}_\star = \begin{pmatrix} \sin(\pi x)\cos(\pi y) \\ -\cos(\pi x)\sin(\pi y) \end{pmatrix}, \quad \phi_\star = \cos(\pi x)\sin(\pi y).$$

We notice that the only external sources of the physical model (1.16) are due to the velocity profile and concentration at the inlet. So, in order to be able to use the above manufactured solution, we introduce artificial volumetric, boundary and interface sources that make this solution to satisfy the equations. Table 1.1 shows the history of convergence for a sequence of quasi-uniform mesh refinements. The experiment confirm the theoretical rate of convergence $\mathcal{O}(h)$, provided by Theorem 1.8. In addition, as initial guess to start the iteration, we consider zero velocity and concentration. The number of iterations required to reach the stopping criterion (1.99) with a tolerance of $1e-6$, was less than or equal to 4.

Example 2: Coupled channels. We set $L = 15\,mm$, $d = 0.74\,mm$. The inlet velocity profiles are consider as in Remark 1.4, and the simulation conditions specified in Section 1.1.2 are in Table 1.2. In Figure 1.2 we display the computed velocity magnitudes, pressure and salt concentration fields, which were built using the fully-mixed $\mathbb{RT}_0 - \mathbf{P}_0$ and $\mathbf{RT}_0 - \mathrm{P}_0 - \mathrm{P}_1$ schemes on a mesh with $h = 0.02$ and $348,140$ triangular elements (actually representing 2,616,096 `dof`). In addition, as initial guess to start the iteration, we consider zero velocity and concentration. The number of iterations required to reach the stopping criterion (1.99) with a tolerance of $1e-6$, was equal to 12. This increment in the number of iterations, compared to the previous example, is due to the value of physical parameters since the contraction properties proved in our analysis depend on these parameters. This aspect can be further explored by studying how sensitive is the number of iterations with respect to the physically meaningful parameters, and it is part of an ongoing research. We see that the parabolic profile remains in both channels (top panel). The velocity magnitude in the feed channel decreases along the axial axis, while the opposite occurs in the permeate channel. This is expected because water flows from the feed channel to the permeate across the membrane. Also, a pressure loss is observed along the entire channels (center panel), which, for laminar flows, is related to the friction between the fluid and the channel walls, as well as to the accumulation of salt near the membrane [103]. This type of accumulation, as shown in the bottom panel, is typical in reverse osmosis processes.

$\mathbb{RT}_0 - \mathbf{P}_0$ and $\mathbf{RT}_0 - \mathrm{P}_0 - \mathrm{P}_1$ approximation								
dof	$e(\boldsymbol{\sigma}_\mathrm{f})$	$r(\boldsymbol{\sigma}_\mathrm{f})$	$e(\mathbf{u}_\mathrm{f})$	$r(\mathbf{u}_\mathrm{f})$	$e(p_\mathrm{f})$	$r(p_\mathrm{f})$	$e(\mathbf{t}_\mathrm{f})$	$r(\mathbf{t}_\mathrm{f})$
1161	$1.62e+00$	$*$	$9.43e-02$	$*$	$2.06e-01$	$*$	$5.16e-01$	$*$
4527	$7.74e-01$	0.99	$4.59e-02$	0.96	$9.30e-02$	1.07	$2.50e-01$	0.97
17559	$3.86e-01$	1.17	$2.30e-02$	1.17	$4.60e-02$	1.19	$1.27e-01$	1.14
68913	$1.94e-01$	1.06	$1.16e-02$	1.05	$2.29e-02$	1.08	$6.35e-02$	1.07
280476	$9.55e-02$	1.05	$5.74e-03$	1.04	$1.13e-02$	1.04	$3.14e-02$	1.04
1106742	$4.79e-02$	1.08	$2.89e-03$	1.08	$5.64e-03$	1.10	$1.58e-02$	1.08
h	$e(\phi_\mathrm{f})$	$r(\phi_\mathrm{f})$	$e(\xi_\mathrm{f})$	$r(\xi_\mathrm{f})$	$e(\boldsymbol{\sigma}_\mathrm{p})$	$r(\boldsymbol{\sigma}_\mathrm{p})$	$e(\mathbf{u}_\mathrm{p})$	$r(\mathbf{u}_\mathrm{p})$
0.1863	$7.46e-02$	$*$	$2.51e-01$	$*$	$1.63e+00$	$*$	$9.60e-02$	$*$
0.0884	$3.50e-02$	1.01	$1.13e-01$	1.08	$7.79e-01$	1.19	$4.65e-02$	1.17
0.0488	$1.77e-02$	1.15	$5.62e-02$	1.17	$3.80e-01$	0.96	$2.31e-02$	0.93
0.0255	$8.79e-03$	1.07	$2.86e-02$	1.04	$1.90e-01$	1.10	$1.16e-02$	1.08
0.0130	$4.33e-03$	1.05	$1.41e-02$	1.05	$9.36e-02$	1.09	$5.72e-03$	1.09
0.0069	$2.18e-03$	1.08	$7.13e-03$	1.07	$4.71e-02$	1.22	$2.88e-03$	1.21
iter	$e(p_\mathrm{p})$	$r(p_\mathrm{p})$	$e(\mathbf{t}_\mathrm{p})$	$r(\mathbf{t}_\mathrm{p})$	$e(\phi_\mathrm{p})$	$r(\phi_\mathrm{p})$	$e(\xi_\mathrm{p})$	$r(\xi_\mathrm{p})$
4	$3.07e-01$	$*$	$5.12e-01$	$*$	$7.10e-02$	$*$	$2.15e-01$	$*$
3	$1.26e-01$	1.43	$2.53e-01$	1.13	$3.52e-02$	1.13	$9.55e-02$	1.31
3	$5.65e-02$	1.07	$1.27e-01$	0.92	$1.74e-02$	0.94	$4.62e-02$	0.97
3	$2.76e-02$	1.13	$6.34e-02$	1.09	$8.76e-03$	1.08	$2.30e-02$	1.10
3	$1.35e-02$	1.10	$3.14e-02$	1.08	$4.31e-03$	1.09	$1.14e-02$	1.08
3	$6.80e-03$	1.22	$1.58e-02$	1.22	$2.18e-03$	1.21	$5.72e-03$	1.23

Table 1.1: Example 1, number of degrees of freedom, meshsizes, iterations, errors, and rates of convergence for the $\mathbb{RT}_0 - \mathbf{P}_0 - \mathbf{RT}_0 - \mathrm{P}_0 - \mathrm{P}_1$ approximations of the Navier–Stokes/transport model, and convergence of the P_0-approximation of the postprocessed pressures field.

Parameter	Meaning	Value	Units
T	System temperature	298	K
R	Ideal gas constant	8.314	$Jmol^{-1}K^{-1}$
i	Number of ions from salt solution	2	$-$
$\mathrm{u}_{\mathrm{in,f}}/\mathrm{u}_{\mathrm{in,p}}$	Inlet mean feed/permeate fluid velocity	0.01/0.001	$m\,s^{-1}$
$\widetilde{\phi}_{\mathrm{in,f}}/\widetilde{\phi}_{\mathrm{in,p}}$	Inlet feed/permeate salt molar concentration	600/6	$mol\,m^{-3}$
$\varDelta P$	Hydrostatic transmembrane pressure	5575875	Pa
ρ	Feed/permeate fluid density	1027.2	$kg\,m^{-3}$
κ	Feed/permeate diffusivity of salt in water	1.611×10^{-9}	m^2s^{-1}
ν	Feed/permeate fluid dynamic viscosity	8.9×10^{-4}	$kg\,m^{-1}s^{-1}$
A	Membrane water permeability	2.5×10^{-12}	$ms^{-1}\,Pa^{-1}$
B	Membrane salt permeability	2.5×10^{-8}	$m\,s^{-1}$

Table 1.2: Simulation conditions [14, 33, 89].

1.7 Appendix

A.1. Boundedness of $\mathbf{b}_\mathbf{T}$. We proceed similarly to [26, Section 4.1]. Given $\star \in \{\mathrm{f},\mathrm{p}\}$, we let $\mathbf{s}_\star \in \mathbb{H}^\star_\mathrm{S}$ and $\eta_\star \in \mathrm{M}^\star_\mathrm{T}$. Thus, by (1.2) we have

$$\langle \mathbf{s}_\star \cdot \mathbf{n}_\star, \eta_\star \rangle_{\Gamma^\mathrm{c}_{\mathrm{in},\star}} = \langle \mathbf{s}_\star \cdot \mathbf{n}_\star, E_{0,\Gamma^\mathrm{c}_{\mathrm{in},\star}}(\eta_\star) \rangle_{\partial\Omega_\star} = \int_{\Omega_\star} \mathbf{s}_\star \cdot \nabla \widetilde{\gamma}_0^{-1}(E_{0,\Gamma^\mathrm{c}_{\mathrm{in},\star}}(\eta_\star)) + \int_{\Omega_\star} \widetilde{\gamma}_0^{-1}(E_{0,\Gamma^\mathrm{c}_{\mathrm{in},\star}}(\eta_\star)) \mathrm{div}(\mathbf{s}_\star),$$

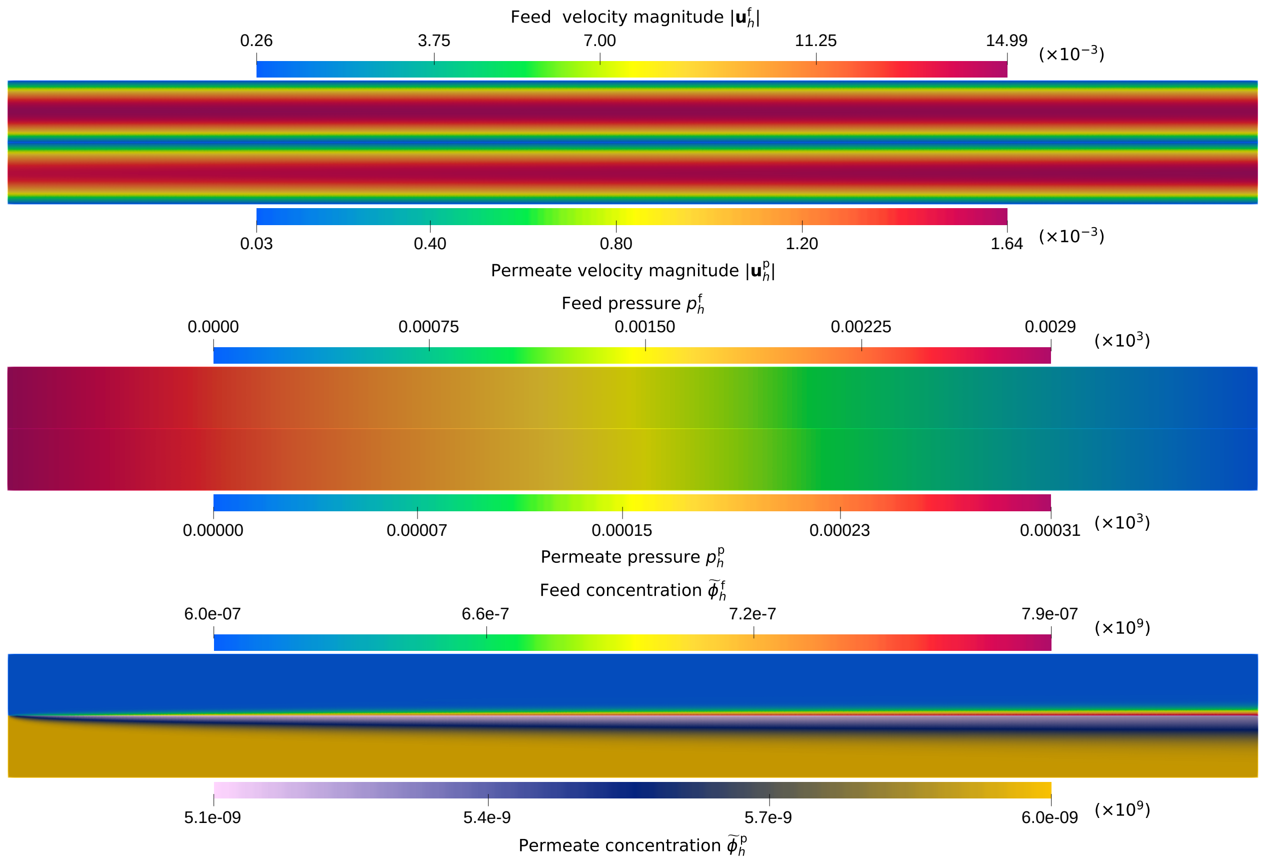

Figure 1.2: *Example 2, approximations with* $\texttt{dof} = 2,616,096$ *for the velocity magnitudes of the fluid, pressure fields and concentration levels in the whole domain.*

where $\widetilde{\gamma}_0^{-1} : \mathrm{H}^{1/2}(\partial\Omega_\star) \to [\mathrm{H}_0^1(\Omega_\star)]^\perp$ is the right inverse of the trace operator $\gamma_0 : \mathrm{H}^1(\Omega_\star) \to \mathrm{H}^{1/2}(\partial\Omega_\star)$ (see, [67, Section 1.3.4]). Thus, applying Hölder's inequality, we obtain

$$|\langle \mathbf{s}_\star \cdot \mathbf{n}_\star, \eta_\star \rangle_{\Gamma^{\mathrm{c}}_{\mathrm{in},\star}}| \leq \|\mathbf{s}_\star\|_{0,\Omega_\star} \|\nabla \widetilde{\gamma}_0^{-1}(E_{0,\Gamma^{\mathrm{c}}_{\mathrm{in},\star}}(\eta_\star))\|_{0,\Omega_\star} + \|\widetilde{\gamma}_0^{-1}(E_{0,\Gamma^{\mathrm{c}}_{\mathrm{in},\star}}(\eta_\star))\|_{0,4;\Omega_\star} \|\mathrm{div}(\mathbf{s}_\star)\|_{0,4/3;\Omega_\star}.$$

Next, thanks to the continuous injection $i_4^\star : \mathrm{H}^1(\Omega_\star) \to \mathrm{L}^4(\Omega_\star)$, we have that $\|\widetilde{\gamma}_0^{-1}(E_{0,\Gamma^{\mathrm{c}}_{\mathrm{in},\star}}(\eta_\star))\|_{0,4;\Omega_\star} \leq \|i_4^\star\| \, \|\widetilde{\gamma}_0^{-1}(E_{0,\Gamma^{\mathrm{c}}_{\mathrm{in},\star}}(\eta_\star))\|_{1,\Omega_\star}$. Moreover, since $E_{0,\Gamma^{\mathrm{c}}_{\mathrm{in},\star}}(\eta_\star)$ belongs to $\mathrm{H}^{1/2}(\partial\Omega_\star)$, we get (cf. [67, Lemma 1.3])

$$\|\widetilde{\gamma}_0^{-1}(E_{0,\Gamma^{\mathrm{c}}_{\mathrm{in},\star}}(\eta_\star))\|_{0,4;\Omega_\star} \leq \|i_4^\star\| \|E_{0,\Gamma^{\mathrm{c}}_{\mathrm{in},\star}}(\eta_\star)\|_{1/2,\partial\Omega_\star} = \|i_4^\star\| \|\eta_\star\|_{1/2,00,\Gamma^{\mathrm{c}}_{\mathrm{in},\star}},$$

whence, $|\langle \mathbf{s}_\star \cdot \mathbf{n}_\star, \eta_\star \rangle_{\Gamma^{\mathrm{c}}_{\mathrm{in},\star}}| \leq \max\big\{1, \|i_4^\star\|\big\} \|\mathbf{s}_\star\|_{\mathrm{div}_{4/3};\Omega_\star} \|\eta_\star\|_{1/2,00,\Gamma^{\mathrm{c}}_{\mathrm{in},\star}}$.
As a consequence of the latter and Hölder's inequality, we deduce (1.35a).

A.2. Boundedness of $\mathbf{d}_{\mathrm{T}}$. We recall from [60, Theorem B.46] (see also [53, Theorem 6.10]) that $\mathrm{H}^{1/2}(\partial\Omega_\star)$ is continuously embedded in $\mathrm{L}^t(\partial\Omega_\star)$ for any $t \in [1, +\infty)$. In other words, for any $\zeta_\star \in \mathrm{H}^{1/2}(\partial\Omega_\star)$, there exists a positive constant $c_t^\star$, depending only on $\partial\Omega_\star$, such that $\|\zeta_\star\|_{0;t,\partial\Omega_\star} \leq$

$c_t^\star \|\zeta_\star\|_{1/2,\partial\Omega_\star}$, $\forall\, t \in [1,+\infty)$. In this way, given $\eta_\star \in \mathrm{H}_{00}^{1/2}(\Gamma_{\mathrm{in},\star}^{\mathrm{c}})$ it follows that

$$\|\eta_\star\|_{0,t;\Gamma_{\mathrm{in},\star}^{\mathrm{c}}} = \|E_{0,\Gamma_{\mathrm{in},\star}^{\mathrm{c}}}(\eta_\star)\|_{0,t;\partial\Omega_\star} \leq c_t^\star \|E_{0,\Gamma_{\mathrm{in},\star}^{\mathrm{c}}}(\eta_\star)\|_{1/2,\partial\Omega_\star} = c_t^\star \|\eta_\star\|_{1/2,00,\Gamma_{\mathrm{in},\star}^{\mathrm{c}}}. \tag{1.100}$$

Thus, by the Cauchy–Schwarz inequality and (1.100), we obtain (1.35b).

A.3. Boundedness of $\mathbf{F}_{\vec{\chi}}$. Given $\vec{\chi} = (\chi_{\mathrm{f}}, \chi_{\mathrm{p}}) \in \mathrm{M}$, we stress that to bound the functional $\mathbf{F}_{\vec{\chi}}$, one cannot proceed in a direct way as when applying the Cauchy–Schwarz or Hölder inequalities since the dual parity defining the functional $\mathbf{F}_{\vec{\chi}}$ involves the data $\mathbf{g}_\star$ and $\mathbf{g}_\star^{\chi}$ (cf. (1.22)), which are defined by parts on the boundary $\Gamma_{\mathrm{out},\star}^{\mathrm{c}}$ and belong to $\mathbf{H}^{1/2}(\Gamma_{\mathrm{out},\star}^{\mathrm{c}})$, for $\star \in \{\mathrm{f},\mathrm{p}\}$. Therefore, we will make use of the results of Section 1.1.1 to properly bound each one of these data providing details for $\star = \mathrm{f}$ since $\star = \mathrm{p}$ is analogous. For that, we write

$$\langle \boldsymbol{\tau}_{\mathrm{f}}\, \mathbf{n}_{\mathrm{f}},\, \mathbf{g}_{\mathrm{f}} + \mathbf{g}_{\mathrm{f}}^{\chi}\rangle_{\Gamma_{\mathrm{out,f}}^{\mathrm{c}}} = \langle \boldsymbol{\tau}_{\mathrm{f}}\, \mathbf{n}_{\mathrm{f}},\, \mathbf{g}_{\mathrm{f}}\rangle_{\Gamma_{\mathrm{out,f}}^{\mathrm{c}}} + \langle \boldsymbol{\tau}_{\mathrm{f}}\, \mathbf{n}_{\mathrm{f}},\, \mathbf{g}_{\mathrm{f}}^{\chi}\rangle_{\Gamma_{\mathrm{out,f}}^{\mathrm{c}}}, \tag{1.101}$$

For the first term on the right-hand side of (1.101), one can define the extension $\boldsymbol{E}_{\Gamma_{\mathrm{out,f}}^{\mathrm{c}}}(\mathbf{g}_{\mathrm{f}}) := \mathbf{z}_{\mathrm{f}}|_{\partial\Omega_{\mathrm{f}}}$, where $\mathbf{z}_{\mathrm{f}} \in \mathbf{H}^1(\Omega_{\mathrm{f}})$ is the unique solution to (1.5), with $\mathbf{g}_{\mathrm{f}}$, $\mathbf{n}_{\mathrm{f}}$, $\Gamma_{\mathrm{out,f}}^{\mathrm{c}}$ and $\Gamma_{\mathrm{out,f}}$ instead of η, $\mathbf{n}$, $\widetilde{\Gamma}$ and $\widetilde{\Gamma}^{\mathrm{c}}$, respectively. Moreover, there exists a constant $C_{\mathrm{f}} > 0$, such that

$$\|\boldsymbol{E}_{\Gamma_{\mathrm{out,f}}^{\mathrm{c}}}(\mathbf{g}_{\mathrm{f}})\|_{1/2,\partial\Omega_{\mathrm{f}}} \leq C_{\mathrm{f}}\, \|\mathbf{g}_{\mathrm{f}}\|_{1/2,\Gamma_{\mathrm{out,f}}^{\mathrm{c}}}. \tag{1.102}$$

Next, we recall from the last part of Section 1.1.1 that since $\boldsymbol{E}_{\Gamma_{\mathrm{out,f}}^{\mathrm{c}}}(\mathbf{g}_{\mathrm{f}}) \in \mathbf{H}^{1/2}(\partial\Omega_{\mathrm{f}})$, there exist unique elements $\boldsymbol{\zeta}_{\Gamma_{\mathrm{out,f}}^{\mathrm{c}}} \in \mathbf{H}^{1/2}(\Gamma_{\mathrm{out,f}}^{\mathrm{c}})$ and $\boldsymbol{\zeta}_{\Gamma_{\mathrm{out,f}}} \in \mathbf{H}_{00}^{1/2}(\Gamma_{\mathrm{out,f}})$ such that

$$\langle \boldsymbol{\tau}_{\mathrm{f}}\mathbf{n}_{\mathrm{f}}, \boldsymbol{E}_{\Gamma_{\mathrm{out,f}}^{\mathrm{c}}}(\mathbf{g}_{\mathrm{f}})\rangle_{\partial\Omega_{\mathrm{f}}} := \langle \boldsymbol{\tau}_{\mathrm{f}}\mathbf{n}_{\mathrm{f}}, \boldsymbol{E}_{\Gamma_{\mathrm{out,f}}^{\mathrm{c}}}(\boldsymbol{\zeta}_{\Gamma_{\mathrm{out,f}}^{\mathrm{c}}})\rangle_{\partial\Omega_{\mathrm{f}}} + \langle \boldsymbol{\tau}_{\mathrm{f}}\mathbf{n}_{\mathrm{f}}, \boldsymbol{E}_{0,\Gamma_{\mathrm{out,f}}}(\boldsymbol{\zeta}_{\Gamma_{\mathrm{out,f}}})\rangle_{\partial\Omega_{\mathrm{f}}},$$

$\boldsymbol{E}_{\Gamma_{\mathrm{out,f}}^{\mathrm{c}}}(\mathbf{g}_{\mathrm{f}})|_{\Gamma_{\mathrm{out,f}}^{\mathrm{c}}} = \boldsymbol{\zeta}_{\Gamma_{\mathrm{out,f}}^{\mathrm{c}}}$ and $\boldsymbol{E}_{\Gamma_{\mathrm{out,f}}^{\mathrm{c}}}(\mathbf{g}_{\mathrm{f}})|_{\Gamma_{\mathrm{out,f}}} = \boldsymbol{\zeta}_{\Gamma_{\mathrm{out,f}}}$. Moreover, by uniqueness we have that $\boldsymbol{\zeta}_{\Gamma_{\mathrm{out,f}}^{\mathrm{c}}} = \mathbf{g}_{\mathrm{f}}$. This means that (cf. (1.4))

$$\langle \boldsymbol{\tau}_{\mathrm{f}}\mathbf{n}_{\mathrm{f}}, \boldsymbol{E}_{\Gamma_{\mathrm{out,f}}^{\mathrm{c}}}(\mathbf{g}_{\mathrm{f}})\rangle_{\partial\Omega_{\mathrm{f}}} = \langle \boldsymbol{\tau}_{\mathrm{f}}\mathbf{n}_{\mathrm{f}}, \mathbf{g}_{\mathrm{f}}\rangle_{\Gamma_{\mathrm{out,f}}^{\mathrm{c}}} \quad \forall\, \boldsymbol{\tau}_{\mathrm{f}} \in \mathbb{H}_{\Gamma_{\mathrm{out}}}(\mathbf{div}_{4/3};\Omega_{\mathrm{f}}). \tag{1.103}$$

As a consequence, employing the identity (1.103) and same arguments for bounding $\mathbf{b}_{\mathrm{T}}$, but now with the continuous injection $\mathbf{i}_4^{\mathrm{f}} : \mathbf{H}^1(\Omega_{\mathrm{f}}) \to \mathbf{L}^4(\Omega_{\mathrm{f}})$ (see, [48, Section 3.1]) and (1.102), we obtain

$$|\langle \boldsymbol{\tau}_{\mathrm{f}}\, \mathbf{n}_{\mathrm{f}},\, \mathbf{g}_{\mathrm{f}}\rangle_{\Gamma_{\mathrm{out,f}}^{\mathrm{c}}}| \leq \max\big\{1, \|\mathbf{i}_4^{\mathrm{f}}\|\big\} C_{\mathrm{f}} \|\boldsymbol{\tau}_{\mathrm{f}}\|_{\mathbf{div}_{4/3};\Omega_{\mathrm{f}}} \|\mathbf{g}_{\mathrm{f}}\|_{1/2,\Gamma_{\mathrm{out,f}}^{\mathrm{c}}}. \tag{1.104}$$

It remains to deal with the second term on the right-hand side of (1.101). Therefore, in what follows, we make use of a convenient extension operator to define an appropriated $\mathbf{G}_{\mathrm{f},\vec{\chi}} \in \mathbf{H}^{1/2}(\partial\Omega_{\mathrm{f}})$ such that its restriction to $\Gamma_{\mathrm{out,f}}^{\mathrm{c}}$ coincides precisely with $\mathbf{g}_{\mathrm{f}}^{\chi}$. Since $\chi_{\mathrm{p}} \in \mathrm{H}_{00}^{1/2}(\Gamma_{\mathrm{in,p}}^{\mathrm{c}})$, that is $E_{0,\Gamma_{\mathrm{in,p}}^{\mathrm{c}}}(\chi_{\mathrm{p}}) \in \mathrm{H}^{1/2}(\partial\Omega_{\mathrm{p}})$ we note that $E_{0,\Gamma_{\mathrm{in,p}}^{\mathrm{c}}}(\chi_{\mathrm{p}})|_{\Sigma} = \chi_{\mathrm{p}} \in \mathrm{H}^{1/2}(\Sigma)$ and $\chi_{\mathrm{p}} = 0$ on $\Gamma_{\mathrm{in,p}}$. Thus, one could define $E_{\Sigma,\mathrm{f}}(\chi_{\mathrm{p}}) := z_{\mathrm{f}}|_{\partial\Omega_{\mathrm{f}}}$, where $z_{\mathrm{f}} \in \mathrm{H}^1(\Omega_{\mathrm{f}})$ is the unique solution to the boundary value problem

$$\triangle z_{\mathrm{f}} = 0 \quad \text{in} \quad \Omega_{\mathrm{f}}, \quad z_{\mathrm{f}} = \chi_{\mathrm{p}} \quad \text{on} \quad \Sigma, \quad z_{\mathrm{f}} = 0 \quad \text{on} \quad \Gamma_{\mathrm{in,f}} \quad \text{and} \quad \nabla z_{\mathrm{f}} \cdot \mathbf{n}_{\mathrm{f}} = 0 \quad \text{on} \quad \Gamma_{\mathrm{w,f}} \cup \Gamma_{\mathrm{out,f}},$$

and show that there exists a constant $C_{\Sigma,\mathrm{f}} > 0$, such that $\|E_{\Sigma,\mathrm{f}}(\chi_\mathrm{p})\|_{1/2,\partial\Omega_\mathrm{f}} \leq C_{\Sigma,\mathrm{f}}\|\chi_\mathrm{p}\|_{1/2,\Sigma}$. On the other hand, from the fact that

$$\|\chi_\mathrm{p}\|_{1/2,\Sigma} = \|E_{0,\Gamma^\mathrm{c}_{\mathrm{in,p}}}(\chi_\mathrm{p})|_\Sigma\|_{1/2,\Sigma} \leq \|E_{0,\Gamma^\mathrm{c}_{\mathrm{in,p}}}(\chi_\mathrm{p})\|_{1/2,\partial\Omega_\mathrm{p}} = \|\chi_\mathrm{p}\|_{1/2,00,\Gamma^\mathrm{c}_{\mathrm{in,p}}},$$

we get

$$\|E_{\Sigma,\mathrm{f}}(\chi_\mathrm{p})\|_{1/2,\partial\Omega_\mathrm{f}} \leq C_{\Sigma,\mathrm{f}}\|\chi_\mathrm{p}\|_{1/2,00,\Gamma^\mathrm{c}_{\mathrm{in,p}}}. \tag{1.105}$$

Now, we define

$$\mathbf{G}_{\mathrm{f},\chi} := (E_{0,\Gamma^\mathrm{c}_{\mathrm{in,f}}}(\chi_\mathrm{f}) - E_{\Sigma,\mathrm{f}}(\chi_\mathrm{p}))\mathcal{Q}_\mathrm{f}\,\mathbf{n}_\mathrm{f} \in \mathbf{H}^{1/2}(\partial\Omega_\mathrm{f}),$$

where $\mathcal{Q}_\mathrm{f}$ can be any function in $C^\infty(\Omega_\mathrm{f})$, such that $\mathcal{Q}_\mathrm{f} = a_1$ an Σ, $\mathcal{Q}_\mathrm{f} = 0$ on $\Gamma_{\mathrm{w,f}}$ and $\|\mathcal{Q}_\mathrm{f}\|_{0,\infty;\Omega_\mathrm{f}} \leq a_1$. For example, we can consider $\mathcal{Q}_\mathrm{f}(x,y) = \dfrac{a_1}{d}(d-y)$, where $\Omega_\mathrm{f} = (0,L)\times(0,d)$, $\Sigma = (0,L)\times\{0\}$ and $\Gamma_{\mathrm{w,f}} = (0,L)\times\{d\}$. In turn, noticing that $\mathbf{G}_{\mathrm{f},\chi}|_{\Gamma^\mathrm{c}_{\mathrm{out,f}}} = \mathbf{g}^\chi_\mathrm{f} \in \mathrm{H}^{1/2}(\Gamma^\mathrm{c}_{\mathrm{out,f}})$, and proceeding similarly as we did for (1.103), it is easy to see that

$$\langle\boldsymbol{\tau}_\mathrm{f}\mathbf{n}_\mathrm{f}, \mathbf{G}_{\mathrm{f},\chi}\rangle_{\partial\Omega_\mathrm{f}} = \langle\boldsymbol{\tau}_\mathrm{f}\mathbf{n}_\mathrm{f}, \mathbf{g}^\chi_\mathrm{f}\rangle_{\Gamma^\mathrm{c}_{\mathrm{out,f}}} \quad \forall\,\boldsymbol{\tau}_\mathrm{f} \in \mathbb{H}_{\Gamma_\mathrm{out}}(\mathbf{div}_{4/3};\Omega_\mathrm{f}).$$

Thus, knowing that $\|E_{0,\Gamma^\mathrm{c}_{\mathrm{in,f}}}(\chi_\mathrm{f})\|_{1/2,\partial\Omega_\mathrm{f}} = \|\chi_\mathrm{f}\|_{1/2,00,\Gamma^\mathrm{c}_{\mathrm{in,f}}}$, and employing (1.105), as well as applying similar arguments to those used in (1.104), we find that

$$|\langle\boldsymbol{\tau}_\mathrm{f}\,\mathbf{n}_\mathrm{f},\,\mathbf{g}^\chi_\mathrm{f}\rangle_{\Gamma^\mathrm{c}_{\mathrm{out,f}}}| \leq a_1\max\left\{1,\|\mathbf{i}^\mathrm{f}_4\|\right\}\max\{C_{\Sigma,\mathrm{f}},1\}\,\|\boldsymbol{\tau}_\mathrm{f}\|_{\mathbf{div}_{4/3};\Omega_\mathrm{f}}\|\vec{\chi}\|_\mathrm{M}. \tag{1.106}$$

The analogous conclusion is obtained by setting $\star = \mathrm{p}$, in order to write

$$\langle\boldsymbol{\tau}_\mathrm{p}\,\mathbf{n}_\mathrm{p},\,\mathbf{g}_\mathrm{p} + \mathbf{g}^\chi_\mathrm{p}\rangle_{\Gamma^\mathrm{c}_{\mathrm{out,p}}} = \langle\boldsymbol{\tau}_\mathrm{p}\,\mathbf{n}_\mathrm{p},\,\mathbf{g}_\mathrm{p}\rangle_{\Gamma^\mathrm{c}_{\mathrm{out,p}}} + \langle\boldsymbol{\tau}_\mathrm{p}\,\mathbf{n}_\mathrm{p},\,\mathbf{g}^\chi_\mathrm{p}\rangle_{\Gamma^\mathrm{c}_{\mathrm{out,p}}},$$

and obtain

$$|\langle\boldsymbol{\tau}_\mathrm{p}\,\mathbf{n}_\mathrm{p},\,\mathbf{g}_\mathrm{p}\rangle_{\Gamma^\mathrm{c}_{\mathrm{out,p}}}| \leq \max\left\{1,\|\mathbf{i}^\mathrm{p}_4\|\right\}C_\mathrm{p}\|\boldsymbol{\tau}_\mathrm{p}\|_{\mathbf{div}_{4/3};\Omega_\mathrm{p}}\|\mathbf{g}_\mathrm{p}\|_{1/2,\Gamma^\mathrm{c}_{\mathrm{out,p}}}, \quad \text{and} \tag{1.107}$$

$$|\langle\boldsymbol{\tau}_\mathrm{p}\,\mathbf{n}_\mathrm{p},\,\mathbf{g}^\chi_\mathrm{p}\rangle_{\Gamma^\mathrm{c}_{\mathrm{out,p}}}| \leq a_1\max\left\{1,\|\mathbf{i}^\mathrm{p}_4\|\right\}\max\{C_{\Sigma,\mathrm{p}},1\}\,\|\boldsymbol{\tau}_\mathrm{p}\|_{\mathbf{div}_{4/3};\Omega_\mathrm{p}}\|\vec{\chi}\|_\mathrm{M}. \tag{1.108}$$

As a consequence, employing the bounds (1.104), (1.106), (1.107) and (1.108), we obtain (1.36).

CHAPTER 2

Further numerical simulations for coupled fluid channels

2.1 Introduction

According to [72], the total volume of freshwater stocks is around the 2.5% (35 million km^3) of the total stock of water in the hydrosphere. Moreover, a large fraction of the freshwater (24 million km^3, or 68.7%) is in the form of ice and permanent snow cover in the Antarctic and Arctic regions. The rising apprehension regarding the future accessibility of freshwater resources has led to a surge in the establishment of seawater desalination plants. As we mentioned in Section 1.1, RO takes a prominent position, being employed in 69% of industrial desalination plants globally [59].

The main purpose of RO is removing all colloidal matter and dissolved particles larger than 0.1-1.0 nm in size from a liquid solution [98]. The conventional process includes three major stages. The initial phase, known as pre-treatment, focuses on the removal of coarse solids such as algae and smaller solid particles like fine sand (see Figure 1 in [98]). Once seawater has undergone this pre-treatment, the main RO stage begins. At this point, pre-treated water flows at high pressure through the feed channel, allowing the water to pass through the pores of the semi-permeable membrane housed in a membrane module (see Figure 2 in [98]). Finally, the post-treatment stage is conducted to achieve mineral enrichment by introducing ions, such as magnesium and calcium, to the permeate water. This three-stage process ensures effective water purification through RO technology.

However, it is well known that a major challenge in separation processes such as RO, is concentration polarization, which induces fouling (the undesired accumulation of materials) and reduces flux at the membrane. This phenomenon occurs because solutes are rejected at the membrane wall while convective transport delivers solutes to the membrane surface faster than diffusive transport can return them to the bulk streamflow. As a result, the solute concentration significantly increases at the membrane surface. To address this issue, spacers (small obstacles placed within the channel) are used to maintain separation between membrane layers and promote mass transfer. Research on spacer filament distribution and design structure has notably increased over the past decade, aiming to identify optimal configurations based on specific requirements. Notable contributions in this field include works by [2,33,77,78,85,104], among others. In this context, and to contribute to a better understanding of the processes underlying RO technology, we propose new numerical discretizations based on the approach outlined in Chapter 1. These discretizations aim to accurately simulate three scenarios. The first

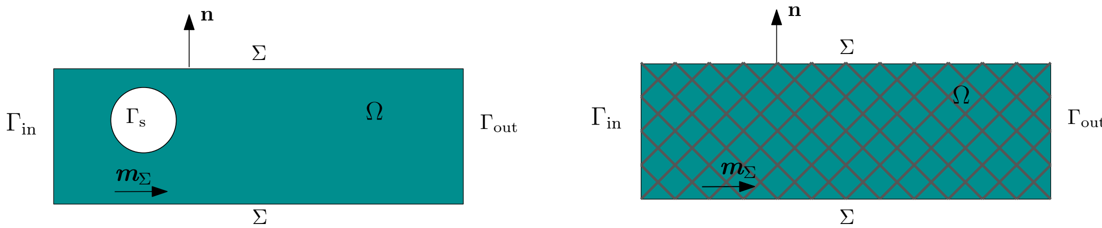

Figure 2.1: *Sketch of a single channel with explicit spacer (left) and implicit spacers (right).*

scenario includes explicit spacers located inside the desalination channels. The second scenario features a channel without spacers (from now on referred as empty channel). The third scenario emulates the effect of spacers implicitly by distributing their effect in the entire region and modeling the domain of simulation as a porous medium. For the first scenario, we employ the coupled Navier–Stokes/transport equations for simulation, while the Brinkman–Forchheimer/transport equations model is used for the third scenario.

The main purpose of this chapter is to give a detailed explanation of the numerical models to be considered, as well as their discrete formulations and their respective matrix block structures. In addition, we performed several numerical simulations for different scenarios in order to show the applicability of the method. In particular, we will first consider simulations in a single channel, which are commonly reported in the literature. In addition, we will numerically investigate the performance of two coupled feed and permeate channels.

The chapter is structured as follows. In Section 2.2 we introduce the model problem of interest in a single channel and define the unknowns to be considered in the variational formulation. Subsequently, in the same section we set the saddle point structure of the discrete variational system and its corresponding matrix block structure. Additionally, the mixed finite element discretization in two coupled domains is explained and its resolution strategy by means of a fixed point algorithm is carried out. Next, numerical simulations that illustrate the applicability of the methods and a detailed discussion are reported in Section 2.3. To conclude, we provide some final remarks in Chapter 4.

2.2 Theoretical description

2.2.1 A single channel

Brinkman–Forchheimer/transport equations. Let Ω be a bounded polygonal domain in $\mathbb{R}^2$ with boundary $\partial\Omega$ as shown in Figure 2.1 and assume that the boundary is decomposed into an inlet Γ_{in}, an outlet Γ_{out}, and two portions describing the membrane, denoted by Σ, i.e., $\partial\Omega = \overline{\Gamma}_{\text{in}} \cup \overline{\Gamma}_{\text{out}} \cup \overline{\Sigma}$. In addition, we denote by $\mathbf{n}$ the unit outward normal vector on $\partial\Omega$ and by $\boldsymbol{m}_\Sigma$ the tangent vector on Σ. The mathematical model describing the behavior of saline water in a RO module consists of a coupled set of partial differential equations where the Brinkman–Forchheimer equations, used to describe the fluid dynamics, are coupled with a transport equation employed to model the concentration of salt within the channel Ω. More precisely, we consider the following coupled system of equations [5, 92]:

$$\begin{aligned} -\nu \triangle \frac{\widehat{\mathbf{u}}}{\varepsilon} + \rho \, \mathbf{div}\Big(\frac{\widehat{\mathbf{u}}}{\varepsilon} \otimes \frac{\widehat{\mathbf{u}}}{\varepsilon}\Big) + \nabla p = -\widehat{\mathtt{D}}\widehat{\mathbf{u}} - \widehat{\mathtt{F}}|\widehat{\mathbf{u}}|\widehat{\mathbf{u}}, \quad \mathrm{div}\Big(\frac{\widehat{\mathbf{u}}}{\varepsilon}\Big) = 0 \quad \text{in} \quad \Omega, \\ -\kappa \triangle \phi + \frac{\widehat{\mathbf{u}}}{\varepsilon} \cdot \nabla \phi = 0 \quad \text{in} \quad \Omega, \end{aligned} \tag{2.1}$$

where $\widehat{\mathbf{u}}$ is the fluid velocity, p the fluid pressure and ϕ the salt concentration occupying the domain Ω. The given data are the fluid dynamic viscosity ν, the fluid density ρ, the solute diffusivity through the solvent κ and the porosity of the medium ε. All these parameters are assumed to be positive constants. In turn, $\widehat{\mathtt{D}}$ and $\widehat{\mathtt{F}}$ are the Darcy and Forchheimer coefficients, respectively, assumed to be either positive constants or equal to zero. The case where $\widehat{\mathtt{D}} > 0$ and $\widehat{\mathtt{F}} > 0$ will be used to describe the situation with implicit spacers. Conversely, when $\widehat{\mathtt{D}}$ and $\widehat{\mathtt{F}}$ are zero, the system (2.1) reduces to the Navier–Stokes/transport problem, which will be used to describe the case with explicit spacers. For the sake of simplicity, in what follows, we introduce the changes of variables $\mathbf{u} := \widehat{\mathbf{u}}/\epsilon$, $\mathtt{D} := \varepsilon \widehat{\mathtt{D}}$ and $\mathtt{F} := \varepsilon^2 \widehat{\mathtt{F}}$.

We complement these equations with suitable boundary conditions on each part of the boundary as described as follows.

Inlet and outlet boundaries. In the inlet boundary Γ_{in}, we consider a given velocity profile $\mathbf{u}_{\text{in}}$ and constant concentration ϕ_{in}. In the outlet of the channel, denoted by Γ_{out}, we consider a do-nothing boundary condition and zero diffusion of salt. That is

$$\mathbf{u} = \mathbf{u}_{\text{in}}, \quad \phi = \phi_{\text{in}} \quad \text{on} \quad \Gamma_{\text{in}} \quad \text{and} \quad (\nu \nabla \mathbf{u} - p\mathbb{I})\mathbf{n} = \mathbf{0}, \quad \kappa \nabla \phi \cdot \mathbf{n} = 0 \quad \text{on} \quad \Gamma_{\text{out}}. \tag{2.2}$$

Remark 2.1. As noticed in [83, Section 1] (see also [85, Section 2.2]), the open boundary condition (second equation in (2.2)), is usually considered thinking of truncating a bigger physical domain (e.g., outflow profile for flow in a bifurcated channel), allowing the fluid to flow naturally.

Imperfect membrane boundary conditions. At membrane surface, velocity and salt concentration are coupled through the following relations (see [33])

$$\mathbf{u} \cdot \boldsymbol{m}_\Sigma = 0, \quad \mathbf{u} \cdot \mathbf{n} = c_0 - c_1 \phi\,, \quad (\phi \mathbf{u} - \kappa \nabla \phi) \cdot \mathbf{n} \, = \, c_2 \phi \quad \text{on} \quad \Sigma,$$

where $c_0 := A\Delta P$, $c_1 := AiRT$ and $c_2 := B$ are positive constants specified later on in Table 2.1. Notice that, a simple algebraic manipulation allows us to rewrite this condition as follows:

$$\mathbf{u} \cdot \boldsymbol{m}_\Sigma = 0, \quad \mathbf{u} \cdot \mathbf{n} = c_0 - c_1 \phi\,, \quad \kappa \nabla \phi \cdot \mathbf{n} + c_1 \phi^2 + c_3 \phi \, = \, 0 \quad \text{on} \quad \Sigma, \tag{2.3}$$

where $c_3 = c_2 - c_0$.

We conclude this section by outlining the considerations to be taken into account when using either explicit or implicit spacers.

Explicit spacers. Explicit spacers are obstacles placed inside the channel with the aim of enhancing the permeate flux. These obstacles are assumed to have a circular shape with boundary $\mathit{\Gamma}_{\mathrm{s}}$ (see Figure 2.1).

As previously mentioned, when introducing explicit spacers in the channel, $\widehat{\mathtt{D}}$ and $\widehat{\mathtt{F}}$ are set to zero, reducing the set of equations (2.1) to a Navier–Stokes/transport coupled problem. Additionally, on $\mathit{\Gamma}_{\mathrm{s}}$, the following boundary conditions must be considered (see [33]):

$$\kappa\nabla\phi\cdot\mathbf{n} = 0 \quad \text{on} \quad \mathit{\Gamma}_{\mathrm{s}} \quad \text{and} \quad \mathbf{u} = \mathbf{0} \quad \text{on} \quad \mathit{\Gamma}_{\mathrm{s}}. \tag{2.4}$$

Implicit spacers. In the second scenario, the spacers are treated implicitly. In this case, we consider $\mathit{\Gamma}_{\mathrm{s}} = \emptyset$ and the effect of the spacers is emulated by making the fluid to flow through a porous media. This means we solve the Darcy–Forchheimer equation, where $\widehat{\mathtt{D}} := \dfrac{\nu}{\widehat{K}}$ and $\widehat{\mathtt{F}} := \dfrac{1.75\,\rho\,\varepsilon}{\sqrt{150\,\varepsilon^3\widehat{K}}}$ are the Darcy and Forchheimer coefficients [92, 93], and $\widehat{K}$ and ε, are the porous medium permeability and the porosity of the medium, respectively. In turn, we keep in mind that spacers are treated implicitly. That is, if we want to emulate the effect of $\mathtt{N_{sp}}$ spacers of diameter d_{s}, the porosity of the medium can be calculated as [79, eq. (1)]

$$\varepsilon = \frac{\mathtt{A_{tot}} - \mathtt{A_{sp}}}{\mathtt{A_{tot}}} = \frac{\mathtt{A_{tot}} - \mathtt{N_{sp}}\pi(0.25)d_{\mathrm{s}}^2}{\mathtt{A_{tot}}}, \tag{2.5}$$

where $\mathtt{A_{tot}}$ and $\mathtt{A_{sp}}$ stand for the total area of the domain and the area occupied for the spacers, respectively. Next, the permeability is determined using the Kozeny–Carman equation [97, Section 2]

$$\widehat{K} = \mathit{\Phi}^2\frac{d_{\mathrm{s}}^2}{180}\frac{\varepsilon^3}{(1-\varepsilon)^2}, \tag{2.6}$$

where $\mathit{\Phi}$ is the sphericity of the particle forming the porous media.

Remark 2.2. Numerical simulations considering a model of implicit spacers require less computational effort compared to the case of explicit spacers, because the latter configuration need a finer mesh near the spacers. However, the price to pay is that the implicit spacers model cannot detect the local effect of the spacers, since their influence is being averaged along the channel. In fact, the porous medium emulating the effect of the spacers, only takes into account the number of spacers but not their distribution in the channel. We will go back to this point in the numerical simulation section.

Mixed finite element discretization.

We propose a mixed finite element discretization to approximate the solution of the coupled system (2.1)–(2.3). To that end, and as previously mentioned in Section 2.1, we introduce further unknowns and rewrite the system of equations as a first-order set of equations. In fact, we let $\boldsymbol{\sigma} := \nu\nabla\mathbf{u} - p\mathbb{I}$ and $\mathbf{t} := \kappa\nabla\phi$ and proceed similarly to [34] to rewrite (2.1) equivalently as follows

$$\frac{1}{\nu}\boldsymbol{\sigma}^{\mathtt{d}} = \nabla\mathbf{u}, \quad \mathbf{div}(\boldsymbol{\sigma}) - \frac{\rho}{\nu}\boldsymbol{\sigma}^{\mathtt{d}}\,\mathbf{u} - \mathtt{D}\mathbf{u} - \mathtt{F}|\mathbf{u}|\mathbf{u} = \mathbf{0}, \quad \mathbf{t} = \kappa\,\nabla\phi \quad \text{and} \quad \kappa\,\mathrm{div}(\mathbf{t}) = \mathbf{u}\cdot\mathbf{t}. \tag{2.7}$$

We observe that employing the incompressibility condition $\mathrm{div}(\mathbf{u}) = 0$ in Ω, we have eliminated the pressure from the system (see [69] for more details), which however can be recovered by means of the postprocessing formula

$$p = -\frac{1}{2}\mathrm{tr}(\boldsymbol{\sigma}).$$

In turn, using these new variables $\boldsymbol{\sigma}$ and $\mathbf{t}$, we rewrite (2.2) as

$$\mathbf{u} = \mathbf{u}_{\mathrm{in}} \quad \text{on} \quad \Gamma_{\mathrm{in}}, \quad \boldsymbol{\sigma}\mathbf{n} = \mathbf{0} \quad \text{on} \quad \Gamma_{\mathrm{out}}, \quad \phi = \phi_{\mathrm{in}} \quad \text{on} \quad \Gamma_{\mathrm{in}} \quad \text{and} \quad \mathbf{t}\cdot\mathbf{n} = 0 \quad \text{on} \quad \Gamma_{\mathrm{out}}. \tag{2.8}$$

Finally, due to technical reasons discussed in [10] and [69], we let $\Gamma_{\mathrm{in}}^{\mathrm{c}} := \partial\Omega \setminus \Gamma_{\mathrm{in}}$ and introduce the additional variable $\xi := -\phi|_{\Gamma_{\mathrm{in}}^{\mathrm{c}}}$, known as Lagrange multiplier in the context of mixed finite element methods. Then, rewrite (2.3) as

$$\mathbf{u}\cdot\boldsymbol{m}_{\Sigma} = 0, \quad \mathbf{u}\cdot\mathbf{n} = c_0 + c_1\xi\,, \quad \mathbf{t}\cdot\mathbf{n} + c_1\xi^2 - c_3\xi \;=\; 0 \quad \text{on} \quad \Sigma. \tag{2.9}$$

Now, we let $\{\mathcal{T}_h\}_{h>0}$ be a family of shape regular partition of the domain Ω formed by triangles K of diameter h_K, and denote by $h := \max\{h_K : K \in \mathcal{T}_h\}$ its corresponding meshsize. On each K we define the local Raviart-Thomas element of order 0 as (see [67] for further details)

$$\mathbf{RT}_0(K) := \left\{ \mathbf{v} : K \to \mathbb{R}^2 : \mathbf{v}(x_1,x_2) := \begin{pmatrix} a \\ b \end{pmatrix} + c\begin{pmatrix} x_1 \\ x_2 \end{pmatrix}, \quad a,b,c \in \mathbb{R} \right\},$$

and denote by $\mathrm{P}_0(K)$ the spaces of polynomials of degree 0 in K. Then, we introduce, respectively, the following finite element spaces for the variables $\mathbf{t}$, $\boldsymbol{\sigma}$, ϕ and $\mathbf{u}$:

$$\begin{aligned}
&\mathbf{H}_h := \Big\{ \mathbf{s} : \Omega \to \mathbb{R}^2 : \quad \mathbf{s}|_K \in \mathbf{RT}_0(K) \quad \forall\, K \in \mathcal{T}_h \Big\},\\
&\mathbb{H}_h := \Big\{ \boldsymbol{\tau} = (\boldsymbol{\tau}_{ij}) : \Omega \to \mathbb{R}^{2\times 2} : (\boldsymbol{\tau}_{i,1}, \boldsymbol{\tau}_{i,2})^t \in \mathbf{H}_h,\, i \in \{1,2\} \quad \text{and} \quad \boldsymbol{\tau}\mathbf{n} = \mathbf{0} \quad \text{on} \quad \Gamma_{\mathrm{out}} \Big\},\\
&\mathrm{X}_h := \{ \psi : \Omega \to \mathbb{R} : \psi|_K \in \mathrm{P}_0(K) \quad \forall\, K \in \mathcal{T}_h \},\\
&\mathbf{Q}_h := \{ \mathbf{v} = (v_1, v_2)^t : \Omega \to \mathbb{R}^2 : v_i \in \mathrm{X}_h,\, i \in \{1,2\} \}.
\end{aligned} \tag{2.10}$$

It remains to introduce the finite element space to approximate the Lagrange multiplier ξ. To that end, we proceed similarly to [69] and denote by $\Gamma_{\mathrm{in},h}^{\mathrm{c}}$ the partition of $\Gamma_{\mathrm{in}}^{\mathrm{c}}$ inherited from $\mathcal{T}_h$. Let us assume, without loss of generality, that the number of edges of $\Gamma_{\mathrm{in},h}^{\mathrm{c}}$ is even. Then, we let $\Gamma_{\mathrm{in},2h}^{\mathrm{c}}$ be the partition of $\Gamma_{\mathrm{in}}^{\mathrm{c}}$ arising by joining pairs of adjacent edges of $\Gamma_{\mathrm{in},h}^{\mathrm{c}}$. If the number of edges of $\Gamma_{\mathrm{in},h}^{\mathrm{c}}$ is odd, we simply reduce it to the even case by adding one node to the discretization of the interface and locally modify the triangulation to keep the mesh conformity and regularity. According to the above, we define the following finite element space for the unknown ξ:

$$\mathrm{M}_h := \Big\{ \eta_h \in \mathcal{C}(\Gamma_{\mathrm{in}}^{\mathrm{c}}) : \quad \eta_h|_e \in \mathrm{P}_1(e) \quad \forall \text{ edge } e \in \Gamma_{\mathrm{in},2h}^{\mathrm{c}} \Big\},$$

where $\mathrm{P}_1(e)$ is the space of linear polynomials defined on an edge e of $\Gamma_{\mathrm{in},2h}^{\mathrm{c}}$. In this way, having introduced the finite element spaces for each unknown, the discrete nonlinear system of equations to approximate the solution of (2.7)–(2.9), reads: Find $\boldsymbol{\sigma}_h \in \mathbb{H}_h$, $\mathbf{u}_h \in \mathbf{Q}_h$, $\mathbf{t}_h \in \mathbf{H}_h$, $\phi_h \in \mathrm{X}_h$ and

$\xi_h \in \mathrm{M}_h$, such that

$$\frac{1}{\nu}\int_\Omega \boldsymbol{\sigma}_h^{\mathtt{d}} : \boldsymbol{\tau}_h + \int_\Omega \mathbf{u}_h \cdot \mathbf{div}\boldsymbol{\tau}_h = \int_{\Gamma_{\mathrm{out}}^{\mathrm{c}}} (\boldsymbol{\tau}_h \mathbf{n}) \cdot \mathbf{u}_{\mathrm{D},\xi_h} \quad \forall \boldsymbol{\tau}_h \in \mathbb{H}_h, \tag{2.11a}$$

$$\int_\Omega \mathbf{v}_h \cdot \mathbf{div}\boldsymbol{\sigma}_h - \mathtt{D}\int_\Omega \mathbf{u}_h \cdot \mathbf{v}_h - \mathtt{F}\int_\Omega |\mathbf{u}_h|\mathbf{u}_h \cdot \mathbf{v}_h - \frac{\rho}{\nu}\int_\Omega \boldsymbol{\sigma}_h^{\mathtt{d}} \mathbf{u}_h \cdot \mathbf{v}_h = 0 \quad \forall \mathbf{v}_h \in \mathbf{Q}_h, \tag{2.11b}$$

$$\frac{1}{\kappa}\int_\Omega \mathbf{t}_h \cdot \mathbf{s}_h + \int_\Omega \phi_h \mathrm{div}\mathbf{s}_h + \int_{\Gamma_{\mathrm{in}}^{\mathrm{c}}} (\mathbf{s}_h \cdot \mathbf{n})\xi_h = \int_{\Gamma_{\mathrm{in}}} (\mathbf{s}_h \cdot \mathbf{n})\phi_{\mathrm{in}} \quad \forall \mathbf{s}_h \in \mathbf{H}_h, \tag{2.11c}$$

$$\int_\Omega \psi_h \mathrm{div}\mathbf{t}_h - \frac{1}{\kappa}\int_\Omega \mathbf{u}_h \cdot \mathbf{t}_h \psi_h = 0 \quad \forall \psi_h \in \mathrm{X}_h, \tag{2.11d}$$

$$\int_{\Gamma_{\mathrm{in}}^{\mathrm{c}}} (\mathbf{t}_h \cdot \mathbf{n})\eta_h - c_3\int_\Sigma \xi_h \eta_h + c_1\int_\Sigma \xi_h^2\, \eta_h = 0 \quad \forall \eta_h \in \mathrm{M}_h, \tag{2.11e}$$

where for each $\chi_h \in \mathrm{M}_h$, $\mathbf{u}_{\mathrm{D},\chi_h}$ is defined as:

$$\mathbf{u}_{\mathrm{D},\chi_h} = \begin{cases} \mathbf{u}_{\mathrm{in}} & \text{on} \quad \Gamma_{\mathrm{in}}, \\ (c_1\chi_h + c_0)\mathbf{n} & \text{on} \quad \Sigma. \end{cases} \tag{2.12}$$

We observe that equations (2.11a), (2.11b), (2.11c) and (2.11d) correspond to the discretization of the first, second, third and fourth equations of (2.7), respectively, whereas (2.11e) is the discrete version of the third equation of (2.9).

Remark 2.3. When introducing explicit spacers in the channel, the boundary conditions set in (2.4), which are rewritten as

$$\mathbf{t} \cdot \mathbf{n} = 0 \quad \text{on} \quad \Gamma_{\mathrm{s}} \quad \text{and} \quad \mathbf{u} = \mathbf{0} \quad \text{on} \quad \Gamma_{\mathrm{s}}, \tag{2.13}$$

suggest to slightly modify the third term of (2.11c), the first term of (2.11e) and the boundary datum $\mathbf{u}_{\mathrm{D},\chi_h}$ by

$$\int_{\Gamma_{\mathrm{in}}^{\mathrm{c}} \cup \Gamma_{\mathrm{s}}} (\mathbf{s}_h \cdot \mathbf{n})\xi_h, \quad \int_{\Gamma_{\mathrm{in}}^{\mathrm{c}} \cup \Gamma_{\mathrm{s}}} (\mathbf{t}_h \cdot \mathbf{n})\eta_h \quad \text{and} \quad \mathbf{u}_{\mathrm{D},\chi_h} = \begin{cases} \mathbf{0} & \text{on} \quad \Gamma_{\mathrm{s}}, \\ \mathbf{u}_{\mathrm{in}} & \text{on} \quad \Gamma_{\mathrm{in}}, \\ (c_1\chi_h + c_0)\mathbf{n} & \text{on} \quad \Sigma, \end{cases}$$

respectively.

Solving strategy.

The nonlinear numerical scheme (2.11a)–(2.11e) will be solved by a fixed point iteration. To explain clearly this strategy, and for the sake of presentation, we will express the set of equations in a block structure. We begin by noticing that the discrete system can be rewritten more compactly as follows:

Find $\boldsymbol{\sigma}_h \in \mathbb{H}_h$, $\mathbf{u}_h \in \mathbf{Q}_h$, $\mathbf{t}_h \in \mathbf{H}_h$, $\phi_h \in \mathrm{X}_h$, $\xi_h \in \mathrm{M}_h$, such that

$$\begin{aligned}
&\mathbf{a_S}(\boldsymbol{\sigma}_h,\boldsymbol{\tau}_h) + \mathbf{b_S}(\boldsymbol{\tau}_h,\mathbf{u}_h) && && = \mathbf{F}(\xi_h;\boldsymbol{\tau}_h) && \forall\, \boldsymbol{\tau}_h \in \mathbb{H}_h,\\
&\mathbf{b_S}(\boldsymbol{\sigma}_h,\mathbf{v}_h) - \mathbf{d_S}(\mathbf{u}_h;\mathbf{u}_h,\mathbf{v}_h) && -\mathbf{O_S}(\mathbf{u}_h;\boldsymbol{\sigma}_h,\mathbf{v}_h) && = 0 && \forall\, \mathbf{v}_h \in \mathbf{Q}_h,\\
&\mathbf{a_T}(\mathbf{t}_h,\mathbf{s}_h) + \mathbf{b}_{\mathbf{T},1}(\mathbf{s}_h,\phi_h) && +\mathbf{b}_{\mathbf{T},2}(\mathbf{s}_h,\xi_h) && = \boldsymbol{\mathcal{H}}(\mathbf{s}_h) && \forall\, \mathbf{s}_h \in \mathbf{H}_h,\\
&\mathbf{b}_{\mathbf{T},1}(\mathbf{t}_h,\psi_h) && -\mathbf{O_T}(\mathbf{u}_h;\mathbf{t}_h,\psi_h) && = 0 && \forall\, \psi_h \in \mathrm{X}_h,\\
&\mathbf{b}_{\mathbf{T},2}(\mathbf{t}_h,\eta_h) && -\mathbf{d_T}(\xi_h,\eta_h) + \mathbf{C_T}(\xi_h;\xi_h,\eta_h) && = 0 && \forall\, \eta_h \in \mathrm{M}_h.
\end{aligned} \tag{2.14}$$

where $\mathbf{a_S}(\cdot,\cdot)$, $\mathbf{b_S}(\cdot,\cdot)$, $\mathbf{a_T}(\cdot,\cdot)$, $\mathbf{b}_{\mathbf{T},1}(\cdot,\cdot)$, $\mathbf{b}_{\mathbf{T},2}(\cdot,\cdot)$ and $\mathbf{d_T}(\cdot,\cdot)$ are the bilinear forms defined as

$$\begin{aligned}
&\mathbf{a_S}(\boldsymbol{\sigma}_h,\boldsymbol{\tau}_h) := \frac{1}{\nu}\int_\Omega \boldsymbol{\sigma}_h^{\mathrm{d}} : \boldsymbol{\tau}_h^{\mathrm{d}}, \quad \mathbf{b_S}(\boldsymbol{\tau}_h,\mathbf{v}_h) := \int_\Omega \mathbf{u}_h \cdot \mathbf{div}(\boldsymbol{\tau}_h), \quad \mathbf{a_T}(\mathbf{t}_h,\,\mathbf{s}_h) := \frac{1}{\kappa}\int_\Omega \mathbf{t}_h \cdot \mathbf{s}_h,\\
&\mathbf{b}_{\mathbf{T},1}(\mathbf{s}_h,\psi_h) := \int_\Omega \psi_h \mathrm{div}(\mathbf{s}_h), \quad \mathbf{b}_{\mathbf{T},2}(\mathbf{s}_h,\eta_h) := \int_{\Gamma_{\mathrm{in}}^{\mathrm{c}}} (\mathbf{s}_h \cdot \mathbf{n})\,\eta_h, \quad \mathbf{d_T}(\xi_h,\eta_h) := c_3 \int_\Sigma \xi_h \eta_h;
\end{aligned} \tag{2.15}$$

and, for each $\chi_h \in \mathrm{M}_h$, $\mathbf{F}(\chi_h;\cdot)$ and $\mathbf{C_T}(\chi_h;\cdot,\cdot)$ are given by

$$\mathbf{F}(\chi_h;\boldsymbol{\tau}_h) \;:=\; \int_{\Gamma_{\mathrm{out}}^{\mathrm{c}}} (\boldsymbol{\tau}_h\mathbf{n})\,\mathbf{u}_{\mathrm{D},\,\chi_h}, \quad \mathbf{C_T}(\chi_h;\xi_h,\eta_h) \;:=\; c_1 \int_\Sigma \chi_h\,\xi_h\,\eta_h. \tag{2.16}$$

For each $\mathbf{w}_h \in \mathbf{Q}_h$, $\mathbf{O_S}(\mathbf{w}_h;\cdot,\cdot)$, $\mathbf{O_T}(\mathbf{w}_h;\cdot,\cdot)$ and $\mathbf{d_S}(\mathbf{w}_h;\cdot,\cdot)$ are defined by

$$\begin{aligned}
&\mathbf{O_S}(\mathbf{w}_h;\boldsymbol{\sigma}_h,\mathbf{v}_h) \;:=\; \frac{\rho}{\nu}\int_\Omega \boldsymbol{\sigma}_h^{\mathrm{d}}\mathbf{w}_h \cdot \mathbf{v}_h, \quad \mathbf{O_T}(\mathbf{w}_h;\mathbf{t}_h,\psi_h) \;:=\; \frac{1}{\kappa}\int_\Omega \mathbf{w}_h \cdot \mathbf{t}_h\psi_h,\\
&\mathbf{d_S}(\mathbf{w}_h;\mathbf{u}_h,\mathbf{v}_h) \;:=\; \mathtt{D}\int_\Omega \mathbf{u}_h \cdot \mathbf{v}_h + \mathtt{F}\int_\Omega |\mathbf{w}_h|\mathbf{u}_h \cdot \mathbf{v}_h.
\end{aligned} \tag{2.17}$$

Finally, $\boldsymbol{\mathcal{H}}(\cdot)$ is the linear functional given by

$$\boldsymbol{\mathcal{H}}(\mathbf{s}_h) := \int_{\Gamma_{\mathrm{in}}} (\mathbf{s}_h \cdot \mathbf{n})\phi_{\mathrm{in}}. \tag{2.18}$$

In what follows, in abuse of notation, we denote by $\boldsymbol{\sigma}_h$, $\mathbf{u}_h$, $\mathbf{t}_h$, ϕ_h, and ξ_h the degrees of freedom associated to the unknowns of (2.14). In turn, $\mathbf{a_S}$, $\mathbf{a_T}$, $\mathbf{b_S}$, $\mathbf{b}_{\mathbf{T},1}$, $\mathbf{b}_{\mathbf{T},2}$, $\mathbf{d_T}$, $\mathbf{O_S}(\mathbf{w}_h)$, $\mathbf{O_T}(\mathbf{w}_h)$, $\mathbf{d_S}(\mathbf{w}_h)$ and $\mathbf{C_T}(\chi_h)$ will denote the corresponding finite element matrices associated to the bilinear forms in (2.15)-(2.17), and $\mathbf{F}(\chi_h)$ and $\boldsymbol{\mathcal{H}}$ will denote the vectors associated to $\mathbf{F}(\chi_h;\cdot)$ and $\boldsymbol{\mathcal{H}}(\cdot)$, defined in (2.16) and (2.18), respectively. Then from (2.14) we obtain the following system

$$\left(\begin{array}{c|c} \mathcal{A}_{\mathbf{S}}(\mathbf{u}_h) & \mathbf{0} \\ \hline \mathbf{0} & \mathcal{A}_{\mathbf{T}}(\mathbf{u}_h,\xi_h) \end{array}\right) \begin{pmatrix} \boldsymbol{\sigma}_h \\ \mathbf{u}_h \\ \hline \mathbf{t}_h \\ \phi_h \\ \xi_h \end{pmatrix} = \begin{pmatrix} \mathbf{F}(\xi_h) \\ \mathbf{0} \\ \boldsymbol{\mathcal{H}} \\ \mathbf{0} \\ \mathbf{0} \end{pmatrix}, \tag{2.19}$$

where

$$\mathcal{A}_{\mathbf{S}}(\mathbf{u}_h) := \left(\begin{array}{c|c} \mathbf{a}_{\mathbf{S}} & \mathbf{b}_{\mathbf{S}} \\ \hdashline (\mathbf{b}_{\mathbf{S}})^t - \mathbf{O}_{\mathbf{S}}(\mathbf{u}_h) & -\mathbf{d}_{\mathbf{S}}(\mathbf{u}_h) \end{array}\right) \tag{2.20}$$

and

$$\mathcal{A}_{\mathbf{T}}(\mathbf{u}_h, \xi_h) := \left(\begin{array}{c|c|c} \mathbf{a}_{\mathbf{T}} & \mathbf{b}_{\mathbf{T},1} & \mathbf{b}_{\mathbf{T},2} \\ \hdashline (\mathbf{b}_{\mathbf{T},1})^t - \mathbf{O}_{\mathbf{T}}(\mathbf{u}_h) & \mathbf{0} & \mathbf{0} \\ \hdashline (\mathbf{b}_{\mathbf{T},2})^t & \mathbf{0} & -\mathbf{d}_{\mathbf{T}} + \mathbf{C}_{\mathbf{T}}(\xi_h) \end{array}\right). \tag{2.21}$$

Now we turn to explain the iterative scheme to solve (2.19). To that end, we let ξ_h^0 and $\mathbf{u}_h^0$ be initial guesses. Then, for each $n \geq 1$, first we solve the linear system: Find $(\boldsymbol{\sigma}_h^n, \mathbf{u}_h^n)$, such that

$$\mathcal{A}_{\mathbf{S}}(\mathbf{u}_h^{n-1}) \begin{pmatrix} \boldsymbol{\sigma}_h^n \\ \mathbf{u}_h^n \end{pmatrix} = \begin{pmatrix} \mathbf{F}(\xi_h^{n-1}) \\ \mathbf{0} \end{pmatrix},$$

and after computing $\boldsymbol{\sigma}_h^n$ and $\mathbf{u}_h^n$, we solve the linear system: Find $(\mathbf{t}_h^n, \phi_h^n, \xi_h^n)$, such that

$$\mathcal{A}_{\mathbf{T}}(\mathbf{u}_h^n, \xi_h^{n-1}) \begin{pmatrix} \mathbf{t}_h^n \\ \phi_h^n \\ \xi_h^n \end{pmatrix} = \begin{pmatrix} \boldsymbol{\mathcal{H}} \\ \mathbf{0} \\ \mathbf{0} \end{pmatrix}.$$

The iterative algorithm stops when certain criteria (see Section 2.3) is satisfied.

2.2.2 Coupled feed and permeate channels

We consider a model for two coupled channels where water with salt concentration flows through the feed channel Ω_{f} and passes through a membrane Σ to the permeate channel Ω_{p}. In order to describe the geometry, we let Ω_{f} and Ω_{p} be two bounded polygonal domains in R^2 such that $\partial\Omega_{\mathrm{f}} \cap \partial\Omega_{\mathrm{p}} = \Sigma \neq \emptyset$ and $\Omega_{\mathrm{f}} \cap \Omega_{\mathrm{p}} = \emptyset$, and set $\Omega := \Omega_{\mathrm{f}} \cup \Sigma \cup \Omega_{\mathrm{p}}$. In turn, for each $\star \in \{\mathrm{f}, \mathrm{p}\}$ we denote $\Gamma_\star := \partial\Omega_\star \setminus \overline{\Sigma} = \Gamma_{\mathrm{in},\star} \cup \overline{\Gamma}_{\mathrm{w},\star} \cup \Gamma_{\mathrm{out},\star}$, where $\Gamma_{\mathrm{w},\star}$ denotes the top ($\star = \mathrm{f}$) and bottom ($\star = \mathrm{p}$) boundaries of the channel (see Figure 2.2), and by $\mathbf{n}_\star$ we denote the unit normal vector, which is chosen pointing outwards from $\Omega_\star$, thus $\mathbf{n}_{\mathrm{f}} = -\mathbf{n}_{\mathrm{p}}$ on Σ. We also consider a unit tangent vector $\boldsymbol{m}_\Sigma$ on Σ as in Figure 2.2. On each channel $\Omega_\star$, with $\star \in \{\mathrm{f}, \mathrm{p}\}$, the fluid and salt concentration satisfy the equations stated in Section 2.2.1, and the boundary conditions at the inlet and outlet are the ones specified in equations (2.2). More precisely, after introducing the further variables $\boldsymbol{\sigma}_\star := \nu_\star \nabla \mathbf{u}_\star - p_\star \mathbb{I}$ and $\mathbf{t}_\star := \kappa_\star \nabla \phi_\star$ in $\Omega_\star$ ($\star \in \{\mathrm{f}, \mathrm{p}\}$), we consider the first-order set of equations:

$$\begin{gathered} \frac{1}{\nu}\boldsymbol{\sigma}_\star^{\mathtt{d}} = \nabla \mathbf{u}_\star, \quad \mathbf{div}(\boldsymbol{\sigma}_\star) - \frac{\rho}{\nu}\boldsymbol{\sigma}_\star^{\mathtt{d}}\mathbf{u}_\star - \mathtt{D}\mathbf{u}_\star - \mathtt{F}|\mathbf{u}_\star|\mathbf{u}_\star = \mathbf{0}, \\ \mathbf{t}_\star = \kappa \nabla \phi_\star \quad \text{and} \quad \kappa \,\mathrm{div}(\mathbf{t}_\star) = \mathbf{u}_\star \cdot \mathbf{t}_\star, \end{gathered} \tag{2.22}$$

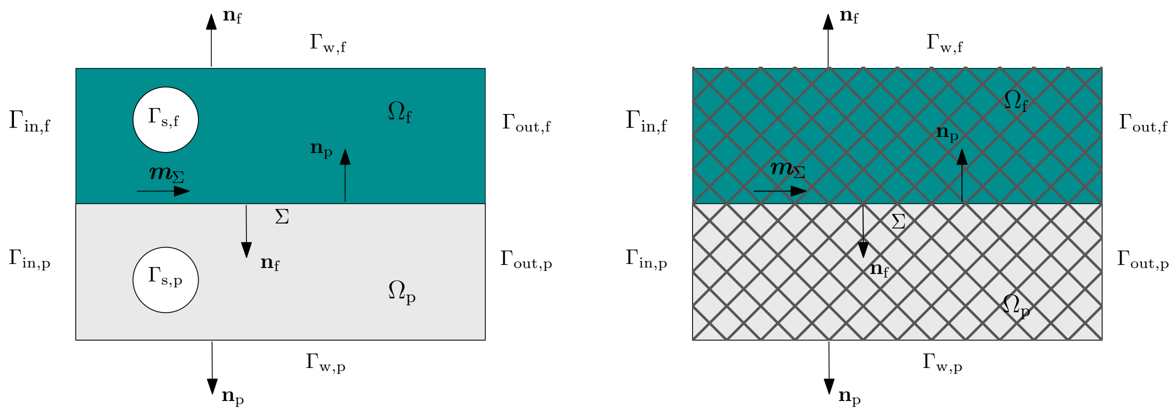

Figure 2.2: *Sketch of the coupled feed and permeate channels. Explicit spacers (left) and implicit spacers (right).*

and on $\mathit{\Gamma}_{\mathrm{in},\star}$ and $\mathit{\Gamma}_{\mathrm{out},\star}$, we consider the boundary conditions

$$\begin{aligned} \mathbf{u}_\star = \mathbf{u}_{\mathrm{in},\star} \quad \text{on} \quad \mathit{\Gamma}_{\mathrm{in},\star}, \quad \boldsymbol{\sigma}_\star \mathbf{n}_\star = \mathbf{0} \quad \text{on} \quad \mathit{\Gamma}_{\mathrm{out}_\star}, \\ \phi_\star = \phi_{\mathrm{in},\star} \quad \text{on} \quad \mathit{\Gamma}_{\mathrm{in},\star} \quad \text{and} \quad \mathbf{t}_\star \cdot \mathbf{n}_\star = 0 \quad \text{on} \quad \mathit{\Gamma}_{\mathrm{out},\star}. \end{aligned} \tag{2.23}$$

Both channels are coupled through a membrane $\mathit{\Sigma}$ by means of the transmission conditions :

$$\begin{aligned} \mathbf{u}_\star \cdot \boldsymbol{m}_{\mathit{\Sigma}} = 0, \quad \mathbf{u}_\mathrm{f} \cdot \mathbf{n}_\mathrm{f} \; = \; -\mathbf{u}_\mathrm{p} \cdot \mathbf{n}_\mathrm{p}, \quad \mathbf{u}_\mathrm{f} \cdot \mathbf{n}_\mathrm{f} = c_0 - c_1(\phi_\mathrm{f} - \phi_\mathrm{p}) \quad \text{on} \quad \mathit{\Sigma}, \\ \mathbf{t}_\mathrm{f} \cdot \mathbf{n}_\mathrm{f} + c_1(\phi_\mathrm{f} - \phi_\mathrm{p})\phi_\mathrm{f} + c_{3,\mathrm{f}}\phi_\mathrm{f} \; = \; c_2\phi_\mathrm{p}, \quad \mathbf{t}_\mathrm{p} \cdot \mathbf{n}_\mathrm{p} + c_1(\phi_\mathrm{p} - \phi_\mathrm{f})\phi_\mathrm{p} + c_{3,\mathrm{p}}\phi_\mathrm{p} \; = \; c_2\phi_\mathrm{f} \quad \text{on} \quad \mathit{\Sigma}, \end{aligned} \tag{2.24}$$

where $c_{3,\mathrm{f}} = c_2 - c_0$ and $c_{3,\mathrm{p}} = c_2 + c_0$. In turn, since the membrane is defined only as $\partial\mathit{\Omega}_\mathrm{f} \cap \partial\mathit{\Omega}_\mathrm{p} \; = \; \mathit{\Sigma}$, we consider the following wall-boundary conditions

$$\mathbf{u}_\star = \mathbf{0} \quad \text{on} \quad \mathit{\Gamma}_{\mathrm{w},\star}, \quad \text{and} \quad \mathbf{t}_\star \cdot \mathbf{n}_\star \; = \; 0 \quad \text{on} \quad \mathit{\Gamma}_{\mathrm{w},\star}. \tag{2.25}$$

Remark 2.4. In real applications of RO, the water in the permeate channel flows into the page of Figure 2.2 and does not contain spacers. Therefore, our two-dimensional simulations are not fully representative of the real model. However, our goal is to numerically explore the performance of our proposed scheme (2.14) in different scenarios where two channels are coupled, and both contain small obstacles. This is why we employ the same terminology and refer to the top and bottom channels of Figure 2.2 as the feed and permeate channels, respectively.

Mixed finite element discretization and solving strategy.

Let $\mathcal{T}_h^\mathrm{f}$ and $\mathcal{T}_h^\mathrm{p}$ be the respective triangulations of the domains $\mathit{\Omega}_\mathrm{f}$ and $\mathit{\Omega}_\mathrm{p}$ formed by shape-regular triangles of diameter h_K and denote by h_f and h_p their corresponding meshsizes. Assume that they match on $\mathit{\Sigma}$ so that $\mathcal{T}_h := \mathcal{T}_h^\mathrm{f} \cup \mathcal{T}_h^\mathrm{p}$ is a triangulation of $\mathit{\Omega}$. Hereafter, $h := \max\{h_\mathrm{f}, h_\mathrm{p}\}$. Since this two channel model is originated by coupling two single channels, from (2.19) we can deduce that the block structure of the non linear system of equations is the following:

$$\left(\begin{array}{c|c|c|c} \mathcal{A}_{\mathbf{S}}^{\mathrm{f}}(\mathbf{u}_{\mathrm{f},h}) & \mathbf{0} & \mathbf{0} & \mathbf{0} \\ \hline \mathbf{0} & \mathcal{A}_{\mathbf{S}}^{\mathrm{p}}(\mathbf{u}_{\mathrm{p},h}) & \mathbf{0} & \mathbf{0} \\ \hline \mathbf{0} & \mathbf{0} & \mathcal{A}_{\mathbf{T}}^{\mathrm{f}}(\mathbf{u}_{\mathrm{f},h}, \xi_{h,\mathrm{f}} - \xi_{h,\mathrm{p}}) & \mathbf{0} \\ \hline \mathbf{0} & \mathbf{0} & \mathbf{0} & \mathcal{A}_{\mathbf{T}}^{\mathrm{p}}(\mathbf{u}_{\mathrm{p},h}, \xi_{h,\mathrm{p}} - \xi_{h,\mathrm{f}}) \end{array}\right) \begin{pmatrix} \mathbf{X}_{\mathrm{f}} \\ \mathbf{X}_{\mathrm{p}} \\ \mathbf{Y}_{\mathrm{f}} \\ \mathbf{Y}_{\mathrm{p}} \end{pmatrix} = \begin{pmatrix} \mathbf{G}^{\mathrm{f}}(\xi_{\mathrm{f},h} - \xi_{\mathrm{p},h}) \\ \mathbf{G}^{\mathrm{p}}(\xi_{\mathrm{f},h} - \xi_{\mathrm{p},h}) \\ \mathcal{G}^{\mathrm{f}}(\xi_{\mathrm{p},h}) \\ \mathcal{G}^{\mathrm{p}}(\xi_{\mathrm{f},h}) \end{pmatrix},$$

where for $\star \in \{\mathrm{f}, \mathrm{p}\}$, $\mathcal{A}_{\mathbf{S}}^{\star}(\mathbf{u}_{\star,h})$ and $\mathcal{A}_{\mathbf{T}}^{\star}(\mathbf{u}_{\star,h}, \chi_h)$ are defined exactly as in (2.20) and (2.21), respectively, considering in this case that the integrals and functions in the bilinear forms that induce these matrices (cf. (2.15)–(2.17)), take values in $\Omega_\star$. In addition, for each $\star \in \{\mathrm{f}, \mathrm{p}\}$:

$$\mathbf{X}_\star := (\boldsymbol{\sigma}_{\star,h}, \mathbf{u}_{\star,h})^t \in \mathbb{H}_h^\star \times \mathbf{Q}_h^\star \quad \text{and} \quad \mathbf{Y}_\star := (\mathbf{t}_{\star,h}, \phi_{\star,h}, \xi_{\star,h})^t \in \mathbf{H}_h^\star \times \mathrm{X}_h^\star \times \mathrm{M}_h^\star,$$

where $\mathbb{H}_h^\star$, $\mathbf{Q}_h^\star$, $\mathbf{H}_h^\star$, $\mathrm{X}_h^\star$ and $\mathrm{M}_h^\star$ are the discrete spaces introduced in (2.10) adapted to $\Omega_\star$. Also, $\mathcal{G}^\star$ and $\mathbf{G}^\star$ are given by

$$\mathcal{G}^{\mathrm{f}}(\xi_{\mathrm{p},h}) := (\boldsymbol{\mathcal{H}}^{\mathrm{f}}, \mathbf{0}, \mathcal{F}^{\mathrm{f}}(\xi_{\mathrm{p},h}))^t, \quad \mathcal{G}^{\mathrm{p}}(\xi_{\mathrm{f},h}) := (\boldsymbol{\mathcal{H}}^{\mathrm{p}}, \mathbf{0}, \mathcal{F}^{\mathrm{p}}(\xi_{\mathrm{f},h}))^t \quad \text{and} \quad \mathbf{G}^\star(\xi_{\mathrm{f},h} - \xi_{\mathrm{p},h}) := (\mathbf{F}_{\mathsf{c}}^\star(\xi_{\mathrm{f},h} - \xi_{\mathrm{p},h}), \mathbf{0})^t.$$

Here, $\mathbf{F}_{\mathsf{c}}^\star(\xi_{\mathrm{f},h} - \xi_{\mathrm{p},h})$ is the vector associated to the functional that involves the Dirichlet boundary condition, defined as $\mathbf{F}_{\mathsf{c}}^\star(\xi_{\mathrm{f},h} - \xi_{\mathrm{p},h}; \boldsymbol{\tau}_{\star,h}) := \displaystyle\int_{\Gamma_{\mathrm{out},\star}^{\mathrm{c}}} (\boldsymbol{\tau}_{\star,h}\mathbf{n}_\star) \cdot \mathbf{u}_{\mathrm{D},\,\xi_{\mathrm{f},h} - \xi_{\mathrm{p},h}}$, where

$$\mathbf{u}^\star_{\mathrm{D},\,\xi_{\mathrm{f},h} - \xi_{\mathrm{p},h}} = \mathbf{u}_\star|_{\Gamma_{\mathrm{out},\star}^{\mathrm{c}}} = \begin{cases} \mathbf{0} & \text{on} \quad \Gamma_{\mathrm{w},\star}, \\ \mathbf{u}_{\mathrm{in},\star} & \text{on} \quad \Gamma_{\mathrm{in},\star}, \\ c_1(\xi_{\mathrm{f},h} - \xi_{\mathrm{p},h} + c_0)\mathbf{n}_{\mathrm{f}} & \text{on} \quad \Sigma, \end{cases} \tag{2.26}$$

with $\star \in \{\mathrm{f}, \mathrm{p}\}$. Moreover, $\boldsymbol{\mathcal{H}}^{\mathrm{f}}$ and $\boldsymbol{\mathcal{H}}^{\mathrm{p}}$ are suitably defined as in (2.18). Finally, $\mathcal{F}^{\mathrm{f}}(\xi_{\mathrm{p},h})$ and $\mathcal{F}^{\mathrm{p}}(\xi_{\mathrm{f},h})$ are the vectors associated to the functionals that arise from coupling terms in (1.17), given by

$$\mathcal{F}^{\mathrm{f}}(\xi_{\mathrm{p},h}; \eta_{\mathrm{f},h}) := -c_2 \int_\Sigma \xi_{\mathrm{p},h}\, \eta_{\mathrm{f},h} \quad \text{and} \quad \mathcal{F}^{\mathrm{p}}(\xi_{\mathrm{f},h}; \eta_{\mathrm{p},h}) := -c_2 \int_\Sigma \xi_{\mathrm{f},h}\, \eta_{\mathrm{p},h}, \tag{2.27}$$

respectively. Finally, the resulting fixed point algorithm is similar to that of Section 2.2.1. Indeed, given $\xi_{\star,h}^{n-1}$ and $\mathbf{u}_{\star,h}^{n-1}$, we look for $\mathbf{X}_\star^n := (\boldsymbol{\sigma}_{\star,h}^n, \mathbf{u}_{\star,h}^n)^t$, with $\star \in \{\mathrm{f}, \mathrm{p}\}$, such that

$$\left(\begin{array}{c|c} \mathcal{A}_{\mathbf{S}}^{\mathrm{f}}(\mathbf{u}_{\mathrm{f},h}^{n-1}) & \mathbf{0} \\ \hline \mathbf{0} & \mathcal{A}_{\mathbf{S}}^{\mathrm{p}}(\mathbf{u}_{\mathrm{p},h}^{n-1}) \end{array}\right) \begin{pmatrix} \mathbf{X}_{\mathrm{f}}^n \\ \mathbf{X}_{\mathrm{p}}^n \end{pmatrix} = \begin{pmatrix} \mathbf{G}^{\mathrm{f}}(\xi_{\mathrm{f},h}^n - \xi_{\mathrm{p},h}^n) \\ \mathbf{G}^{\mathrm{p}}(\xi_{\mathrm{f},h}^n - \xi_{\mathrm{p},h}^n) \end{pmatrix}.$$

Then, after $\mathbf{X}_\star^n := (\boldsymbol{\sigma}_{\star,h}^n, \mathbf{u}_{\star,h}^n)^t$ is computed, we find for $\mathbf{Y}_\star^n := (\mathbf{t}_{\star,h}^n, \phi_{\star,h}^n, \xi_{h,\star}^n)^t$, with $\star \in \{\mathrm{f}, \mathrm{p}\}$, such that

$$\left(\begin{array}{c|c} \mathcal{A}_{\mathbf{T}}^{\mathrm{f}}(\mathbf{u}_{\mathrm{f},h}^n, \xi_{h,\mathrm{f}}^{n-1} - \xi_{h,\mathrm{p}}^{n-1}) & \mathbf{0} \\ \hline \mathbf{0} & \mathcal{A}_{\mathbf{T}}^{\mathrm{p}}(\mathbf{u}_{\mathrm{p},h}^n, \xi_{h,\mathrm{p}}^{n-1} - \xi_{h,\mathrm{f}}^{n-1}) \end{array}\right) \begin{pmatrix} \mathbf{Y}_{\mathrm{f}}^n \\ \mathbf{Y}_{\mathrm{p}}^n \end{pmatrix} = \begin{pmatrix} \mathcal{G}^{\mathrm{f}}(\xi_{\mathrm{p},h}^{n-1}) \\ \mathcal{G}^{\mathrm{p}}(\xi_{\mathrm{f},h}^{n-1}) \end{pmatrix}.$$

2.2.3 Comments on the well-posedness of the numerical schemes

At this point, we note that the theoretical foundations provided in Chapter 1 offer a fairly general framework since they consider two coupled domains. Clearly, these results can be slightly adapted to establish the well-posedness of the Navier–Stokes/transport equations in a single channel. On the other hand, when the Brinkman–Forchheimer equations are considered instead of the Navier–Stokes equations, two additional terms appear in the variational scheme, as reflected in equation (2.11b). These terms constitute the bilinear form $\mathbf{d}_{\mathbf{S}}$, which is present in equation (2.14), and can be addressed, for instance, by proceeding as in [32, Theorem 4.1]. More precisely, this involves applying the theory developed in [50] to the Brinkman–Forchheimer equations instead of the one employed in Chapter 1 for the Navier–Stokes equations.

2.3 Numerical simulations

Inspired by the RO process, we now turn to the computational results to illustrate a variety of examples in both single and coupled channel systems, and considering explicit and implicit spacers. The computational implementation is based on a `FreeFem++` code (cf. [73]) and the use of the direct linear solvers UMFPACK (cf. [51]). The iterative method comes straightforward from the uncoupling strategy presented in Sections 2.2.1 and 2.2.2 and the iterations are terminated once the relative error of the entire coefficient vectors between two consecutive iterates is sufficiently small, that is

$$\frac{\|\mathbf{coeff}^{m+1} - \mathbf{coeff}^{m}\|_{l^2}}{\|\mathbf{coeff}^{m+1}\|_{l^2}} \leq \mathtt{tol} := 10^{-6}\,,$$

where $\|\cdot\|_{l^2}$ stands for the usual Euclidean norm in $\mathbb{R}^{\mathtt{dof}}$, with `dof` denoting the total number of degrees of freedom defining the finite element subspaces $\mathbb{H}_h$, $\mathbf{Q}_h$, $\mathbf{H}_h$, X_h, and M_h, when considering a single channel, and $\mathbb{H}_h^\star$, $\mathbf{Q}_h^\star$, $\mathbf{H}_h^\star$, $\mathrm{X}_h^\star$ and $\mathrm{M}_h^\star$, with $\star \in \{\mathrm{f}, \mathrm{p}\}$ for the case of two channels. In this way, the physical parameters specified in Section 2.2.1 are taken in Table 2.1 [33, 104].

Parameter	Meaning	Value	Units
T	System temperature	298	K
R	Ideal gas constant	8.314	$Jmol^{-1}K^{-1}$
i	Number of ions from salt solution	2	–
$\varDelta P$	Hydrostatic transmembrane pressure	$\varDelta P_1 := 4053000$ $\varDelta P_2 := 5575875$	Pa
ρ	Feed/permeate fluid density	1027.2	$kg\,m^{-3}$
κ	Feed/permeate diffusivity of salt in water	1.611×10^{-9}	m^2s^{-1}
ν	Feed/permeate fluid dynamic viscosity	8.9×10^{-4}	$kg\,m^{-1}s^{-1}$
A	Membrane water permeability	2.5×10^{-12}	$ms^{-1}\,Pa^{-1}$
B	Membrane salt permeability	2.5×10^{-8}	$m\,s^{-1}$

Table 2.1: Physical parameters

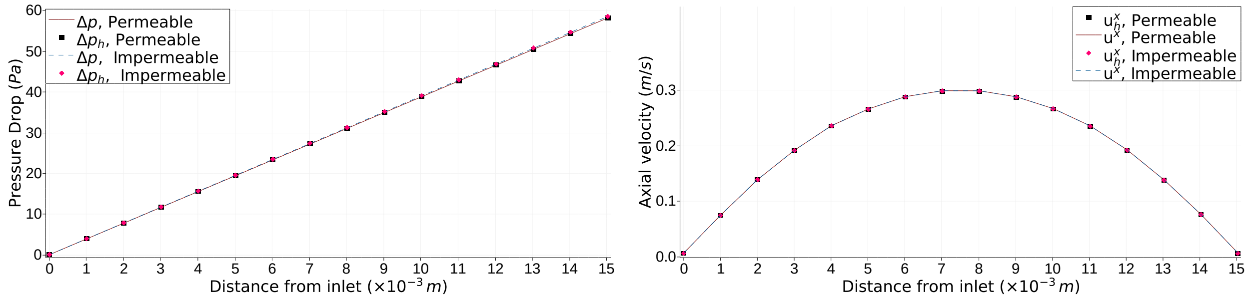

Figure 2.3: *Comparison of exact vs. approximate pressure drop (left) and axial velocity (right) for a single channel. Simulation conditions:* $\mathrm{u_{in}} = 0.2\,m/s$, $\varDelta P = \varDelta P_2$ *and clean water, for Poiseuille (impermeable) and Berman (permeable) flows.*

2.3.1 A single feed channel.

We consider the computational domain $\varOmega = (0, L) \times (0, d)$, where $L = 15\,mm$ and $d = 0.74\,mm$. In turn, the inlet velocity profile is set as follows

$$\mathbf{u}_{\rm in} := \Big(6\mathrm{u}_{\rm in}\frac{y}{d}\Big(1-\frac{y}{d}\Big), 2(c_0 - c_1\phi_{\rm in})\frac{y}{d} - (c_0 - c_1\phi_{\rm in})\Big)^t, \quad y \in [0, d], \tag{2.28}$$

where $\mathrm{u_{in,f}}$ stands for the inlet mean feed fluid velocity.

Simulation 1. A feed channel with no salt concentration. We consider a channel without explicit spacers and the numerical method is tested against classic analytical models of momentum transport in membrane modules, that is, those of Poiseuille and Berman flow models, by comparison of the pressure drop, denoted by $\varDelta p := p(0, d/2) - p(x, d/2)$. This validation implies the simulation of a uniform permeation of pure solvent ($\phi_{\rm f} = 0$), and then the pressure drop is obtained by solving the equations of motion with the following boundary conditions

$$\mathbf{u}\cdot\mathbf{n} = c_0 \text{ (for Berman flow)} \quad \text{on} \quad \varSigma \quad \text{and} \quad \mathbf{u}\cdot\mathbf{n} = 0 \text{ (for Poiseuille flow)} \quad \text{on} \quad \varSigma.$$

We recall that for the Poiseuille flow the boundary condition on the membrane means that $A = 0$ (impermeable walls). In the case of Berman flow model, we have the following exact pressure drop equation

$$\varDelta p(x, d/2) := \Big(\frac{1}{2}\rho \mathrm{u}_{\rm in}^2\Big)\Big(\frac{24}{Re} - \frac{648}{35}\frac{Re_{\mathbf{n}}}{Re}\Big)\Big(1 - \frac{2Re_{\mathbf{n}}x}{Re\,d}\Big)\Big(\frac{2x}{d}\Big), \tag{2.29}$$

where $Re := \dfrac{2\,\rho\,d\,\mathrm{u}_{\rm in}}{\nu}$ is the cross flow Reynolds number, and $Re_{\mathbf{n}} := \dfrac{\rho\,d\,(\mathbf{u}\cdot\mathbf{n})}{2\,\nu}$ is the Reynolds number at the channel walls. We note that the reduced pressure drop for the Poiseuille flow is obtained using the fact that $Re_{\mathbf{n}} = 0$, that is

$$\varDelta p(x, d/2) := \Big(\frac{1}{2}\rho_{\rm f}\mathrm{u}_{\rm in}^2\Big)\Big(\frac{24}{Re}\Big)\Big(\frac{2x}{d}\Big). \tag{2.30}$$

We simulate the case where $\mathrm{u_{in}} = 0.2 m/s$ and $\varDelta P = \varDelta P_2$. Figure 2.3 (left) shows the analytical pressure drop predicted by the equation (2.29), compared with the discrete pressure drop, denoted by

$\Delta p_h(x, d/2)$. We observe that our mixed finite element model accurately captures the axial pressure drops for both, the permeable and impermeable walls. In addtion, in Figure 2.3 (right) we plot the axial velocity along the segment starting at $(0, 0)$ and ending at (L, d). We observe that the numerical approximation agrees with the exact solution given by (2.28). We would like to remark that even though the analytical solution obtained by Berman [13], does not consider the boundary condition (2.2) at the outlet, it is commonly used to validate the numerical simulations [33, 104]. Since the channel is sufficiently long, the effect of the outlet boundary condition in the behaviour of the solution will be negligible away from the outlet.

Simulation 2. A feed channel with salt concentration with explicit and implicit spacers. We now employ our numerical method to compare the behaviour of the system considering three different cases: (S.1) channel without spacers, (S.2) with explicit submerged spacers and (S.3) implicit spacers. For a single channel with a constant inlet salt concentration of $\phi_{\text{in}} = 600 \, \frac{mol}{m^3}$, varying the inlet mean feed fluid velocities $\text{u}_{\text{in}} \in \{0.1m/s, 0.2m/s\}$, and $\Delta P \in \{\Delta P_1, \Delta P_2\}$, we perform a total of twelve scenarios. Also, for the cases (S.2) and (S.3), we consider a number of spacers $\mathtt{N_{sp}} = 3$ of diameter $d_{\text{s}} = 0.36 \, mm$. In particular, the spacers for (S.2) centered at $(L/4, d/2), (L/2, d/2)$ and $(3L/4, d/2)$. In addition for (S.3), taking into account that the sphericity of the particles is $\Phi = 1$, we find that the porosity of the medium and the porous medium permeability become $\varepsilon = 0.97249$ and $\widehat{K} = 8.74987 \times 10^{-7} \, m^2$, respectively. Consequently, the resulting Darcy and Forchheimer coefficients are $\widehat{\mathtt{D}} = 1.01716 \times 10^3 \, \frac{kg}{sm^3}$ and $\widehat{\mathtt{F}} = 1.59112 \times 10^5 \, \frac{kg}{m^4}$, respectively. Darcy's coefficient gives a linear relationship between the pressure drop and the velocity of the fluid, its value depends on physicochemical parameters such as the permeability and viscosity of the medium. For values of the Darcy number ($\mathtt{Da} = \widehat{K}/d^2$) above 10^{-3} (in our case $\mathtt{Da} = 1.59$), an additional term is needed to account for nonlinear effects between pressure drop and velocity [82]. These are attributed to the insurgence of inertial effects within the laminar flow regime. For these nonlinear relationship we use the Forchheimer term, which is proportional to the fluid density and to the second power of the flow rate [22].

As is usual in this type of simulations, and with the end of avoiding potential errors due to improper meshing, we employ our mixed method scheme combined to a high resolution mesh near the interface. This approach has been demonstrated to be crucial for achieving optimal results [74, 104].

Discussion. Representative velocity profiles (left), concentration fields (middle), and pressure drops (right) are shown in Figure 2.4. In an empty feed channel (case (S.1)), the parabolic velocity profile is preserved along the entire region. Similar results are observed for the porous cases (S.3), but as expected, the value of the axial velocity profile is slightly smaller than the one of case (S.1). In fact, for an empty channel there is not any material affecting the fluid flow allowing higher velocities in comparison with a porous channel where the fluid passes through spaces between small obstacles. On the other hand, as shown in the center panel of Figure 2.4 (case (S.2)), a submerged spacer produces an increment in the fluid velocity in the region surrounding the spacer. As a consequence, we observe abrupt changes in the pressure drop for the submerged configuration (case (S.2) in Figure 2.4) in the whole transversal section near the spacer, which is commonly attributed to be momentum losses due to the changes in the flow direction. Here, we also observe a pressure drop in the case (S.3) because the effect of the spacers is been distributed as a porous medium. On the other hand, we note that the empty channel produces a thicker salt concentration layer compared to the others, this is because the submerged spacers have a local thinning effect on the salt layer. In turn, the same effect is produced by the porous channel but in a distributed way. To see this effect more clearly in Figure 2.5 we display the concentration along the vertical line at $x = 7.7mm$, $y \in [0, 0.1]\, mm$, for the three cases. We recall that a circular spacer of diameter $d_\mathrm{s} = 0.36\, mm$ and centered at the point $(7.5\, mm, 0.37\, mm)$ is placed in the channel. Then, the segment $x = 7.7\, mm$ is located immediately $0.02\, mm$ at the right of the circular obstacle with the goal of observing the effect of the spacer in the concentration. As expected, the concentration of salt is higher near the membrane. We also notice that the values of the concentration and thickness of the salt layer decrease when the inlet velocity increases while maintaining a fixed hydrostatic transmembrane pressure, which in turn leads to a higher permeate velocity (see Figures 2.6 and 2.7). In turn, the concentration increases when the hydrostatic transmembrane pressure increases. On the other hand, the concentration in the empty channel (case (S.1)) is higher compared to cases (S.2) and (S.3). In other words, the presence of explicit or implicit spacers lowers the salt concentration near the membrane. Moreover, the concentration in case (S.3) is higher that in case (S.2) due to the local effect of the spacer, as we can observe in the bottom panels of Figures 2.6 and 2.7. Here, for the case (S.2), we observe three local minima when the distance from the inlet is approximately $3.75\, mm$, $7.5\, mm$ and $11.25\, mm$, respectively. This values correspond to the horizontal component the center of each circular spacers.

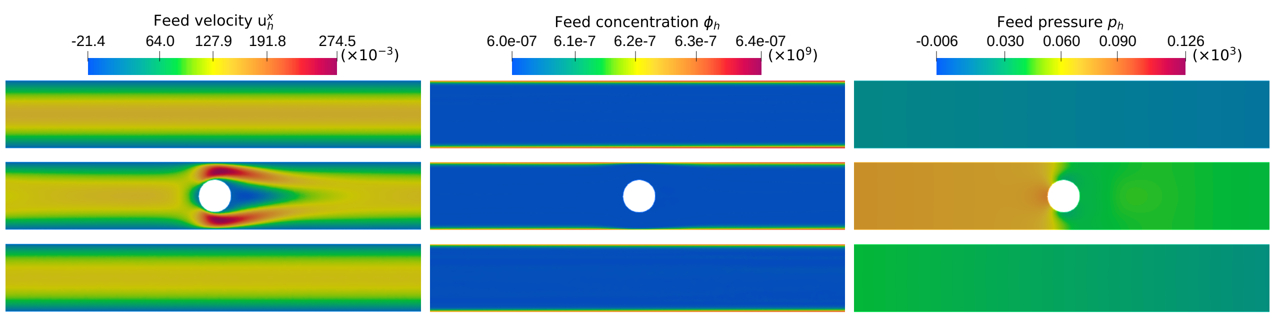

Figure 2.4: *Zoom in the region* $[5, 10]\, mm \times [0, 0.74]\, mm$*. From left to right: axial velocity profiles (left), concentration fields (middle), and pressure drops (right). From top to bottom, cases (S.1), (S.2) and (S.3). Simulation conditions:* $\mathrm{u_{in}} = 0.1\, m/s$*,* $\Delta P = \Delta P_1$*.*

Now, looking at the plots in Figures 2.6 and 2.7, we observe that for each case ((S.1), (S.2) or (S.3)), the hydrostatic transmembrane pressure $\Delta P = \Delta P_1$ (top-left panel) and $\Delta P = \Delta P_2$ (top-right panel), has no influence on the pressure drop. Nevertheless, its increment produces a higher permeate velocity flow, as we can see in the middle panels, yielding an inlet permeation velocity of $2.69 \times 10^{-6}\, m/s$ and $6.50 \times 10^{-6}\, m/s$, for ΔP_1 and ΔP_2, respectively. If the transmembrane pressure were even higher we could observe a subtle decrease in the pressure drop, since there would be more permeate flow and less velocity gradients near the bottleneck formed at the spacers. However, the permeate velocity is 6 orders of magnitude lower than the inlet flow, so it is not possible to evidence this phenomenon. For the same reason we can say that the transmembrane pressure does not have a major impact on the hydrodynamics of the channel [33]. In turn, the increment of ΔP has as a consequence in a higher salt concentration (bottom panels) on the membrane.

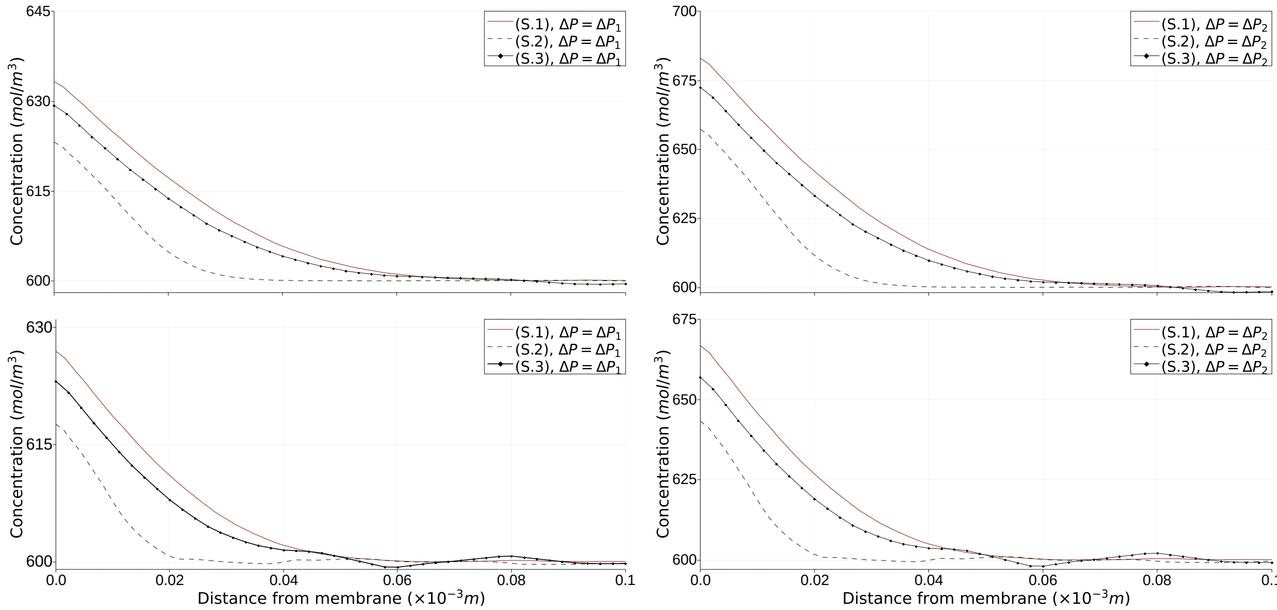

Figure 2.5: *Salt concentration along the vertical line at $x = 7.7\,mm$, $y \in [0, 0.1]\,mm$ for the three cases (S.1), (S.2) and (S.3). Simulation conditions: $\mathrm{u_{in}}$ equal to $0.1\,m/s$ (top panels) and $0.2\,m/s$ (bottom panels); and ΔP equal to ΔP_1 (left panels) and ΔP_2 (right panels).*

Next, we focus on analyzing comparatively the three proposed configurations. We observe in the empty channel (S.1) that the salt concentration (bottom panels) at the membrane is monotonically increasing with respect to the distance from the inlet, which means a higher salt concentration as the fluid passes through the membrane. This implies a lower permeate velocity (center panels). In this way, the spacers in the feed channel play a key roll since they generally enhance mixing, reduce (rejected) solute concentration and increase in permeate production (total permeate flow per unit length $\dot{V}/W$, to be defined below) compared to the absence of spacers, as demonstrated in previous works [2,78,104]. Within the limits of the current study, for the single channel with two permeable walls, we consider the particular case of submerged spacers (case (S.2)), since it has been shown to exhibit the highest permeate production compared to cavity and zig-zag spacers [33]. If we compare the cases (S.1) and (S.2) in Figures 2.6 and 2.7, we observe that not only the values of the salt concentration in (S.2) are lower than those of (S.1) throughout the regions influenced by the spacers, but also the former are lower than the latter in the regions between the spacers, under the same operating conditions. In addition, we know that the concentration has a direct effect on the permeate velocity (see second equation in (2.3)). This fact, is also confirmed in our simulations (middle and bottom panels of Figures 2.6 and 2.7), where the behaviour of the permeate velocity and concentration is opposite.

On the other hand, as we mentioned before, case (S.3) consists of emulating the spacer-filled channel as a porous medium, where its porosity is calculated by distributing in the entire channel the effect of the spacer. As a consequence, the model will no detect the local effect. Instead, as we can see in Figures 2.6 and 2.7, the black lines show a global behaviour of the variables. In addition, as we mentioned before, an increment in the inlet mass flow while maintaining a fixed hydrostatic transmembrane pressure, reduces the concentration at the membrane, leading to a higher permeate velocity and larger pressure losses (higher energy cost). In fact, the pressure drop is an unavoidable phenomenon along

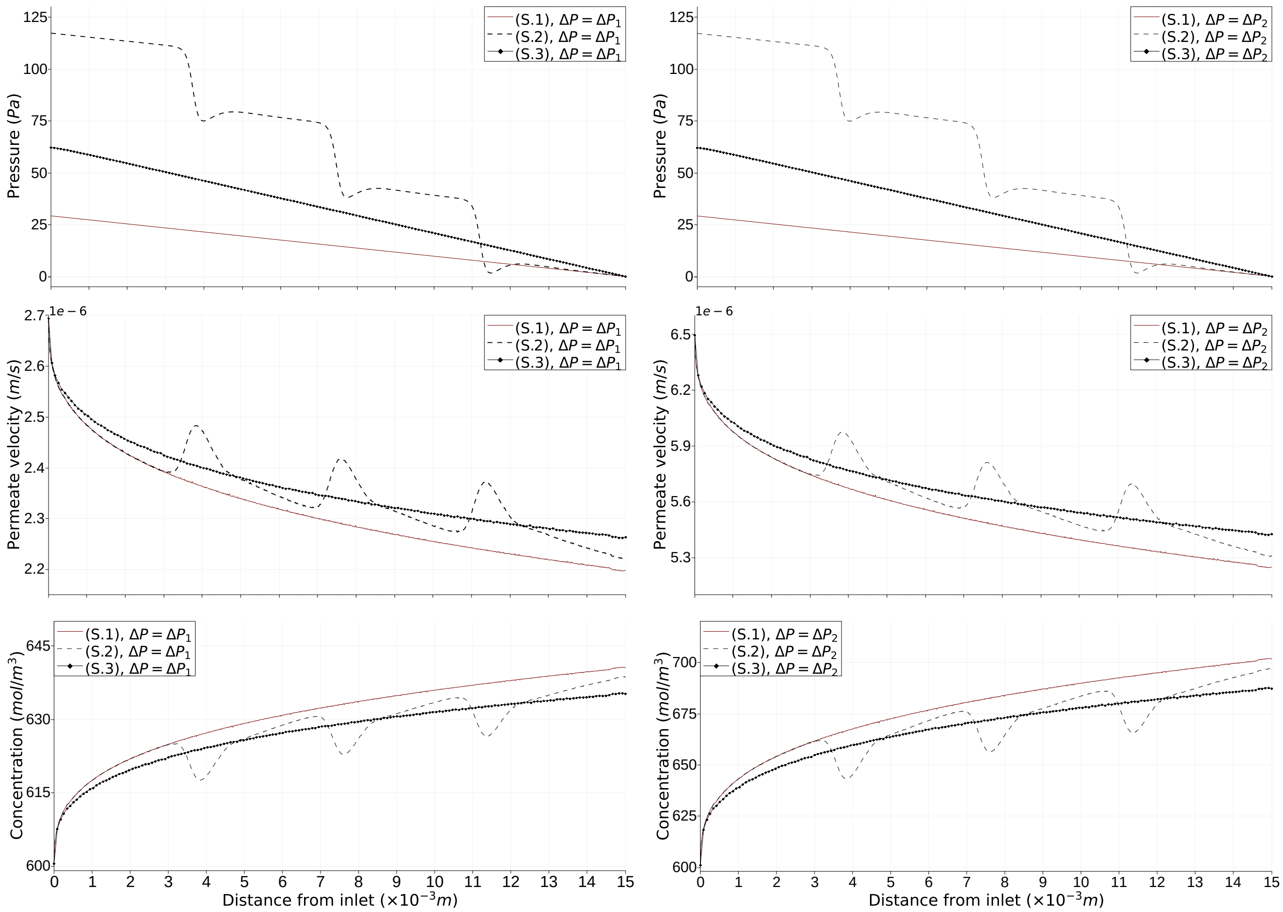

Figure 2.6: *Relative pressure drop (top panels), permeate velocity (middle) and concentration level (bottom panels) at the membrane $y = 0\,mm$ without spacers (S.1), with submerged explicit spacers (S.2), and implicit spacers (S.3). Simulation conditions:* $\mathrm{u_{in}} = 0.1\,m/s$*; and ΔP equal to ΔP_1 (left panels) and ΔP_2 (right panels).*

the entire channel, being the empty channel case (S.1) the one with the lowest pressure drop, whereas the case (S.2) exhibits a larger pressure drop, due to the presence of submerged spacers.

Now, to measure the impact of each case on permeate production, we compute the total volumetric flow per unit width. The channel in Figure 2.1, is actually a cross section of the region $[0, L] \times [0, d] \times [0, W]$, for a positive width W. Then, we utilize the following definition of the volumetric flow from the flux:

$$\frac{\dot{V}}{W} = \int_{\Sigma} |\mathbf{u}_h(s) \cdot \mathbf{n}| ds, \tag{2.31}$$

where $\dot{V}$ is the total volumetric flow of the permeate from the membrane walls and we recall that $\mathbf{u}_h(s) \cdot \mathbf{n}$ is the approximation of the permeate flux at a distance s from the inlet, obtained by our numerical scheme. In the simulations W is taken to be equal to L.

We report the values of $\dot{V}/W$ obtained in different scenarios in Table 2.2. The results show differences up to 2.5 times comparing the lowest ($\mathrm{u_{in}} = 0.1\,m/s$, $\Delta P = \Delta P_1$, case (S.1)) and the highest ($\mathrm{u_{in}} = 0.2\,m/s$, $\Delta P = \Delta P_2$, case (S.3)) permeate production values. In turn, Table 2.3 shows the increment

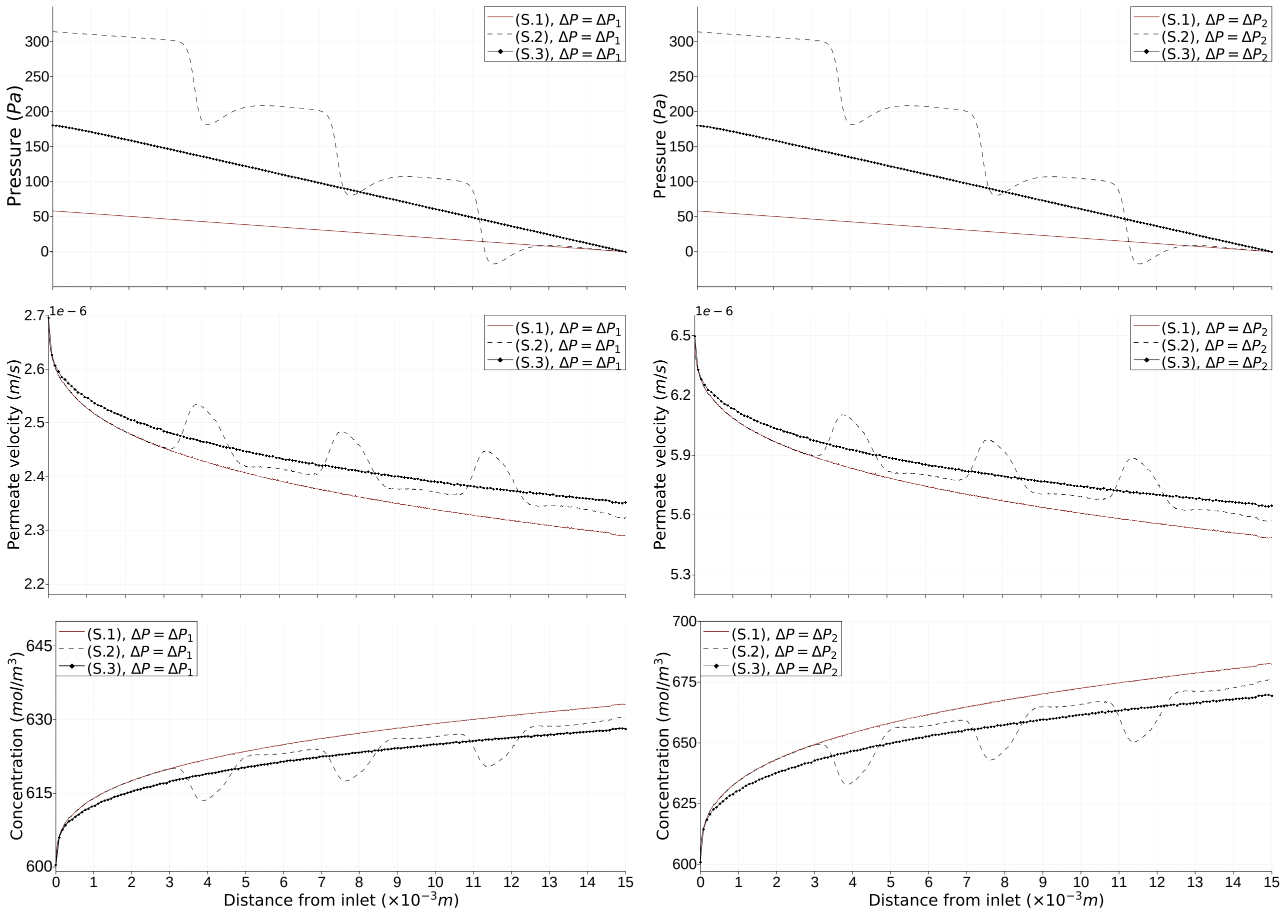

Figure 2.7: *Same as Figure 2.6 but considering* $\mathrm{u_{in}} = 0.2\,m/s$.

($\rightarrow$) rate of the values of the permeate production $\dot{V}/W$ reported in Table 2.2. For example, the third row and second column reads as follows: A simulation considering $\mathrm{u_{in}} = 0.1\,m/s$ and case (S.2) produces an increment of 139.56% when varying ΔP from ΔP_1 by ΔP_2. It is worth noting that the largest differences in the permeate production are due to the increment in the hydrostatic transmembrane pressure for all configurations, as we observe in the second and third row of Table 2.3. However, it is important to bear in mind that this leads to an increment in the concentration on the membrane. As a Consequence, we would need to increase the inlet velocity to remove the salt near the membrane, but this leads to a higher pressure drop (energy loss), as we have observed in Figures 2.6 and 2.7. In other words in order to determine the optimal values of all the parameters, we need to employ a constrained optimization algorithm and further numerical investigations will be carried out in a future work.

Finally, we compare how well the porous medium model (case (S.3)) emulate the case of submerged explicit spacers (S.2). In Table 2.3 (last column, fifth to eight rows), we observe that the case (S.3), in a very rough sense, differs from (S.2) only between 0.16% and 0.26% of the total permeate flow. This means, as we know, that considering implicit spacers allow us to predict a global behaviour with lower computational cost compared to the case of explicit spacers.

	$\Delta P = \Delta P_1$		$\Delta P = \Delta P_2$	
case	$\mathrm{u_{in}}$ (m/s)	$\dot{V}/W$ (m^2/s)	$\mathrm{u_{in}}$ (m/s)	$\dot{V}/W$ (m^2/s)
(S.1)	0.1	6.92222×10^{-8}	0.1	1.65829×10^{-7}
	0.2	7.14278×10^{-8}	0.2	1.71444×10^{-7}
(S.2)	0.1	7.04797×10^{-8}	0.1	1.69034×10^{-7}
	0.2	7.26112×10^{-8}	0.2	1.74439×10^{-7}
(S.3)	0.1	7.05906×10^{-8}	0.1	1.69470×10^{-7}
	0.2	7.27309×10^{-8}	0.2	1.74816×10^{-7}

Table 2.2: Total permeate flow per unit length $\dot{V}/W$ in a single channel for different values of $\mathrm{u_{in}}$ and ΔP, of the three cases (S.1), (S.2) and (S.3).

ΔP_1−(S.1): $0.1\,m/s \xrightarrow{3.19\%} 0.2\,m/s$	ΔP_1−(S.2): $0.1\,m/s \xrightarrow{3.02\%} 0.2\,m/s$	ΔP_1− (S.3): $0.1\,m/s \xrightarrow{3.03\%} 0.2\,m/s$
ΔP_2−(S.1): $0.1\,m/s \xrightarrow{3.39\%} 0.2\,m/s$	ΔP_2−(S.2): $0.1\,m/s \xrightarrow{3.20\%} 0.2\,m/s$	ΔP_2−(S.3): $0.1\,m/s \xrightarrow{3.15\%} 0.2\,m/s$
$0.1\,m/s$−(S.1): $\Delta P_1 \xrightarrow{139.56\%} \Delta P_2$	$0.1\,m/s$−(S.2): $\Delta P_1 \xrightarrow{139.83\%} \Delta P_2$	$0.1\,m/s$−(S.3): $\Delta P_1 \xrightarrow{140.07\%} \Delta P_2$
$0.2\,m/s$−(S.1): $\Delta P_1 \xrightarrow{140.02\%} \Delta P_2$	$0.2\,m/s$−(S.2): $\Delta P_1 \xrightarrow{140.24\%} \Delta P_2$	$0.2\,m/s$−(S.3): $\Delta P_1 \xrightarrow{140.36\%} \Delta P_2$
$0.1\,m/s - \Delta P_1$: (S.1) $\xrightarrow{1.82\%}$ (S.2)	$0.1\,m/s - \Delta P_1$: (S.1) $\xrightarrow{1.98\%}$ (S.3)	$0.1\,m/s - \Delta P_1$: (S.2) $\xrightarrow{0.16\%}$ (S.3)
$0.2\,m/s - \Delta P_1$: (S.1) $\xrightarrow{1.66\%}$ (S.2)	$0.2\,m/s - \Delta P_1$: (S.1) $\xrightarrow{1.82\%}$ (S.3)	$0.2\,m/s - \Delta P_1$: (S.2) $\xrightarrow{0.16\%}$ (S.3)
$0.1\,m/s - \Delta P_2$: (S.1) $\xrightarrow{1.93\%}$ (S.2)	$0.1\,m/s - \Delta P_2$: (S.1) $\xrightarrow{2.20\%}$ (S.3)	$0.1\,m/s - \Delta P_2$: (S.2) $\xrightarrow{0.26\%}$ (S.3)
$0.2\,m/s - \Delta P_2$: (S.1) $\xrightarrow{1.75\%}$ (S.2)	$0.2\,m/s - \Delta P_2$: (S.1) $\xrightarrow{1.97\%}$ (S.3)	$0.2\,m/s - \Delta P_2$: (S.2) $\xrightarrow{0.22\%}$ (S.3)

Table 2.3: Increment rate in the value of $\dot{V}/W$ reported in Table 2.2, with respect to the variation of the velocity (first and second rows), hydrostatic transmembrane pressure (third and fourth rows) and configurations (fifth to eight rows).

2.3.2 Coupled feed and permeate channel.

We also consider $L = 15\,mm$ and $d = 0.74\,mm$, and the computational domain $\Omega = \Omega_{\mathrm{f}} \cup \Omega_{\mathrm{p}} \cup \Sigma$, where $\Omega_{\mathrm{f}} = (0, L) \times (d, 2d)$, $\Omega_{\mathrm{p}} = (0, L) \times (0, d)$, and $\Sigma = (0, L) \times \{d\}$. Here, we consider the inlet velocity profiles of the feed and permeate channels as

$$\begin{aligned}
\mathbf{u}_{\mathrm{in,f}} &:= \left(6\mathrm{u}_{\mathrm{in,f}}\Big(1 - \frac{y}{d}\Big)\left(\frac{y}{d} - 2\right), (c_0 - c_1(\phi_{\mathrm{in,f}} - \phi_{\mathrm{in,p}}))\Big(\frac{y}{d} - 2\Big)\right)^t, \quad y \in [d, 2d], \\
\mathbf{u}_{\mathrm{in,p}} &:= \left(6\mathrm{u}_{\mathrm{in,p}}\frac{y}{d}\Big(1 - \frac{y}{d}\Big), -(c_0 - c_1(\phi_{\mathrm{in,f}} - \phi_{\mathrm{in,p}}))\frac{y}{d}\right)^t, \quad y \in [0, d],
\end{aligned} \tag{2.32}$$

respectively, where $\mathrm{u}_{\mathrm{in,f}}$ and $\mathrm{u}_{\mathrm{in,p}}$ stand for the inlet mean feed and permeate fluid velocities, respectively.

Simulation 3. Coupled feed and permeate channel with salt concentration with explicit and implicit spacers. We now investigate the behaviour of the system that consists of a feed channel coupled to the permeate channel where the interface is the membrane. We consider five different cases: (C.1) channels without spacers, (C.2) with submerged spacers, (C.3) with zig-zag distributed spacers,

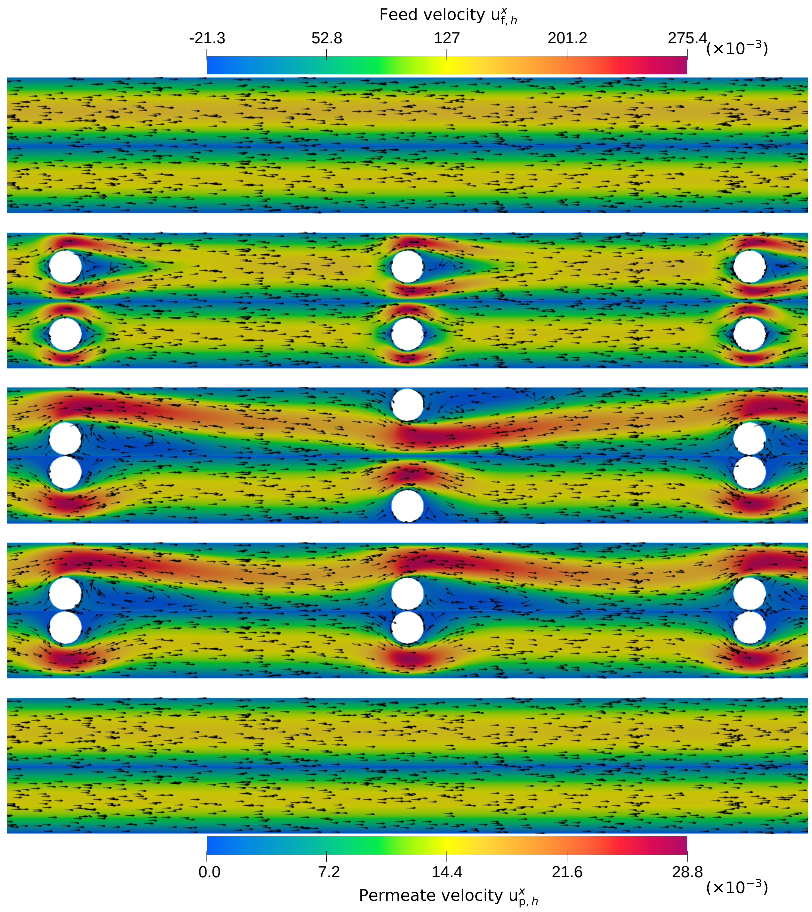

Figure 2.8: *Axial velocities in the region* $[3, 12]\,mm \times [0, 1.48]\,mm$. *From top to bottom: cases (C.1), (C.2), (C.3), (C.4) and (C.5). Simulation conditions:* $\mathrm{u_{in,f}} = 0.1\,m/s$, $\mathrm{u_{in,p}} = 0.01\,m/s$, $\mathit{\Delta P} = \mathit{\Delta P}_2$.

(C.4) with cavity spacers, and (C.5) implicit spacers. We set a constant inlet salt concentration of $\phi_{\mathrm{in,f}} = 600\,\frac{mol}{m^3}$ and $\phi_{\mathrm{in,p}} = 6\,\frac{mol}{m^3}$, for the feed and permeate channels, respectively. For this analysis, we focus exclusively on the scenario where $\mathit{\Delta P} = \mathit{\Delta P}_2$, motivated by the fact that higher values of the hydrostatic transmembrane pressure produces a higher permeate production. The inlet mean feed and permeate fluid velocities are set as $0.1\,m/s$ and $0.01\,m/s$, respectively. Furthermore, we maintain three spacers for each channel of diameter $0.36\,mm$ with centers located according to Table 2.4.

	(C.2)	(C.3)	(C.4)
Feed channel	$\left(\frac{L}{4}, \frac{3d}{2}\right)$, $\left(\frac{L}{2}, \frac{3d}{2}\right)$, $\left(\frac{3L}{4}, \frac{3d}{2}\right)$.	$\left(\frac{L}{4}, \frac{5d}{4}\right)$, $\left(\frac{L}{2}, \frac{5d}{4}\right)$, $\left(\frac{3L}{4}, \frac{5d}{4}\right)$.	$\left(\frac{L}{4}, \frac{5d}{4}\right)$, $\left(\frac{L}{2}, \frac{7d}{4}\right)$, $\left(\frac{3L}{4}, \frac{5d}{4}\right)$.
Permeate channel	$\left(\frac{L}{4}, \frac{d}{2}\right)$, $\left(\frac{L}{2}, \frac{d}{2}\right)$, $\left(\frac{3L}{4}, \frac{d}{2}\right)$.	$\left(\frac{L}{4}, \frac{d}{4}\right)$, $\left(\frac{L}{2}, \frac{d}{4}\right)$, $\left(\frac{3L}{4}, \frac{d}{4}\right)$.	$\left(\frac{L}{4}, \frac{d}{4}\right)$, $\left(\frac{L}{2}, \frac{3d}{4}\right)$, $\left(\frac{3L}{4}, \frac{d}{4}\right)$.

Table 2.4: Coordinates of the center of the circular spacers located inside the feed and permeate channels.

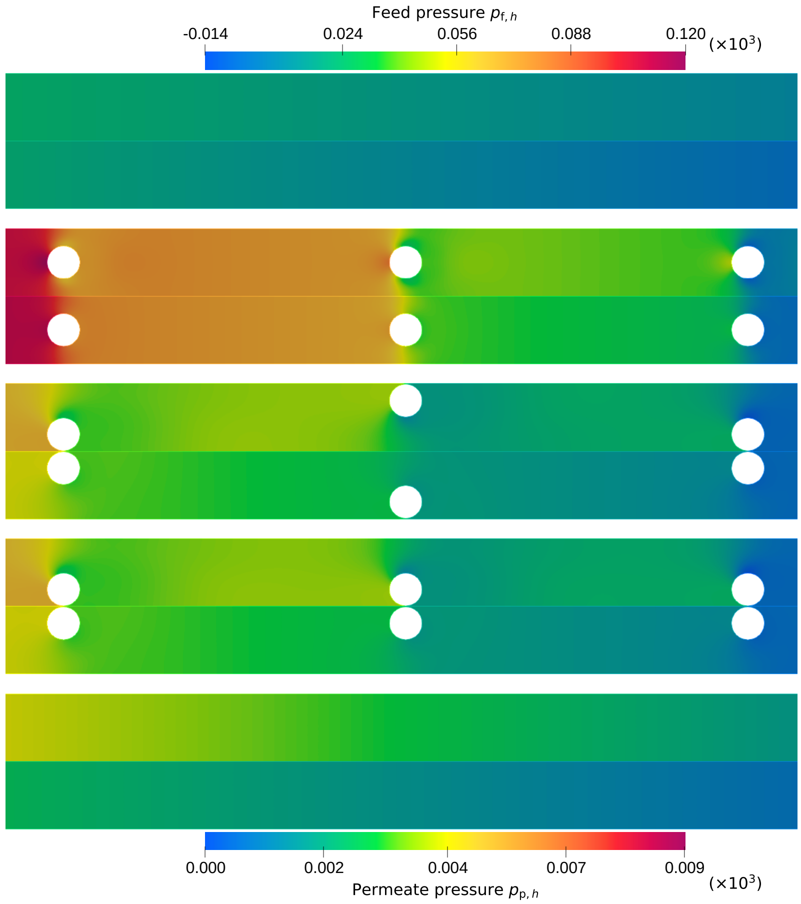

Figure 2.9: *Pressure drop in the region* $[3, 12]\,mm \times [0, 1.48]\,mm$. *From top to bottom: cases (C.1), (C.2), (C.3), (C.4) and (C.5). Simulation conditions:* $\mathrm{u_{in,f}} = 0.1\,m/s$, $\mathrm{u_{in,p}} = 0.01\,m/s$, $\Delta P = \Delta P_2$.

Discussion. Velocity profiles in both, feed and permeate channels, for all cases are depicted in Figure 2.8. The axial velocity in cases (C.1) and (C.5) exhibits similar behaviours to those obtained for a single channel (cases (S.1) and (S.3), respectively). On the other hand, we notice that the obstacles produce increment in the velocities for the three explicit spacer configurations. This effect is due to the fluid being forced to flow through a reduced cross-section of the channel. For instance, in an empty feed channel with inlet mean feed velocity of $0.1\,m/s$, the maximum velocity achieved is $0.15\,m/s$. In contrast, the maximum velocity using submerged spacers (case (C.2)), is $0.275\,m/s$, whereas for both zig-zag (case (C.3)) and cavity (case (C.4)) spacers, the velocity is $0.265\,m/s$. In turn, in an empty permeate channel with inlet mean permeate velocity of $0.01\,m/s$, the maximum velocity is $0.015\,m/s$, whereas the maximum velocities for the three configurations with explicit spacers are around $0.0289\,m/s$. In addition, when we compare the effect of the obstacles in the feed channel with those of the permeate channel, we observe that the high feed velocities (red regions in Figure 2.8) do not significantly decay along the channel for the zig-zag and cavity spacers. However, in the case (C.2) there is an increment of the velocity near the membrane and the wall, but this occurs close to the spacers, decreasing the velocity away from them. Also, as shown in Figure 2.9, the submerged obstacles produce the highest pressure drop compared to the other configurations. In addition, we observe similar pressure drops when we use the zig-zag or cavity configurations. Now, an unavoidable effect due to

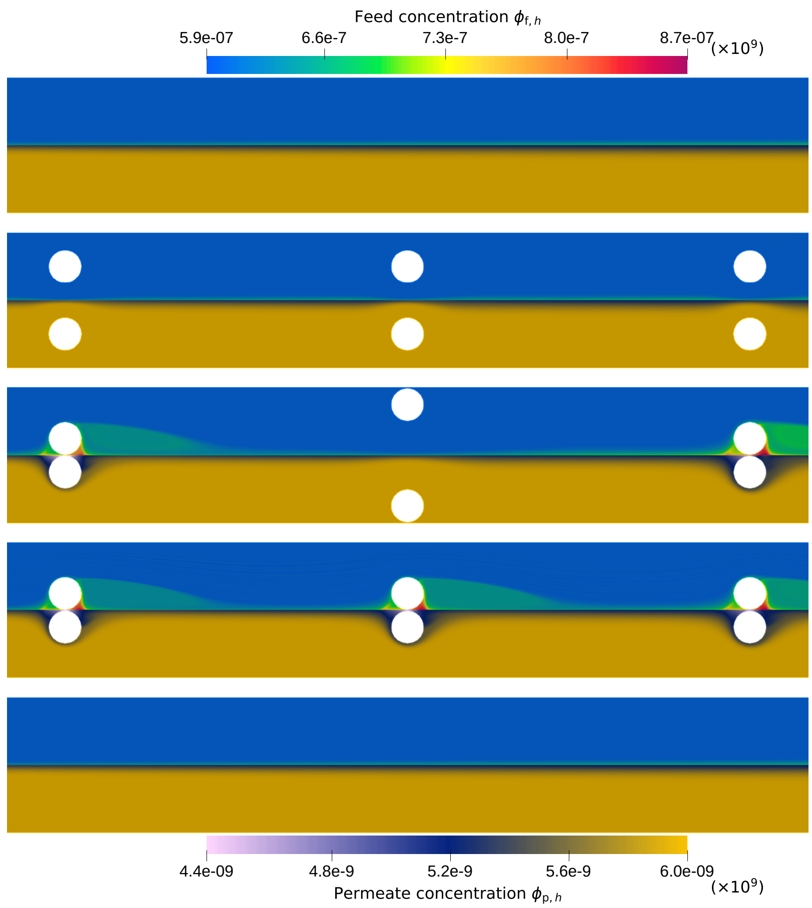

Figure 2.10: *Salt concentration in the region* $[3, 12]\,mm \times [0, 1.48]\,mm$*. From top to bottom: cases (C.1), (C.2), (C.3), (C.4) and (C.5). Simulation conditions:* $\mathrm{u_{in,f}} = 0.1\,m/s$*,* $\mathrm{u_{in,p}} = 0.01\,m/s$*,* $\Delta P = \Delta P_2$*.*

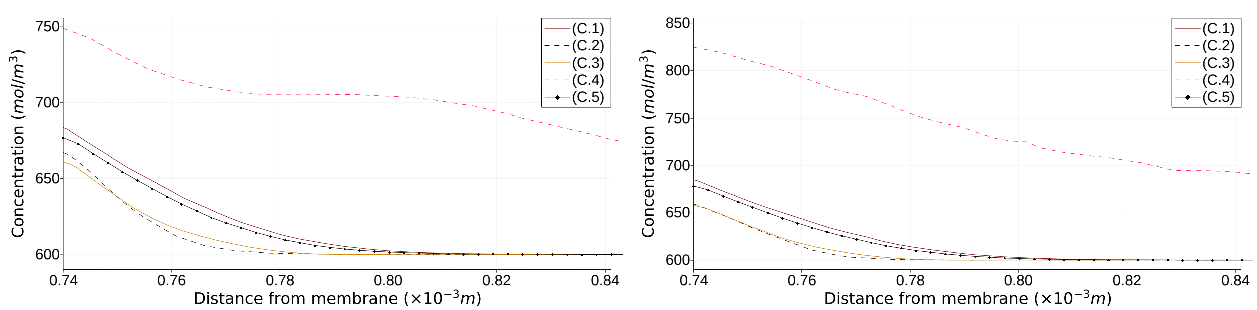

Figure 2.11: *Salt concentration along the vertical lines at* $x = 7.3\,mm$ *(left panel) and* $x = 7.7\,mm$ *(right panel),* $y \in [0.74, 1.15]\,mm$ *for the five cases (C.1), (C.2), (C.3), (C.4) and (C.5). Simulation conditions:* $\mathrm{u_{in,f}} = 0.1\,m/s$*,* $\mathrm{u_{in,p}} = 0.01\,m/s$*,* $\Delta P = \Delta P_2$*.*

the use of spacer-filled channels, is the formation of recirculation zones. This is a particular issue for spacers placed on the surface of the membrane, where it is desirable to have a concentration to be as low as possible [104]. For submerged spacers (C.2), the recirculation is located in the centre of the channel behind the spacers (Figure 2.8, second panel), and away from the membrane. In contrast, the

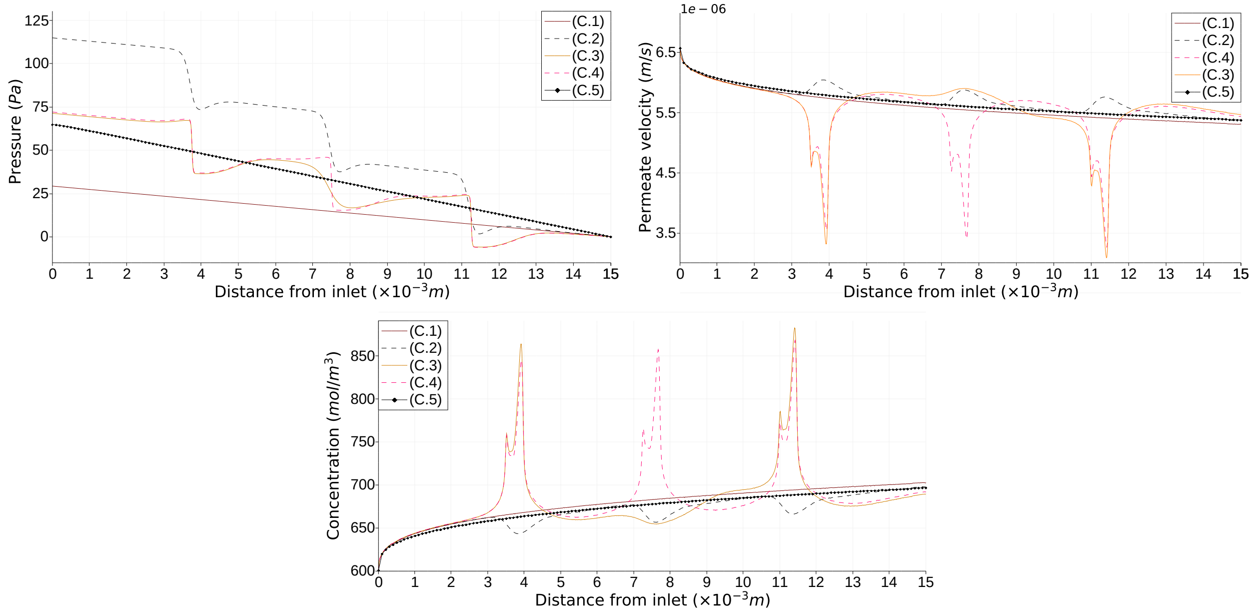

Figure 2.12: *Feed channel. Relative pressure drop (top-left panel), permeate velocity (top-right panel) and concentration level (bottom panel) at the membrane ($y = 0.74\,mm$) for all cases (C.1)-(C.5). Simulation conditions:* $\mathrm{u_{in,f}} = 0.1\,m/s$, $\mathrm{u_{in,p}} = 0.01\,m/s$, $\mathit{\Delta P} = \mathit{\Delta P}_2$.

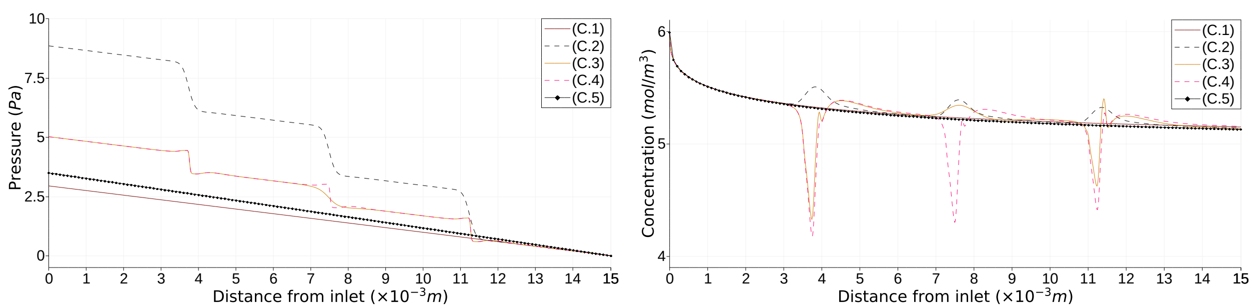

Figure 2.13: *Permeate channel. Relative pressure drop (left panel) and concentration level (right panel) at the membrane ($y = 0.74\,mm$) for all cases (C.1)-(C.5). Simulation conditions:* $\mathrm{u_{in,f}} = 0.1\,m/s$, $\mathrm{u_{in,p}} = 0.01\,m/s$, $\mathit{\Delta P} = \mathit{\Delta P}_2$.

recirculation effect for the other two cases not only covers a larger region, but also occurs close to the membrane, as it is immediately evident from Figure 2.8 (third and fourth panels). Here, cavity spacer configuration produces a larger recirculation zones compared to the zig-zag spacers configuration. This leads to strong concentration in the regions close to the spacers that attached to the membrane, as depicted in the third and fourth panels of Figure 2.10. In turn, the middle spacer in case (C.3) has a positive effect in lowering the values of the concentration near the membrane. It is evident that the fluid permeating through the membrane has a lower concentration than the inlet permeate concentration as we observe in the bottom channels of Figure 2.10. This difference since the former is 99% less than the latter. In Figure 2.11 we show the behaviour of the concentration in the feed channel immediately to the left and to the right of the middle spacer along the vertical lines at $x = 7.3\,mm$ and $x = 7.7\,mm$, $y \in [0.74, 1.15]\,mm$, for the five cases. We observe that (C.4) is the case that shows the highest concentration near the membrane. Moreover, an abrupt increment is observable when we compare the region at the left (left panel) of the spacer with the one of the right (right panel).

In Figure 2.12, we display the values of the variables of interest at the membrane from the side of the feed channel. The concentration/permeate velocity in cases (C.3) and (C.4) shows the highest/lowest local maxima/minima of all proposed configurations in the places where the spacers are attached to the membrane. This validates the fact that the concentration has a direct effect on the permeate velocity (third equation of the first row in (2.24)). On the other hand, we observe in the top-left panel, that case (C.2) has the highest pressure drop, whereas case (C.3) has a similar behaviour in pressure drop to that of case (C.4). This behaviour is also similar for the pressure at the membrane (left panel) in the permeate channel, as shown in Figure 2.13, where we plot the pressure and concentration at the membrane from the permeate channel. However, the concentration on the membrane in the permeate channel (right panel) has a larger reduction for configurations (C.3) and (C.4). This is caused by the effect of the spacers attached to the membrane.

We now compute the total permeate flow per unit length $\dot{V}/W$ (cf. (2.31)) for the coupled channels configurations. In contrast to the single channel configurations, in this case the total permeate flow per unit length depends on both, the feed and permeate concentrations on the membrane, according to the third equation of the first row in (2.24). We show in Table 2.5 the permeate production for the all coupled configurations. In the particular cases when we use explicit spacers, we observe that the largest permeate production is due to the submerged spacers configuration, while the cavity spacer configuration is the lowest. To see this more clearly, in Table 2.6, we show the increment ($\rightarrow$) rates of the values of the total permeate flow per unit length $\dot{V}/W$ reported in Table 2.5, where having submerged spacers produces 1.87% of increment in $\dot{V}/W$ compared to the empty channel configuration. In this table, we also want to compare how well implicit spacers emulates the different cases of explicit spacers. We observe that case (C.5) always has a larger permeate flux than case (C.1). This implies that the use of implicit spacers tends to emulate those cases where explicit spacers also reduce the salt concentration compared to case (C.1). From the latter, we note that the porous case emulates more accurately the case (C.2), since differs by only 0.86%.

	(C.1)	(C.2)	(C.3)	(C.4)	(C.5)
$\dot{V}/W\,(m^2/s)$	8.37876×10^{-8}	8.53812×10^{-8}	8.36789×10^{-8}	8.27399×10^{-8}	8.46516×10^{-8}

Table 2.5: Total permeate flow per unit length $\dot{V}/W$ in coupled channels for $\mathrm{u_{in,f}} = 0.1\,m/s$, $\mathrm{u_{in,p}} = 0.01\,m/s$ and $\mathit{\Delta} P = \mathit{\Delta} P_2$, of the five cases (C.1), (C.2), (C.3), (C.4) and (C.5).

(C.1) $\xrightarrow{1.87\%}$ (C.2)	(C.4) $\xrightarrow{1.27\%}$ (C.1)	(C.5) $\xrightarrow{0.86\%}$ (C.2)	(C.4) $\xrightarrow{2.26\%}$ (C.5)
(C.3) $\xrightarrow{0.13\%}$ (C.1)	(C.1) $\xrightarrow{1.02\%}$ (C.5)	(C.3) $\xrightarrow{1.14\%}$ (C.5)	

Table 2.6: Increment rate in the value of $\dot{V}/W$ reported in Table 2.5, with respect to the variation of configurations.

CHAPTER 3

An HDG method for Stokes/Darcy coupling on dissimilar meshes

3.1 Introduction

During the last decade, the development of new non-body-fitted numerical methods for partial differential equations (PDEs) has become of interest in the community, especially with focus on high order schemes. One of the most popular is the cut finite element method (CutFEM). Roughly speaking, the CutFEM method considers a background grid where the domain is immersed and a Nitsche's approach is employed to impose the transmission conditions in the elements cut by the interface. A review can be found in [23] and recent works have also proposed conservative CutFEM schemes [62,81]. CutFEM requires special quadrature rules to compute the integrals over the interface, in contrast with the recently developed ϕ-FEM method [56–58]. The main idea there is to introduce an auxiliary variable that depends on the level-set function in such a way that the homogeneous Dirichlet boundary condition is automatically satisfied.

A different approach to handle transmission/boundary conditions with unfitted methods is based on a Taylor expansion of the function near the interface/boundary. In this direction, in the literature we can find two methods: the Shifted Boundary Method (SBM) [7,86] and the Transfer Path Method (TPM) [47,91,94]. The former considers a primal formulation and the residual of the Taylor expansion vanishes at discrete level. The TPM, on the other hand, is based on a mixed formulation where the residual of the Taylor expansion does not vanish but it involves the mixed variable that is then approximated by the numerical scheme. Our work focuses on the latter with the aim to demonstrate that the TPM can be a useful technique to handle situations where two meshes of different sizes are apart from each other. In addition, as a byproduct, our analysis also covers the case where the interface is fitted by the two meshes, allowing the presence of hanging nodes.

When the domain of a PDE is discretized by the union of different computational subdomains, it is possible to identify two configurations. In the first one, the interface is not fitted by the triangulations, generating *dissimilar meshes* with gaps and overlaps appearing between the grids associated to each subdomains, as the one depicted in Figure 3.1 (left). Therefore, the discrete interfaces of neighboring grids need to be properly connected. In the second configuration the interface is fitted by the grids, but it presents hanging nodes as portrayed in Figure 3.1 (right). This causes a non-conformity at the intersection of the subdomains in which adjacent elements do not necessarily share a complete face or edge. This is why we prefer to consider a discontinuous Galerkin method (DG) to discretize the PDE. In particular, we focus on the hybridizable DG (HDG) method.

Furthermore, to the best of our knowledge, there are only two works that analyze the HDG method for non-conforming triangulations [38, 39]. In the first approach the authors perform an analysis for the convection-diffusion equations in non-conforming meshes. In particular, using polynomial approximations of degree k in all elements, they obtained suboptimal order of convergence $h^{k+1/2}$ for the diffusive flux and optimal convergence h^{k+1} for the projection of the error in the scalar variable. The second approach is similar to the first one, but uses the so-called *semimatching* nonconforming meshes. Then, both optimal convergence for the diffusive flux and superconvergence of the projection of the error in the scalar variable is obtained.

With the aim of developing a high-order method to handle geometries with complex interfaces, we present an HDG method for coupled problems on dissimilar and non-conforming meshes. More precisely, we focus on the coupling of fluid and porous media flows across a discrete interface that does not necessarily match the true interface. To this end, we rely on the TPM [44–46, 94] originally designed for handling boundary value problems in curved domains, but recently employed for coupling dissimilar meshes in the context of a single PDE in the entire domain [87, 101]. It is worth noting that, in the last decade, several HDG methods addressing the Stokes-Darcy coupling problem have emerged in the literature. For instance, [36, 37] present a strongly conservative discretization of the velocity–pressure formulation of the Stokes equations, coupled with Darcy-transport and Darcy equations, respectively. Likewise, the approach developed in [63] guarantees exact mass conservation, where the Stokes flow is discretized using a divergence-conforming HDG method, while the Darcy flow is addressed by a mixed finite element method. Another contribution presented in [71] employs a fully mixed formulation, selecting stress, vorticity, velocity, and velocity trace as main variables in the Stokes domain, and velocity, pressure, and pressure trace in the Darcy domain. HDG schemes for the coupled Navier–Stokes and Darcy equations have also been developed. For instance, in [35] a strongly conservative HDG for the time dependent case was proposed. All of these methods successfully demonstrate optimal convergence rates. Our work proposes and analyzes a new method for Stokes/Darcy coupling, following a similar scheme developed in [71]. More precisely, let Ω_{s} and Ω_{d} be bounded and simply connected polyhedral domains in $\mathbb{R}^n$, $n \in \{2,3\}$, with outward unit normal vectors $\mathbf{n}_{\mathrm{s}}$ and $\mathbf{n}_{\mathrm{d}}$, respectively, such that $\mathcal{I} := \overline{\Omega}_{\mathrm{s}} \cap \overline{\Omega}_{\mathrm{d}}$ is the interface that separates them, and let $\Gamma_{\mathrm{s}} := \partial\Omega_{\mathrm{s}} \setminus \mathcal{I}$, $\Gamma_{\mathrm{d}} := \partial\Omega_{\mathrm{d}} \setminus \mathcal{I}$. On $\mathcal{I}$, we also consider unit tangent vectors, $\boldsymbol{m}_1$ when $n = 2$ and $\{\boldsymbol{m}_1, \boldsymbol{m}_2\}$ when $n = 3$. The model consists of two separate groups of equations and a set of coupling terms. In the fluid region Ω_{s}, the governing equations are those of the Stokes problem, which can be written as follows:

$$\begin{gathered} \mathrm{L}_{\mathrm{s}} - \nabla \mathbf{u}_{\mathrm{s}} = \mathbf{0} \quad \text{in} \quad \Omega_{\mathrm{s}}, \quad -\nabla\cdot(\nu \mathrm{L}_{\mathrm{s}} - P_{\mathrm{s}}\mathrm{I}) = \mathbf{f}_{\mathrm{s}} \quad \text{in} \quad \Omega_{\mathrm{s}}, \quad \nabla\cdot\mathbf{u}_{\mathrm{s}} = 0 \quad \text{in} \quad \Omega_{\mathrm{s}}, \\ \mathbf{u}_{\mathrm{s}} = \mathbf{0} \quad \text{on} \quad \Gamma_{\mathrm{s}}, \quad \text{and} \quad \int_{\Omega_{\mathrm{s}}} P_{\mathrm{s}} = 0, \end{gathered} \tag{3.1a}$$

where $\nu > 0$ is the fluid dynamic viscosity, $\mathbf{f}_{\mathrm{s}} \in \mathbf{L}^2(\Omega_{\mathrm{s}})$ is the volumetric force acting on the fluid, $\mathbf{u}_{\mathrm{s}}$ is the fluid velocity, L_{s} is the velocity gradient tensor, P_{s} is the pressure, and I is the $n \times n$ identity matrix. In turn, in the porous medium region Ω_{d} we consider the following Darcy model:

$$\mathbf{u}_{\mathrm{d}} + \kappa\nabla p_{\mathrm{d}} = \mathbf{0} \quad \text{in} \quad \Omega_{\mathrm{d}}, \quad \nabla\cdot\mathbf{u}_{\mathrm{d}} = \mathrm{f}_{\mathrm{d}} \quad \text{in} \quad \Omega_{\mathrm{d}}, \quad \text{and} \quad \mathbf{u}_{\mathrm{d}}\cdot\mathbf{n}_{\mathrm{d}} = 0 \quad \text{on} \quad \Gamma_{\mathrm{d}}, \tag{3.1b}$$

where κ is a tensor valued function, which describes the permeability of Ω_{d}, satisfies $\kappa^{\mathtt{t}} = \kappa$, and has $L^{\infty}(\Omega_{\mathrm{d}})$ components, $\mathrm{f}_{\mathrm{d}} \in L^2(\Omega_{\mathrm{d}})$ is a given source term such that $\displaystyle\int_{\Omega_{\mathrm{d}}} \mathrm{f}_{\mathrm{d}} = 0$, and $\mathbf{u}_{\mathrm{d}}$ and p_{d} denote the velocity and pressure, respectively. Also, we assume that there exist positive constants $\underline{\kappa}$ and $\overline{\kappa}$ such that $\underline{\kappa} \leq \|\kappa\|_{\infty,\Omega_{\mathrm{d}}} \leq \overline{\kappa}$. Finally, the transmission conditions on $\mathcal{I}$ are given by

$$\mathbf{u}_{\mathrm{s}} \cdot \mathbf{n}_{\mathrm{s}} + \mathbf{u}_{\mathrm{d}} \cdot \mathbf{n}_{\mathrm{d}} = 0 \quad \text{and} \quad (\nu \mathrm{L}_{\mathrm{s}} - P_{\mathrm{s}} \mathrm{I}) \mathbf{n}_{\mathrm{s}} + \sum_{\ell=1}^{n-1} \omega_{\ell}^{-1} (\mathbf{u}_{\mathrm{s}} \cdot \boldsymbol{m}_{\ell}) \boldsymbol{m}_{\ell} = p_{\mathrm{d}} \mathbf{n}_{\mathrm{d}} \quad \text{on} \quad \mathcal{I}, \tag{3.1c}$$

where $\{\omega_1, ..., \omega_{n-1}\}$ is a set of positive frictional constants that can be determined experimentally. The first equation in (3.1c) is based on mass conservation, whereas the second one establishes the balance of normal forces and the Beavers–Joseph–Saffman law. Well-posedness of weak formulations associated to (3.1) can be found, for instance, in [69, 70] and references therein.

We end this section by mentioning that our work continues the development of the TPM applied to dissimilar meshes started in [87, 101] and therefore we employ similar techniques. However, in this manuscript other issues arise due to the fact that two different equations are being coupled. Here, the primal variable of the Stokes system is coupled to the mixed variable of the Darcy equations and vice-versa. This adds more difficulties in designing and analyzing the scheme compared to the cases in [87, 101] where a single equation holds in the entire domain. We will come back to this point in Remark 3.2 after introducing the discrete setting.

This chapter is organized as follows. In Section 3.2, we introduce the notation related to the discretization and transferring segments, as well as some preliminaries and definitions related to the computational domain and the approximation spaces. Next, in Section 3.3, the HDG method is introduced along with the proposed transmission conditions. In Section 3.4, we show the stability of the method and present the error estimates in Section 3.5. Several numerical experiments validating the performance of the method and confirming the rates of convergence are reported in Section 3.6. Finally, we conclude the study providing final remarks in Chapter 4.2.

3.2 Preliminaries

We begin by introducing some preliminary notations related to the geometric discretization, the approximation spaces and the HDG scheme. In turn, we introduce the main tools to address the discretization of the interface.

The computational domain. Let $\Omega^{\mathrm{s}}_{h_{\mathrm{s}}}$ and $\Omega^{\mathrm{d}}_{h_{\mathrm{d}}}$ be triangulations of the domains Ω_{s} and Ω_{d}, with meshsizes h_{s}, $h_{\mathrm{d}} > 0$ and boundaries $\mathcal{S}_{\mathrm{s},h_{\mathrm{s}}}, \mathcal{S}_{\mathrm{d},h_{\mathrm{d}}}$, respectively. Without loss of generality, we suppose $h_{\mathrm{d}} \geq h_{\mathrm{s}}$ and drop the sub-index $\star \in \{\mathrm{s}, \mathrm{d}\}$ when there is no confusion; for example, we just write Ω^{s}_h, and Ω^{d}_h henceforth. We also denote the set of all faces of the triangulation $\Omega^{\star}_h$ by $\mathcal{E}^{\star}_h$. Furthermore, since $\overline{\Omega}^{\mathrm{s}}_h \cap \overline{\Omega}^{\mathrm{d}}_h$ is not necessarily equal to $\mathcal{I}$, then, for $\star \in \{\mathrm{s}, \mathrm{d}\}$, we define the discrete interfaces $\mathcal{I}^{\star}_h \coloneqq \mathcal{S}_{\star,h} \setminus \Gamma_{\star,h}$, where $\Gamma_{\star,h}$ denotes the discretization of $\Gamma_{\star}$. Bearing in mind the above, we consider outward normal vectors for the new interfaces $\mathcal{I}^{\mathrm{s}}_h$ and $\mathcal{I}^{\mathrm{d}}_h$, which will be denoted by $\mathbf{n}_{\mathrm{s},h}$ and $\mathbf{n}_{\mathrm{d},h}$, respectively. The family of triangulations $\{\Omega^{\star}_h\}_{h>0}$ is assumed to be shape-regular, i.e., there exists a constant $\kappa_\star > 0$ such that for all elements $K \in \Omega_h^\star$ and all $h > 0$, $h_K/\rho_K \leq \kappa_\star$, where h_K is the diameter of K and ρ_K is the diameter of the largest ball contained in K. For every element K, we denote by $\mathbf{n}_K$ the outward unit normal vector to K, writting $\mathbf{n}$ instead of $\mathbf{n}_K$ when there is no confusion. In this work, we consider the two configurations depicted in Figure 3.1. In the first one, a uniform gap of size δ separates the two triangulations. In the second setting, the interface is piecewise flat and both meshes are fitted to it, but with different meshsizes.

Spaces and norms. We use the standard notation for Sobolev spaces and their associated norms and seminorms, where vector-valued functions and their corresponding spaces are denoted in bold face font, and roman font in the tensor-valued case. In addition, let D be an open bounded region of $\mathbb{R}^n$ or $\mathbb{R}^{n-1}$. We denote by $(\cdot,\cdot)_D$ and $\langle\cdot,\cdot\rangle_{\partial D}$ the $L^2(D)$ and $L^2(\partial D)$ inner products, respectively, with induced norms $\|\cdot\|_D$ and $\|\cdot\|_{\partial D}$. Given an integer $k \geq 0$, we use the usual notation to denote the space of polynomials of degree at most k as $P_k(D)$, and set $\mathbf{P}_k(D) \coloneqq [P_k(D)]^n$ and $\mathrm{P}_k(D) \coloneqq [P_k(D)]^{n\times n}$.

We introduce now the finite-dimensional spaces

$$\begin{aligned}
\mathrm{G}_h^{\mathrm{s}} &\coloneqq \Big\{\mathrm{G} \in \mathrm{L}^2(\Omega_h^{\mathrm{s}}) : \mathrm{G}|_K \in \mathrm{P}_k(K) \quad \forall\, K \in \Omega_h^{\mathrm{s}}\Big\},\\
\mathbf{V}_h^\star &\coloneqq \Big\{\mathbf{v} \in \mathbf{L}^2(\Omega_h^\star) : \mathbf{v}|_K \in \mathbf{P}_k(K) \quad \forall\, K \in \Omega_h^\star\Big\},\\
Q_h^\star &\coloneqq \Big\{q \in L^2(\Omega_h^\star) : q|_K \in P_k(K) \quad \forall\, K \in \Omega_h^\star\Big\},
\end{aligned}$$

for intra-element variables, and

$$\begin{aligned}
M_h^{\mathrm{d}} &\coloneqq \Big\{\mu \in L^2(\mathcal{E}_h^{\mathrm{d}}) : \mu|_e \in P_k(e) \quad \forall\, e \in \mathcal{E}_{\mathrm{d}}\Big\},\\
\mathbf{M}_h^{\mathrm{s}} &\coloneqq \Big\{\boldsymbol{\mu} \in \mathbf{L}^2(\mathcal{E}_h^{\mathrm{s}}) : \boldsymbol{\mu}|_e \in \mathbf{P}_k(e) \quad \forall\, e \in \mathcal{E}_{\mathrm{s}}\Big\}
\end{aligned}$$

for trace variables. We denote by N_h^{d} and $\mathbf{N}_h^{\mathrm{s}}$ the restrictions of M_h^{d} and $\mathbf{M}_h^{\mathrm{s}}$ to the discrete interfaces $\mathcal{I}_h^{\mathrm{d}}$ and $\mathcal{I}_h^{\mathrm{s}}$, respectively. The mesh-dependent inner products are defined as

$$(\cdot,\cdot)_{\Omega_h^\star} \coloneqq \sum_{K\in\Omega_h^\star} (\cdot,\cdot)_K, \quad \langle\cdot,\cdot\rangle_{\partial\Omega_h^\star} = \sum_{K\in\Omega_h^\star} \langle\cdot,\cdot\rangle_{\partial K} \quad \text{and} \quad \langle\cdot,\cdot\rangle_{\mathcal{I}_h^\star} = \sum_{e\in\mathcal{I}_h^\star} \langle\cdot,\cdot\rangle_e,$$

and their corresponding norms denoted by

$$\|\cdot\|_{\Omega_h^\star} \coloneqq \left(\sum_{K\in\Omega_h^\star} \|\cdot\|_K^2\right)^{1/2}, \quad \|\cdot\|_{\partial\Omega_h^\star} = \left(\sum_{K\in\Omega_h^\star} \|\cdot\|_{\partial K}^2\right)^{1/2} \quad \text{and} \quad \|\cdot\|_{\mathcal{I}_h^\star} = \left(\sum_{e\in\mathcal{I}_h^\star} \|\cdot\|_e^2\right)^{1/2}.$$

To avoid proliferation of unimportant constants, we use the terminology $a \lesssim b$ whenever $a \leq Cb$ and C is a positive constant independent of h and the gap between both discrete interfaces.

Transfer Paths. For $\star \in \{\mathrm{s}, \mathrm{d}\}$, we introduce a mapping $\boldsymbol{\psi}_\star : \mathcal{I} \to \mathcal{I}_h^\star$, such that for each point $\boldsymbol{x} \in \mathcal{I}$, we associate a point $\boldsymbol{x}_\star = \boldsymbol{\psi}_\star(\boldsymbol{x}) \in \mathcal{I}_h^\star$. We also define a mapping $\boldsymbol{\psi} : \mathcal{I}_h^{\mathrm{d}} \to \mathcal{I}_h^{\mathrm{s}}$ as $\boldsymbol{\psi} = \boldsymbol{\psi}_{\mathrm{s}} \circ \boldsymbol{\psi}_{\mathrm{d}}^{-1}$, which means that for each $\boldsymbol{x}_{\mathrm{d}} \in \mathcal{I}_h^{\mathrm{d}}$, we associate a point $\boldsymbol{x}_{\mathrm{s}} = \boldsymbol{\psi}(\boldsymbol{x}_{\mathrm{d}}) \in \mathcal{I}_h^{\mathrm{s}}$. We denote by $\sigma_\star(\boldsymbol{x}_\star)$ the segment starting at $\boldsymbol{x}_\star$ and ending at $\boldsymbol{x}$, with unit tangent vector $\boldsymbol{t}_\star$ and length $|\sigma_\star(\boldsymbol{x}_\star)|$. Then, keeping in mind the configuration of the interfaces, i.e., piece-wise polynomial if the meshes coincide or flat interfaces for the case with gap, as depicted in Figure 3.1, it follows immediately that for each $e \in \mathcal{I}_h^\star$, $\boldsymbol{t}_\star = \mathbf{n}_{\star,h} = \mathbf{n}_\star$ with $\star \in \{\mathrm{s},\mathrm{d}\}$, and $\boldsymbol{t}_\mathrm{d} = -\boldsymbol{t}_\mathrm{s}$. This means that the direction of the segment $\sigma_\star(\boldsymbol{x}_\star)$ must be parallel to the normals computed at its ends. Therefore, from now on, when no confusion arise, we will write $\mathbf{n}_\star$, to refer to the vector associated with $\sigma_\star(\boldsymbol{x}_\star)$, with $\star \in \{\mathrm{s},\mathrm{d}\}$. Then, $\sigma(\boldsymbol{x}_\mathrm{d})$ is the segment that starts at $\boldsymbol{x}_\mathrm{d}$ and ends at $\boldsymbol{x}_\mathrm{s}$, with unit tangent vector $\mathbf{n}_\mathrm{d}$ and length $|\sigma(\boldsymbol{x}_\mathrm{d})|$. The segment $\sigma(\boldsymbol{x}_\mathrm{d})$ is referred as the *Transfer Path* associated with $\boldsymbol{x}_\mathrm{d}$ and is assumed to satisfy two conditions: it does not intersect the interior of another transfer path and its length $|\sigma(\boldsymbol{x}_\mathrm{d})|$ is of order at most $\max\{h_\mathrm{s}, h_\mathrm{d}\} = h_\mathrm{d}$.

Remark 3.1. From the implementation point of view, the mapping $\psi_\star$ is only computed at the quadrature points needed to calculate the integrals in (3.8). Given a quadrature point $\boldsymbol{x}_\star$ at the discrete interface $\mathcal{I}_h^\star$, we need to find a point $\boldsymbol{x}$ at the true interface $\mathcal{I}$. In principle, $\boldsymbol{x}$ can be any point, as long as the following conditions are satisfied [47]: the distance between $\boldsymbol{x}$ and $\boldsymbol{x}_\star$ is of order δ, the interior of the segment connecting $\boldsymbol{x}_\star$ and $\boldsymbol{x}$ does not intersect the interior of the domain $\Omega_h^\star$, and the unit tangent vector $\boldsymbol{t}_\star$ does not deviate too much from the normal vector $\mathbf{n}_{\star,h}$. For instance, we can consider the closest point projection or the algorithm provided in [47, Section 2.4] to construct the mapping in the two dimensional case. The previous conditions are valid for Dirichlet boundary problems. Now, for Neumann or interface conditions, in addition we must require $\mathbf{n}_{\star,h}$ to be sufficiently close to $\mathbf{n}_\star$. From the point of view of the analysis, we needed to make the further assumption on this mapping asking $\mathbf{n}_{\star,h}$ and $\mathbf{n}_\star$ to be equal, which limit its construction in general scenarios. This is why the analysis presented in this manuscript covers the cases depicted in Fig. 3.1, but we believe it can be extended to the case when $\|\mathbf{n}_\star - \mathbf{n}_{\star,h}\|_\infty$ is of order δ^α, for some $\alpha > 0$, being this a subject of ongoing work.

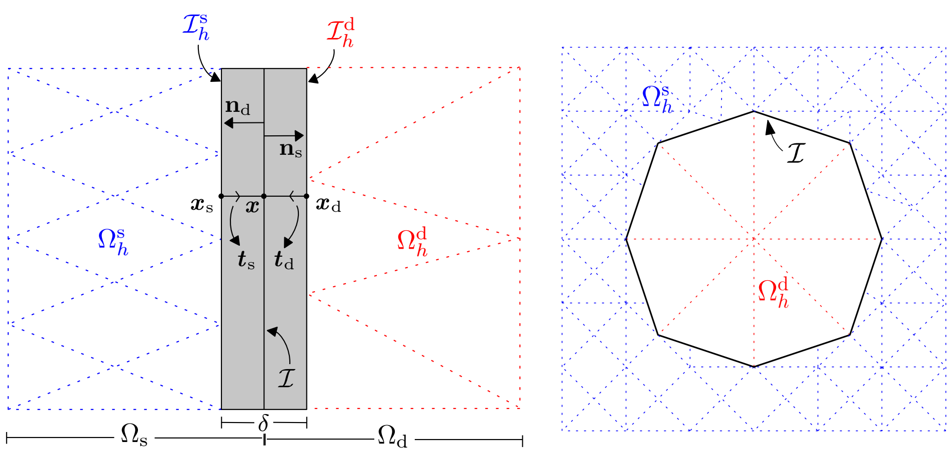

Figure 3.1: *Left: Example of dissimilar meshes separated by a uniform gap of size δ. Right: A piecewise polygonal interface separating two regions discretized by diferent meshes.*

The treatment of the pressure. Since the computational domain Ω_h^s does not necessarily coincide with the physical domain Ω_s, we adopt a similar approach to that developed in [102] by introducing a decomposition $P_\mathrm{s} = \alpha_\mathrm{s} + p_\mathrm{s}$ that imposes a zero-mean condition on the pressure, with $\alpha_\mathrm{s} := \frac{1}{|\Omega_h^\mathrm{s}|}\int_{\Omega_h^\mathrm{s}} P_\mathrm{s}$

and $p_{\rm s} \in L^2_0(\Omega_h^{\rm s})$ ($L^2(\Omega_h^{\rm s})$-function with zero mean in $\Omega_h^{\rm s}$). In turn, since $P_{\rm s}$ will be eliminated from the system, we need to rewrite $\alpha_{\rm s}$ in terms of $p_{\rm s}$. By using the fifth equation of (3.1a), we deduce that

$$\alpha_{\rm s} = \frac{-1}{|\Omega_{\rm s}|}\int_{\Omega_{\rm s}\setminus\Omega_h^{\rm s}} p_{\rm s}. \tag{3.2}$$

Then, $P_{\rm s}$ can be recovered after the approximation of $p_{\rm s}$ is computed.

Extrapolation operator. The region enclosed by $\Omega_h^{\rm s}$ and $\Omega_h^{\rm d}$ (shaded area in Figure 3.1) is denoted by $\Omega_h^{\tt ext}$. We notice that $\Omega_h^{\tt ext}$ is not meshed and, as a consequence, we do not have an HDG approximation in there. That is why the HDG approximation of the velocity gradient $\mathrm{L}_{\rm s}$, the pressure field $p_{\rm s}$ (to be defined below), and the flux $\mathbf{u}_{\rm d}$, will be locally extrapolated from the computational domain $\Omega_h^{\rm d}\cup\Omega_h^{\rm s}$ to $\Omega_h^{\tt ext}$. More precisely, let $\star\in\{{\rm s},{\rm d}\}$. Given a face $e\in\mathcal{I}_h^\star$ belonging to the element $K_e\in\Omega_h^\star$, we define the *extrapolation patch* as $K_e^{\tt ext} := \Big\{\boldsymbol{x}+\mathbf{n}_\star t : 0\le t\le|\sigma_\star(\boldsymbol{x})|,\ \boldsymbol{x}\in e\Big\}$, and let q be a tensor, vector, or scalar-valued polynomial function defined on an element K in $\Omega_h^{\rm d}\cup\Omega_h^{\rm s}$ such that $\overline{K}\cap\overline{K_e^{\tt ext}} = e$. We denote by $\boldsymbol{E}_q(\boldsymbol{y})$, the extrapolation of q evaluated at $\boldsymbol{y}\in K_e^{\tt ext}$.

The HDG projections. Let $(\mathrm{L}_{\rm s},\mathbf{u}_{\rm s},p_{\rm s})\in \mathrm{H}^1(\Omega_h^{\rm s})\times\mathbf{H}^1(\Omega_h^{\rm s})\times H^1(\Omega_h^{\rm s})$. For the Stokes problem, we recall from [42] its HDG projection $\mathit{\Pi}_{\rm s}(\mathrm{L}_{\rm s},\mathbf{u}_{\rm s},p_{\rm s}) = (\mathit{\Pi}^{\rm s}_{\rm G}\mathrm{L}_{\rm s},\mathit{\Pi}^{\rm s}_{\mathbf{V}}\mathbf{u}_{\rm s},\mathit{\Pi}^{\rm s}_{Q}p_{\rm s})$ as the element of $\mathrm{G}_h^{\rm s}\times\mathbf{V}_h^{\rm s}\times Q_h^{\rm s}$ defined as follows: on an arbitrary element K of $\Omega_h^{\rm s}$, the values of the projected function on K are determined by requiring that

$$(\mathit{\Pi}^{\rm s}_{\rm G}\mathrm{L}_{\rm s},\mathrm{G})_K = (\mathrm{L}_{\rm s},\mathrm{G})_K \quad \forall\,\mathrm{G}\in\mathrm{P}_{k-1}(K), \qquad (\mathit{\Pi}^{\rm s}_{\mathbf{V}}\mathbf{u}_{\rm s},\mathbf{v})_K = (\mathbf{u}_{\rm s},\mathbf{v})_K \quad \forall\,\mathbf{v}\in\mathbf{P}_{k-1}(K), \tag{3.3a}$$

$$(\mathit{\Pi}^{\rm s}_{Q}p_{\rm s},q)_K = (p_{\rm s},q)_K \quad \forall\,q\in P_{k-1}(K), \qquad (\mathrm{tr}\mathit{\Pi}^{\rm s}_{\rm G}\mathrm{L}_{\rm s},q)_K = (\mathrm{tr}\mathrm{L}_{\rm s},q)_K \quad \forall\,q\in P_k(K), \tag{3.3b}$$

$$\langle\nu\mathit{\Pi}^{\rm s}_{\rm G}\mathrm{L}_{\rm s}\mathbf{n}_{\rm s} - \mathit{\Pi}^{\rm s}_{Q}p_{\rm s}\mathbf{n}_{\rm s} - \tau\nu\mathit{\Pi}^{\rm s}_{\mathbf{V}}\mathbf{u}_{\rm s},\boldsymbol{\mu}\rangle_e = \langle\nu\mathrm{L}_{\rm s}\mathbf{n}_{\rm s} - p_{\rm s}\mathbf{n}_{\rm s} - \tau\nu\mathbf{u}_{\rm s},\boldsymbol{\mu}\rangle_e \quad \forall\,\boldsymbol{\mu}\in\mathbf{P}_k(e)\,\forall\,e\subset\partial K, \tag{3.3c}$$

where $\tau>0$ is the stabilization parameter of the HDG method. For the case $k=0$, the projections are well-defined considering only the second equation of (3.3b) and (3.3c). Furthermore, if $(\mathrm{L}_{\rm s},\mathbf{u}_{\rm s},p_{\rm s})\in \mathrm{H}^{l_\sigma+1}(\Omega_h^{\rm s})\times\mathbf{H}^{l_{\mathbf{u}_{\rm s}}+1}(\Omega_h^{\rm s})\times H^{l_\sigma+1}(\Omega_h^{\rm s})$, for $l_{\mathbf{u}_{\rm s}},\,l_\sigma\in[0,k]$, the above projection satisfies (cf. [42, Theorem 2.1]) the following properties:

$$\|\mathbf{u}_{\rm s}-\mathit{\Pi}^{\rm s}_{\mathbf{V}}\mathbf{u}_{\rm s}\|_K \lesssim h_K^{l_{\mathbf{u}_{\rm s}}+1}|\mathbf{u}_{\rm s}|_{\mathbf{H}^{l_{\mathbf{u}_{\rm s}}+1}(K)} + h_K^{l_\sigma+1}(\tau\nu)^{-1}|\nabla\cdot(\nu\mathrm{L}_{\rm s}-p_{\rm s}\mathrm{I})|_{\mathbf{H}^{l_\sigma}(K)}, \tag{3.4a}$$

$$\begin{aligned}\|\nu(\mathrm{L}_{\rm s}-\mathit{\Pi}^{\rm s}_{\rm G}\mathrm{L}_{\rm s})\|_K + \|p_{\rm s}-\mathit{\Pi}^{\rm s}_{Q}p_{\rm s}\|_K \lesssim\ & h_K^{l_\sigma+1}|\nu\mathrm{L}_{\rm s}-p_{\rm s}\mathrm{I}|_{\mathrm{H}^{l_\sigma+1}(K)} + h_K^{l_u+1}\tau\nu|\mathbf{u}_{\rm s}|_{\mathbf{H}^{l_u+1}(K)}\\ &+\tau\nu\|\mathbf{u}_{\rm s}-\mathit{\Pi}^{\rm s}_{\mathbf{V}}\mathbf{u}_{\rm s}\|_K,\end{aligned} \tag{3.4b}$$

for all $K\in\Omega_h^{\rm s}$, where I is the identity tensor. Similarly, given $(\mathbf{u}_{\rm d},p_{\rm d})\in\mathbf{H}^1(\Omega_h^{\rm d})\times H^1(\Omega_h^{\rm d})$ for the Darcy problem, we recall from [43] its HDG projection $\mathit{\Pi}_{\rm d}(\mathbf{u}_{\rm d},p_{\rm d}) = (\mathit{\Pi}^{\rm d}_{\mathbf{V}}\mathbf{u}_{\rm d},\mathit{\Pi}^{\rm d}_{Q}p_{\rm d})$ as the element of $\mathbf{V}_h^{\rm d}\times Q_h^{\rm d}$ defined as the unique element-wise solution of

$$(\mathit{\Pi}^{\rm d}_{\mathbf{V}}\mathbf{u}_{\rm d},\mathbf{v})_K = (\mathbf{u}_{\rm d},\mathbf{v})_K \quad \forall\,\mathbf{v}\in\mathbf{P}_{k-1}(K), \quad (\mathit{\Pi}^{\rm d}_{Q}p_{\rm d},q)_K = (p_{\rm d},q)_K \quad \forall\,q\in P_{k-1}(K), \tag{3.5a}$$

$$\langle\mathit{\Pi}^{\rm d}_{\mathbf{V}}\mathbf{u}_{\rm d}\cdot\mathbf{n}_{\rm d} + \tau\mathit{\Pi}^{\rm d}_{Q}p_{\rm d},\mu\rangle_e = \langle\mathbf{u}_{\rm d}\cdot\mathbf{n}_{\rm d} + \tau\mathcal{P}^{\rm d}p_{\rm d},\mu\rangle_e \quad \forall\,\mu\in P_k(e),\ \forall\,e\subset\partial K, \tag{3.5b}$$

for every element $K \in \Omega_h^{\rm d}$. Similarly to the projections in the Stokes domain, for the case $k = 0$, the projections in the Darcy domain are well-defined considering only (3.5b). Given constants $l_{\mathbf{u}_{\rm d}}$, $l_{p_{\rm d}} \in [0,k]$, if $(\mathbf{u}_{\rm d}, p_{\rm d}) \in \mathbf{H}^{l_{\mathbf{u}_{\rm d}}+1}(\Omega_h^{\rm d}) \times H^{l_{p_{\rm d}}+1}(\Omega_h^{\rm d})$, there hold (cf. [43])

$$\|\mathbf{u}_{\rm d} - \Pi_{\mathbf{V}}^{\rm d}\mathbf{u}_{\rm d}\|_K \lesssim h_K^{l_{\mathbf{u}_{\rm d}}+1}|\mathbf{u}_{\rm d}|_{\mathbf{H}^{l_{\mathbf{u}_{\rm d}}+1}(K)} + h_K^{l_{p_{\rm d}}+1}|p_{\rm d}|_{H^{l_{p_{\rm d}}+1}(K)}, \tag{3.6a}$$

$$\|p_{\rm d} - \Pi_{Q}^{\rm d}p_{\rm d}\|_K \lesssim h_K^{l_{p_{\rm d}}+1}|p_{\rm d}|_{H^{l_{p_{\rm d}}+1}(K)} + h_K^{l_{\mathbf{u}_{\rm d}}+1}|\nabla\cdot\mathbf{u}_{\rm d}|_{H^{l_{\mathbf{u}_{\rm d}}}(K)}, \tag{3.6b}$$

for all $K \in \Omega_h^{\rm d}$. We end this section by mentioning that in this chapter, $\boldsymbol{\mathcal{P}}^\star : \mathbf{L}^2(e) \to \mathbf{P}_k(e)$ and $\mathcal{P}^\star : L^2(e) \to P_k(e)$ are the respective $\mathbf{L}^2$ and L^2 orthogonal projections for all facet e of $\mathcal{E}_h^\star$. In abuse of notation, the global projections will be also denoted by $\boldsymbol{\mathcal{P}}^\star$ and $\mathcal{P}^\star$.

3.3 The HDG method

The HDG formulation of the coupled system (3.1a)-(3.1b) reduces to:
Find $(\mathrm{L}_{{\rm s},h}, \mathbf{u}_{{\rm s},h}, p_{{\rm s},h}, \widehat{\mathbf{u}}_{{\rm s},h}, \mathbf{u}_{{\rm d},h}, p_{{\rm d},h}, \widehat{p}_{{\rm d},h}) \in \mathrm{G}_h^{\rm s} \times \mathbf{V}_h^{\rm s} \times Q_h^{\rm s} \times \mathbf{M}_h^{\rm s} \times \mathbf{V}_h^{\rm d} \times Q_h^{\rm d} \times M_h^{\rm d}$ such that

$$\begin{aligned}
(\mathrm{L}_{{\rm s},h}, \mathrm{G}_{{\rm s},h})_{\Omega_h^{\rm s}} + (\mathbf{u}_{{\rm s},h}, \nabla\cdot\mathrm{G}_{{\rm s},h})_{\Omega_h^{\rm s}} - \langle\widehat{\mathbf{u}}_{{\rm s},h}, \mathrm{G}_{{\rm s},h}\mathbf{n}_{\rm s}\rangle_{\partial\Omega_h^{\rm s}} &= 0\,, && (3.7a)\\
(\boldsymbol{\sigma}_{{\rm s},h}, \nabla\mathbf{v}_{{\rm s},h})_{\Omega_h^{\rm s}} - \langle\widehat{\boldsymbol{\sigma}}_{{\rm s},h}\mathbf{n}_{\rm s}, \mathbf{v}_{{\rm s},h}\rangle_{\partial\Omega_h^{\rm s}} &= (\mathbf{f}_{\rm s}, \mathbf{v}_{{\rm s},h})_{\Omega_h^{\rm s}}\,, && (3.7b)\\
-(\mathbf{u}_{{\rm s},h}, \nabla q_{{\rm s},h})_{\Omega_h^{\rm s}} + \langle\widehat{\mathbf{u}}_{{\rm s},h}\cdot\mathbf{n}_{\rm s}, q_{{\rm s},h}\rangle_{\partial\Omega_h^{\rm s}} &= 0\,, && (3.7c)\\
\langle\widehat{\mathbf{u}}_{{\rm s},h}, \boldsymbol{\mu}_{{\rm s},h}\rangle_{\Gamma_{{\rm s},h}} &= 0\,, && (3.7d)\\
(p_{{\rm s},h}, 1)_{\Omega_h^{\rm s}} &= 0\,, && (3.7e)\\
\langle\widehat{\boldsymbol{\sigma}}_{{\rm s},h}\mathbf{n}_{\rm s}, \boldsymbol{\mu}_{{\rm s},h}\rangle_{\partial\Omega_h^{\rm s}\setminus(\Gamma_{{\rm s},h}\cup\mathcal{I}_h^{\rm s})} &= 0\,, && (3.7f)\\
(\kappa^{-1}\mathbf{u}_{{\rm d},h}, \mathbf{v}_{{\rm d},h})_{\Omega_h^{\rm d}} - (p_{{\rm d},h}, \nabla\cdot\mathbf{v}_{{\rm d},h})_{\Omega_h^{\rm d}} + \langle\mathbf{v}_{{\rm d},h}\cdot\mathbf{n}_{\rm d}, \widehat{p}_{{\rm d},h}\rangle_{\partial\Omega_h^{\rm d}} &= 0\,, && (3.7g)\\
-(\mathbf{u}_{{\rm d},h}, \nabla q_{{\rm d},h})_{\Omega_h^{\rm d}} + \langle\widehat{\mathbf{u}}_{{\rm d},h}\cdot\mathbf{n}_{\rm d}, q_{{\rm d},h}\rangle_{\partial\Omega_h^{\rm d}} &= (\mathrm{f}_{\rm d}, q_{{\rm d},h})_{\Omega_h^{\rm d}}, && (3.7h)\\
\langle\widehat{\mathbf{u}}_{{\rm d},h}\cdot\mathbf{n}_{\rm d}, \mu_{{\rm d},h}\rangle_{\partial\Omega_h^{\rm d}\setminus\mathcal{I}_h^{\rm d}} &= 0\,, && (3.7i)
\end{aligned}$$

for all $(\mathrm{G}_{{\rm s},h}, \mathbf{v}_{{\rm s},h}, q_{{\rm s},h}, \boldsymbol{\mu}_{{\rm s},h}, \mathbf{v}_{{\rm d},h}, q_{{\rm d},h}, \mu_{{\rm d},h}) \in \mathrm{G}_h^{\rm s} \times \mathbf{V}_h^{\rm s} \times Q_h^{\rm s} \times \mathbf{M}_h^{\rm s} \times \mathbf{V}_h^{\rm d} \times Q_h^{\rm d} \times M_h^{\rm d}$, where

$$\begin{aligned}
\boldsymbol{\sigma}_{{\rm s},h} &= \nu\mathrm{L}_{{\rm s},h} - p_{{\rm s},h}\mathrm{I}\,,\\
\widehat{\mathbf{u}}_{{\rm d},h}\cdot\mathbf{n}_{\rm d} &= \mathbf{u}_{{\rm d},h}\cdot\mathbf{n}_{\rm d} + \tau(p_{{\rm d},h} - \widehat{p}_{{\rm d},h}) \quad \text{on} \quad \partial\Omega_h^{\rm d}\,, && (3.8a)\\
\widehat{\boldsymbol{\sigma}}_{{\rm s},h}\mathbf{n}_{\rm s} &= \boldsymbol{\sigma}_{{\rm s},h}\mathbf{n}_{\rm s} - \tau\nu(\mathbf{u}_{{\rm s},h} - \widehat{\mathbf{u}}_{{\rm s},h}) \quad \text{on} \quad \partial\Omega_h^{\rm s}\,, && (3.8b)
\end{aligned}$$

and we recall that τ is a positive stabilization function defined in $\partial\Omega_h^{\rm s}\cup\partial\Omega_h^{\rm d}$, assumed to be uniformly bounded. For simplicity of the exposition, we assume τ is constant everywhere. The above equations must be complemented with suitable transmission conditions across the interfaces $\mathcal{I}_h^{\rm s}$ and $\mathcal{I}_h^{\rm d}$, which we proceed to derive now and this constitutes the novelty of our work. Indeed, we propose the following conditions:

$$-\langle\widetilde{\mathbf{u}}_{{\rm s},h}\cdot\mathbf{n}_{\rm d}, \mu_{{\rm d},h}\rangle_{\mathcal{I}_h^{\rm d}} + \langle\widetilde{\mathbf{u}}_{{\rm d},h}\cdot\mathbf{n}_{\rm d}, \mu_{{\rm d},h}\rangle_{\mathcal{I}_h^{\rm d}} = 0 \quad \forall\,\mu_{{\rm d},h} \in N_h^{\rm d}, \tag{3.9a}$$

$$\langle \widetilde{\boldsymbol{\sigma}}_{\mathrm{s},h}\mathbf{n}_{\mathrm{s}} + \sum_{\ell=1}^{n-1} \omega_\ell^{-1}(\widetilde{\mathbf{u}}_{\mathrm{s},h} \circ \boldsymbol{\psi}^{-1} \cdot \boldsymbol{m}_\ell)\boldsymbol{m}_\ell, \boldsymbol{\mu}_{\mathrm{s},h}\rangle_{\mathcal{I}_h^{\mathrm{s}}} - \langle \widetilde{p}_{\mathrm{d},h}\mathbf{n}_{\mathrm{d}}, \boldsymbol{\mu}_{\mathrm{s},h}\rangle_{\mathcal{I}_h^{\mathrm{s}}} \;=\; 0 \quad \forall\, \boldsymbol{\mu}_{\mathrm{s},h} \in \mathbf{N}_h^{\mathrm{s}}, \tag{3.9b}$$

where $\widetilde{\mathbf{u}}_{\mathrm{s},h}$, $\widetilde{p}_{\mathrm{d},h}$, $\widetilde{\boldsymbol{\sigma}}_{\mathrm{s},h}\mathbf{n}_{\mathrm{s}}$, and $\widetilde{\mathbf{u}}_{\mathrm{d},h}$ stand for the approximations of $\mathbf{u}_{\mathrm{s}}|_{\mathcal{I}_h^{\mathrm{s}}}$, $p_{\mathrm{d}}|_{\mathcal{I}_h^{\mathrm{d}}}$, $(\nu \mathrm{L}_{\mathrm{s}} - p_{\mathrm{s}}\mathrm{I})\mathbf{n}_{\mathrm{s}}|_{\mathcal{I}_h^{\mathrm{s}}}$ and $\mathbf{u}_{\mathrm{d}}|_{\mathcal{I}_h^{\mathrm{d}}}$, respectively, based on suitable extensions (constructed below) of $\widehat{\mathbf{u}}_{\mathrm{s},h}$, $\widehat{p}_{\mathrm{d},h}$, $\widehat{\boldsymbol{\sigma}}_{\mathrm{s},h}\mathbf{n}_{\mathrm{s}}$ and $\widehat{\mathbf{u}}_{\mathrm{d},h}$ outside their corresponding computational domains. More precisely, employing the transferring technique of [47] (see also [45, 87, 101]), the tilde variables are constructed as follows: let $\boldsymbol{x}_\star \in \mathcal{I}_h^\star$ and its corresponding point $\boldsymbol{x} \in \mathcal{I}$. Integrating the first equation of (3.1a) along the transferring path $\sigma_{\mathrm{s}}(\boldsymbol{x}_{\mathrm{s}})$ and using the first equation of (3.1c), we obtain

$$\mathbf{u}_{\mathrm{s}} \circ \boldsymbol{\psi}_{\mathrm{d}}^{-1}(\boldsymbol{x}_{\mathrm{d}}) \cdot \mathbf{n}_{\mathrm{s}} + (\mathbf{u}_{\mathrm{d}} \circ \boldsymbol{\psi}_{\mathrm{d}}^{-1})(\boldsymbol{x}_{\mathrm{d}}) \cdot \mathbf{n}_{\mathrm{d}} = 0, \tag{3.10}$$

where $\mathbf{u}_{\mathrm{s}} \circ \boldsymbol{\psi}_{\mathrm{d}}^{-1}(\boldsymbol{x}_{\mathrm{d}}) = \mathbf{u}_{\mathrm{s}}(\boldsymbol{x}_{\mathrm{s}}) + |\sigma_{\mathrm{s}}(\boldsymbol{x}_{\mathrm{s}})| \displaystyle\int_0^1 \mathrm{L}_{\mathrm{s}}(\boldsymbol{y}_{\mathrm{s}}(t))\mathbf{n}_{\mathrm{s}} dt$, being $\boldsymbol{y}_{\mathrm{s}}(t) = \boldsymbol{x}_{\mathrm{s}} + (\boldsymbol{x} - \boldsymbol{x}_{\mathrm{s}})t$ with $t \in [0,1]$ the parametrization of $\sigma_{\mathrm{s}}(\boldsymbol{x}_{\mathrm{s}})$. Similarly, integrating the first equation of (3.1b) along the connecting segment $\sigma_{\mathrm{d}}(\boldsymbol{x}_{\mathrm{d}})$ and using the second equation of (3.1c), it follows that

$$((\nu \mathrm{L}_{\mathrm{s}} - P_{\mathrm{s}}\mathrm{I}) \circ \boldsymbol{\psi}_{\mathrm{s}}^{-1})(\boldsymbol{x}_{\mathrm{s}})\mathbf{n}_{\mathrm{s}} + \sum_{\ell=1}^{n-1} \omega_\ell^{-1}(\mathbf{u}_{\mathrm{s}} \circ \boldsymbol{\psi}_{\mathrm{s}}^{-1}(\boldsymbol{x}_{\mathrm{s}}) \cdot \boldsymbol{m}_\ell)\boldsymbol{m}_\ell - p_{\mathrm{d}} \circ \boldsymbol{\psi}_{\mathrm{s}}^{-1}(\boldsymbol{x}_{\mathrm{s}})\mathbf{n}_{\mathrm{d}} = \mathbf{0}, \tag{3.11}$$

where $p_{\mathrm{d}} \circ \boldsymbol{\psi}_{\mathrm{s}}^{-1}(\boldsymbol{x}_{\mathrm{s}}) = p_{\mathrm{d}}(\boldsymbol{x}_{\mathrm{d}}) - |\sigma_{\mathrm{d}}(\boldsymbol{x}_{\mathrm{d}})| \displaystyle\int_0^1 \kappa^{-1}\mathbf{u}_{\mathrm{d}}(\boldsymbol{y}_{\mathrm{d}}(t)) \cdot \mathbf{n}_{\mathrm{d}} dt$, being $\boldsymbol{y}_{\mathrm{d}}(t) = \boldsymbol{x}_{\mathrm{d}} + (\boldsymbol{x} - \boldsymbol{x}_{\mathrm{d}})t$ with $t \in [0,1]$ the parametrization of $\sigma_{\mathrm{d}}(\boldsymbol{x}_{\mathrm{d}})$.

Hence, motivated by these expressions and based on the form of the HDG numerical fluxes (3.8a) and (3.8b), we define

$$\begin{aligned}
\widetilde{p}_{\mathrm{d},h}(\boldsymbol{x}_{\mathrm{s}}) \;&\coloneqq\; \widehat{p}_{\mathrm{d},h}(\boldsymbol{x}_{\mathrm{d}}) - |\sigma_{\mathrm{d}}(\boldsymbol{x}_{\mathrm{d}})| \int_0^1 \kappa^{-1}\boldsymbol{E}_{\mathbf{u}_{\mathrm{d},h}}(\boldsymbol{y}_{\mathbf{d}}(t)) \cdot \mathbf{n}_{\mathrm{d}} dt, && (3.12\mathrm{a})\\
\widetilde{\mathbf{u}}_{\mathrm{s},h}(\boldsymbol{x}_{\mathrm{d}}) \;&\coloneqq\; \widehat{\mathbf{u}}_{\mathrm{s},h}(\boldsymbol{x}_{\mathrm{s}}) + |\sigma_{\mathrm{s}}(\boldsymbol{x}_{\mathrm{s}})| \int_0^1 \boldsymbol{E}_{\mathrm{L}_{\mathrm{s},h}}(\boldsymbol{y}_{\mathrm{s}}(t))\mathbf{n}_{\mathrm{s}} dt, && (3.12\mathrm{b})\\
\widetilde{\mathbf{u}}_{\mathrm{d},h}(\boldsymbol{x}_{\mathrm{d}}) \cdot \mathbf{n}_{\mathrm{d}} \;&\coloneqq\; \boldsymbol{E}_{\mathbf{u}_{\mathrm{d},h}} \circ \boldsymbol{\psi}_{\mathrm{d}}^{-1}(\boldsymbol{x}_{\mathrm{d}}) \cdot \mathbf{n}_{\mathrm{d}} + \tau(p_{\mathrm{d},h} - \widehat{p}_{\mathrm{d},h})(\boldsymbol{x}_{\mathrm{d}}), && (3.12\mathrm{c})\\
\widetilde{\boldsymbol{\sigma}}_{\mathrm{s},h}(\boldsymbol{x}_{\mathrm{s}})\mathbf{n}_{\mathrm{s}} \;&\coloneqq\; \boldsymbol{E}_{\boldsymbol{\sigma}_{\mathrm{s},h}} \circ \boldsymbol{\psi}_{\mathrm{s}}^{-1}(\boldsymbol{x}_{\mathrm{s}})\mathbf{n}_{\mathrm{s}} - \alpha_{\mathrm{s},h}\mathbf{n}_{\mathrm{s}} - \nu\tau(\mathbf{u}_{\mathrm{s},h} - \widehat{\mathbf{u}}_{\mathrm{s},h})(\boldsymbol{x}_{\mathrm{s}}), && (3.12\mathrm{d})
\end{aligned}$$

where $\alpha_{\mathrm{s},h} \coloneqq \dfrac{1}{|\Omega_{\mathrm{s}}|} \displaystyle\int_{\Omega_{\mathrm{s}} \setminus \Omega_h^{\mathrm{s}}} \boldsymbol{E}_{p_{\mathrm{s},h}}$, and $\boldsymbol{E}$ denotes the local extrapolation defined in Section 3.2.

In the particular case of matching interfaces, namely $\mathcal{I} = \overline{\Omega}_h^{\mathrm{s}} \cap \overline{\Omega}_h^{\mathrm{d}} = \mathcal{I}_h^{\mathrm{s}} = \mathcal{I}_h^{\mathrm{d}}$, the transmission conditions (3.9) become

$$\langle \widehat{\mathbf{u}}_{\mathrm{s},h} \cdot \mathbf{n}_{\mathrm{s}}, \mu_{\mathrm{d},h}\rangle_{\mathcal{I}} + \langle \widehat{\mathbf{u}}_{\mathrm{d},h} \cdot \mathbf{n}_{\mathrm{d}}, \mu_{\mathrm{d},h}\rangle_{\mathcal{I}} \;=\; 0 \quad \forall\, \mu_{\mathrm{d},h} \in N_h^{\mathrm{d}}, \tag{3.13a}$$

$$\langle \widehat{\boldsymbol{\sigma}}_{\mathrm{s},h}\mathbf{n}_{\mathrm{s}} + \sum_{\ell=1}^{n-1} \omega_\ell^{-1}(\widehat{\mathbf{u}}_{\mathrm{s},h} \cdot \boldsymbol{m}_\ell)\boldsymbol{m}_\ell, \boldsymbol{\mu}_{\mathrm{s},h}\rangle_{\mathcal{I}} - \langle \widehat{p}_{\mathrm{d},h}\mathbf{n}_{\mathrm{d}}, \boldsymbol{\mu}_{\mathrm{s},h}\rangle_{\mathcal{I}} \;=\; 0 \quad \forall\, \boldsymbol{\mu}_{\mathrm{s},h} \in \mathbf{N}_h^{\mathrm{s}}, \tag{3.13b}$$

and the resulting HDG formulation is very similar to the one presented in [71].

Remark 3.2. In [87, 101], a single equation is satisfied in the entire domain, which implies that one of the transmission conditions involves only the primal variable (continuity of the solution), whereas only the mixed variables are present in the other transmission condition (continuity of the normal fluxes). For the former, the numerical trace in the interface of one subdomain, let say $\widehat{u}_h^{(1)}$, is transferred by the TPM to the interface of the other subdomain with numerical trace $\widehat{u}_h^{(2)}$. If we denote by $\mathrm{TPM}(\widehat{u}_h^{(1)})$ the transfer operator applied to $\widehat{u}_h^{(1)}$, a weak continuity is imposed by coupling $\mathrm{TPM}(\widehat{u}_h^{(1)})$ to $\widehat{u}_h^{(2)}$. Regarding the other transmission, denoting by $\widehat{\boldsymbol{q}}_h^{(1)}$ and $\widehat{\boldsymbol{q}}_h^{(2)}$ the discretization of the fluxes in each subdomain, $\widehat{\boldsymbol{q}}_h^{(2)}$ is extrapolated to the other subdomain by an expression similar to that of (3.12c) and then coupled to $\widehat{\boldsymbol{q}}_h^{(1)}$. In other words, in each transmission condition, only one variable is transferred or extrapolated, whereas the other is not. In the current manuscript, two different equations hold in each subdomain, where the primal variable of the Stokes system is coupled to the mixed variable of the Darcy equations, and vice-versa. Then, all the variables are being extrapolated or transferred. In fact, according to (3.9a), the TPM (3.12b) is applied to the primal variable of Stokes, where the extrapolation (3.12c) is used for the mixed variable of Darcy. For the condition (3.9b), the opposite happens.

3.4 Stability analysis

In this section we show a stability estimate associated with (3.7) and (3.8). For that, we recall some important estimates and assumptions required to carry out our analysis.

Further notation and auxiliary estimates. Let $\star \in \{\mathrm{s}, \mathrm{d}\}$. Given a face $e \in \mathcal{I}_h^\star$ belonging to the element $K_e \in \Omega_h^\star$, we recall that the *extrapolation patch* is $K_e^{\mathtt{ext}} := \Big\{\boldsymbol{x} + \mathbf{n}_\star t : 0 \le t \le |\sigma_\star(\boldsymbol{x})|,\, \boldsymbol{x} \in e\Big\}$, and denote by $h_e^\perp$ (resp. δ_e) the largest distance of a point inside K_e (resp. $K_e^{\mathtt{ext}}$) to the plane determined by the face e. In other words, $h_e^\perp = \max_{\boldsymbol{x}\in K_e} |\mathrm{dist}(\boldsymbol{x}, e)|, \quad \delta_e = \max_{\boldsymbol{x}\in e} |\sigma_\star(\boldsymbol{x})|$, where $\mathrm{dist}(\boldsymbol{x}, e)$ denotes the distance from $\boldsymbol{x}$ to the face e. We note that δ_e is a measure of the local size of the gap and $\delta := \max_e \delta_e$ is an upper bound of the size of the gap. We define the ratio $r_e := \delta_e / h_e^\perp$ and, for $e \in \mathcal{I}_h^{\mathrm{s}} \cup \mathcal{I}_h^{\mathrm{d}}$, $\boldsymbol{\mathcal{N}}^k := \Big\{\mathbf{q} \in \mathbf{P}_k(K_e^{\mathtt{ext}}), \quad \mathbf{q}\cdot\mathbf{n}_e \neq 0 \text{ on each } e \subset \partial K_e^{\mathtt{ext}}\Big\}$, where we denoted by $\mathbf{n}_e$ the interior normal vector to $K_e^{\mathtt{ext}}$ along the face e, that is, the exterior normal vector to K_e pointing in the direction of $K_e^{\mathtt{ext}}$. We can then introduce the constants

$$C_e^{\mathtt{ext}} := \frac{1}{\sqrt{r_e}} \sup_{\mathbf{q}\in\boldsymbol{\mathcal{N}}^k} \frac{\|\mathbf{q}\cdot\mathbf{n}_e\|_{K_e^{\mathtt{ext}}}}{\|\mathbf{q}\cdot\mathbf{n}_e\|_{K_e}}, \quad C_e^{\mathtt{inv}} := h_e^\perp \sup_{\mathbf{q}\in\boldsymbol{\mathcal{N}}^k} \frac{\|\partial_{\mathbf{n}_e}\mathbf{q}\|_{K_e^{\mathtt{ext}}}}{\|\mathbf{q}\cdot\mathbf{n}_e\|_{K_e}}. \tag{3.14}$$

As proved in [45, Lemma A.2], these constants are independent of the meshsize, but depend on the polynomial degree k. The superscripts in $C_e^{\mathtt{ext}}$ and $C_e^{\mathtt{inv}}$ refer to an extrapolation constant and an inverse inequality constant.

On the other hand, proceeding as in [45], we introduce the following auxiliary functions: let $e \in \mathcal{I}_h^\star$ that belongs to K_e and $K_e^{\mathtt{ext}}$. For a function $\mathbf{q}$, we define

$$\Lambda_{\mathbf{q}|_{K_e}}(\boldsymbol{x}_\star) := \frac{1}{|\sigma_\star(\boldsymbol{x}_\star)|} \int_0^{|\sigma_\star(\boldsymbol{x}_\star)|} \big(\mathbf{q}_{K_e}(\boldsymbol{x}_\star + \mathbf{n}_\star y) - \mathbf{q}_{K_e}(\boldsymbol{x}_\star)\big)\cdot\mathbf{n}_\star dy, \tag{3.15}$$

for $\star \in \{\mathrm{s}, \mathrm{d}\}$, where $\boldsymbol{x}_{\mathrm{d}} \in e$ and $\boldsymbol{x}_{\mathrm{s}} \in \mathcal{I}_h^{\mathrm{s}}$ are connected by the segment $\sigma(\boldsymbol{x}_{\mathrm{d}})$. They satisfy (cf. [45, Lemma 5.2]),

$$\left\| |\sigma_\star|^{1/2} \Lambda_{\mathbf{q}|_{K_e}} \right\|_e \leq \frac{1}{\sqrt{3}} r_e^{3/2} C_e^{\mathtt{ext}} C_e^{\mathtt{inv}} \|\mathbf{q}\|_{K_e} \qquad \forall\, \mathbf{q} \in \mathbf{P}_k(K_e), \tag{3.16}$$

$$\left\| |\sigma_\star|^{1/2} \Lambda_{\mathbf{q}|_{K_e}} \right\|_e \leq \frac{1}{\sqrt{3}} r_e \left\| h_e^{\perp} \partial_n \mathbf{q} \cdot \mathbf{n} \right\|_{K_e^{\mathtt{ext}}} \qquad \forall\, \mathbf{q} \in \mathbf{H}^1(K_e^{\mathtt{ext}}). \tag{3.17}$$

Another important tool in the analysis of this method, which is based on the Taylor series expansion of a function defined on $\mathcal{I}$ around a point $\mathcal{I}_h^\star$, is the following lemma ([101, Lemma 2.1] or [87, Lemma 2]).

Lemma 1. Suppose that $\boldsymbol{\psi}_\star : \mathcal{I} \to \mathcal{I}_h^\star$ is a bijection for each $\star \in \{\mathrm{s}, \mathrm{d}\}$. The following assertions hold true: If $\boldsymbol{\phi}_\star \in \mathbf{H}^2(\Omega_\star)$ and $\Phi_\star := \nabla \boldsymbol{\phi}_\star$, then

$$\left\| |\sigma_\star|^{-1/2} (\boldsymbol{\phi}_\star - \boldsymbol{\phi}_\star \circ \boldsymbol{\psi}_\star^{-1}) + |\sigma_\star|^{1/2} (\Phi_\star \circ \boldsymbol{\psi}_\star^{-1}) \mathbf{n}_\star \right\|_{\mathcal{I}_h^\star} \lesssim \delta \|\boldsymbol{\phi}_\star\|_{\mathbf{H}^2(\Omega_\star)}, \tag{3.18}$$

$$\left\| |\sigma_\star|^{-1/2} (\boldsymbol{\phi}_\star - \boldsymbol{\phi}_\star \circ \boldsymbol{\psi}_\star^{-1}) \right\|_{\mathcal{I}_h^\star} \lesssim \delta^{1/2} \|\boldsymbol{\phi}_\star\|_{\mathbf{H}^2(\Omega_\star)}, \tag{3.19}$$

If $\Phi_\star \in \mathrm{H}^1(\Omega_\star)$ then

$$\left\| |\sigma_\star|^{-1/2} (\Phi_\star - \Phi_\star \circ \boldsymbol{\psi}_\star^{-1}) \mathbf{n}_\star \right\|_{\mathcal{I}_h^\star} \lesssim \|\Phi_\star\|_{\mathrm{H}^1(\Omega_\star)}. \tag{3.20}$$

Let $e \in \mathcal{I}$, $e_\star = \boldsymbol{\psi}_\star(e) \in \mathcal{I}_h^\star$ and $K_{e_\star}$ the element to which $e_\star$ belongs. If $p \in P_k(K_{e_\star})$, then

$$\|p - p \circ \boldsymbol{\psi}_\star^{-1}\|_{e_\star} \lesssim C_e^{\mathtt{ext}} \delta_e h_e^{-3/2} \|p\|_{K_{e_\star}}. \tag{3.21}$$

In addition, we recall the discrete trace inequality (cf. [54, Lemma 1.46]), which establishes that if ϕ is a scalar, vector or tensor-valued polynomial in K_e, there exists a positive constant C_e^{tr}, independent of the meshsize but depends on the polynomial degree, such that

$$\|\phi\|_e \leq C_e^{\mathrm{tr}} h_e^{-1/2} \|\phi\|_{K_e}. \tag{3.22}$$

We stress that the identities and inequalities established throughout this section hold true for the tensor, vector or scalar-valued cases as required.

Assumptions. Here we outline a set of assumptions under which our analysis holds. More precisely, we assume that

(A.1) $\Omega_h^{\mathrm{s}} \cap \Omega_h^{\mathrm{d}} = \emptyset$,

(A.2) the mappings $\boldsymbol{\psi}_\star : \mathcal{I} \to \mathcal{I}_\star$ for $\star \in \{\mathrm{s}, \mathrm{d}\}$, and $\boldsymbol{\psi} : \mathcal{I}_h^{\mathrm{d}} \to \mathcal{I}_h^{\mathrm{s}}$ are bijections,

(A.3) $4 \max\left\{1, \nu^{-1}, 2\sum_{\ell=1}^{n-1} \omega_\ell^{-2}\right\} \tau^{-1/2} C_{\delta_\star, h} \max_{e \in \mathcal{I}_h^\star} \left(\delta_e^{-10/14}\right) + 8 \max_{e \in \mathcal{I}_h^\star} \left(\widehat{C}_e^\star \delta_e^{12/7} h_e^{-3} (C_e^{\mathtt{ext}})^2 \tau^{-1}\right) \leq \frac{1}{4}$, where $C_{\delta_\star, h}$ depends on h and δ (cf. Lemma 2), and $\widehat{C}_e^\star$ is a positive constant appearing in the proof of Lemma 4,

(A.4) $C_{\delta,h} := \widetilde{C}_1 C^{\mathcal{S}}_{\delta,h} + \left((C^{p}_{\delta,h})^2 + \widetilde{C}_2\right)\widetilde{C}_{is}$ is small enough, where $C^{\mathcal{S}}_{\delta,h} := h^2 + (C^{u_{\mathrm{d}},L_{\mathrm{s}}}_{\delta,h})^2 + (C^{\widehat{u}_{\mathrm{s}},\widehat{p}_{\mathrm{d}}}_{\delta,h})^2$,

$$\widetilde{C}_1 := \max\{\nu,1\}\sum_{\star\in\{\mathrm{s},\mathrm{d}\}}\left(4\max_{e\in\mathcal{I}_h^\star}\left(\left(C_e^{\mathrm{tr}}\right)^2\delta_e^{2/7}h_e^{-1}\tau\right) + \max_{e\in\mathcal{I}_h^\star}\left(\frac{(C_e^{\mathrm{tr}})^{-2}h_e^{-\beta}}{2}\right)\right),$$

$$\widetilde{C}_2 := \frac{8}{\nu}\max_{e\in\mathcal{I}_h^{\mathrm{s}}}\left(\widehat{C}_e^{\mathrm{s}}\delta_e^{12/7}h_e^{-3}(C_e^{\mathtt{ext}})^2\tau^{-1}\right) + 4\frac{C_\alpha^2}{\nu}\max_{e\in\mathcal{I}_h^{\mathrm{s}}}\left(\delta_e^{-2/7}\right),$$

$$C^{u_{\mathrm{d}},L_{\mathrm{s}}}_{\delta,h} := \max\{\nu^{-1},1\}\sum_{\star\in\{\mathrm{s},\mathrm{d}\}}\left(\max_{e\in\mathcal{I}_h^\star}\left(\delta_e h_e^{-3/2}C_e^{\mathtt{ext}}\right) + \max_{e\in\mathcal{I}_h^\star}\left(\delta_e^{1/2}C^{1/2}_{\delta_\star,h}\right)\right),$$

$$C^{\widehat{u}_{\mathrm{s}},\widehat{p}_{\mathrm{d}}}_{\delta,h} := \max\{\nu^{-1},1\}\sum_{\star\in\{\mathrm{s},\mathrm{d}\}}\left(\max_{e\in\mathcal{I}_h^\star}\left(\delta_e^{6/7}\tau^{-1/2}\right) + \max_{e\in\mathcal{I}_h^\star}\left(\delta_e^{5/14}\tau^{-1/2}\right)\right) + \delta,$$

$$C^{p}_{\delta,h} := \nu^{-1}\max_{e\in\mathcal{I}_h^{\mathrm{s}}}\left(\delta_e h_e^{-3/2}C_e^{\mathtt{ext}}\right) + \nu^{-1}C_\alpha,$$

$\widetilde{C}_{is}$ is related to an inf-sup condition of Lemma 6, β is a nonnegative parameter whose range will be determined later, and C_α is positive constant, which will appear in the proof of Lemma 4.

Let us briefly comment on these assumptions. Note that Assumptions **(A.1)** and **(A.2)** hold true, for instance, in the illustrations of Figure 3.1. In particular, the assumption **(A.1)** ensures that there is no overlap between subdomains, and is intended to simplify the analysis, whereas, the assumption **(A.2)** is the key to "tie" the interfaces $\mathcal{I}_h^{\mathrm{s}}$ and $\mathcal{I}_h^{\mathrm{d}}$ that cause the gap. The remaining assumptions are technical and define the relationship between the gap size δ and the mesh size h, which is essential for ensuring the convergence and optimality of the method. For example, **(A.3)** is always satisfied for h small enough if $\delta \lesssim h^{7/4}$. To analyze the feasibility of other assumptions, let us write $\delta = C_{\mathrm{g}}h^{1+\gamma}$ with $C_{\mathrm{g}} \geq 0$ and $\gamma > 0$ constants independent of the meshsize. Assumption **(A.4)** is satisfied for all $\gamma > 3/4$ and $\beta \in [0,2]\cap[0,2\gamma-1)$, if h is small enough, as we will explain in Corollaries 2 and 3. These are the strongest assumptions, since they indicate that our analysis holds if the gap size is at most of order $h^{7/4}$, however we will present numerical evidence suggesting that the method is still optimal when the gap is of order h. Finally, we highlight that the remaining constants are defined in the subsequent results presented below. In turn, in order to begin with the analysis, we establish the following result.

Lemma 2. Suppose that Assumptions **(A.1)**-**(A.2)** hold, then it follows that

$$\left\||\sigma_{\mathrm{s}}|^{-1/2}(\widetilde{\mathbf{u}}_{\mathrm{s},h}\circ\boldsymbol{\psi}^{-1} - \widehat{\mathbf{u}}_{\mathrm{s},h})\right\|_{\mathcal{I}_h^{\mathrm{s}}} \leq C^{1/2}_{\delta_{\mathrm{s}},h}\left\|\mathrm{L}_{\mathrm{s},h}\right\|_{\Omega_h^{\mathrm{s}}}, \quad \text{and} \tag{3.23a}$$

$$\left\||\sigma_{\mathrm{d}}|^{-1/2}(\widetilde{p}_{\mathrm{d},h}\circ\boldsymbol{\psi} - \widehat{p}_{\mathrm{d},h})\right\|_{\mathcal{I}_h^{\mathrm{d}}} \leq C^{1/2}_{\delta_{\mathrm{d}},h}\left\|\kappa^{-1}\mathbf{u}_{\mathrm{d},h}\right\|_{\Omega_h^{\mathrm{d}}}, \tag{3.23b}$$

where $C_{\delta_\star,h} = 2\max_{e\in\mathcal{I}_h^\star}\left(\delta_e h_e^{-1}(C_e^{\mathrm{tr}})^2 + \frac{1}{3}\delta_e^3 h_e^{-3}\kappa_\star^3(C_e^{\mathtt{ext}}C_e^{\mathtt{inv}})^2\right)$ for $\star\in\{\mathrm{s},\mathrm{d}\}$.

Proof. It suffices to prove for $\star = \mathrm{d}$, since the proof for $\star = \mathrm{s}$ follows almost verbatim. We begin by stressing that $\boldsymbol{y}_{\mathrm{d}}(t) = \boldsymbol{x}_{\mathrm{d}} + (\boldsymbol{x}-\boldsymbol{x}_{\mathrm{d}})t = \boldsymbol{x}_{\mathrm{d}} + \mathbf{n}_{\mathrm{d}}|\sigma_{\mathrm{d}}(\boldsymbol{x}_{\mathrm{d}})|t$ for all $t\in[0,1]$. Thus, from (3.12a) we deduce that

$$\begin{aligned}\widetilde{p}_{\mathrm{d},h}(\boldsymbol{x}_{\mathrm{s}}) &= \widehat{p}_{\mathrm{d},h}(\boldsymbol{x}_{\mathrm{d}}) - |\sigma_{\mathrm{d}}(\boldsymbol{x}_{\mathrm{d}})| \int_0^1 \kappa^{-1} \boldsymbol{E}_{\mathbf{u}_{\mathrm{d},h}}(\boldsymbol{y}_{\mathbf{d}}(t)) \cdot \mathbf{n}_{\mathrm{d}} dt \\ &= \widehat{p}_{\mathrm{d},h}(\boldsymbol{x}_{\mathrm{d}}) - \int_0^{|\sigma_{\mathrm{d}}(\boldsymbol{x}_{\mathrm{d}})|} \kappa^{-1} \boldsymbol{E}_{\mathbf{u}_{\mathrm{d},h}}(\boldsymbol{x}_{\mathrm{d}} + \mathbf{n}_{\mathrm{d}} t) \cdot \mathbf{n}_{\mathrm{d}} dt \\ &= \widehat{p}_{\mathrm{d},h}(\boldsymbol{x}_{\mathrm{d}}) - \int_0^{|\sigma_{\mathrm{d}}(\boldsymbol{x}_{\mathrm{d}})|} \kappa^{-1} \Big(\boldsymbol{E}_{\mathbf{u}_{\mathrm{d},h}}(\boldsymbol{x}_{\mathrm{d}} + \mathbf{n}_{\mathrm{d}} t) - \mathbf{u}_{\mathrm{d},h}(\boldsymbol{x}_{\mathrm{d}}) \Big) \cdot \mathbf{n}_{\mathrm{d}} dt - \kappa^{-1} |\sigma_{\mathrm{d}}(\boldsymbol{x}_{\mathrm{d}})| \mathbf{u}_{\mathrm{d},h}(\boldsymbol{x}_{\mathrm{d}}) \cdot \mathbf{n}_{\mathrm{d}} \\ &= \widehat{p}_{\mathrm{d},h}(\boldsymbol{x}_{\mathrm{d}}) - \kappa^{-1} |\sigma_{\mathrm{d}}(\boldsymbol{x}_{\mathrm{d}})| \Lambda_{\mathbf{u}_{\mathrm{d},h}}(\boldsymbol{x}_{\mathrm{d}}) - \kappa^{-1} |\sigma_{\mathrm{d}}(\boldsymbol{x}_{\mathrm{d}})| \mathbf{u}_{\mathrm{d},h}(\boldsymbol{x}_{\mathrm{d}}) \cdot \mathbf{n}_{\mathrm{d}},\end{aligned}$$

where we have used (3.15). This implies that $\mathbf{u}_{\mathrm{d},h}(\boldsymbol{x}_{\mathrm{d}}) \cdot \mathbf{n}_{\mathrm{d}} = -\kappa |\sigma_{\mathrm{d}}(\boldsymbol{x}_{\mathrm{d}})|^{-1} (\widetilde{p}_{\mathrm{d},h} \circ \boldsymbol{\psi} - \widehat{p}_{\mathrm{d},h}) - \Lambda_{\mathbf{u}_{\mathrm{d},h}}(\boldsymbol{x}_{\mathrm{d}})$.

By the Cauchy–Schwarz and Young inequalities, and the estimate (3.16), we obtain

$$\begin{aligned}\| |\sigma_{\mathrm{d}}|^{-1/2} (\widetilde{p}_{\mathrm{d},h} \circ \boldsymbol{\psi} - \widehat{p}_{\mathrm{d},h}) \|^2_{\mathcal{I}_h^{\mathrm{d}}} &\le 2 \left(\| \kappa^{-1} |\sigma_{\mathrm{d}}|^{1/2} \mathbf{u}_{\mathrm{d},h} \|^2_{\mathcal{I}_h^{\mathrm{d}}} + \| \kappa^{-1} |\sigma_{\mathrm{d}}|^{1/2} \Lambda_{\mathbf{u}_{\mathrm{d},h}} \|^2_{\mathcal{I}_h^{\mathrm{d}}} \right) \\ &\le 2 \Big(\| \kappa^{-1} |\sigma_{\mathrm{d}}|^{1/2} \mathbf{u}_{\mathrm{d},h} \|^2_{\mathcal{I}_h^{\mathrm{d}}} + \frac{1}{3} \max_{e \in \mathcal{I}_h^{\mathrm{d}}} \left(r_e^3 (C_e^{\mathtt{ext}} C_e^{\mathtt{inv}})^2 \right) \| \kappa^{-1} \mathbf{u}_{\mathrm{d},h} \|^2_{\mathcal{I}_h^{\mathrm{d}}} \Big).\end{aligned}$$

Finally, by the discrete trace inequality (3.22) and the fact that $r_e \le \delta_e h_e^{-1} \kappa_{\mathrm{d}}$, where we recall that κ_{d} is the mesh regularity constant of Ω_h^{d}, we obtain (3.23b). We omit further details. ■

In order to use this analysis to establish both, well-posedness and error bounds, we consider the problem (3.7), but (3.7a) and (3.7g) are replaced by

$$(\mathrm{L}_{\mathrm{s},h}, \mathrm{G}_{\mathrm{s},h})_{\Omega_h^{\mathrm{s}}} + (\mathbf{u}_{\mathrm{s},h}, \nabla \cdot \mathrm{G}_{\mathrm{s},h})_{\Omega_h^{\mathrm{s}}} - \langle \widehat{\mathbf{u}}_{\mathrm{s},h}, \mathrm{G}_{\mathrm{s},h} \mathbf{n}_{\mathrm{s}} \rangle_{\partial \Omega_h^{\mathrm{s}}} = (\mathrm{J}_{\mathrm{s}}, \mathrm{G}_{\mathrm{s},h})_{\Omega_h^{\mathrm{s}}}, \tag{3.24a}$$

$$(\kappa^{-1} \mathbf{u}_{\mathrm{d},h}, \mathbf{v}_{\mathrm{d},h})_{\Omega_h^{\mathrm{d}}} - (p_{\mathrm{d},h}, \nabla \cdot \mathbf{v}_{\mathrm{d},h})_{\Omega_h^{\mathrm{d}}} + \langle \mathbf{v}_{\mathrm{d},h} \cdot \mathbf{n}_{\mathrm{d}}, \widehat{p}_{\mathrm{d},h} \rangle_{\partial \Omega_h^{\mathrm{d}}} = (\mathbf{J}_{\mathrm{d}}, \mathbf{v}_{\mathrm{d},h})_{\Omega_h^{\mathrm{d}}}, \tag{3.24b}$$

where $\mathrm{J}_{\mathrm{s}} \in \mathrm{L}^2(\Omega_h^{\mathrm{s}})$, $\mathbf{J}_{\mathrm{d}} \in \mathbf{L}^2(\Omega_h^{\mathrm{d}})$ are given functions orthogonal to polynomials of degree $k-1$ and (3.9) is replaced by

$$\langle \widetilde{\mathbf{u}}_{\mathrm{s},h} \cdot \mathbf{n}_{\mathrm{s}}, \mu_{\mathrm{d},h} \rangle_{\mathcal{I}_h^{\mathrm{d}}} + \langle \widetilde{\mathbf{u}}_{\mathrm{d},h} \cdot \mathbf{n}_{\mathrm{d}}, \mu_{\mathrm{d},h} \rangle_{\mathcal{I}_h^{\mathrm{d}}} = \langle j_{\mathrm{d}}^{\mathrm{nc}} + j_{\mathrm{d}}^{\delta}, \mu_{\mathrm{d},h} \rangle_{\mathcal{I}_h^{\mathrm{d}}}, \tag{3.25a}$$

$$\langle \widetilde{\boldsymbol{\sigma}}_{\mathrm{s},h} \mathbf{n}_{\mathrm{s}} + \sum_{\ell=1}^{n-1} \omega_\ell^{-1} (\widetilde{\mathbf{u}}_{\mathrm{s},h} \circ \boldsymbol{\psi}^{-1} \cdot \boldsymbol{m}_\ell) \boldsymbol{m}_\ell, \boldsymbol{\mu}_{\mathrm{s},h} \rangle_{\mathcal{I}_h^{\mathrm{s}}} - \langle \widetilde{p}_{\mathrm{d},h} \mathbf{n}_{\mathrm{d}}, \boldsymbol{\mu}_{\mathrm{s},h} \rangle_{\mathcal{I}_h^{\mathrm{s}}} = \langle \mathbf{j}_{\mathrm{s}}^{\mathrm{nc}} + \mathbf{j}_{\mathrm{s}}^{\delta}, \boldsymbol{\mu}_{\mathrm{s},h} \rangle_{\mathcal{I}_h^{\mathrm{s}}}, \tag{3.25b}$$

for all $(\mu_{\mathrm{d},h}, \boldsymbol{\mu}_{\mathrm{s},h}) \in N_h^{\mathrm{d}} \times \mathbf{N}_h^{\mathrm{s}}$, where $j_{\mathrm{d}}^{\mathrm{nc}}$ and $\mathbf{j}_{\mathrm{s}}^{nc}$ are given functions associated with the non-conformity that occurs at the interface, belonging to $L^2(\mathcal{I}_h^{\mathrm{d}})$ and $\mathbf{L}^2(\mathcal{I}_h^{\mathrm{s}})$, respectively. Similarly, j_{d}^{δ} and $\mathbf{j}_{\mathrm{s}}^{\delta}$ are associated with the gap between the discrete interfaces $\mathcal{I}_h^{\mathrm{s}}$ and $\mathcal{I}_h^{\mathrm{d}}$, also belonging to $L^2(\mathcal{I}_h^{\mathrm{d}})$ and $\mathbf{L}^2(\mathcal{I}_h^{\mathrm{s}})$, respectively. We emphasize that the motivation to introduce these given functions is only to unify the well-posedness and error analysis in a compact way. In particular, as we will see below in Corollary 1, to show well-posedness, J_{s}, $\mathbf{J}_{\mathrm{d}}$, $j_{\mathrm{d}}^{\mathrm{nc}}$, $\mathbf{j}_{\mathrm{s}}^{\mathrm{nc}}$, j_{d}^{δ} and $\mathbf{j}_{\mathrm{s}}^{\delta}$ will be zero. On the other hand, as we will see in Section 3.5, J_{s} and $\mathbf{J}_{\mathrm{d}}$ are associated with projection errors when proving the error bounds, and will appear in the terms on the right-hand side of (3.43a) and (3.43f). Similarly, $j_{\mathrm{d}}^{\mathrm{nc}}$, $\mathbf{j}_{\mathrm{s}}^{\mathrm{nc}}$, j_{d}^{δ} and $\mathbf{j}_{\mathrm{s}}^{\delta}$ will appear in the terms on the right-hand side of (3.46a) and (3.46b).

3.4.1 An energy argument

Before presenting the energy estimate, we proceed to deduce how the transmission conditions (3.9) connect $\langle \widehat{\boldsymbol{\sigma}}_{\mathrm{s},h}\mathbf{n}_{\mathrm{s}}, \widehat{\mathbf{u}}_{\mathrm{s},h}\rangle_{\mathcal{I}_h^{\mathrm{s}}}$ and $\langle \widehat{\mathbf{u}}_{\mathrm{d},h}\cdot\mathbf{n}_{\mathrm{d}}, \widehat{p}_{\mathrm{d},h}\rangle_{\mathcal{I}_h^{\mathrm{d}}}$. To this end, we define $\mathbb{T} = -\langle \widehat{\boldsymbol{\sigma}}_{\mathrm{s},h}\mathbf{n}_{\mathrm{s}}, \widehat{\mathbf{u}}_{\mathrm{s},h}\rangle_{\mathcal{I}_h^{\mathrm{s}}} + \langle \widehat{\mathbf{u}}_{\mathrm{d},h}\cdot\mathbf{n}_{\mathrm{d}}, \widehat{p}_{\mathrm{d},h}\rangle_{\mathcal{I}_h^{\mathrm{d}}}$ and we write it in terms associated with the mismatch between $\mathcal{I}_h^{\mathrm{s}}$ and $\mathcal{I}_h^{\mathrm{d}}$. More precisely, we prove the following lemma.

Lemma 3. It holds that

$$
\begin{aligned}
\mathbb{T} =& \langle \left(\boldsymbol{E}_{\boldsymbol{\sigma}_{\mathrm{s},h}}\circ\boldsymbol{\psi}_{\mathrm{s}}^{-1} - \boldsymbol{\sigma}_{\mathrm{s},h}\right)\mathbf{n}_{\mathrm{s}}, \widehat{\mathbf{u}}_{\mathrm{s},h}\rangle_{\mathcal{I}_h^{\mathrm{s}}} + \langle \left(\mathbf{u}_{\mathrm{d},h} - \boldsymbol{E}_{\mathbf{u}_{\mathrm{d},h}}\circ\boldsymbol{\psi}_{\mathrm{d}}^{-1}\right)\cdot\mathbf{n}_{\mathrm{d}}, \widehat{p}_{\mathrm{d},h}\rangle_{\mathcal{I}_h^{\mathrm{d}}} - \langle \alpha_{\mathrm{s},h}\mathbf{n}_{\mathrm{s}}, \widehat{\mathbf{u}}_{\mathrm{s},h}\rangle_{\mathcal{I}_h^{\mathrm{s}}}\\
&+\langle (\widetilde{p}_{\mathrm{d},h}\circ\boldsymbol{\psi} - \widehat{p}_{\mathrm{d},h})\mathbf{n}_{\mathrm{d}}, \widehat{\mathbf{u}}_{\mathrm{s},h}\circ\boldsymbol{\psi}\rangle_{\mathcal{I}_h^{\mathrm{d}}} - \langle \mathbf{j}_{\mathrm{s}}^{\mathrm{nc}} + \mathbf{j}_{\mathrm{s}}^{\delta}, \widehat{\mathbf{u}}_{\mathrm{s},h}\rangle_{\mathcal{I}_h^{\mathrm{s}}} + \langle (\widetilde{\mathbf{u}}_{\mathrm{s},h}\circ\boldsymbol{\psi}^{-1} - \widehat{\mathbf{u}}_{\mathrm{s},h})\cdot\mathbf{n}_{\mathrm{s}}, \widehat{p}_{\mathrm{d},h}\circ\boldsymbol{\psi}^{-1}\rangle_{\mathcal{I}_h^{\mathrm{s}}}\\
&+ \langle j_{\mathrm{d}}^{\mathrm{nc}} + j_{\mathrm{d}}^{\delta}, \widehat{p}_{\mathrm{d},h}\rangle_{\mathcal{I}_h^{\mathrm{d}}} + \nu\langle \delta_e^{2/7}\tau\widehat{\mathbf{u}}_{\mathrm{s},h}, \widehat{\mathbf{u}}_{\mathrm{s},h}\rangle_{\mathcal{I}_h^{\mathrm{s}}} + \nu\langle \delta_e^{2/7}\tau(\mathbf{u}_{\mathrm{s},h} - \widehat{\mathbf{u}}_{\mathrm{s},h}), \widehat{\mathbf{u}}_{\mathrm{s},h}\rangle_{\mathcal{I}_h^{\mathrm{s}}} - \nu\langle \delta_e^{2/7}\tau\mathbf{u}_{\mathrm{s},h}, \widehat{\mathbf{u}}_{\mathrm{s},h}\rangle_{\mathcal{I}_h^{\mathrm{s}}}\\
&+ \langle \delta_e^{2/7}\tau\widehat{p}_{\mathrm{d},h}, \widehat{p}_{\mathrm{d},h}\rangle_{\mathcal{I}_h^{\mathrm{d}}} + \langle \delta_e^{2/7}\tau(p_{\mathrm{d},h} - \widehat{p}_{\mathrm{d},h}), \widehat{p}_{\mathrm{d},h}\rangle_{\mathcal{I}_h^{\mathrm{d}}} - \langle \delta_e^{2/7}\tau p_{\mathrm{d},h}, \widehat{p}_{\mathrm{d},h}\rangle_{\mathcal{I}_h^{\mathrm{d}}}\\
&+ \sum_{\ell=1}^{n-1}\omega_\ell^{-1}\langle (\widetilde{\mathbf{u}}_{\mathrm{s},h}\circ\boldsymbol{\psi}^{-1} - \widehat{\mathbf{u}}_{\mathrm{s},h})\cdot\boldsymbol{m}_\ell, \widehat{\mathbf{u}}_{\mathrm{s},h}\cdot\boldsymbol{m}_\ell\rangle_{\mathcal{I}_h^{\mathrm{s}}} + \sum_{\ell=1}^{n-1}\omega_\ell^{-1}\|\widehat{\mathbf{u}}_{\mathrm{s},h}\cdot\boldsymbol{m}_\ell\|^2_{\mathcal{I}_h^{\mathrm{s}}}.
\end{aligned}
$$

Before proving this result, we point out that in the particular case when $\mathcal{I}_h^{\mathrm{s}} = \mathcal{I}_h^{\mathrm{d}}$, we have coincident meshes free of hanging nodes, from which it is easily seen that $\mathbb{T} = 0$.

Proof. It follows straightforwardly from simple algebraic manipulations. Indeed, we first use the definition of the numerical fluxes (3.8) to rewrite the two last terms in (3.12c) and (3.12d). Next, using the transmission conditions (3.25), we obtain

$$
\begin{aligned}
\mathbb{T} =& -\langle \boldsymbol{\sigma}_{\mathrm{s},h}\mathbf{n}_{\mathrm{s}}, \widehat{\mathbf{u}}_{\mathrm{s},h}\rangle_{\mathcal{I}_h^{\mathrm{s}}} + \langle \mathbf{u}_{\mathrm{d},h}\cdot\mathbf{n}_{\mathrm{d}}, \widehat{p}_{\mathrm{d},h}\rangle_{\mathcal{I}_h^{\mathrm{d}}} + \langle \tau(p_{\mathrm{d},h} - \widehat{p}_{\mathrm{d},h}), \widehat{p}_{\mathrm{d},h}\rangle_{\mathcal{I}_h^{\mathrm{d}}} + \langle \tau\nu(\mathbf{u}_{\mathrm{s},h} - \widehat{\mathbf{u}}_{\mathrm{s},h}), \widehat{\mathbf{u}}_{\mathrm{s},h}\rangle_{\mathcal{I}_h^{\mathrm{s}}}\\
=& \langle \left(\boldsymbol{E}_{\boldsymbol{\sigma}_{\mathrm{s},h}}\circ\boldsymbol{\psi}_{\mathrm{s}}^{-1} - \boldsymbol{\sigma}_{\mathrm{s},h}\right)\mathbf{n}_{\mathrm{s}}, \widehat{\mathbf{u}}_{\mathrm{s},h}\rangle_{\mathcal{I}_h^{\mathrm{s}}} + \langle \left(\mathbf{u}_{\mathrm{d},h} - \boldsymbol{E}_{\mathbf{u}_{\mathrm{d},h}}\circ\boldsymbol{\psi}_{\mathrm{d}}^{-1}\right)\cdot\mathbf{n}_{\mathrm{d}}, \widehat{p}_{\mathrm{d},h}\rangle_{\mathcal{I}_h^{\mathrm{d}}} - \langle \alpha_{\mathrm{s},h}\mathbf{n}_{\mathrm{s}}, \widehat{\mathbf{u}}_{\mathrm{s},h}\rangle_{\mathcal{I}_h^{\mathrm{s}}}\\
&+ \langle j_{\mathrm{d}}^{\mathrm{nc}} + j_{\mathrm{d}}^{\delta}, \widehat{p}_{\mathrm{d},h}\rangle_{\mathcal{I}_h^{\mathrm{d}}} + \langle (\widetilde{p}_{\mathrm{d},h}\circ\boldsymbol{\psi} - \widehat{p}_{\mathrm{d},h})\mathbf{n}_{\mathrm{d}}, \widehat{\mathbf{u}}_{\mathrm{s},h}\circ\boldsymbol{\psi}\rangle_{\mathcal{I}_h^{\mathrm{d}}} - \langle \mathbf{j}_{\mathrm{s}}^{\mathrm{nc}} + \mathbf{j}_{\mathrm{s}}^{\delta}, \widehat{\mathbf{u}}_{\mathrm{s},h}\rangle_{\mathcal{I}_h^{\mathrm{s}}}\\
&+ \langle (\widetilde{\mathbf{u}}_{\mathrm{s},h}\circ\boldsymbol{\psi}^{-1} - \widehat{\mathbf{u}}_{\mathrm{s},h})\cdot\mathbf{n}_{\mathrm{s}}, \widehat{p}_{\mathrm{d},h}\circ\boldsymbol{\psi}^{-1}\rangle_{\mathcal{I}_h^{\mathrm{s}}} + \sum_{\ell=1}^{n-1}\omega_\ell^{-1}\langle (\widetilde{\mathbf{u}}_{\mathrm{s},h}\circ\boldsymbol{\psi}^{-1}\cdot\boldsymbol{m}_\ell)\boldsymbol{m}_\ell, \widehat{\mathbf{u}}_{\mathrm{s},h}\rangle_{\mathcal{I}_h^{\mathrm{s}}}.
\end{aligned}
$$

Moreover, for all $\ell \in \{1, ..., n-1\}$, we have that

$$
\langle (\widetilde{\mathbf{u}}_{\mathrm{s},h}\circ\boldsymbol{\psi}^{-1}\cdot\boldsymbol{m}_\ell)\boldsymbol{m}_\ell, \widehat{\mathbf{u}}_{\mathrm{s},h}\rangle_{\mathcal{I}_h^{\mathrm{s}}} = \langle (\widetilde{\mathbf{u}}_{\mathrm{s},h}\circ\boldsymbol{\psi}^{-1} - \widehat{\mathbf{u}}_{\mathrm{s},h})\cdot\boldsymbol{m}_\ell, \widehat{\mathbf{u}}_{\mathrm{s},h}\cdot\boldsymbol{m}_\ell\rangle_{\mathcal{I}_h^{\mathrm{s}}} + \|\widehat{\mathbf{u}}_{\mathrm{s},h}\cdot\boldsymbol{m}_\ell\|^2_{\mathcal{I}_h^{\mathrm{s}}}.
$$

Finally, in order to obtain the terms $\nu\|\delta_e^{1/7}\tau^{1/2}\widehat{\mathbf{u}}_{\mathrm{s},h}\|_{\mathcal{I}_h^{\mathrm{s}}}$ and $\|\delta_e^{1/7}\tau^{1/2}\widehat{p}_{\mathrm{d},h}\|_{\mathcal{I}_h^{\mathrm{d}}}$ on the left-hand side of the stability estimate, we add

$$
\begin{aligned}
0 =& \nu\langle \delta_e^{2/7}\tau\widehat{\mathbf{u}}_{\mathrm{s},h}, \widehat{\mathbf{u}}_{\mathrm{s},h}\rangle_{\mathcal{I}_h^{\mathrm{s}}} + \nu\langle \delta_e^{2/7}\tau(\mathbf{u}_{\mathrm{s},h} - \widehat{\mathbf{u}}_{\mathrm{s},h}), \widehat{\mathbf{u}}_{\mathrm{s},h}\rangle_{\mathcal{I}_h^{\mathrm{s}}} - \nu\langle \delta_e^{2/7}\tau\mathbf{u}_{\mathrm{s},h}, \widehat{\mathbf{u}}_{\mathrm{s},h}\rangle_{\mathcal{I}_h^{\mathrm{s}}}\\
&+ \langle \delta_e^{2/7}\tau\widehat{p}_{\mathrm{d},h}, \widehat{p}_{\mathrm{d},h}\rangle_{\mathcal{I}_h^{\mathrm{d}}} + \langle \delta_e^{2/7}\tau(p_{\mathrm{d},h} - \widehat{p}_{\mathrm{d},h}), \widehat{p}_{\mathrm{d},h}\rangle_{\mathcal{I}_h^{\mathrm{d}}} - \langle \delta_e^{2/7}\tau p_{\mathrm{d},h}, \widehat{p}_{\mathrm{d},h}\rangle_{\mathcal{I}_h^{\mathrm{d}}},
\end{aligned}
$$

which finishes the proof. ∎

In what follows, we define

$$\mathcal{Q}\big(\mathrm{L}_{\mathrm{s},h},\mathbf{u}_{\star,h},\widehat{\mathbf{u}}_{\mathrm{s},h},p_{\mathrm{d},h},\widehat{p}_{\mathrm{d},h}\big) := \Big\{\nu\|\mathrm{L}_{\mathrm{s},h}\|^2_{\Omega^{\mathrm{s}}_h}+\|\kappa^{-1}\mathbf{u}_{\mathrm{d},h}\|^2_{\Omega^{\mathrm{d}}_h}+\nu\|\tau^{1/2}(\mathbf{u}_{\mathrm{s},h}-\widehat{\mathbf{u}}_{\mathrm{s},h})\|^2_{\partial\Omega^{\mathrm{s}}_h}$$
$$+\|\delta_e^{1/7}\tau^{1/2}\widehat{p}_{\mathrm{d},h}\|^2_{\mathcal{I}^{\mathrm{d}}_h}+\|\tau^{1/2}(p_{\mathrm{d},h}-\widehat{p}_{\mathrm{d},h})\|^2_{\partial\Omega^{\mathrm{d}}_h}+\nu\|\delta_e^{1/7}\tau^{1/2}\widehat{\mathbf{u}}_{\mathrm{s},h}\|^2_{\mathcal{I}^{\mathrm{s}}_h}+\sum_{\ell=1}^{n-1}\omega_\ell^{-1}\|\widehat{\mathbf{u}}_{\mathrm{s},h}\cdot\boldsymbol{m}_\ell\|^2_{\mathcal{I}^{\mathrm{s}}_h}\Big\}^{1/2}, \tag{3.26}$$

and provide an upper bound for this energy term $\mathcal{Q}(\mathrm{L}_{\mathrm{s},h},\mathbf{u}_{\star,h},\widehat{\mathbf{u}}_{\mathrm{s},h},p_{\mathrm{d},h},\widehat{p}_{\mathrm{d},h})$. This bound depends, in addition to the sources, on the norms of the approximations of the velocity $\mathbf{u}_{\mathrm{s},h}$, pressures $p_{\mathrm{s},h}$, and $p_{\mathrm{d},h}$.

Lemma 4. Assume that $\mathrm{f}_\mathrm{d}=0$ and $\mathbf{f}_\mathrm{s}=\mathbf{0}$. If assumptions **(A.1)** – **(A.3)** hold and $\star\in\{\mathrm{s},\mathrm{d}\}$, then

$$\frac{5}{16}\mathcal{Q}(\mathrm{L}_{\mathrm{s},h},\mathbf{u}_{\star,h},\widehat{\mathbf{u}}_{\mathrm{s},h},p_{\mathrm{d},h},\widehat{p}_{\mathrm{d},h})^2 \le \widetilde{C}_1\big(\|\mathbf{u}_{\mathrm{s},h}\|^2_{\Omega^{\mathrm{s}}_h}+\|p_{\mathrm{d},h}\|^2_{\Omega^{\mathrm{d}}_h}\big)+\widetilde{C}_2\|p_{\mathrm{s},h}\|^2_{\Omega^{\mathrm{s}}_h}+4\|\kappa\mathbf{J}_\mathrm{d}\|^2_{\Omega^{\mathrm{d}}_h}+4\nu\|\mathrm{J}_\mathrm{s}\|^2_{\Omega^{\mathrm{s}}_h}$$
$$+\|h_e^{(\beta-1)/2}(j^{\mathrm{nc}}_\mathrm{d}+j^{\delta}_\mathrm{d})\|^2_{\mathcal{I}^{\mathrm{d}}_h}+\|h_e^{(\beta-1)/2}(\mathbf{j}^{\mathrm{nc}}_\mathrm{s}+\mathbf{j}^{\delta}_\mathrm{s})\|^2_{\mathcal{I}^{\mathrm{s}}_h}, \tag{3.27}$$

where β is a non-negative parameter whose range will be chosen later.

Proof. Taking $\mathrm{G}_{\mathrm{s},h}=\nu\mathrm{L}_{\mathrm{s},h}$, $\mathbf{v}_{\mathrm{s},h}=\mathbf{u}_{\mathrm{s},h}$, $q_{\mathrm{s},h}=p_{\mathrm{s},h}$, and $\boldsymbol{\mu}_{\mathrm{s},h}=\widehat{\mathbf{u}}_{\mathrm{s},h}$ in (3.24a), (3.7b), (3.7c), and (3.7d), along with (3.8b), we easily obtain

$$\nu\|\mathrm{L}_{\mathrm{s},h}\|^2_{\Omega^{\mathrm{s}}_h}+\nu\|\tau^{1/2}(\mathbf{u}_{\mathrm{s},h}-\widehat{\mathbf{u}}_{\mathrm{s},h})\|^2_{\partial\Omega^{\mathrm{s}}_h}-\langle\widehat{\boldsymbol{\sigma}}_{\mathrm{s},h}\mathbf{n}_\mathrm{s},\widehat{\mathbf{u}}_{\mathrm{s},h}\rangle_{\mathcal{I}^{\mathrm{s}}_h} = (\nu\mathrm{J}_\mathrm{s},\mathrm{L}_{\mathrm{s},h})_{\Omega^{\mathrm{s}}_h}. \tag{3.28}$$

Similarly, taking $\mathbf{v}_{\mathrm{d},h}=\mathbf{u}_{\mathrm{d},h}$, $q_{\mathrm{d},h}=p_{\mathrm{d},h}$, $\mu_{\mathrm{d},h}=\widehat{p}_{\mathrm{d},h}$ in (3.24b), (3.7h), and (3.7i), along with (3.8a), we find that

$$(\kappa^{-1}\mathbf{u}_{\mathrm{d},h},\mathbf{u}_{\mathrm{d},h})_{\Omega^{\mathrm{d}}_h}+\|\tau^{1/2}(p_{\mathrm{d},h}-\widehat{p}_{\mathrm{d},h})\|^2_{\partial\Omega^{\mathrm{d}}_h}+\langle\widehat{\mathbf{u}}_{\mathrm{d},h}\cdot\mathbf{n}_\mathrm{d},\widehat{p}_{\mathrm{d},h}\rangle_{\mathcal{I}^{\mathrm{d}}_h}=(\mathbf{J}_\mathrm{d},\mathbf{u}_{\mathrm{d},h})_{\Omega^{\mathrm{d}}_h}. \tag{3.29}$$

Next, adding (3.29) and (3.28), it follows that

$$\begin{aligned}&\nu\|\mathrm{L}_{\mathrm{s},h}\|^2_{\Omega^{\mathrm{s}}_h}+\nu\|\tau^{1/2}(\mathbf{u}_{\mathrm{s},h}-\widehat{\mathbf{u}}_{\mathrm{s},h})\|^2_{\partial\Omega^{\mathrm{s}}_h}+(\kappa^{-1}\mathbf{u}_{\mathrm{d},h},\mathbf{u}_{\mathrm{d},h})_{\Omega^{\mathrm{d}}_h}+\|\tau^{1/2}(p_{\mathrm{d},h}-\widehat{p}_{\mathrm{d},h})\|^2_{\partial\Omega^{\mathrm{d}}_h}+\mathbb{T}\\ &\quad = (\nu\mathrm{J}_\mathrm{s},\mathrm{L}_{\mathrm{s},h})_{\Omega^{\mathrm{s}}_h}+(\mathbf{J}_\mathrm{d},\mathbf{u}_{\mathrm{d},h})_{\Omega^{\mathrm{d}}_h}.\end{aligned}$$

In this way, by combining this identity with the expression for $\mathbb{T}$ given in Lemma 3, we obtain

$$\mathcal{Q}(\mathrm{L}_{\mathrm{s},h},\mathbf{u}_{\star,h},\widehat{\mathbf{u}}_{\mathrm{s},h},p_{\mathrm{d},h},\widehat{p}_{\mathrm{d},h})^2=\sum_{i=1}^{12}I_i+(\nu\mathrm{J}_\mathrm{s},\mathrm{L}_{\mathrm{s},h})_{\Omega^{\mathrm{s}}_h}+(\mathbf{J}_\mathrm{d},\mathbf{u}_{\mathrm{d},h})_{\Omega^{\mathrm{d}}_h}, \tag{3.30}$$

where $\mathcal{Q}$ is the energy term defined in (3.26), and

$$\begin{aligned}
I_1 &:= -\langle(\widetilde{p}_{\mathrm{d},h}\circ\boldsymbol{\psi}-\widehat{p}_{\mathrm{d},h})\mathbf{n}_\mathrm{d},\widehat{\mathbf{u}}_{\mathrm{s},h}\circ\boldsymbol{\psi}\rangle_{\mathcal{I}^{\mathrm{d}}_h}, & I_2 &:= -\langle(\widetilde{\mathbf{u}}_{\mathrm{s},h}\circ\boldsymbol{\psi}^{-1}-\widehat{\mathbf{u}}_{\mathrm{s},h})\cdot\mathbf{n}_\mathrm{s},\widehat{p}_{\mathrm{d},h}\circ\boldsymbol{\psi}^{-1}\rangle_{\mathcal{I}^{\mathrm{s}}_h},\\
I_3 &:= -\langle\big(\boldsymbol{E}_{\boldsymbol{\sigma}_{\mathrm{s},h}}\circ\boldsymbol{\psi}_\mathrm{s}^{-1}-\boldsymbol{\sigma}_{\mathrm{s},h}\big)\,\mathbf{n}_\mathrm{s},\widehat{\mathbf{u}}_{\mathrm{s},h}\rangle_{\mathcal{I}^{\mathrm{s}}_h}, & I_4 &:= -\langle\big(\mathbf{u}_{\mathrm{d},h}-\boldsymbol{E}_{\mathbf{u}_{\mathrm{d},h}}\circ\boldsymbol{\psi}_\mathrm{d}^{-1}\big)\cdot\mathbf{n}_\mathrm{d},\widehat{p}_{\mathrm{d},h}\rangle_{\mathcal{I}^{\mathrm{d}}_h},\\
I_5 &:= \langle\mathbf{j}^{\mathrm{nc}}_\mathrm{s}+\mathbf{j}^{\delta}_\mathrm{s},\widehat{\mathbf{u}}_{\mathrm{s},h}\rangle_{\mathcal{I}^{\mathrm{s}}_h}, & I_6 &:= -\langle j^{\mathrm{nc}}_\mathrm{d}+j^{\delta}_\mathrm{d},\widehat{p}_{\mathrm{d},h}\rangle_{\mathcal{I}^{\mathrm{d}}_h},\\
I_7 &:= \langle\alpha_{\mathrm{s},h}\mathbf{n}_\mathrm{s},\widehat{\mathbf{u}}_{\mathrm{s},h}\rangle_{\mathcal{I}^{\mathrm{s}}_h}, & I_8 &:= -\nu\langle\delta_e^{2/7}\tau(\mathbf{u}_{\mathrm{s},h}-\widehat{\mathbf{u}}_{\mathrm{s},h}),\widehat{\mathbf{u}}_{\mathrm{s},h}\rangle_{\mathcal{I}^{\mathrm{s}}_h},
\end{aligned}$$

$$I_9 := -\langle \delta_e^{2/7}\tau(p_{\mathrm{d},h} - \widehat{p}_{\mathrm{d},h}), \widehat{p}_{\mathrm{d},h}\rangle_{\mathcal{I}_h^{\mathrm{d}}}, \qquad I_{10} := \nu\langle \delta_e^{2/7}\tau\mathbf{u}_{\mathrm{s},h}, \widehat{\mathbf{u}}_{\mathrm{s},h}\rangle_{\mathcal{I}_h^{\mathrm{s}}},$$

$$I_{11} := \langle \delta_e^{2/7}\tau p_{\mathrm{d},h}, \widehat{p}_{\mathrm{d},h}\rangle_{\mathcal{I}_h^{\mathrm{d}}} \qquad I_{12} := \sum_{\ell=1}^{n-1}\omega_\ell^{-1}\langle(\widehat{\mathbf{u}}_{\mathrm{s},h} - \widetilde{\mathbf{u}}_{\mathrm{s},h}\circ\boldsymbol{\psi}^{-1})\cdot\boldsymbol{m}_\ell, \widehat{\mathbf{u}}_{\mathrm{s},h}\cdot\boldsymbol{m}_\ell\rangle_{\mathcal{I}_h^{\mathrm{s}}}.$$

Now, recalling the properties of κ^{-1}, τ and ν, we apply the Cauchy–Schwarz and Young inequalities to bound each of these terms as follows. First,

$$\begin{aligned}
I_1 &\leq 4\tau^{-1}\nu^{-1}C_{\delta_{\mathrm{d}},h}\|\delta_e^{-5/14}\kappa^{-1}\mathbf{u}_{\mathrm{d},h}\|^2_{\Omega_h^{\mathrm{d}}} + \frac{\nu}{16}\|\delta_e^{1/7}\tau^{1/2}\widehat{\mathbf{u}}_{\mathrm{s},h}\|^2_{\mathcal{I}_h^{\mathrm{s}}},\\
I_2 &\leq 4\tau^{-1}C_{\delta_{\mathrm{s}},h}\|\delta_e^{-5/14}\mathrm{L}_{\mathrm{s},h}\|^2_{\Omega_h^{\mathrm{s}}} + \frac{1}{16}\|\delta_e^{1/7}\tau^{1/2}\widehat{p}_{\mathrm{d},h}\|^2_{\mathcal{I}_h^{\mathrm{d}}}, \quad \text{and}\\
I_{12} &\leq 8\sum_{\ell=1}^{n-1}\omega_\ell^{-2}\,\tau^{-1}\nu^{-1}C_{\delta_{\mathrm{s}},h}\|\delta_e^{-5/14}\mathrm{L}_{\mathrm{s},h}\|^2_{\Omega_h^{\mathrm{s}}} + \frac{\nu}{16}\|\delta_e^{1/7}\tau^{1/2}\widehat{\mathbf{u}}_{\mathrm{s},h}\|^2_{\mathcal{I}_h^{\mathrm{s}}},
\end{aligned}$$

where we have used (3.23b) for I_1, and (3.23a) for I_2 and I_{12}. For I_3 and I_4, it follows from the estimate (3.21), that there exist positive constants $\widehat{C}_{\mathrm{s}}^e$ and $\widehat{C}_e^{\mathrm{d}}$, such that

$$\begin{aligned}
I_3 &\leq \frac{8}{\nu}\max_{e\in\mathcal{I}_h^{\mathrm{s}}}\left(\widehat{C}_e^{\mathrm{s}}\delta_e^{12/7}h_e^{-3}(C_e^{\mathtt{ext}})^2\tau^{-1}\right)\left(\nu^2\|\mathrm{L}_{\mathrm{s},h}\|^2_{\Omega_h^{\mathrm{s}}} + \|p_{\mathrm{s},h}\|^2_{\Omega_h^{\mathrm{s}}}\right) + \frac{\nu}{16}\|\delta_e^{1/7}\tau^{1/2}\widehat{\mathbf{u}}_{\mathrm{s},h}\|^2_{\mathcal{I}_h^{\mathrm{s}}}, \quad \text{and}\\
I_4 &\leq 4\max_{e\in\mathcal{I}_h^{\mathrm{d}}}\left(\widehat{C}_e^{\mathrm{d}}\delta_e^{12/7}h_e^{-3}(C_e^{\mathtt{ext}})^2\tau^{-1}\right)\|\kappa^{-1}\mathbf{u}_{\mathrm{d},h}\|^2_{\Omega_h^{\mathrm{d}}} + \frac{1}{16}\|\delta_e^{1/7}\tau^{1/2}\widehat{p}_{\mathrm{d},h}\|^2_{\mathcal{I}_h^{\mathrm{d}}}.
\end{aligned}$$

For I_5 and I_6, we have

$$\begin{aligned}
I_5 &\leq \|h_e^{(\beta-1)/2}(\mathbf{j}_{\mathrm{s}}^{\mathrm{nc}} + \mathbf{j}_{\mathrm{s}}^{\delta})\|^2_{\mathcal{I}_h^{\mathrm{s}}} + \frac{1}{2}\|h_e^{(1-\beta)/2}(\widehat{\mathbf{u}}_{\mathrm{s},h} - \mathbf{u}_{\mathrm{s},h})\|^2_{\mathcal{I}_h^{\mathrm{s}}} + \max_{e\in\mathcal{I}_h^{\mathrm{s}}}\left(\frac{(C_e^{\mathrm{tr}})^{-2}h_e^{-\beta}}{2}\right)\|\mathbf{u}_{\mathrm{s},h}\|^2_{\Omega_h^{\mathrm{s}}}, \quad \text{and}\\
I_6 &\leq \|h_e^{(\beta-1)/2}(j_{\mathrm{d}}^{\mathrm{nc}} + j_{\mathrm{d}}^{\delta})\|^2_{\mathcal{I}_h^{\mathrm{d}}} + \frac{1}{2}\|h_e^{(1-\beta)/2}(\widehat{p}_{\mathrm{d},h} - p_{\mathrm{d},h})\|^2_{\mathcal{I}_h^{\mathrm{d}}} + \max_{e\in\mathcal{I}_h^{\mathrm{d}}}\left(\frac{(C_e^{\mathrm{tr}})^{-2}h_e^{-\beta}}{2}\right)\|p_{\mathrm{d},h}\|^2_{\Omega_h^{\mathrm{d}}}.
\end{aligned}$$

Next, noticing that $I_7 \leq \|\alpha_{\mathrm{s},h}\|_{\mathcal{I}_h^{\mathrm{s}}}\|\widehat{\mathbf{u}}_{\mathrm{s},h}\|_{\mathcal{I}_h^{\mathrm{s}}}$, and $\|\alpha_{\mathrm{s},h}\|_{\mathcal{I}_h^{\mathrm{s}}} \leq C_\alpha\|p_{\mathrm{s},h}\|_{\Omega_h^{\mathrm{s}}}$, where

$$C_\alpha := |\mathcal{I}_h^{\mathrm{s}}|^{1/2}\frac{|\Omega_{\mathrm{s}}\setminus\Omega_h^{\mathrm{s}}|^{1/2}}{|\Omega_{\mathrm{s}}|}\max_{e\in\mathcal{I}_h^{\mathrm{s}}}\left(\delta_e^{1/2}h_e^{-1/2}C_e^{\mathtt{ext}}\right),$$

it follows that

$$I_7 \leq 4\frac{C_\alpha^2}{\nu}\|\delta_e^{-1/7}p_{\mathrm{s},h}\|^2_{\Omega_h^{\mathrm{s}}} + \frac{\nu}{16}\|\delta_e^{1/7}\tau^{1/2}\widehat{\mathbf{u}}_{\mathrm{s},h}\|^2_{\mathcal{I}_h^{\mathrm{s}}}.$$

For I_8 and I_9, we easily obtain

$$\begin{aligned}
I_8 &\leq 4\nu\|\delta_e^{1/7}\tau^{1/2}(\mathbf{u}_{\mathrm{s},h} - \widehat{\mathbf{u}}_{\mathrm{s},h})\|^2_{\mathcal{I}_h^{\mathrm{s}}} + \frac{\nu}{16}\|\delta_e^{1/7}\tau^{1/2}\widehat{\mathbf{u}}_{\mathrm{s},h}\|^2_{\mathcal{I}_h^{\mathrm{s}}}, \quad \text{and}\\
I_9 &\leq 4\|\delta_e^{1/7}\tau^{1/2}(p_{\mathrm{d},h} - \widehat{p}_{\mathrm{d},h})\|^2_{\mathcal{I}_h^{\mathrm{d}}} + \frac{1}{16}\|\delta_e^{1/7}\tau^{1/2}\widehat{p}_{\mathrm{d},h}\|^2_{\mathcal{I}_h^{\mathrm{d}}}.
\end{aligned}$$

In turn, using the discrete trace inequality (3.22), we find that

$$\begin{aligned} I_{10} &\leq 4\nu \max_{e\in\mathcal{I}_h^{\mathrm{s}}} \left(\left(C_e^{\mathrm{tr}}\right)^2 \delta_e^{2/7} h_e^{-1}\tau \right) \|\mathbf{u}_{\mathrm{s},h}\|^2_{\Omega_h^{\mathrm{s}}} + \frac{\nu}{16}\|\delta_e^{1/7}\tau^{1/2}\widehat{\mathbf{u}}_{\mathrm{s},h}\|^2_{\mathcal{I}_h^{\mathrm{s}}}, \\ I_{11} &\leq 4 \max_{e\in\mathcal{I}_h^{\mathrm{d}}} \left(\left(C_e^{\mathrm{tr}}\right)^2 \delta_e^{2/7} h_e^{-1}\tau \right) \|p_{\mathrm{d},h}\|^2_{\Omega_h^{\mathrm{d}}} + \frac{1}{16}\|\delta_e^{1/7}\tau^{1/2}\widehat{p}_{\mathrm{d},h}\|^2_{\mathcal{I}_h^{\mathrm{d}}}. \end{aligned}$$

Finally, rearranging terms and bearing in mind the Assumption **(A.3)**, we obtain (3.27). We omit further details. ■

Our next goal is to provide an estimate for the L^2-norm of $\mathbf{u}_{\mathrm{s},h}$, $p_{\mathrm{s},h}$, and $p_{\mathrm{d},h}$. To bound $\|\mathbf{u}_{\mathrm{s},h}\|_{\Omega_h^{\mathrm{s}}}$ and $\|p_{\mathrm{d},h}\|_{\Omega_h^{\mathrm{d}}}$ we employ a duality argument, whereas for $\|p_{\mathrm{s},h}\|_{\Omega_h^{\mathrm{s}}}$ we use an inf-sup condition.

3.4.2 A duality argument

In order to estimate $\|\mathbf{u}_{\mathrm{s},h}\|_{\Omega_h^{\mathrm{s}}}+\|p_{\mathrm{d},h}\|_{\Omega_h^{\mathrm{d}}}$, we now proceed as in [71,87,101] and incorporate a suitable auxiliary problem. More precisely, in what follows we consider the continuous problem (3.1a)-(3.1b)-(3.1c) with sources given by $\mathbf{f}_{\mathrm{s}} := \boldsymbol{\Theta}_{\mathrm{s}} \in \mathbf{L}^2(\Omega_{\mathrm{s}})$ and $\mathrm{f}_{\mathrm{d}} := \Theta_{\mathrm{d}} \in L^2(\Omega_{\mathrm{d}})$, that is:

$$\Phi_{\mathrm{s}} = \nabla\boldsymbol{\phi}_{\mathrm{s}}, \quad \nabla\cdot(\nu\Phi_{\mathrm{s}} - \widetilde{\varphi}_{\mathrm{s}}\mathrm{I}) = \boldsymbol{\Theta}_{\mathrm{s}}, \quad \nabla\cdot\boldsymbol{\phi}_{\mathrm{s}} = 0 \quad \text{in} \quad \Omega_{\mathrm{s}}, \quad \boldsymbol{\phi}_{\mathrm{s}} = \mathbf{0} \quad \text{on} \quad \Gamma_{\mathrm{s}}, \quad \int_{\Omega_{\mathrm{s}}} \widetilde{\varphi}_{\mathrm{s}} = 0, \tag{3.31a}$$

$$\nabla\cdot\boldsymbol{\phi}_{\mathrm{d}} = \Theta_{\mathrm{d}}, \quad \boldsymbol{\phi}_{\mathrm{d}} + \kappa\nabla\varphi_{\mathrm{d}} = \mathbf{0} \quad \text{in} \quad \Omega_{\mathrm{d}}, \qquad \boldsymbol{\phi}_{\mathrm{d}}\cdot\mathbf{n}_{\mathrm{d}} = 0 \quad \text{on} \quad \Gamma_{\mathrm{d}}, \tag{3.31b}$$

$$\boldsymbol{\phi}_{\mathrm{s}}\cdot\mathbf{n}_{\mathrm{s}} + \boldsymbol{\phi}_{\mathrm{d}}\cdot\mathbf{n}_{\mathrm{d}} = 0, \quad \text{and} \quad (\nu\Phi_{\mathrm{s}} - \widetilde{\varphi}_{\mathrm{s}}\mathrm{I})\mathbf{n}_{\mathrm{s}} + \sum_{\ell=1}^{n-1}\omega_\ell^{-1}(\boldsymbol{\phi}_{\mathrm{s}}\cdot\boldsymbol{m}_\ell)\boldsymbol{m}_\ell = \varphi_{\mathrm{d}}\mathbf{n}_{\mathrm{d}} \quad \text{on} \quad \mathcal{I}. \tag{3.31c}$$

In addition, we proceed to carry out the same decomposition performed for the pressure of the continuous problem, that is $\widetilde{\varphi}_{\mathrm{s}} = \widetilde{\alpha}_{\mathrm{s}} + \varphi_{\mathrm{s}}$, where $\varphi_{\mathrm{s}} \in L_0^2(\Omega_h^{\mathrm{s}})$, and $\widetilde{\alpha}_{\mathrm{s}} = \dfrac{-1}{|\Omega_{\mathrm{s}}|}\displaystyle\int_{\Omega_{\mathrm{s}}\setminus\Omega_h^{\mathrm{s}}} \varphi_{\mathrm{s}}$, is the constant similar to (3.2). Furthermore, suppose that elliptic regularity holds, that is,

$$\nu\|\Phi_{\mathrm{s}}\|_{\mathrm{H}^1(\Omega_{\mathrm{s}})} + \nu\|\boldsymbol{\phi}_{\mathrm{s}}\|_{\mathbf{H}^2(\Omega_{\mathrm{s}})} + \|\varphi_{\mathrm{s}}\|_{H^1(\Omega_{\mathrm{s}})} + \|\boldsymbol{\phi}_{\mathrm{d}}\|_{\mathbf{H}^1(\Omega_{\mathrm{d}})} + \|\varphi_{\mathrm{d}}\|_{H^2(\Omega_{\mathrm{d}})} \leq C_{\mathbf{r}}\Big\{\|\Theta_{\mathrm{s}}\|_{\Omega_{\mathrm{s}}} + \|\Theta_{\mathrm{d}}\|_{\Omega_{\mathrm{d}}}\Big\}. \tag{3.32}$$

Lemma 5. Suppose Assumptions **(A)** and (3.32) hold true. There exist $h_0 \in (0,1)$ and a positive constant C such that, for all $h < h_0$,

$$\begin{aligned} \|\mathbf{u}_{\mathrm{s},h}\|^2_{\Omega_h^{\mathrm{s}}} + \|p_{\mathrm{d},h}\|^2_{\Omega_h^{\mathrm{d}}} \leq C\Big\{ & C^{\mathcal{S}}_{\delta,h}\mathcal{Q}(\mathrm{L}_{\mathrm{s},h}, \mathbf{u}_{\star,h}, \widehat{\mathbf{u}}_{\mathrm{s},h}, p_{\mathrm{d},h}, \widehat{p}_{\mathrm{d},h})^2 + \|\mathbf{j}_{\mathrm{s}}^{\mathrm{nc}} + \mathbf{j}_{\mathrm{s}}^{\delta}\|^2_{\mathcal{I}_h^{\mathrm{s}}} + \|j_{\mathrm{d}}^{\mathrm{nc}} + j_{\mathrm{d}}^{\delta}\|^2_{\mathcal{I}_h^{\mathrm{d}}} \\ & + (C^{p}_{\delta,h})^2\|p_{\mathrm{s},h}\|^2_{\Omega_h^{\mathrm{s}}} + h^{2\min\{1,k\}}\|\mathbf{J}_{\mathrm{d}}\|^2_{\Omega_h^{\mathrm{d}}} + h^{2\min\{1,k\}}\|\mathrm{J}_{\mathrm{s}}\|^2_{\Omega_h^{\mathrm{s}}}\Big\}, \end{aligned} \tag{3.33}$$

where $C^{\mathcal{S}}_{\delta,h}$ and $C^{p}_{\delta,h}$ are constants defined in **(A.4)**.

Proof. We proceeded as in [71, Lemma 4.6]. First, from (3.31a) and (3.31b), we have

$$
\begin{aligned}
&(\mathbf{u}_{\mathrm{s},h}, \Theta_{\mathrm{s}})_{\Omega_h^{\mathrm{s}}} + (p_{\mathrm{d},h}, \Theta_{\mathrm{d}})_{\Omega_h^{\mathrm{d}}} \\
&\quad = (\mathbf{u}_{\mathrm{s},h}, \nabla\cdot(\nu\Phi_{\mathrm{s}} - \widetilde{\varphi}_{\mathrm{s}}\mathrm{I}))_{\Omega_h^{\mathrm{s}}} + (p_{\mathrm{d},h}, \nabla\cdot\boldsymbol{\phi}_{\mathrm{d}})_{\Omega_h^{\mathrm{d}}} + (\nu\mathrm{L}_{\mathrm{s},h}, \Phi_{\mathrm{s}} - \nabla\boldsymbol{\phi}_{\mathrm{s}})_{\Omega_h^{\mathrm{s}}} - (\mathbf{u}_{\mathrm{d},h}, \kappa^{-1}\boldsymbol{\phi}_{\mathrm{d}} + \nabla\varphi_{\mathrm{d}})_{\Omega_h^{\mathrm{d}}}.
\end{aligned}
$$

Now, using the properties of the HDG projectors, L^2-projectors, and performing some algebraic manipulations along with the transmission conditions given by (3.25) and (3.31c), we deduce that

$$
\begin{aligned}
&(\mathbf{u}_{\mathrm{s},h}, \Theta_{\mathrm{s}})_{\Omega_h^{\mathrm{s}}} + (p_{\mathrm{d},h}, \Theta_{\mathrm{d}})_{\Omega_h^{\mathrm{d}}} \\
&= -(\nu\mathrm{L}_{\mathrm{s},h}, \Pi_{\mathrm{G}}^{\mathrm{s}}\Phi_{\mathrm{s}} - \Phi_{\mathrm{s}})_{\Omega_h^{\mathrm{s}}} - (\mathrm{J}_{\mathrm{s}}, \nu\Pi_{\mathrm{G}}^{\mathrm{s}}\Phi_{\mathrm{s}})_{\Omega_h^{\mathrm{s}}} + (\mathbf{J}_{\mathrm{d}}, \Pi_{\mathbf{V}}^{\mathrm{d}}\boldsymbol{\phi}_{\mathrm{d}} - \boldsymbol{\phi}_{\mathrm{d}})_{\Omega_h^{\mathrm{d}}} - (\mathbf{J}_{\mathrm{d}}, \kappa\nabla\varphi_{\mathrm{d}})_{\Omega_h^{\mathrm{d}}} + \langle\boldsymbol{\phi}_{\mathrm{d}}\cdot\mathbf{n}_{\mathrm{d}}, \widehat{p}_{\mathrm{d},h}\rangle_{\mathcal{I}_h^{\mathrm{d}}} \\
&\quad + (\kappa^{-1}\mathbf{u}_{\mathrm{d},h}, \Pi_{\mathbf{V}}^{\mathrm{d}}\boldsymbol{\phi}_{\mathrm{d}} - \boldsymbol{\phi}_{\mathrm{d}})_{\Omega_h^{\mathrm{d}}} + \langle\widehat{\mathbf{u}}_{\mathrm{s},h}, (\nu\Phi_{\mathrm{s}} - \mathrm{I}\widetilde{\varphi}_{\mathrm{s}})\mathbf{n}_{\mathrm{s}}\rangle_{\mathcal{I}_h^{\mathrm{s}}} - \langle(\nu\widehat{\mathrm{L}}_{\mathrm{s},h} - \mathrm{I}\widehat{p}_{\mathrm{s},h})\mathbf{n}_{\mathrm{s}}, \boldsymbol{\phi}_{\mathrm{s}}\rangle_{\partial\Omega_h^{\mathrm{s}}} - \langle\widehat{\mathbf{u}}_{\mathrm{d},h}\cdot\mathbf{n}_{\mathrm{d}}, \varphi_{\mathrm{d}}\rangle_{\partial\Omega_h^{\mathrm{d}}} \\
&= \mathbb{T}_1 + \mathbb{T}_2,
\end{aligned}
$$

where

$$
\begin{aligned}
\mathbb{T}_1 = &-(\nu\mathrm{L}_{\mathrm{s},h}, \Pi_{\mathrm{G}}^{\mathrm{s}}\Phi_{\mathrm{s}} - \Phi_{\mathrm{s}})_{\Omega_h^{\mathrm{s}}} - (\mathrm{J}_{\mathrm{s}}, \nu(\Pi_{\mathrm{G}}^{\mathrm{s}}\Phi_{\mathrm{s}} - \Phi_{\mathrm{s}}))_{\Omega_h^{\mathrm{s}}} - (\mathrm{J}_{\mathrm{s}}, \nu(\Phi_{\mathrm{s}} - \boldsymbol{P}_{k-1}(\Phi_{\mathrm{s}})))_{\Omega_h^{\mathrm{s}}} + (\mathbf{J}_{\mathrm{d}}, \Pi_{\mathbf{V}}^{\mathrm{d}}\boldsymbol{\phi}_{\mathrm{d}} - \boldsymbol{\phi}_{\mathrm{d}})_{\Omega_h^{\mathrm{d}}} \\
&- (\mathbf{J}_{\mathrm{d}}, \kappa(\nabla\varphi_{\mathrm{d}} - P_{k-1}(\nabla\varphi_{\mathrm{d}})))_{\Omega_h^{\mathrm{d}}} + (\kappa^{-1}\mathbf{u}_{\mathrm{d},h}, \Pi_{\mathbf{V}}^{\mathrm{d}}\boldsymbol{\phi}_{\mathrm{d}} - \boldsymbol{\phi}_{\mathrm{d}})_{\Omega_h^{\mathrm{d}}},
\end{aligned}
$$

and

$$
\begin{aligned}
\mathbb{T}_2 = &\langle\big(\boldsymbol{E}_{\mathbf{u}_{\mathrm{d},h}}\circ\boldsymbol{\psi}_{\mathrm{d}}^{-1} - \mathbf{u}_{\mathrm{d},h}\big)\cdot\mathbf{n}_{\mathrm{d}}, \mathcal{P}^{\mathrm{d}}\varphi_{\mathrm{d}}\rangle_{\mathcal{I}_h^{\mathrm{d}}} + \langle\boldsymbol{\mathcal{P}}^{\mathrm{s}}\boldsymbol{\phi}_{\mathrm{s}}, \big(\boldsymbol{E}_{\boldsymbol{\sigma}_{\mathrm{s},h}}\circ\boldsymbol{\psi}_{\mathrm{s}}^{-1} - \boldsymbol{\sigma}_{\mathrm{s},h}\big)\,\mathbf{n}_{\mathrm{s}}\rangle_{\mathcal{I}_h^{\mathrm{s}}} - \langle\mathbf{j}_{\mathrm{s}}^{\mathrm{nc}} + \mathbf{j}_{\mathrm{s}}^{\delta}, \boldsymbol{\mathcal{P}}^{\mathrm{s}}\boldsymbol{\phi}_{\mathrm{s}}\rangle_{\mathcal{I}_h^{\mathrm{s}}} \\
&- \langle j_{\mathrm{d}}^{\mathrm{nc}} + j_{\mathrm{d}}^{\delta}, \mathcal{P}^{\mathrm{d}}\varphi_{\mathrm{d}}\rangle_{\mathcal{I}_h^{\mathrm{d}}} + \langle\big(\widehat{p}_{\mathrm{d},h}\circ\boldsymbol{\psi}^{-1} - \widetilde{p}_{\mathrm{d},h}\big)\,\mathbf{n}_{\mathrm{d}}, \boldsymbol{\mathcal{P}}^{\mathrm{s}}\boldsymbol{\phi}_{\mathrm{s}}\rangle_{\mathcal{I}_h^{\mathrm{s}}} + \langle(\widetilde{\mathbf{u}}_{\mathrm{s},h} - \widehat{\mathbf{u}}_{\mathrm{s},h}\circ\boldsymbol{\psi})\cdot\mathbf{n}_{\mathrm{s}}, \mathcal{P}^{\mathrm{d}}\varphi_{\mathrm{d}}\rangle_{\mathcal{I}_h^{\mathrm{d}}} \\
&- \langle\widehat{\mathbf{u}}_{\mathrm{s},h}, (\mathcal{P}^{\mathrm{d}}\varphi_{\mathrm{d}} - \varphi_{\mathrm{d}})\mathbf{n}_{\mathrm{d}}\circ\boldsymbol{\psi}^{-1}\rangle_{\mathcal{I}_h^{\mathrm{s}}} + \langle(\boldsymbol{\mathcal{P}}^{\mathrm{s}}\boldsymbol{\phi}_{\mathrm{s}} - \boldsymbol{\phi}_{\mathrm{s}})\circ\boldsymbol{\psi}\cdot\mathbf{n}_{\mathrm{s}}, \widehat{p}_{\mathrm{d},h}\rangle_{\mathcal{I}_h^{\mathrm{d}}} - \langle\alpha_{\mathrm{s},h}\mathbf{n}_{\mathrm{s}}, \boldsymbol{\mathcal{P}}^{\mathrm{s}}\boldsymbol{\phi}_{\mathrm{s}}\rangle_{\mathcal{I}_h^{\mathrm{s}}} \\
&- \langle\widehat{p}_{\mathrm{d},h}\circ\boldsymbol{\psi}^{-1}, \big(\boldsymbol{\phi}_{\mathrm{s}}\circ\boldsymbol{\psi}_{\mathrm{s}}^{-1} - \boldsymbol{\phi}_{\mathrm{s}}\big)\cdot\mathbf{n}_{\mathrm{s}}\rangle_{\mathcal{I}_h^{\mathrm{s}}} + \langle\widehat{\mathbf{u}}_{\mathrm{s},h}, \big(\nu\Phi_{\mathrm{s}} - \varphi_{\mathrm{s}}\mathrm{I} - (\nu\Phi_{\mathrm{s}} - \varphi_{\mathrm{s}}\mathrm{I})\circ\boldsymbol{\psi}_{\mathrm{s}}^{-1}\big)\mathbf{n}_{\mathrm{s}}\rangle_{\mathcal{I}_h^{\mathrm{s}}} \\
&+ \langle\widehat{p}_{\mathrm{d},h}, \big(\boldsymbol{\phi}_{\mathrm{d}} - \boldsymbol{\phi}_{\mathrm{d}}\circ\boldsymbol{\psi}_{\mathrm{d}}^{-1}\big)\cdot\mathbf{n}_{\mathrm{d}}\rangle_{\mathcal{I}_h^{\mathrm{d}}} + \langle\widehat{\mathbf{u}}_{\mathrm{s},h}\circ\boldsymbol{\psi}, \big(\varphi_{\mathrm{d}}\circ\boldsymbol{\psi}_{\mathrm{d}}^{-1} - \varphi_{\mathrm{d}}\big)\,\mathbf{n}_{\mathrm{d}}\rangle_{\mathcal{I}_h^{\mathrm{d}}} \\
&+ \sum_{\ell=1}^{n-1}\omega_\ell^{-1}\langle(\widetilde{\mathbf{u}}_{\mathrm{s},h}\circ\boldsymbol{\psi}^{-1} - \widehat{\mathbf{u}}_{\mathrm{s},h})\cdot\boldsymbol{m}_\ell, \boldsymbol{\mathcal{P}}^{\mathrm{s}}\boldsymbol{\phi}_{\mathrm{s}}\cdot\boldsymbol{m}_\ell\rangle_{\mathcal{I}_h^{\mathrm{s}}} + \sum_{\ell=1}^{n-1}\omega_\ell^{-1}\langle(\boldsymbol{\phi}_{\mathrm{s}} - \boldsymbol{\phi}_{\mathrm{s}}\circ\boldsymbol{\psi}_{\mathrm{s}}^{-1})\cdot\boldsymbol{m}_\ell, \widehat{\mathbf{u}}_{\mathrm{s},h}\cdot\boldsymbol{m}_\ell\rangle_{\mathcal{I}_h^{\mathrm{s}}}.
\end{aligned}
$$

Here $\boldsymbol{P}_{k-1}|_{\widetilde{K}}$ and $P_{k-1}|_K$ are the projections $\mathbf{L}^2(\widetilde{K})$ and $L^2(K)$ onto $\mathbf{P}_{k-1}(\widetilde{K})$ and $P_{k-1}(K)$ for each $\widetilde{K}\in\Omega_h^{\mathrm{s}}$ and $K\in\Omega_h^{\mathrm{d}}$. Hence, applying the Cauchy–Schwarz inequality, it follows that

$$
\begin{aligned}
\mathbb{T}_1 \le &\Big\{\|\mathrm{L}_{\mathrm{s},h}\|_{\Omega_h^{\mathrm{s}}} + \|\mathrm{J}_{\mathrm{s}}\|_{\Omega_h^{\mathrm{s}}} + (1+\overline{\kappa})\|\mathbf{J}_{\mathrm{d}}\|_{\Omega_h^{\mathrm{d}}} + \|\kappa^{-1}\mathbf{u}_{\mathrm{d},h}\|_{\Omega_h^{\mathrm{d}}}\Big\}\Big\{\|\nu(\Pi_{\mathrm{G}}^{\mathrm{s}}\mathrm{L}_{\mathrm{s}} - \Phi_{\mathrm{s}})\|_{\Omega_h^{\mathrm{s}}} \\
&+ \|\nu(\Phi_{\mathrm{s}} - \boldsymbol{P}_{k-1}(\Phi_{\mathrm{s}}))\|_{\Omega_h^{\mathrm{s}}} + \|\Pi_{\mathbf{V}}^{\mathrm{d}}\boldsymbol{\phi}_{\mathrm{d}} - \boldsymbol{\phi}_{\mathrm{d}}\|_{\Omega_h^{\mathrm{d}}} + \|\nabla\varphi_{\mathrm{d}} - P_{k-1}(\nabla\varphi_{\mathrm{d}})\|_{\Omega_h^{\mathrm{d}}}\Big\}.
\end{aligned}
$$

Thus, invoking [54, Lemma 1.58], the approximation properties given by (3.4) and (3.6), and the regularity assumption (cf. (3.32)) we obtain

$$
\begin{aligned}
\mathbb{T}_1 &\le C_1 h\Big\{\|\mathrm{L}_{\mathrm{s},h}\|_{\Omega_h^{\mathrm{s}}} + \|\mathrm{J}_{\mathrm{s}}\|_{\Omega_h^{\mathrm{s}}} + (1+\overline{\kappa})\|\mathbf{J}_{\mathrm{d}}\|_{\Omega_h^{\mathrm{d}}} + \|\kappa^{-1}\mathbf{u}_{\mathrm{d},h}\|_{\Omega_h^{\mathrm{d}}}\Big\}\Big\{\|\nu\Phi_{\mathrm{s}}\|_{1,\Omega_h^{\mathrm{s}}} + \|\varphi_{\mathrm{s}}\|_{1,\Omega_h^{\mathrm{s}}} \\
&\qquad + \|\nu\boldsymbol{\phi}_{\mathrm{s}}\|_{2,\Omega_h^{\mathrm{s}}} + \|\Theta_{\mathrm{s}}\|_{\Omega_h^{\mathrm{s}}} + \|\boldsymbol{\phi}_{\mathrm{d}}\|_{1,\Omega_h^{\mathrm{d}}} + \|\varphi_{\mathrm{d}}\|_{2,\Omega_h^{\mathrm{d}}}\Big\} \\
&\le 2C_1 C_{\mathbf{r}} h\Big\{\|\mathrm{L}_{\mathrm{s},h}\|_{\Omega_h^{\mathrm{s}}} + \|\mathrm{J}_{\mathrm{s}}\|_{\Omega_h^{\mathrm{s}}} + (1+\overline{\kappa})\|\mathbf{J}_{\mathrm{d}}\|_{\Omega_h^{\mathrm{d}}} + \|\kappa^{-1}\mathbf{u}_{\mathrm{d},h}\|_{\Omega_h^{\mathrm{d}}}\Big\}\Big\{\|\Theta_{\mathrm{s}}\|_{\Omega_h^{\mathrm{s}}} + \|\Theta_{\mathrm{d}}\|_{\Omega_h^{\mathrm{d}}}\Big\}. \qquad (3.34)
\end{aligned}
$$

In turn, for $\mathbb{T}_2$ we write

$$
\begin{aligned}
\mathbb{B}_1 &:= \langle (\boldsymbol{E}_{\mathbf{u}_{\mathrm{d},h}} \circ \boldsymbol{\psi}_{\mathrm{d}}^{-1} - \mathbf{u}_{\mathrm{d},h}) \cdot \mathbf{n}_{\mathrm{d}}, \mathcal{P}^{\mathrm{d}}\varphi_{\mathrm{d}} \rangle_{\mathcal{I}_h^{\mathrm{d}}}, & \mathbb{B}_2 &:= \langle \boldsymbol{\mathcal{P}}^{\mathrm{s}}\boldsymbol{\phi}_{\mathrm{s}}, (\boldsymbol{E}_{\boldsymbol{\sigma}_{\mathrm{s},h}} \circ \boldsymbol{\psi}_{\mathrm{s}}^{-1} - \boldsymbol{\sigma}_{\mathrm{s},h})\,\mathbf{n}_{\mathrm{s}} \rangle_{\mathcal{I}_h^{\mathrm{s}}}, \\
\mathbb{B}_3 &:= -\langle \mathbf{j}_{\mathrm{s}}^{\mathrm{nc}} + \mathbf{j}_{\mathrm{s}}^{\delta}, \boldsymbol{\mathcal{P}}^{\mathrm{s}}\boldsymbol{\phi}_{\mathrm{s}} \rangle_{\mathcal{I}_h^{\mathrm{s}}}, & \mathbb{B}_4 &:= -\langle j_{\mathrm{d}}^{\mathrm{nc}} + j_{\mathrm{d}}^{\delta}, \mathcal{P}^{\mathrm{d}}\varphi_{\mathrm{d}} \rangle_{\mathcal{I}_h^{\mathrm{d}}}, \\
\mathbb{B}_5 &:= \langle (\widehat{p}_{\mathrm{d},h} \circ \boldsymbol{\psi}^{-1} - \widetilde{p}_{\mathrm{d},h})\,\mathbf{n}_{\mathrm{d}}, \boldsymbol{\mathcal{P}}^{\mathrm{s}}\boldsymbol{\phi}_{\mathrm{s}} \rangle_{\mathcal{I}_h^{\mathrm{s}}}, & \mathbb{B}_6 &:= \langle (\widetilde{\mathbf{u}}_{\mathrm{s},h} - \widehat{\mathbf{u}}_{\mathrm{s},h} \circ \boldsymbol{\psi}) \cdot \mathbf{n}_{\mathrm{s}}, \mathcal{P}^{\mathrm{d}}\varphi_{\mathrm{d}} \rangle_{\mathcal{I}_h^{\mathrm{d}}}, \\
\mathbb{B}_7 &:= \langle \widehat{\mathbf{u}}_{\mathrm{s},h}, (\varphi_{\mathrm{d}} - \mathcal{P}^{\mathrm{d}}\varphi_{\mathrm{d}})\mathbf{n}_{\mathrm{d}} \circ \boldsymbol{\psi}^{-1} \rangle_{\mathcal{I}_h^{\mathrm{s}}}, & \mathbb{B}_8 &:= \langle (\boldsymbol{\mathcal{P}}^{\mathrm{s}}\boldsymbol{\phi}_{\mathrm{s}} - \boldsymbol{\phi}_{\mathrm{s}}) \circ \boldsymbol{\psi} \cdot \mathbf{n}_{\mathrm{s}}, \widehat{p}_{\mathrm{d},h} \rangle_{\mathcal{I}_h^{\mathrm{d}}}, \\
\mathbb{B}_9 &:= \langle \widehat{\mathbf{u}}_{\mathrm{s},h} \circ \boldsymbol{\psi}, (\varphi_{\mathrm{d}} \circ \boldsymbol{\psi}_{\mathrm{d}}^{-1} - \varphi_{\mathrm{d}})\,\mathbf{n}_{\mathrm{d}} \rangle_{\mathcal{I}_h^{\mathrm{d}}}, & \mathbb{B}_{10} &:= -\langle \widehat{p}_{\mathrm{d},h} \circ \boldsymbol{\psi}^{-1}, (\boldsymbol{\phi}_{\mathrm{s}} \circ \boldsymbol{\psi}_{\mathrm{s}}^{-1} - \boldsymbol{\phi}_{\mathrm{s}}) \cdot \mathbf{n}_{\mathrm{s}} \rangle_{\mathcal{I}_h^{\mathrm{s}}}, \\
\mathbb{B}_{11} &:= \langle \widehat{\mathbf{u}}_{\mathrm{s},h}, (\nu\varPhi_{\mathrm{s}} - \varphi_{\mathrm{s}}\mathrm{I} - (\nu\varPhi_{\mathrm{s}} - \varphi_{\mathrm{s}}\mathrm{I}) \circ \boldsymbol{\psi}_{\mathrm{s}}^{-1})\mathbf{n}_{\mathrm{s}} \rangle_{\mathcal{I}_h^{\mathrm{s}}}, & \mathbb{B}_{12} &:= \langle \widehat{p}_{\mathrm{d},h}, (\boldsymbol{\phi}_{\mathrm{d}} - \boldsymbol{\phi}_{\mathrm{d}} \circ \boldsymbol{\psi}_{\mathrm{d}}^{-1}) \cdot \mathbf{n}_{\mathrm{s}} \rangle_{\mathcal{I}_h^{\mathrm{d}}}, \\
\mathbb{B}_{13} &:= \sum_{\ell=1}^{n-1} \omega_\ell^{-1} \langle (\widetilde{\mathbf{u}}_{\mathrm{s},h} \circ \boldsymbol{\psi}^{-1} - \widehat{\mathbf{u}}_{\mathrm{s},h}) \cdot \boldsymbol{m}_\ell, \boldsymbol{\mathcal{P}}^{\mathrm{s}}\boldsymbol{\phi}_{\mathrm{s}} \cdot \boldsymbol{m}_\ell \rangle_{\mathcal{I}_h^{\mathrm{s}}}, & \mathbb{B}_{14} &:= -\langle \alpha_{\mathrm{s},h}\mathbf{n}_{\mathrm{s}}, \boldsymbol{\mathcal{P}}^{\mathrm{s}}\boldsymbol{\phi}_{\mathrm{s}} \rangle_{\mathcal{I}_h^{\mathrm{s}}}, \\
\mathbb{B}_{15} &:= \sum_{\ell=1}^{n-1} \omega_\ell^{-1} \langle (\boldsymbol{\phi}_{\mathrm{s}} - \boldsymbol{\phi}_{\mathrm{s}} \circ \boldsymbol{\psi}_{\mathrm{s}}^{-1}) \cdot \boldsymbol{m}_\ell, \widehat{\mathbf{u}}_{\mathrm{s},h} \cdot \boldsymbol{m}_\ell \rangle_{\mathcal{I}_h^{\mathrm{s}}}.
\end{aligned}
$$

In this way, we bound each of these terms applying the Cauchy–Schwarz and trace inequalities, and the regularity Assumption (cf. (3.32)). Indeed, note that

$$
\mathbb{B}_3 \lesssim \nu^{-1}\|\mathbf{j}_{\mathrm{s}}^{\mathrm{nc}} + \mathbf{j}_{\mathrm{s}}^{\delta}\|_{\mathcal{I}_h^{\mathrm{s}}} \|\varTheta_{\mathrm{s}}\|_{\varOmega_h^{\mathrm{s}}}, \quad \mathbb{B}_4 \lesssim \|j_{\mathrm{d}}^{\mathrm{nc}} + j_{\mathrm{d}}^{\delta}\|_{\mathcal{I}_h^{\mathrm{d}}} \|\varTheta_{\mathrm{d}}\|_{\varOmega_h^{\mathrm{d}}}, \quad \mathbb{B}_{14} \lesssim \nu^{-1} C_\alpha \|p_{\mathrm{s},h}\|_{\varOmega_h^{\mathrm{s}}} \|\varTheta_{\mathrm{s}}\|_{\varOmega_h^{\mathrm{s}}}.
$$

In turn, thanks to Lemma 1, it follows that

$$
\begin{aligned}
\mathbb{B}_1 &\lesssim \max_{e \in \mathcal{I}_h^{\mathrm{d}}} \left(\delta_e h_e^{-3/2} C_e^{\mathtt{ext}}\right) \|\mathbf{u}_{\mathrm{d},h}\|_{\varOmega_h^{\mathrm{d}}} \|\varTheta_{\mathrm{d}}\|_{\varOmega_h^{\mathrm{d}}}, & \mathbb{B}_9 &\lesssim \delta \|\widehat{\mathbf{u}}_{\mathrm{s},h}\|_{\mathcal{I}_h^{\mathrm{s}}} \|\varTheta_{\mathrm{d}}\|_{\varOmega_h^{\mathrm{d}}}, \\
\mathbb{B}_2 &\lesssim \nu^{-1} \max_{e \in \mathcal{I}_h^{\mathrm{s}}} \left(\delta_e h_e^{-3/2} C_e^{\mathtt{ext}}\right) \|\boldsymbol{\sigma}_{\mathrm{s},h}\|_{\varOmega_h^{\mathrm{s}}} \|\varTheta_{\mathrm{s}}\|_{\varOmega_h^{\mathrm{s}}}, & \mathbb{B}_{10} &\lesssim \nu^{-1}\delta \|\widehat{p}_{\mathrm{d},h}\|_{\mathcal{I}_h^{\mathrm{d}}} \|\varTheta_{\mathrm{s}}\|_{\varOmega_h^{\mathrm{s}}}, \\
\mathbb{B}_{11} &\lesssim \delta^{1/2} \|\widehat{\mathbf{u}}_{\mathrm{s},h}\|_{\mathcal{I}_h^{\mathrm{s}}} \|\varTheta_{\mathrm{s}}\|_{\varOmega_h^{\mathrm{s}}}, & \mathbb{B}_{12} &\lesssim \delta^{1/2} \|\widehat{p}_{\mathrm{d},h}\|_{\mathcal{I}_h^{\mathrm{d}}} \|\varTheta_{\mathrm{d}}\|_{\varOmega_h^{\mathrm{d}}}, \\
\mathbb{B}_{15} &\lesssim \delta \sum_{\ell=1}^{n-1} \omega_\ell^{-1} \|\widehat{\mathbf{u}}_{\mathrm{s},h} \cdot \boldsymbol{m}_\ell\|_{\mathcal{I}_h^{\mathrm{s}}} \|\varTheta_{\mathrm{s}}\|_{\varOmega_h^{\mathrm{s}}}.
\end{aligned}
$$

Next, from (3.23a) and (3.23b), we obtain

$$
\begin{aligned}
\mathbb{B}_6 &\lesssim \nu^{-1} \delta_e^{1/2} C_{\delta_{\mathrm{s},h}}^{1/2} \|\nu \mathrm{L}_{\mathrm{s},h}\|_{\varOmega_h^{\mathrm{s}}} \|\varTheta_{\mathrm{d}}\|_{\varOmega_h^{\mathrm{d}}}, & \mathbb{B}_5 &\lesssim \nu^{-1} \delta_e^{1/2} C_{\delta_{\mathrm{d},h}}^{1/2} \|\kappa^{-1}\mathbf{u}_{\mathrm{d},h}\|_{\varOmega_h^{\mathrm{s}}} \|\varTheta_{\mathrm{s}}\|_{\varOmega_h^{\mathrm{s}}}, \\
\mathbb{B}_{13} &\lesssim \nu^{-1} \delta_e^{1/2} C_{\delta_{\mathrm{s},h}}^{1/2} \|\nu \mathrm{L}_{\mathrm{s},h}\|_{\varOmega_h^{\mathrm{s}}} \|\varTheta_{\mathrm{s}}\|_{\varOmega_h^{\mathrm{s}}}.
\end{aligned}
$$

On the other hand, from [54, Lemma 1.59], we find that

$$
\begin{aligned}
\mathbb{B}_7 &\lesssim \left(h_e^{3/2} \|\widehat{\mathbf{u}}_{\mathrm{s},h} - \mathbf{u}_{\mathrm{s},h}\|_{\mathcal{I}_h^{\mathrm{s}}} + h_e (C_e^{\mathrm{tr}})^{-1} \|\mathbf{u}_{\mathrm{s},h}\|_{\varOmega_h^{\mathrm{s}}}\right) \|\varTheta_{\mathrm{d}}\|_{\varOmega_h^{\mathrm{d}}}, \\
\mathbb{B}_8 &\lesssim \left(h_e^{3/2} \|\widehat{p}_{\mathrm{d},h} - p_{\mathrm{d},h}\|_{\mathcal{I}_h^{\mathrm{d}}} + h_e (C_e^{\mathrm{tr}})^{-1} \|p_{\mathrm{d},h}\|_{\varOmega_h^{\mathrm{d}}}\right) \|\varTheta_{\mathrm{s}}\|_{\varOmega_h^{\mathrm{s}}}.
\end{aligned}
$$

In summary, adding up all the estimates for $\mathbb{B}_i$ ($i = 1, ..., 15$), we deduce that

$$\begin{aligned}\mathbb{T}_2 \lesssim \Big\{ & C_{\delta,h}^{u_{\rm d},L_{\rm s}} \Big(\|\kappa^{-1}\mathbf{u}_{{\rm d},h}\|_{\Omega_h^{\rm d}} + \|{\rm L}_{{\rm s},h}\|_{\Omega_h^{\rm s}} \Big) + C_{\delta,h}^{\widehat{u}_{\rm s},\widehat{p}_{\rm d}} \Big(\nu \|\delta_e^{1/7}\tau^{1/2}\widehat{\mathbf{u}}_{{\rm s},h}\|_{\mathcal{I}_h^{\rm s}} + \|\delta_e^{1/7}\tau^{1/2}\widehat{p}_{{\rm d},h}\|_{\mathcal{I}_h^{\rm d}} \Big) \\ & + C_{\delta,h}^{p}\|p_{{\rm s},h}\|_{\Omega_h^{\rm s}} + \|\mathbf{j}_{\rm s}^{\rm nc} + \mathbf{j}_{\rm s}^{\delta}\|_{\mathcal{I}_h^{\rm s}} + \|j_{\rm d}^{\rm nc} + j_{\rm d}^{\delta}\|_{\mathcal{I}_h^{\rm d}} + h_e^{3/2}\|\widehat{\mathbf{u}}_{{\rm s},h} - \mathbf{u}_{{\rm s},h}\|_{\mathcal{I}_h^{\rm s}} + C_{\delta,h}^{\widehat{u}_{\rm s},\widehat{p}_{\rm d}} \sum_{\ell=1}^{n-1} \omega_\ell^{-1}\|\widehat{\mathbf{u}}_{{\rm s},h}\|_{\mathcal{I}_h^{\rm s}} \\ & + h_e (C_e^{\rm tr})^{-1}\|\mathbf{u}_{{\rm s},h}\|_{\Omega_h^{\rm s}} + h_e^{3/2}\|\widehat{p}_{{\rm d},h} - p_{{\rm d},h}\|_{\mathcal{I}_h^{\rm d}} + h_e(C_e^{\rm tr})^{-1}\|p_{{\rm d},h}\|_{\Omega_h^{\rm d}} \Big\} \Big\{ \|\Theta_{\rm s}\|_{\Omega_h^{\rm s}} + \|\Theta_{\rm d}\|_{\Omega_h^{\rm d}} \Big\},\end{aligned} \tag{3.35}$$

where $C_{\delta,h}^{u_{\rm d},L_{\rm s}}$, $C_{\delta,h}^{\widehat{u}_{\rm s},\widehat{p}_{\rm d}}$, and $C_{\delta,h}^{p}$ are the constants that have been defined in **(A.4)**. In this way, from (3.34) and (3.35), we find that

$$\begin{aligned}&(\mathbf{u}_{{\rm s},h}, \Theta_{\rm s})_{\Omega_h^{\rm s}} + (p_{{\rm d},h}, \Theta_{\rm d})_{\Omega_h^{\rm d}} \\ &\lesssim \Big\{ \Big(h + C_{\delta,h}^{u_{\rm d},L_{\rm s}} + C_{\delta,h}^{\widehat{u}_{\rm s},\widehat{p}_{\rm d}} \Big) \mathcal{Q}({\rm L}_{{\rm s},h}, \mathbf{u}_{\star,h}, \widehat{\mathbf{u}}_{{\rm s},h}, p_{{\rm d},h}, \widehat{p}_{{\rm d},h}) + C_{\delta,h}^{p}\|p_{{\rm s},h}\|_{\Omega_h^{\rm s}} + \|j_{\rm d}^{\rm nc} + j_{\rm d}^{\delta}\|_{\mathcal{I}_h^{\rm d}} \\ &\quad + \|\mathbf{j}_{\rm s}^{\rm nc} + \mathbf{j}_{\rm s}^{\delta}\|_{\mathcal{I}_h^{\rm s}} + h^{\min\{1,k\}}\big(\|\mathbf{J}_{\rm d}\|_{\Omega_h^{\rm d}} + \|{\rm J}_{\rm s}\|_{\Omega_h^{\rm s}}\big) + h\big(\|p_{{\rm d},h}\|_{\Omega_h^{\rm d}} + \|\mathbf{u}_{{\rm s},h}\|_{\Omega_h^{\rm s}}\big) \Big\} \Big\{ \|\Theta_{\rm s}\|_{\Omega_h^{\rm s}} + \|\Theta_{\rm d}\|_{\Omega_h^{\rm d}} \Big\}.\end{aligned}$$

Hence, taking $\Theta_{\rm s} = \mathbf{u}_{{\rm s},h}$ and $\Theta_{\rm d} = p_{{\rm d},h}$ leads to the required inequality (3.33). ■

Lemma 6. Assume that ${\rm f}_{\rm d} = 0$ and $\mathbf{f}_{\rm s} = \mathbf{0}$. It holds that

$$\|p_{{\rm s},h}\|_{\Omega_h^{\rm s}} \le \widetilde{C}_{is} \Big\{ \nu\|{\rm L}_{{\rm s},h}\|_{\Omega_h^{\rm s}} + \nu\|\tau^{1/2}\left(\mathbf{u}_{{\rm s},h} - \widehat{\mathbf{u}}_{{\rm s},h}\right)\|_{\partial\Omega_h^{\rm s}} \Big\}, \tag{3.36}$$

where $\widetilde{C}_{is} = \widetilde{\beta}\max\Big\{1, \max_{K\in\Omega_h^{\rm s}}(\tau h_K)^{1/2}\Big\}$, and $\widetilde{\beta}$ is a positive constant independent of h.

Proof. See [102, Lemma 2] or [87, Lemma 10]. ■

We are now in position to establish the main result of this section.

Theorem 1. Suppose Assumptions **(A)** and elliptic regularity (cf. (3.32)) hold true. If τ is of order one, $k \ge 1$ and $h < 1$, there exists $h_0 \in (0, 1)$, such that for all $h < h_0$,

$$\begin{aligned}&\mathcal{Q}({\rm L}_{{\rm s},h}, \mathbf{u}_{\star,h}, \widehat{\mathbf{u}}_{{\rm s},h}, p_{{\rm d},h}, \widehat{p}_{{\rm d},h})^2 \\ &\quad \lesssim \|h_e^{(\beta-1)/2}(j_{\rm d}^{\rm nc} + j_{\rm d}^{\delta})\|_{\mathcal{I}_h^{\rm d}}^2 + \|h_e^{(\beta-1)/2}(\mathbf{j}_{\rm s}^{\rm nc} + \mathbf{j}_{\rm s}^{\delta})\|_{\mathcal{I}_h^{\rm s}}^2 + \|\mathbf{J}_{\rm d}\|_{\Omega_h^{\rm d}}^2 + \|\nu{\rm J}_{\rm s}\|_{\Omega_h^{\rm s}}^2,\end{aligned} \tag{3.37}$$

$$\begin{aligned}\|\mathbf{u}_{{\rm s},h}\|_{\Omega_h^{\rm s}}^2 + \|p_{{\rm d},h}\|_{\Omega_h^{\rm d}}^2 \lesssim & \Big\{ C_{\delta,h}^{\mathcal{S}}\mathcal{Q}({\rm L}_{{\rm s},h}, \mathbf{u}_{\star,h}, \widehat{\mathbf{u}}_{{\rm s},h}, p_{{\rm d},h}, \widehat{p}_{{\rm d},h})^2 + \|\mathbf{j}_{\rm s}^{\rm nc} + \mathbf{j}_{\rm s}^{\delta}\|_{\mathcal{I}_h^{\rm s}}^2 + \|j_{\rm d}^{\rm nc} + j_{\rm d}^{\delta}\|_{\mathcal{I}_h^{\rm d}}^2 \\ & + (C_{\delta,h}^{p})^2\|p_{{\rm s},h}\|_{\Omega_h^{\rm s}}^2 + h^{2\min\{1,k\}}\|\mathbf{J}_{\rm d}\|_{\Omega_h^{\rm d}}^2 + h^{2\min\{1,k\}}\|{\rm J}_{\rm s}\|_{\Omega_h^{\rm s}}^2 \Big\}, \quad \text{and}\end{aligned} \tag{3.38}$$

$$\|p_{{\rm s},h}\|_{\Omega_h^{\rm s}}^2 \lesssim \nu\mathcal{Q}({\rm L}_{{\rm s},h}, \mathbf{u}_{\star,h}, \widehat{\mathbf{u}}_{{\rm s},h}, p_{{\rm d},h}, \widehat{p}_{{\rm d},h})^2. \tag{3.39}$$

Proof. We first employ the estimate obtained in Lemma 5 to bound the first and second terms of the right-hand side of Lemma 4. Next, using the estimate for $\|p_{{\rm s},h}\|$ (cf. (3.36)), we obtain

$$(1 - C_{\delta,h})\,\mathcal{Q}({\rm L}_{{\rm s},h}, \mathbf{u}_{\star,h}, \widehat{\mathbf{u}}_{{\rm s},h}, p_{{\rm d},h}, \widehat{p}_{{\rm d},h})^2 \lesssim \|h_e^{(\beta-1)/2}(j_{\rm d}^{\rm nc} + j_{\rm d}^{\delta})\|_{\mathcal{I}_h^{\rm d}}^2 + \|h_e^{(\beta-1)/2}(\mathbf{j}_{\rm s}^{\rm nc} + \mathbf{j}_{\rm s}^{\delta})\|_{\mathcal{I}_h^{\rm s}}^2$$

$$+\|\mathbf{J}_{\rm d}\|^2_{\Omega_h^{\rm d}} + \|\nu \mathrm{J}_{\rm s}\|^2_{\Omega_h^{\rm s}},$$

where $C_{\delta,h}$ is the constant defined in **(A.4)**, since $\delta < 1$, τ is of order one, $k \geq 1$ and $h < 1$. Hence, (3.37) follows by Assumption **(A.4)**. Finally, making use of (3.33) and (3.36), we get (3.38) and (3.39), which finishes the proof. ∎

Corollary 1. The HDG scheme (3.7) has a unique solution.

Proof. We first note that the existence of the solution follows from its uniqueness. Thus, it suffices to show that when the right-hand sides of (3.7) vanish, then $\mathrm{L}_{{\rm s},h}$, $\mathbf{u}_{{\rm d},h}$, $p_{{\rm d},h}$, $\mathbf{u}_{{\rm s},h}$, $\widehat{p}_{{\rm d},h}$, $\widehat{\mathbf{u}}_{{\rm s},h}$ also vanish. Indeed, assuming that $\mathrm{f}_{\rm d} = 0$, $\mathbf{f}_{\rm s} = \mathbf{0}$, $\mathbf{J}_{\rm d} = \mathbf{0}$, $\mathrm{J}_{\rm s} = \mathbf{0}$, $j_{\rm d} = 0$, and $\mathbf{j}_{\rm s} = \mathbf{0}$, we deduce from Theorem 1 that $\mathrm{L}_{{\rm s},h} = \mathbf{0}$, $\mathbf{u}_{{\rm d},h} = \mathbf{0}$, $p_{{\rm d},h} = \widehat{p}_{{\rm d},h} = 0$, $\mathbf{u}_{{\rm s},h} = \widehat{\mathbf{u}}_{{\rm s},h} = \mathbf{0}$, and $p_{{\rm s},h} = 0$. In turn, we notice from Lemma 2 that $\widetilde{p}_{{\rm d},h} = 0$, and $\widetilde{\mathbf{u}}_{{\rm s},h} = \mathbf{0}$, which completes the proof. ∎

3.4.3 Semi-aligned discrete interfaces

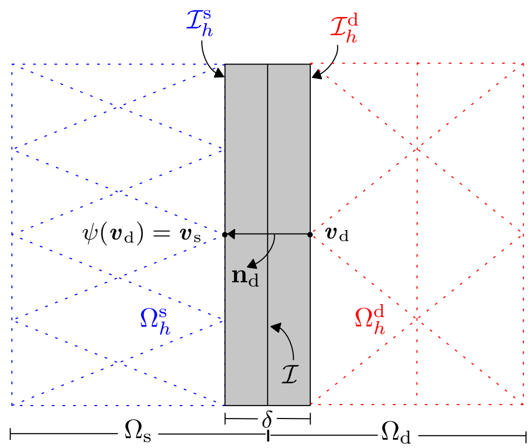

Figure 3.2: *Example of semi-aligned discrete interfaces separated by a uniform gap of size δ.*

With the aim of improving the estimate given in Theorem 1, in this section, we consider a specific structure of nonconforming meshes, where the discrete interfaces satisfy the following: if $\boldsymbol{v}_{\rm d}$ is a vertex in $\mathcal{I}_h^{\rm d}$, then $\boldsymbol{\psi}(\boldsymbol{v}_{\rm d}) := \boldsymbol{v}_{\rm d} + \delta \mathbf{n}_{\rm d}$ is a vertex $\boldsymbol{v}_{\rm s}$ in $\mathcal{I}_h^{\rm s}$ (see Fig 3.2). In this way, we refer to $\mathcal{I}_h^{\rm d}$ and $\mathcal{I}_h^{\rm s}$ as *semi-aligned discrete interfaces.*

Under this condition and the fact that in the error analysis $\mathbf{j}_{\rm s}^{\rm nc} := (\mathcal{P}^{\rm d} p_{\rm d} - p_{\rm d}) \circ \boldsymbol{\psi}^{-1} \mathbf{n}_{\rm d}$ and $j_{\rm d}^{\rm nc} := (\boldsymbol{\mathcal{P}}^{\rm s} \mathbf{u}_{\rm s} - \mathbf{u}_{\rm s}) \circ \boldsymbol{\psi} \cdot \mathbf{n}_{\rm s}$ (see eqs. (3.46) in Lemma 8), it is easy to see that $\langle j_{\rm d}^{\rm nc}, \mu_{{\rm d},h} \rangle_{\mathcal{I}_h^{\rm d}}$ in (3.25a) vanishes. In fact, since $h_{\rm s} \leq h_{\rm d}$, the term $\mu_{{\rm d},h} \mathbf{n}_{\rm s} \circ \boldsymbol{\psi}^{-1}$ belongs to $\mathbf{N}_h^{\rm s}$ and thus $\langle j_{\rm d}^{\rm nc}, \mu_{{\rm d},h} \rangle_{\mathcal{I}_h^{\rm d}} = \langle (\boldsymbol{\mathcal{P}}^{\rm s} \mathbf{u}_{\rm s} - \mathbf{u}_{\rm s}), \mu_{{\rm d},h} \mathbf{n}_{\rm s} \circ \boldsymbol{\psi}^{-1} \rangle_{\mathcal{I}_h^{\rm s}} = 0$. Furthermore, in what follows we show that under this configuration $\langle \mathbf{j}_{\rm s}^{\rm nc}, \boldsymbol{\mathcal{P}}^{\rm d} (\boldsymbol{\phi}_{\rm s} \circ \boldsymbol{\psi}) \circ \boldsymbol{\psi}^{-1} \rangle_{\mathcal{I}_h^{\rm s}}$ and $\langle j_{\rm d}^{\rm nc}, \mathcal{P}^{\rm d} \varphi_{\rm d} \rangle_{\mathcal{I}_h^{\rm d}}$ also vanish. Indeed,

$$\begin{aligned}
\langle \mathbf{j}_{\rm s}^{\rm nc}, \boldsymbol{\mathcal{P}}^{\rm d} (\boldsymbol{\phi}_{\rm s} \circ \boldsymbol{\psi}) \circ \boldsymbol{\psi}^{-1} \rangle_{\mathcal{I}_h^{\rm s}} &= \langle \mathcal{P}^{\rm d} p_{\rm d}, \boldsymbol{\mathcal{P}}^{\rm d} (\boldsymbol{\phi}_{\rm s} \circ \boldsymbol{\psi}) \cdot \mathbf{n}_{\rm d} \rangle_{\mathcal{I}_h^{\rm d}} - \langle p_{\rm d} \mathbf{n}_{\rm d}, \boldsymbol{\mathcal{P}}^{\rm d} (\boldsymbol{\phi}_{\rm s} \circ \boldsymbol{\psi}) \rangle_{\mathcal{I}_h^{\rm d}} \\
&= \langle p_{\rm d}, \boldsymbol{\mathcal{P}}^{\rm d} (\boldsymbol{\phi}_{\rm s} \circ \boldsymbol{\psi}) \cdot \mathbf{n}_{\rm d} \rangle_{\mathcal{I}_h^{\rm d}} - \langle p_{\rm d} \mathbf{n}_{\rm d}, \boldsymbol{\mathcal{P}}^{\rm d} (\boldsymbol{\phi}_{\rm s} \circ \boldsymbol{\psi}) \rangle_{\mathcal{I}_h^{\rm d}} = 0.
\end{aligned}$$

On the other hand, taking into account that $h_{\rm s} \leq h_{\rm d}$, we have

$$\begin{aligned}\langle j_{\rm d}^{\rm nc}, \mathcal{P}^{\rm d}\varphi_{\rm d}\rangle_{\mathcal{I}_h^{\rm d}} &= \langle \boldsymbol{\mathcal{P}}^{\rm s}\mathbf{u}_{\rm s}\circ\boldsymbol{\psi}\cdot\mathbf{n}_{\rm s}, \mathcal{P}^{\rm d}\varphi_{\rm d}\rangle_{\mathcal{I}_h^{\rm d}} - \langle \mathbf{u}_{\rm s}\circ\boldsymbol{\psi}\cdot\mathbf{n}_{\rm s}, \mathcal{P}^{\rm d}\varphi_{\rm d}\rangle_{\mathcal{I}_h^{\rm d}}\\ &= \langle \boldsymbol{\mathcal{P}}^{\rm s}\mathbf{u}_{\rm s}, \mathcal{P}^{\rm d}\varphi_{\rm d}\circ\boldsymbol{\psi}^{-1}\mathbf{n}_{\rm s}\rangle_{\mathcal{I}_h^{\rm s}} - \langle \mathbf{u}_{\rm s}, \mathcal{P}^{\rm d}\varphi_{\rm d}\circ\boldsymbol{\psi}^{-1}\mathbf{n}_{\rm s}\rangle_{\mathcal{I}_h^{\rm s}} = 0,\end{aligned}$$

since $\mathcal{P}^{\rm d}\varphi_{\rm d}\circ\boldsymbol{\psi}^{-1}\mathbf{n}_{\rm s} \in \mathbf{M}_h^{\rm s}$. All these identities imply an improvement of the estimate of Lemma 5. In fact, we recall that $\mathbb{B}_3 = -\langle \mathbf{j}_{\rm s}^{\rm nc}, \boldsymbol{\mathcal{P}}^{\rm s}\boldsymbol{\phi}_{\rm s}\rangle_{\mathcal{I}_h^{\rm s}} - \langle \mathbf{j}_{\rm s}^{\delta}, \boldsymbol{\mathcal{P}}^{\rm s}\boldsymbol{\phi}_{\rm s}\rangle_{\mathcal{I}_h^{\rm s}}$. Then, we have

$$\begin{aligned}\langle \mathbf{j}_{\rm s}^{\rm nc}, \boldsymbol{\mathcal{P}}^{\rm s}\boldsymbol{\phi}_{\rm s}\rangle_{\mathcal{I}_h^{\rm s}} &= \langle \mathbf{j}_{\rm s}^{\rm nc}, \boldsymbol{\mathcal{P}}^{\rm s}\boldsymbol{\phi}_{\rm s} - \boldsymbol{\phi}_{\rm s}\rangle_{\mathcal{I}_h^{\rm s}} - \langle \mathbf{j}_{\rm s}^{\rm nc}, \boldsymbol{\mathcal{P}}^{\rm d}(\boldsymbol{\phi}_{\rm s}\circ\boldsymbol{\psi})\circ\boldsymbol{\psi}^{-1} - \boldsymbol{\phi}_{\rm s}\rangle_{\mathcal{I}_h^{\rm s}} + \langle \mathbf{j}_{\rm s}^{\rm nc}, \boldsymbol{\mathcal{P}}^{\rm d}(\boldsymbol{\phi}_{\rm s}\circ\boldsymbol{\psi})\circ\boldsymbol{\psi}^{-1}\rangle_{\mathcal{I}_h^{\rm s}}\\ &\lesssim h^{3/2}\|\mathbf{j}_{\rm s}^{\rm nc}\|_{\mathcal{I}_h^{\rm s}}\,|\boldsymbol{\phi}_{\rm s}|_{\mathbf{H}^2(\Omega_{\rm s})} + \|\mathbf{j}_{\rm s}^{\rm nc}\|_{\mathcal{I}_h^{\rm s}}\|\boldsymbol{\mathcal{P}}^{\rm d}(\boldsymbol{\phi}_{\rm s}\circ\boldsymbol{\psi}) - \boldsymbol{\phi}_{\rm s}\circ\boldsymbol{\psi}\|_{\mathcal{I}_h^{\rm d}}\\ &\lesssim h^{3/2}\|\mathbf{j}_{\rm s}^{\rm nc}\|_{\mathcal{I}_h^{\rm s}}\,|\boldsymbol{\phi}_{\rm s}|_{\mathbf{H}^2(\Omega_{\rm s})} + h^{3/2}\|\mathbf{j}_{\rm s}^{\rm nc}\|_{\mathcal{I}_h^{\rm s}}|\boldsymbol{\phi}_{\rm s}\circ\boldsymbol{\psi}|_{\mathbf{H}^{3/2}(\mathcal{I}_h^{\rm d})}\\ &\lesssim \nu^{-1}h^{3/2}\|\mathbf{j}_{\rm s}^{\rm nc}\|_{\mathcal{I}_h^{\rm s}}\,\|\Theta_{\rm s}\|_{\Omega_{\rm s}},\end{aligned}$$

which implies that

$$\mathbb{B}_3 \lesssim \nu^{-1}h^{3/2}\|\mathbf{j}_{\rm s}^{\rm nc}\|_{\mathcal{I}_h^{\rm s}}\,\|\Theta_{\rm s}\|_{\Omega_{\rm s}} + \nu^{-1}\|\mathbf{j}_{\rm s}^{\delta}\|_{\mathcal{I}_h^{\rm s}}\,\|\Theta_{\rm s}\|_{\Omega_{\rm s}}. \tag{3.40}$$

On the other hand, since $\langle j_{\rm d}^{\rm nc}, \mathcal{P}^{\rm d}\varphi_{\rm d}\rangle_{\mathcal{I}_h^{\rm d}} = 0$, by applying the continuous trace inequality and (3.32), it follows that

$$\mathbb{B}_4 \;=\; -\langle j_{\rm d}^{\rm nc}, \mathcal{P}^{\rm d}\varphi_{\rm d}\rangle_{\mathcal{I}_h^{\rm d}} - \langle j_{\rm d}^{\delta}, \mathcal{P}^{\rm d}\varphi_{\rm d}\rangle_{\mathcal{I}_h^{\rm d}} = -\langle j_{\rm d}^{\delta}, \mathcal{P}^{\rm d}\varphi_{\rm d}\rangle_{\mathcal{I}_h^{\rm d}} \lesssim \|j_{\rm d}^{\delta}\|_{\mathcal{I}_h^{\rm d}}\,\|\Theta_{\rm d}\|_{\Omega_{\rm d}}. \tag{3.41}$$

We now have the following result.

Lemma 7. Under the same assumptions of Lemma 5, if we have *semi-aligned discrete interfaces*, we get

$$\begin{aligned}\|\mathbf{u}_{{\rm s},h}\|^2_{\Omega_h^{\rm s}} + \|p_{{\rm d},h}\|^2_{\Omega_h^{\rm d}} \leq C\Big\{&C^{\mathcal{S}}_{\delta,h}\mathcal{Q}(\mathrm{L}_{{\rm s},h}, \mathbf{u}_{\star,h}, \widehat{\mathbf{u}}_{{\rm s},h}, p_{{\rm d},h}, \widehat{p}_{{\rm d},h})^2 + h^{3/2}\|\mathbf{j}_{\rm s}^{\rm nc}\|^2_{\mathcal{I}_h^{\rm s}} + \|\mathbf{j}_{\rm s}^{\delta}\|^2_{\mathcal{I}_h^{\rm s}} + \|j_{\rm d}^{\delta}\|^2_{\mathcal{I}_h^{\rm d}}\\ &+ (C^{p}_{\delta,h})^2\|p_{{\rm s},h}\|^2_{\Omega_h^{\rm s}} + h^{2\min\{1,k\}}\|\mathbf{J}_{\rm d}\|^2_{\Omega_h^{\rm d}} + h^{2\min\{1,k\}}\|\mathrm{J}_{\rm s}\|^2_{\Omega_h^{\rm s}}\Big\}.\end{aligned} \tag{3.42}$$

Proof. The proof follows almost verbatim as in Lemma 5, but now considering the estimates (3.40) and (3.41). ■

3.5 Error Analysis

Our first goal in this section is to derive the error estimates of the proposed method. We employ the stability estimate deduced in previous sections. In what follows, we introduce the projection of the errors, namely $\varepsilon^{\mathrm{L}_{\rm s}} := \mathit{\Pi}^{\rm s}_{\rm G}\mathrm{L}_{\rm s} - \mathrm{L}_{{\rm s},h}$, $\varepsilon^{\mathbf{u}_\star} := \mathit{\Pi}^{\star}_{\mathbf{V}}\mathbf{u}_\star - \mathbf{u}_{\star,h}$, $\varepsilon^{\widehat{\mathbf{u}}_\star} := \boldsymbol{\mathcal{P}}^{\star}\mathbf{u}_\star - \widehat{\mathbf{u}}_{\star,h}$, $\varepsilon^{p_\star} := \mathit{\Pi}^{\star}_{P}p_\star - p_{\star,h}$, $\varepsilon^{\widehat{p}_{\rm d}} := \mathcal{P}^{\rm d}p_{\rm d} - \widehat{p}_{{\rm d},h}$, and $\varepsilon^{\alpha_{\rm s}} := \mathit{\Pi}^{\rm s}_{Q}\alpha_{\rm s} - \alpha_{{\rm s},h}$. In turn, the error of the projections are given by $\mathrm{I}^{\rm s}_{\mathrm{L}} := \mathrm{L}_{\rm s} - \mathit{\Pi}^{\rm s}_{\rm G}\mathrm{L}_{\rm s}$, $\mathrm{I}^{\star}_{\mathbf{u}} := \mathbf{u}_\star - \mathit{\Pi}^{\star}_{\mathbf{V}}\mathbf{u}_\star$, $\mathrm{I}^{\star}_{p} := p_\star - \mathit{\Pi}^{\star}_{P}p_\star$, and $\mathrm{I}^{\rm s}_{\alpha} := \alpha_{\rm s} - \mathit{\Pi}^{\rm s}_{Q}\alpha_{\rm s}$, and note that $\mathrm{I}^{\rm s}_{\alpha} = 0$.

Lemma 8. The projection of the errors satisfies

$$
\begin{aligned}
(\varepsilon^{\mathrm{L_s}}, \mathrm{G}_{\mathrm{s},h})_{\Omega_h^{\mathrm{s}}} + (\varepsilon^{\mathbf{u}_\mathrm{s}}, \nabla\cdot \mathrm{G}_{\mathrm{s},h})_{\Omega_h^{\mathrm{s}}} - \langle \varepsilon^{\widehat{\mathbf{u}}_\mathrm{s}}, \mathrm{G}_{\mathrm{s},h}\mathbf{n}_\mathrm{s}\rangle_{\partial\Omega_h^{\mathrm{s}}} &= -\,(\mathrm{I}_{\mathrm{L}}^{\mathrm{s}}, \mathrm{G}_{\mathrm{s},h})_{\Omega_h^{\mathrm{s}}}\,, &&(3.43a)\\
(\varepsilon^{\mathrm{L_s}}, \nabla\mathbf{v}_{\mathrm{s},h})_{\Omega_h^{\mathrm{s}}} - (\varepsilon^{p_\mathrm{s}}, \nabla\cdot\mathbf{v}_{\mathrm{s},h})_{\Omega_h^{\mathrm{s}}} - \langle (\nu\varepsilon^{\widehat{\mathrm{L}}_\mathrm{s}} - \varepsilon^{\widehat{p}_\mathrm{s}})\mathbf{n}_\mathrm{s}, \mathbf{v}_{\mathrm{s},h}\rangle_{\partial\Omega_h^{\mathrm{s}}} &= 0\,, &&(3.43b)\\
-(\varepsilon^{\mathbf{u}_\mathrm{s}}, \nabla q_{\mathrm{s},h})_{\Omega_h^{\mathrm{s}}} + \langle \varepsilon^{\widehat{\mathbf{u}}_\mathrm{s}}\cdot\mathbf{n}_\mathrm{s}, q_{\mathrm{s},h}\rangle_{\partial\Omega_h^{\mathrm{s}}} &= 0\,, &&(3.43c)\\
\langle \varepsilon^{\widehat{\mathbf{u}}_\mathrm{s}}, \boldsymbol{\mu}_{\mathrm{s},h}\rangle_{\Gamma_{\mathrm{s},h}} &= 0\,, &&(3.43d)\\
\langle (\nu\varepsilon^{\widehat{\mathrm{L}}_\mathrm{s}} - \varepsilon^{\widehat{p}_\mathrm{s}})\mathbf{n}_\mathrm{s}, \boldsymbol{\mu}_{\mathrm{s},h}\rangle_{\partial\Omega_h^{\mathrm{s}}\setminus(\Gamma_{\mathrm{s},h}\cup\mathcal{I}_h^{\mathrm{s}})} &= 0\,, &&(3.43e)\\
(\kappa^{-1}\varepsilon^{\mathbf{u}_\mathrm{d}}, \mathbf{v}_{\mathrm{d},h})_{\Omega_h^{\mathrm{d}}} - (\varepsilon^{p_\mathrm{d}}, \nabla\cdot\mathbf{v}_{\mathrm{d},h})_{\Omega_h^{\mathrm{d}}} + \langle \mathbf{v}_{\mathrm{d},h}\cdot\mathbf{n}_\mathrm{d}, \varepsilon^{\widehat{p}_\mathrm{d}}\rangle_{\partial\Omega_h^{\mathrm{d}}} &= -\,(\kappa^{-1}\mathrm{I}_{\mathbf{u}}^{\mathrm{d}}, \mathbf{v}_{\mathrm{d},h})_{\Omega_h^{\mathrm{d}}}\,, &&(3.43f)\\
-(\varepsilon^{\mathbf{u}_\mathrm{d}}, \nabla q_{\mathrm{d},h})_{\Omega_h^{\mathrm{d}}} + \langle \varepsilon^{\widehat{\mathbf{u}}_\mathrm{d}}\cdot\mathbf{n}_\mathrm{d}, q_{\mathrm{d},h}\rangle_{\partial\Omega_h^{\mathrm{d}}} &= 0\,, &&(3.43g)\\
\langle \varepsilon^{\widehat{\mathbf{u}}_\mathrm{d}}\cdot\mathbf{n}_\mathrm{d}, \mu_{\mathrm{d},h}\rangle_{\partial\Omega_h^{\mathrm{d}}\setminus\mathcal{I}_h^{\mathrm{d}}} &= 0\,, &&(3.43h)
\end{aligned}
$$

for all $(\mathrm{G}_{\mathrm{s},h}, \mathbf{v}_{\mathrm{s},h}, q_{\mathrm{s},h}, \boldsymbol{\mu}_{\mathrm{s},h}, \mathbf{v}_{\mathrm{d},h}, q_{\mathrm{d},h}, \mu_{\mathrm{d},h}) \in \mathrm{G}_h^{\mathrm{s}}\times\mathbf{V}_h^{\mathrm{s}}\times Q_h^{\mathrm{s}}\times\mathbf{M}_h^{\mathrm{s}}\times\mathbf{V}_h^{\mathrm{d}}\times Q_h^{\mathrm{d}}\times M_h^{\mathrm{d}}$, and

$$
\begin{aligned}
\varepsilon^{\widehat{\mathbf{u}}_\mathrm{d}}\cdot\mathbf{n}_\mathrm{d} &= \varepsilon^{\mathbf{u}_\mathrm{d}}\cdot\mathbf{n}_\mathrm{d} + \tau(\varepsilon^{p_\mathrm{d}} - \varepsilon^{\widehat{p}_\mathrm{d}}) \quad \text{on} \quad \partial\Omega_h^{\mathrm{d}}, &&(3.44a)\\
\varepsilon^{\widehat{\boldsymbol{\sigma}}_\mathrm{s}}\mathbf{n}_\mathrm{s} &= \nu\varepsilon^{\mathrm{L_s}}\mathbf{n}_\mathrm{s} - \varepsilon^{p_\mathrm{s}}\mathbf{I}\mathbf{n}_\mathrm{s} - \tau\nu(\varepsilon^{\mathbf{u}_\mathrm{s}} - \varepsilon^{\widehat{\mathbf{u}}_\mathrm{s}}) \quad \text{on} \quad \partial\Omega_h^{\mathrm{s}}. &&(3.44b)
\end{aligned}
$$

Moreover, for $\boldsymbol{x}_\star \in \mathcal{I}_h^\star$, let

$$
\begin{aligned}
\varepsilon^{\widetilde{p}_\mathrm{d}}(\boldsymbol{x}_\mathrm{s}) &:= \varepsilon^{\widehat{p}_\mathrm{d}}(\boldsymbol{x}_\mathrm{d}) - |\sigma_\mathrm{d}(\boldsymbol{x}_\mathrm{d})|\int_0^1 \boldsymbol{E}_{\varepsilon^{\mathbf{u}_\mathrm{d}}}(\boldsymbol{y}_\mathrm{d}(t))\cdot\mathbf{n}_\mathrm{d}dt, &&(3.45a)\\
\varepsilon^{\widetilde{\mathbf{u}}_\mathrm{s}}(\boldsymbol{x}_\mathrm{d}) &:= \varepsilon^{\widehat{\mathbf{u}}_\mathrm{s}}(\boldsymbol{x}_\mathrm{s}) + |\sigma_\mathrm{s}(\boldsymbol{x}_\mathrm{s})|\int_0^1 \boldsymbol{E}_{\varepsilon^{\mathrm{L_s}}}(\boldsymbol{y}_\mathrm{s}(t))\mathbf{n}_\mathrm{s}dt, &&(3.45b)\\
\varepsilon^{\widetilde{\mathbf{u}}_\mathrm{d}}(\boldsymbol{x}_\mathrm{d}) &:= \boldsymbol{E}_{\varepsilon^{\mathbf{u}_\mathrm{d}}}\circ\boldsymbol{\psi}_\mathrm{d}^{-1}(\boldsymbol{x}_\mathrm{d})\cdot\mathbf{n}_\mathrm{d} + \tau(\varepsilon^{p_\mathrm{d}} - \varepsilon^{\widehat{p}_\mathrm{d}})(\boldsymbol{x}_\mathrm{d}), &&(3.45c)\\
\varepsilon^{\widetilde{\boldsymbol{\sigma}}_\mathrm{s}}(\boldsymbol{x}_\mathrm{s})\mathbf{n}_\mathrm{s} &:= (\nu\boldsymbol{E}_{\varepsilon^{\mathrm{L_s}}} - \boldsymbol{E}_{\varepsilon^{p_\mathrm{s}}}\mathrm{I})\circ\boldsymbol{\psi}_\mathrm{s}^{-1}(\boldsymbol{x}_\mathrm{s})\mathbf{n}_\mathrm{s} - \nu\tau(\varepsilon^{\mathbf{u}_\mathrm{s}} - \varepsilon^{\widehat{\mathbf{u}}_\mathrm{s}})(\boldsymbol{x}_\mathrm{s}) - \varepsilon^{\alpha_\mathrm{s}}\mathbf{n}_\mathrm{s}. &&(3.45d)
\end{aligned}
$$

They satisfy

$$
\begin{aligned}
\langle \varepsilon^{\widetilde{\mathbf{u}}_\mathrm{s}}\cdot\mathbf{n}_\mathrm{s} + \varepsilon^{\widetilde{\mathbf{u}}_\mathrm{d}}\cdot\mathbf{n}_\mathrm{d}, \mu_{\mathrm{d},h}\rangle_{\mathcal{I}_h^{\mathrm{d}}} &= \langle (\boldsymbol{\mathcal{P}}^{\mathrm{s}}\mathbf{u}_\mathrm{s} - \mathbf{u}_\mathrm{s})\circ\boldsymbol{\psi}\cdot\mathbf{n}_\mathrm{s}, \mu_{\mathrm{d},h}\rangle_{\mathcal{I}_h^{\mathrm{d}}} - \langle |\sigma_\mathrm{s}|\Lambda_{\mathrm{I}_{\mathrm{L}}^{\mathrm{s}}}\circ\boldsymbol{\psi}\cdot\mathbf{n}_\mathrm{d}, \mu_{\mathrm{d},h}\rangle_{\mathcal{I}_h^{\mathrm{d}}}\\
&\quad + \langle |\sigma_\mathrm{s}|\mathrm{I}_{\mathrm{L}}^{\mathrm{s}}\circ\boldsymbol{\psi}\mathbf{n}_\mathrm{d}, \mu_{\mathrm{d},h}\mathbf{n}_\mathrm{d}\rangle_{\mathcal{I}_h^{\mathrm{d}}} + \left\langle \left(\mathrm{I}_{\mathbf{u}}^{\mathrm{d}} - \mathrm{I}_{\mathbf{u}}^{\mathrm{d}}\circ\boldsymbol{\psi}_\mathrm{d}^{-1}\right)\cdot\mathbf{n}_\mathrm{d}, \mu_{\mathrm{d},h}\right\rangle_{\mathcal{I}_h^{\mathrm{d}}} \quad \forall\, \mu_{\mathrm{d},h}\in \mathrm{N}_h^{\mathrm{d}},
\end{aligned}
\qquad (3.46a)
$$

$$
\begin{aligned}
&\langle \varepsilon^{\widetilde{\boldsymbol{\sigma}}_\mathrm{s}}\mathbf{n}_\mathrm{s} + \sum_{\ell=1}^{n-1}\omega_\ell^{-1}(\varepsilon^{\widetilde{\mathbf{u}}_\mathrm{s}}\circ\boldsymbol{\psi}^{-1}\cdot\boldsymbol{m}_\ell)\boldsymbol{m}_\ell - \varepsilon^{\widetilde{p}_\mathrm{d}}\mathbf{n}_\mathrm{d}, \boldsymbol{\mu}_{\mathrm{s},h}\rangle_{\mathcal{I}_h^{\mathrm{s}}} = -\langle (\mathcal{P}^{\mathrm{d}}p_\mathrm{d} - p_\mathrm{d})\circ\boldsymbol{\psi}^{-1}\mathbf{n}_\mathrm{d}, \boldsymbol{\mu}_{\mathrm{s},h}\rangle_{\mathcal{I}_h^{\mathrm{s}}}\\
&\quad + \langle \kappa^{-1}|\sigma_\mathrm{d}|\Lambda_{\mathrm{I}_{\mathbf{u}}^{\mathrm{d}}}\mathbf{n}_\mathrm{d}\circ\boldsymbol{\psi}^{-1} - \kappa^{-1}|\sigma_\mathrm{d}|\mathrm{I}_{\mathbf{u}}^{\mathrm{d}}\circ\boldsymbol{\psi}^{-1} - \left((\nu\mathrm{I}_{\mathrm{L}}^{\mathrm{s}} - \mathrm{I}_p^{\mathrm{s}}\mathrm{I}) - (\nu\mathrm{I}_{\mathrm{L}}^{\mathrm{s}} - \mathrm{I}_p^{\mathrm{s}}\mathrm{I})\circ\boldsymbol{\psi}_\mathrm{s}^{-1}\right)\mathbf{n}_\mathrm{s}, \boldsymbol{\mu}_{\mathrm{s},h}\rangle_{\mathcal{I}_h^{\mathrm{s}}} \qquad (3.46b)\\
&\quad + \sum_{\ell=1}^{n-1}\omega_\ell^{-1}\langle ((|\sigma_\mathrm{s}|\Lambda_{\mathrm{I}_{\mathrm{L}}^{\mathrm{s}}} - |\sigma_\mathrm{s}|\mathrm{I}_{\mathrm{L}}^{\mathrm{s}}\mathbf{n}_\mathrm{s})\cdot\boldsymbol{m}_\ell)\boldsymbol{m}_\ell, \boldsymbol{\mu}_{\mathrm{s},h}\rangle_{\mathcal{I}_h^{\mathrm{s}}} \quad \forall\, \boldsymbol{\mu}_{\mathrm{s},h}\in\mathbf{N}_h^{\mathrm{s}}.
\end{aligned}
$$

Proof. The identities (3.43)-(3.44) are straightforwardly obtained from the definition of the projection of the errors and (3.7) (see also [42, Lemma 3.1] and [43, Lemma 3.1]). Now, let $\boldsymbol{x}_\mathrm{s}\in\mathcal{I}_h^{\mathrm{s}}$. By (3.12a) and the definition of the extrapolation defined in Section 3.2, we rewrite (3.45a) as

$$\varepsilon^{\widetilde{p}_{\mathrm{d}}}(\boldsymbol{x}_{\mathrm{s}}) = \mathcal{P}^{\mathrm{d}} p_{\mathrm{d}}(\boldsymbol{x}_{\mathrm{d}}) - |\sigma_{\mathrm{d}}(\boldsymbol{x}_{\mathrm{d}})| \int_0^1 \kappa^{-1} \boldsymbol{E}_{\varPi^{\mathrm{d}}_{\mathbf{V}}\mathbf{u}_{\mathrm{d}}}(\boldsymbol{y}_{\mathrm{d}}(t)) \cdot \mathbf{n}_{\mathrm{d}} dt - \widetilde{p}_{\mathrm{d},h}(\boldsymbol{x}_{\mathrm{s}}).$$

Moreover,

$$\int_0^1 \kappa^{-1} \boldsymbol{E}_{\varPi^{\mathrm{d}}_{\mathbf{V}}\mathbf{u}_{\mathrm{d}}}(\boldsymbol{y}_{\mathrm{d}}(t)) \cdot \mathbf{n}_{\mathrm{d}} dt = -\int_0^1 \kappa^{-1} \mathrm{I}^{\mathrm{d}}_{\mathbf{u}}(\boldsymbol{y}_{\mathrm{d}}(t)) \cdot \mathbf{n}_{\mathrm{d}} dt + \int_0^1 \kappa^{-1} \mathbf{u}_{\mathrm{d}}(\boldsymbol{y}_{\mathrm{d}}(t)) \cdot \mathbf{n}_{\mathrm{d}} dt,$$

from which, proceeding in a similar way as in the proof of Lemma 2, we obtain

$$\begin{aligned}|\sigma_{\mathrm{d}}(\boldsymbol{x}_{\mathrm{d}})| \int_0^1 \kappa^{-1} \boldsymbol{E}_{\varPi^{\mathrm{d}}_{\mathbf{V}}\mathbf{u}_{\mathrm{d}}}(\boldsymbol{y}_{\mathrm{d}}(t)) \cdot \mathbf{n}_{\mathrm{d}} dt \ &= \kappa^{-1} |\sigma_{\mathrm{d}}(\boldsymbol{x}_{\mathrm{d}})| \varLambda_{\mathrm{I}^{\mathrm{d}}_{\mathbf{u}}}(\boldsymbol{x}_{\mathrm{d}}) - |\sigma_{\mathrm{d}}(\boldsymbol{x}_{\mathrm{d}})| \kappa^{-1} \mathrm{I}^{\mathrm{d}}_{\mathbf{u}}(\boldsymbol{x}_{\mathrm{d}}) \cdot \mathbf{n}_{\mathrm{d}} \\ &\quad + p_{\mathrm{d}}(\boldsymbol{x}_{\mathrm{d}}) - p_{\mathrm{d}} \circ \boldsymbol{\psi}_{\mathrm{d}}^{-1}(\boldsymbol{x}_{\mathrm{d}}).\end{aligned}$$

Similarly, it is easy to show that

$$\varepsilon^{\widetilde{\mathbf{u}}_{\mathrm{s}}} \circ \boldsymbol{\psi}^{-1}(\boldsymbol{x}_{\mathrm{s}}) = \boldsymbol{\mathcal{P}}^{\mathrm{s}} \mathbf{u}_{\mathrm{s}}(\boldsymbol{x}_{\mathrm{s}}) - \mathbf{u}_{\mathrm{s}}(\boldsymbol{x}_{\mathrm{s}}) + |\sigma_{\mathrm{s}}(\boldsymbol{x}_{\mathrm{s}})| \left(\varLambda_{\mathrm{I}^{\mathrm{s}}_{\mathrm{L}}}(\boldsymbol{x}_{\mathrm{s}}) - \mathrm{I}^{\mathrm{s}}_{\mathrm{L}}(\boldsymbol{x}_{\mathrm{s}}) \mathbf{n}_{\mathrm{s}} \right) + \mathbf{u}_{\mathrm{s}} \circ \boldsymbol{\psi}_{\mathrm{s}}^{-1}(\boldsymbol{x}_{\mathrm{s}}) - \widetilde{\mathbf{u}}_{\mathrm{s},h} \circ \boldsymbol{\psi}^{-1}(\boldsymbol{x}_{\mathrm{s}}).$$

On the other hand, from (3.12d) and (3.45d), we find that

$$\begin{aligned}\varepsilon^{\widetilde{\boldsymbol{\sigma}}_{\mathrm{s}}}(\boldsymbol{x}_{\mathrm{s}}) \mathbf{n}_{\mathrm{s}} \ :=& -(\nu \widetilde{\mathrm{L}}_{\mathrm{s},h} - \widetilde{p}_{\mathrm{s},h} \mathrm{I})(\boldsymbol{x}_{\mathrm{s}}) \mathbf{n}_{\mathrm{s}} + (\nu \varPi^{\mathrm{s}}_{\mathrm{G}} \mathrm{L}_{\mathrm{s}} - \varPi^{\mathrm{s}}_{Q} p_{\mathrm{s}} \mathrm{I}) \circ \boldsymbol{\psi}_{\mathrm{s}}^{-1}(\boldsymbol{x}_{\mathrm{s}}) \mathbf{n}_{\mathrm{s}} - \nu\tau(\varPi^{\mathrm{s}}_{\mathbf{V}} \mathbf{u}_{\mathrm{s}} - \boldsymbol{\mathcal{P}}^{\mathrm{s}} \mathbf{u}_{\mathrm{s}})(\boldsymbol{x}_{\mathrm{s}}) \\ & - \boldsymbol{E}_{\varPi^{\mathrm{s}}_{Q} \alpha_{\mathrm{s}}} \mathbf{n}_{\mathrm{s}}.\end{aligned}$$

Hence, for $\boldsymbol{\mu}_{\mathrm{s},h} \in \mathbf{N}^{\mathrm{s}}_h$, the above expressions together with (3.3c) and the definition of the L^2-projection $\mathcal{P}^{\mathrm{d}}$, imply

$$\begin{aligned}&\langle \varepsilon^{\widetilde{\boldsymbol{\sigma}}_{\mathrm{s}}} \mathbf{n}_{\mathrm{s}} + \sum_{\ell=1}^{n-1} \omega_\ell^{-1} (\varepsilon^{\widetilde{\mathbf{u}}_{\mathrm{s}}} \circ \boldsymbol{\psi}^{-1} \cdot \boldsymbol{m}_\ell) \boldsymbol{m}_\ell - \varepsilon^{\widetilde{p}_{\mathrm{d}}} \mathbf{n}_{\mathrm{d}}, \boldsymbol{\mu}_{\mathrm{s},h} \rangle_{\mathcal{I}^{\mathrm{s}}_h} = \langle (\nu \varPi^{\mathrm{s}}_{\mathrm{G}} \mathrm{L}_{\mathrm{s}} - \varPi^{\mathrm{s}}_{Q} p_{\mathrm{s}} \mathrm{I}) \circ \boldsymbol{\psi}_{\mathrm{s}}^{-1} \mathbf{n}_{\mathrm{s}}, \boldsymbol{\mu}_{\mathrm{s},h} \rangle_{\mathcal{I}^{\mathrm{s}}_h} \\ &\quad - \langle (\nu \mathrm{I}^{\mathrm{s}}_{\mathrm{L}} - \mathrm{I}^{\mathrm{s}}_{p} \mathrm{I}) \mathbf{n}_{\mathrm{s}}, \boldsymbol{\mu}_{\mathrm{s},h} \rangle_{\mathcal{I}^{\mathrm{s}}_h} - \langle (\mathcal{P}^{\mathrm{d}} p_{\mathrm{d}} - p_{\mathrm{d}}) \circ \boldsymbol{\psi}^{-1} \mathbf{n}_{\mathrm{d}} + \kappa^{-1} (|\sigma_{\mathrm{d}}| \varLambda_{\mathrm{I}^{\mathrm{d}}_{\mathbf{u}}} \mathbf{n}_{\mathrm{d}} - |\sigma_{\mathrm{d}}| \mathrm{I}^{\mathrm{d}}_{\mathbf{u}}) \circ \boldsymbol{\psi}^{-1}, \boldsymbol{\mu}_{\mathrm{s},h} \rangle_{\mathcal{I}^{\mathrm{s}}_h} \\ &\quad - \langle \alpha_{\mathrm{s}} \mathbf{n}_{\mathrm{s}}, \boldsymbol{\mu}_{\mathrm{s},h} \rangle_{\mathcal{I}^{\mathrm{s}}_h} - \langle p_{\mathrm{d}} \circ \boldsymbol{\psi}_{\mathrm{s}}^{-1} \mathbf{n}_{\mathrm{d}}, \boldsymbol{\mu}_{\mathrm{s},h} \rangle_{\mathcal{I}^{\mathrm{s}}_h} + \sum_{\ell=1}^{n-1} \omega_\ell^{-1} \langle ((|\sigma_{\mathrm{s}}| \varLambda_{\mathrm{I}^{\mathrm{s}}_{\mathrm{L}}} - |\sigma_{\mathrm{s}}| \mathrm{I}^{\mathrm{s}}_{\mathrm{L}} \mathbf{n}_{\mathrm{s}} + \mathbf{u}_{\mathrm{s}} \circ \boldsymbol{\psi}_{\mathrm{s}}^{-1}) \cdot \boldsymbol{m}_\ell) \boldsymbol{m}_\ell, \boldsymbol{\mu}_{\mathrm{s},h} \rangle_{\mathcal{I}^{\mathrm{s}}_h},\end{aligned}$$

from which, employing (3.11), we obtain (3.46b). In turn, for $\boldsymbol{x}_{\mathrm{d}} \in \mathcal{I}^{\mathrm{d}}_h$, the identity (3.46a) is proved in a completely analogous way. We omit further details. ■

We observe that the above equations are similar to those of the HDG scheme (3.7), where $\mathrm{I}^{\mathrm{s}}_{\mathrm{L}}$, $\mathrm{I}^{\mathrm{d}}_{\mathbf{u}}$, 0, and $\mathbf{0}$ play the role of J_{s}, $\mathbf{J}_{\mathrm{d}}$, f_{d} and $\mathbf{f}_{\mathrm{s}}$, respectively. Moreover,

$$\begin{aligned}\langle j^{\mathrm{nc}}_{\mathrm{d}} + j^{\delta}_{\mathrm{d}}, \mu_{\mathrm{d},h} \rangle_{\mathcal{I}^{\mathrm{d}}_h} \ &= \langle (\boldsymbol{\mathcal{P}}^{\mathrm{s}} \mathbf{u}_{\mathrm{s}} - \mathbf{u}_{\mathrm{s}}) \circ \boldsymbol{\psi} \cdot \mathbf{n}_{\mathrm{s}} - |\sigma_{\mathrm{s}}| \varLambda_{\mathrm{I}^{\mathrm{s}}_{\mathrm{L}}} \circ \boldsymbol{\psi} \cdot \mathbf{n}_{\mathrm{d}}, \mu_{\mathrm{d},h} \rangle_{\mathcal{I}^{\mathrm{d}}_h} + \langle |\sigma_{\mathrm{s}}| \mathrm{I}^{\mathrm{s}}_{\mathrm{L}} \circ \boldsymbol{\psi} \mathbf{n}_{\mathrm{d}}, \mu_{\mathrm{d},h} \mathbf{n}_{\mathrm{d}} \rangle_{\mathcal{I}^{\mathrm{d}}_h} \\ &\quad + \langle \left(\mathrm{I}^{\mathrm{d}}_{\mathbf{u}} - \mathrm{I}^{\mathrm{d}}_{\mathbf{u}} \circ \boldsymbol{\psi}_{\mathrm{d}}^{-1} \right) \cdot \mathbf{n}_{\mathrm{d}}, \mu_{\mathrm{d},h} \rangle_{\mathcal{I}^{\mathrm{d}}_h}, \\ \langle \mathbf{j}^{\mathrm{nc}}_{\mathrm{s}} + \mathbf{j}^{\delta}_{\mathrm{s}}, \boldsymbol{\mu}_{\mathrm{s},h} \rangle_{\mathcal{I}^{\mathrm{s}}_h} \ &= -\langle (\mathcal{P}^{\mathrm{d}} p_{\mathrm{d}} - p_{\mathrm{d}}) \circ \boldsymbol{\psi}^{-1} \mathbf{n}_{\mathrm{d}} + \kappa^{-1} |\sigma_{\mathrm{d}}| \varLambda_{\mathrm{I}^{\mathrm{d}}_{\mathbf{u}}} \mathbf{n}_{\mathrm{d}} \circ \boldsymbol{\psi}^{-1}, \boldsymbol{\mu}_{\mathrm{s},h} \rangle_{\mathcal{I}^{\mathrm{s}}_h}\end{aligned} \tag{3.47}$$

$$- \langle \kappa^{-1}|\sigma_{\rm d}|\mathrm{I}^{\rm d}_{\mathbf{u}} \circ \boldsymbol{\psi}^{-1} - \left((\nu \mathrm{I}^{\rm s}_{\rm L} - \mathrm{I}^{\rm s}_{p}\mathrm{I}) - (\nu \mathrm{I}^{\rm s}_{\rm L} - \mathrm{I}^{\rm s}_{p}\mathrm{I}) \circ \boldsymbol{\psi}_{\rm s}^{-1}\right) \mathbf{n}_{\rm s}, \boldsymbol{\mu}_{{\rm s},h}\rangle_{\mathcal{I}^{\rm s}_h} \tag{3.48}$$

$$+ \sum_{\ell=1}^{n-1} \omega_\ell^{-1} \langle (|\sigma_{\rm s}|\Lambda_{\mathrm{I}^{\rm s}_{\rm L}} - |\sigma_{\rm s}|\mathrm{I}^{\rm s}_{\rm L}\mathbf{n}_{\rm s}) \cdot \boldsymbol{m}_\ell)\boldsymbol{m}_\ell, \boldsymbol{\mu}_{{\rm s},h}\rangle_{\mathcal{I}^{\rm s}_h}. \tag{3.49}$$

Hence, we consider the result of Theorem 1 applied to this context. More precisely, we notice that

$$\begin{aligned} \|h_e^{(\beta-1)/2}(j^{\rm nc}_{\rm d} + j^{\delta}_{\rm d})\|^2_{\mathcal{I}^{\rm d}_h} \lesssim& \|h_e^{(\beta-1)/2}(\boldsymbol{\mathcal{P}}^{\rm s}\mathbf{u}_{\rm s} \circ \boldsymbol{\psi} - \mathbf{u}_{\rm s} \circ \boldsymbol{\psi})\|^2_{\mathcal{I}^{\rm d}_h} + \|h_e^{(\beta-1)/2}|\sigma_{\rm s}|\Lambda_{\mathrm{I}^{\rm s}_{\rm L}} \circ \boldsymbol{\psi}\|^2_{\mathcal{I}^{\rm d}_h} \\ &+ \|h_e^{(\beta-1)/2}|\sigma_{\rm s}|\mathrm{I}^{\rm s}_{\rm L} \circ \boldsymbol{\psi}\|^2_{\mathcal{I}^{\rm d}_h} + \|h_e^{(\beta-1)/2}\left(\mathrm{I}^{\rm d}_{\mathbf{u}} - \mathrm{I}^{\rm d}_{\mathbf{u}} \circ \boldsymbol{\psi}_{\rm d}^{-1}\right)\|^2_{\mathcal{I}^{\rm d}_h}, \end{aligned} \tag{3.50}$$

and

$$\begin{aligned} \|h_e^{(\beta-1)/2}(\mathbf{j}^{\rm nc}_{\rm s} + \mathbf{j}^{\delta}_{\rm s})\|^2_{\mathcal{I}^{\rm s}_h} \lesssim\;& \|h_e^{(\beta-1)/2}(\mathcal{P}^{\rm d}p_{\rm d} \circ \boldsymbol{\psi}^{-1} - p_{\rm d} \circ \boldsymbol{\psi}^{-1})\|^2_{\mathcal{I}^{\rm s}_h} + \|h_e^{(\beta-1)/2}\kappa^{-1}|\sigma_{\rm d}|\Lambda_{\mathrm{I}^{\rm d}_{\mathbf{u}}} \circ \boldsymbol{\psi}^{-1}\|^2_{\mathcal{I}^{\rm s}_h} \\ &+ \|h_e^{(\beta-1)/2}\kappa^{-1}|\sigma|\mathrm{I}^{\rm d}_{\mathbf{u}} \circ \boldsymbol{\psi}^{-1}\|^2_{\mathcal{I}^{\rm s}_h} + \|h_e^{(\beta-1)/2}(\nu \mathrm{I}^{\rm s}_{\rm L} - \mathrm{I}^{\rm s}_{p}\mathrm{I} - (\nu \mathrm{I}^{\rm s}_{\rm L} - \mathrm{I}^{\rm s}_{p}\mathrm{I}) \circ \boldsymbol{\psi}_{\rm s}^{-1})\|^2_{\mathcal{I}^{\rm s}_h} \\ &+ \|h_e^{(\beta-1)/2}|\sigma_{\rm s}|\Lambda_{\mathrm{I}^{\rm s}_{\rm L}}\|^2_{\mathcal{I}^{\rm s}_h} + \|h_e^{(\beta-1)/2}|\sigma_{\rm s}|\mathrm{I}^{\rm s}_{\rm L}\|^2_{\mathcal{I}^{\rm s}_h}. \end{aligned} \tag{3.51}$$

and observe that the first terms in (3.50) and (3.51) can be bounded using the approximation properties of the L^2-projection over $N^{\rm d}_h$ and $\mathbf{N}^{\rm s}_h$, respectively. In fact, we recall from [54, Lemma 1.59] that there exist positive constants $C_{\rm ns}$ and $C_{\rm nd}$, independent of h, such that

$$\begin{aligned} \|\boldsymbol{\mathcal{P}}^{\rm s}\mathbf{u}_{\rm s} \circ \boldsymbol{\psi} - \mathbf{u}_{\rm s} \circ \boldsymbol{\psi}\|^2_{\mathcal{I}^{\rm d}_h} &\le C_{\rm ns} h^{2l_{\mathbf{u}_{\rm s}}+1}|\mathbf{u}_{\rm s}|^2_{\mathbf{H}^{l_{\mathbf{u}_{\rm s}}+1}(\Omega_{\rm s})}, \\ \|\mathcal{P}^{\rm d}p_{\rm d} \circ \boldsymbol{\psi}^{-1} - p_{\rm d} \circ \boldsymbol{\psi}^{-1}\|^2_{\mathcal{I}^{\rm s}_h} &\le C_{\rm nd} h^{2l_{p_{\rm d}}+1}|p_{\rm d}|^2_{H^{l_{p_{\rm d}}+1}(\Omega_{\rm d})}. \end{aligned}$$

We stress that these constants take into account the nonconformity between the computational interfaces. Thus, we have

$$\|h_e^{(\beta-1)/2}(\boldsymbol{\mathcal{P}}^{\rm s}\mathbf{u}_{\rm s} \circ \boldsymbol{\psi} - \mathbf{u}_{\rm s} \circ \boldsymbol{\psi})\|^2_{\mathcal{I}^{\rm d}_h} \le C_{\rm ns} h^{2l_{\mathbf{u}_{\rm s}}+\beta}|\mathbf{u}_{\rm s}|^2_{\mathbf{H}^{l_{\mathbf{u}_{\rm s}}+1}(\Omega_{\rm s})}, \tag{3.52}$$

$$\|h_e^{(\beta-1)/2}(\mathcal{P}^{\rm d}p_{\rm d} \circ \boldsymbol{\psi}^{-1} - p_{\rm d} \circ \boldsymbol{\psi}^{-1})\|^2_{\mathcal{I}^{\rm s}_h} \le C_{\rm nd} h^{2l_{p_{\rm d}}+\beta}|p_{\rm d}|^2_{H^{l_{p_{\rm d}}+1}(\Omega_{\rm d})}. \tag{3.53}$$

On the other hand, following the proof of [101, Theorem 4.2] we deduce from (3.16), a scaling argument to bound the $L^2(\mathcal{I}^\star_h)$−norm in terms of its $L^2(\Omega^\star_h)$−norm, and Lemma 1, that

$$\begin{aligned} \|h_e^{(\beta-1)/2}(j^{\rm nc}_{\rm d} + j^{\delta}_{\rm d})\|^2_{\mathcal{I}^{\rm d}_h} \lesssim& C_{\rm ns} h^{2l_{\mathbf{u}_{\rm s}}+\beta}|\mathbf{u}_{\rm s}|^2_{\mathbf{H}^{l_{\mathbf{u}_{\rm s}}+1}(\Omega_{\rm s})} + h^\beta\Big(\max_{e\in\mathcal{I}^{\rm s}_h}(\delta_e^4 h_e^{-4}) + \max_{e\in\mathcal{I}^{\rm s}_h}(\delta_e h_e^{-1})^2\Big)\|\mathrm{I}^{\rm s}_{\rm L}\|^2_{\Omega^{\rm s}_h} \\ &+ h^\beta \max_{e\in\mathcal{I}^{\rm d}_h}(\delta_e h_e^{-1})|\kappa^{-1}\mathrm{I}^{\rm d}_{\mathbf{u}}|^2_{\mathbf{H}^1(\Omega^{\rm d}_h)}, \end{aligned}$$

and

$$\begin{aligned} \|h_e^{(\beta-1)/2}(\mathbf{j}^{\rm nc}_{\rm s} + \mathbf{j}^{\delta}_{\rm s})\|^2_{\mathcal{I}^{\rm s}_h} \lesssim\;& C_{\rm nd} h^{2l_{p_{\rm d}}+\beta}|p_{\rm d}|^2_{H^{l_{p_{\rm d}}+1}(\Omega_{\rm d})} + h^\beta \max_{e\in\mathcal{I}^{\rm s}_h}(\delta_e h_e^{-1})|\nu \mathrm{I}^{\rm s}_{\rm L} - \mathrm{I}^{\rm s}_{p}\mathrm{I}|^2_{\mathbf{H}^1(\Omega^{\rm s}_h)} \\ &+ h^\beta\Big(\max_{e\in\mathcal{I}^{\rm d}_h}(\delta_e^4 h_e^{-4}) + \max_{e\in\mathcal{I}^{\rm d}_h}(\delta_e h_e^{-1})\Big)\|\mathrm{I}^{\rm d}_{\mathbf{u}}\|^2_{\Omega^{\rm d}_h} + h^\beta\Big(\max_{e\in\mathcal{I}^{\rm s}_h}(\delta_e^4 h_e^{-4}) + \max_{e\in\mathcal{I}^{\rm s}_h}(\delta_e h_e^{-1})^2\Big)\|\mathrm{I}^{\rm s}_{\rm L}\|^2_{\Omega^{\rm s}_h}. \end{aligned}$$

Next, by Assumptions **(A)**, the fact that $(\delta_e^4 h_e^{-4} h^\beta)$ and $(\delta_e h_e^{-1} h^\beta)$ are bounded, with $\star \in \{\mathrm{s}, \mathrm{d}\}$, it follows that

$$\|h_e^{(\beta-1)/2}(j_{\rm d}^{\rm nc}+j_{\rm d}^{\delta})\|^2_{\mathcal{I}_h^{\rm d}} \lesssim C_{\rm ns}h^{2l_{\mathbf{u}_{\rm s}}+\beta}|\mathbf{u}_{\rm s}|^2_{\mathbf{H}^{l_{\mathbf{u}_{\rm s}}+1}(\Omega_{\rm s})}+\delta^4 h^{\beta-4}\|\mathrm{I}_{\rm L}^{\rm s}\|^2_{\Omega_h^{\rm s}}+\delta h^{\beta-1}|\mathrm{I}_{\mathbf{u}}^{\rm d}|^2_{\mathbf{H}^1(\Omega_h^{\rm d})}, \quad \text{and}$$

$$\|h_e^{(\beta-1)/2}(\mathbf{j}_{\rm s}^{\rm nc}+\mathbf{j}_{\rm s}^{\delta})\|^2_{\mathcal{I}_h^{\rm s}} \lesssim C_{\rm nd}h^{2l_{p_{\rm d}}+\beta}|p_{\rm d}|^2_{H^{l_{p_{\rm d}}+1}(\Omega_{\rm d})}+\delta h^{\beta-1}|\nu\mathrm{I}_{\rm L}^{\rm s}-\mathrm{I}_p^{\rm s}\mathrm{I}|^2_{\mathrm{H}^1(\Omega_h^{\rm s})}+\delta^4 h^{\beta-4}\left(\|\mathrm{I}_{\mathbf{u}}^{\rm d}\|^2_{\Omega_h^{\rm d}}+\|\mathrm{I}_{\rm L}^{\rm s}\|^2_{\Omega_h^{\rm s}}\right).$$

Then, bearing in mind the above, the estimates from Theorem 1 applied to (3.43) become

$$\begin{aligned}\mathcal{Q}(\varepsilon^{\mathrm{L}_{\rm s}},\boldsymbol{\varepsilon}^{\mathbf{u}_\star},\varepsilon^{\widehat{\mathbf{u}}_{\rm s}},\varepsilon^{p_{\rm d}},\varepsilon^{\widehat{p}_{\rm d}})^2 &\lesssim C_{\rm ns}h^{2l_{\mathbf{u}_{\rm s}}+\beta}|\mathbf{u}_{\rm s}|^2_{\mathbf{H}^{l_{\mathbf{u}_{\rm s}}+1}(\Omega_{\rm s})}+\delta h^{\beta-1}|\mathrm{I}_{\mathbf{u}}^{\rm d}|^2_{\mathbf{H}^1(\Omega_h^{\rm d})}+\left(\delta^4 h^{\beta-4}+1\right)\|\mathrm{I}_{\mathbf{u}}^{\rm d}\|^2_{\Omega_h^{\rm d}}\\ &+C_{\rm nd}h^{2l_{p_{\rm d}}+\beta}|p_{\rm d}|^2_{H^{l_{p_{\rm d}}+1}(\Omega_{\rm d})}+\delta h^{\beta-1}|\nu\mathrm{I}_{\rm L}^{\rm s}-\mathrm{I}_p^{\rm s}\mathrm{I}|^2_{\mathrm{H}^1(\Omega_h^{\rm s})}+\left(\nu^{-2}\delta^4 h^{\beta-4}+1\right)\|\nu\mathrm{I}_{\rm L}^{\rm s}\|^2_{\Omega_h^{\rm s}},\end{aligned}$$

and

$$\begin{aligned}\|\varepsilon^{\mathbf{u}_{\rm s}}\|^2_{\Omega_h^{\rm s}}+\|\varepsilon^{p_{\rm d}}\|^2_{\Omega_h^{\rm d}} \lesssim &\left(C^{\mathcal{S}}_{\delta,h}+(C^{p}_{\delta,h})^2\right)\mathcal{Q}(\varepsilon^{\mathrm{L}_{\rm s}},\boldsymbol{\varepsilon}^{\mathbf{u}_\star},\varepsilon^{\widehat{\mathbf{u}}_{\rm s}},\varepsilon^{p_{\rm d}},\varepsilon^{\widehat{p}_{\rm d}})^2+\delta|\nu\mathrm{I}_{\rm L}^{\rm s}-\mathrm{I}_p^{\rm s}\mathrm{I}|^2_{\mathrm{H}^1(\Omega_h^{\rm s})}\\ &+\delta|\mathrm{I}_{\mathbf{u}}^{\rm d}|^2_{\mathbf{H}^1(\Omega_h^{\rm d})}+\left(\delta^4h^{-3}+h^2\right)\|\mathrm{I}_{\mathbf{u}}^{\rm d}\|^2_{\Omega_h^{\rm d}}+\left(\delta^4h^{-3}\nu^{-2}+h^2\right)\|\nu\mathrm{I}_{\rm L}^{\rm s}\|^2_{\Omega_h^{\rm s}}\\ &+C_{\rm ns}h^{2l_{\mathbf{u}_{\rm s}}+1}|\mathbf{u}_{\rm s}|^2_{\mathbf{H}^{l_{\mathbf{u}_{\rm s}}+1}(\Omega_{\rm s})}+C_{\rm nd}h^{2l_{p_{\rm d}}+1}|p_{\rm d}|^2_{H^{l_{p_{\rm d}}+1}(\Omega_{\rm d})}.\end{aligned}$$

which, along with the properties of the HDG projectors (cf. (3.4)-(3.6)), we obtain the following result.

Theorem 2. Let us assume that Assumptions **(A)** and elliptic regularity are satisfied. If τ is of order one, $k\geq 1$, and $(\mathrm{L}_{\rm s},\mathbf{u}_\star,p_\star)\in \mathrm{H}^{l_\sigma+1}(\Omega_h^{\rm s})\times\mathbf{H}^{l_{\mathbf{u}_\star}+1}(\Omega_h^\star)\times H^{l_{p_\star}+1}(\Omega_h^\star)$, for $l_{\mathbf{u}_\star}$, l_σ and $l_{p_\star}\in[0,k]$, with $\star\in\{\mathrm{s},\mathrm{d}\}$, then there exists $h_0\in(0,1)$, such that for all $h<h_0$, the following holds:

$$\begin{aligned}&\|\mathbf{u}_{\rm d}-\mathbf{u}_{{\rm d},h}\|_{\Omega_h^{\rm d}}+\|\nu(\mathrm{L}_{\rm s}-\mathrm{L}_{{\rm s},h})\|_{\Omega_h^{\rm s}}+\|p_{\rm s}-p_{{\rm s},h}\|_{\Omega_h^{\rm s}}\\ \lesssim&\Big(C_{\rm nd}^{\frac12}h^{l_{p_{\rm d}}+\frac{\beta}{2}}+h^{l_{p_{\rm d}}+1}+\delta^{1/2}h^{l_{p_{\rm d}}-\frac{1-\beta}{2}}\Big)|p_{\rm d}|_{H^{l_{p_{\rm d}}+1}(\Omega_{\rm d})}+\Big(h^{l_\sigma+1}+\delta^{1/2}h^{l_\sigma-\frac{1-\beta}{2}}\Big)|\nu\mathrm{L}_{\rm s}-p_{\rm s}\mathrm{I}|_{\mathrm{H}^{l_\sigma+1}(\Omega_{\rm s})}\\ &+\Big(C_{\rm ns}^{\frac12}h^{l_{\mathbf{u}_{\rm s}}+\frac{\beta}{2}}+h^{l_{\mathbf{u}_{\rm s}}+1}+\delta^{1/2}h^{l_{\mathbf{u}_{\rm s}}-\frac{1-\beta}{2}}\Big)|\mathbf{u}_{\rm s}|_{\mathbf{H}^{l_{\mathbf{u}_{\rm s}}+1}(\Omega_{\rm s})}+\Big(h^{l_{\mathbf{u}_{\rm d}}+1}+\delta^{1/2}h^{l_{\mathbf{u}_{\rm d}}-\frac{1-\beta}{2}}\Big)|\mathbf{u}_{\rm d}|_{\mathbf{H}^{l_{\mathbf{u}_{\rm d}}+1}(\Omega_{\rm d})},\\ &\left(\|\varepsilon^{\mathbf{u}_{\rm s}}\|^2_{\Omega_h^{\rm s}}+\|\varepsilon^{p_{\rm d}}\|^2_{\Omega_h^{\rm d}}\right)^{\frac12}\lesssim\Big(C_{\rm nd}^{1/2}\delta h^{\frac{-3+\beta}{2}}+C_{\rm nd}^{1/2}h^{1/2}+\delta h^{-1/2}+h^2\Big)h^{l_{p_{\rm d}}}|p_{\rm d}|_{H^{l_{p_{\rm d}}+1}(\Omega_{\rm d})}\\ &\quad+\Big(\delta^{3/2}h^{\frac{\beta-4}{2}}+\delta^{1/2}+h^2\Big)h^{l_\sigma}|\nu\mathrm{L}_{\rm s}-p_{\rm s}\mathrm{I}|_{\mathrm{H}^{l_\sigma+1}(\Omega_{\rm s})}+\Big(\delta^{3/2}h^{\frac{\beta-4}{2}}+\delta^{1/2}+h^2\Big)h^{l_{\mathbf{u}_{\rm d}}}|\mathbf{u}_{\rm d}|_{\mathbf{H}^{l_{\mathbf{u}_{\rm d}}+1}(\Omega_{\rm d})}\\ &\quad+\Big(C_{\rm ns}^{1/2}\delta h^{\frac{-3+\beta}{2}}+C_{\rm ns}^{1/2}h^{1/2}+\delta h^{-1/2}+h^2\Big)h^{l_{\mathbf{u}_{\rm s}}}|\mathbf{u}_{\rm s}|_{\mathbf{H}^{l_{\mathbf{u}_{\rm s}}+1}(\Omega_{\rm s})},\\ &\|\mathbf{u}_{\rm s}-\mathbf{u}_{{\rm s},h}\|_{\Omega_h^{\rm s}}+\|p_{\rm d}-p_{{\rm d},h}\|_{\Omega_h^{\rm d}}\\ &\quad\lesssim\Big(\|\varepsilon^{\mathbf{u}_{\rm s}}\|^2_{\Omega_h^{\rm s}}+\|\varepsilon^{p_{\rm d}}\|^2_{\Omega_h^{\rm d}}\Big)^{\frac12}+\Big(+h_{\rm d}^{2(l_{p_{\rm d}}+1)}|p_{\rm d}|^2_{H^{l_{p_{\rm d}}+1}(\Omega_{\rm d})}+h_{\rm s}^{2(l_{\mathbf{u}_{\rm s}}+1)}|\mathbf{u}_{\rm s}|^2_{\mathbf{H}^{l_{\mathbf{u}_{\rm s}}+1}(\Omega_{\rm s})}\Big)^{1/2}.\end{aligned}$$

Corollary 2. Suppose that the assumptions of Theorem 2 hold and $(\mathrm{L}_{\rm s},\mathbf{u}_\star,p_\star)\in\mathrm{H}^{k+1}(\Omega_h^{\rm s})\times\mathbf{H}^{k+1}(\Omega_h^\star)\times H^{k+1}(\Omega_h^\star)$. Let $\delta=C_{\rm g}h^{1+\gamma}$ with $C_{\rm g}\geq 0$ and $\gamma\in(3/4,3]$, and $\beta\in[0,2]\cap[0,2\gamma-1)$, with $\star\in\{\mathrm{s},\mathrm{d}\}$. There hold

$$\|\mathbf{u}_{\rm d}-\mathbf{u}_{{\rm d},h}\|_{\Omega_h^{\rm d}}+\|\nu(\mathrm{L}_{\rm s}-\mathrm{L}_{{\rm s},h})\|_{\Omega_h^{\rm s}}+\|p_{\rm s}-p_{{\rm s},h}\|_{\Omega_h^{\rm s}}\lesssim(C_{\rm ns}^{1/2}+C_{\rm nd}^{1/2})h^{k+\frac{\beta}{2}}+h^{k+1}\big(1+C_{\rm g}^{1/2}h^{\frac{\gamma+\beta-2}{2}}\big),$$

$$\big(\|\varepsilon^{\mathbf{u}_{\rm s}}\|^2_{\Omega_h^{\rm s}}+\|\varepsilon^{p_{\rm d}}\|^2_{\Omega_h^{\rm d}}\big)^{1/2}\lesssim h^{k+1}\big(h+(C_{\rm nd}^{1/2}+C_{\rm ns}^{1/2})h^{-1/2}+C_{\rm g}^{1/2}h^{\frac{\gamma-1}{2}}+\big(C_{\rm ns}^{1/2}+C_{\rm nd}^{1/2}\big)C_{\rm g}h^{\gamma+\frac{\beta-3}{2}}\big),$$

$$\|\mathbf{u}_{\mathrm{s}}-\mathbf{u}_{\mathrm{s},h}\|_{\Omega_h^{\mathrm{s}}}+\|p_{\mathrm{d}}-p_{\mathrm{d},h}\|_{\Omega_h^{\mathrm{d}}}\lesssim h^{k+1}\big(1+(C_{\mathrm{nd}}^{1/2}+C_{\mathrm{ns}}^{1/2})h^{-1/2}+C_{\mathrm{g}}^{1/2}h^{\frac{\gamma-1}{2}}+\big(C_{\mathrm{ns}}^{1/2}+C_{\mathrm{nd}}^{1/2}\big)C_{\mathrm{g}}h^{\gamma+\frac{\beta-3}{2}}\big).$$

We now explain the consequences of this corollary for some particular cases.

(C.1) *No-gap and no hanging nodes.* In this case, $C_{\mathrm{ns}}=C_{\mathrm{nd}}=C_{\mathrm{g}}=0$ and our result shows optimal order of convergence of h^{k+1} for all the variables and order h^{k+2} for the projection of the errors $\varepsilon^{\mathbf{u}_{\mathrm{s}}}$ and $\varepsilon^{p_{\mathrm{d}}}$, as expected.

(C.2) *No-gap and hanging nodes.* In this case, $C_{\mathrm{g}}=0$, but $C_{\mathrm{ns}}\neq 0$ and $C_{\mathrm{nd}}\neq 0$. In this situation, since $C_{\mathrm{g}}=0$, we can take $\beta=2$. Therefore, we obtain optimal order of convergence of h^{k+1} for the variables $\mathbf{u}_{\mathrm{d}}$, L_{s} and p_{s}, but suboptimal order of $h^{k+1/2}$ for the projection of the errors $\varepsilon^{\mathbf{u}_{\mathrm{s}}}$ and $\varepsilon^{p_{\mathrm{d}}}$ and also for the errors in $\mathbf{u}_{\mathrm{s}}$ and p_{d}.

(C.3) *Gap δ of order h^2 and no hanging nodes.* Here $\gamma=1$, which implies that $\beta=1-\epsilon$ for all $\epsilon>0$, whereas the nonconformity constants C_{ns} and C_{nd} vanish. This yields, for all the variables, order of convergence $h^{k+1-\epsilon}$ for all $\epsilon>0$.

(C.4) *Gap δ of order h^2 and hanging nodes.* Again, $\gamma=1$ and $\beta=1-\epsilon$ for all $\epsilon>0$, but now $C_{\mathrm{ns}}\neq 0$ and $C_{\mathrm{nd}}\neq 0$. Therefore, an order of convergence of $h^{k+1/2-\epsilon}$ for all $\epsilon>0$ is attained for the variables $\mathbf{u}_{\mathrm{d}}$, L_{s} and p_{s} and $h^{k+1/2}$ for all the other variables.

(C.5) *Gap δ of order $h^{7/4}$ and no hanging nodes.* In this case $\gamma=3/4$, $\beta=1/2-\epsilon$ for all $\epsilon>0$, and $C_{\mathrm{ns}}=C_{\mathrm{nd}}=0$. Then, the order of convergence is $h^{k+5/8-\epsilon}$ for all $\epsilon>0$ for the variables $\mathbf{u}_{\mathrm{d}}$, L_{s} and p_{s} and $h^{k+7/8}$ for the rest of the variables.

(C.6) *Gap δ of order $h^{7/4}$ and hanging nodes.* Here $\gamma=3/4$ and $\beta=1/2-\epsilon$ for all $\epsilon>0$, whereas $C_{\mathrm{ns}}\neq 0$ and $C_{\mathrm{nd}}\neq 0$. Hence, an order of convergence of $h^{k+1/4-\epsilon}$ for all $\epsilon>0$ is attained for the variables $\mathbf{u}_{\mathrm{d}}$, L_{s} and p_{s} and $h^{k+1/2}$ for the rest of the variables.

We observe that the introduction of the constant β as exponent in the first term of the right-hand side of the first equation of Corollary 2 slightly improves the theoretical convergence rate of the variables involved there, despite the presence of the non-conformity constants.

We end this section by considering the particular case where the discrete interfaces $\mathcal{I}_h^{\mathrm{d}}$ and $\mathcal{I}_h^{\mathrm{s}}$ satisfy the requirement set out in Section 3.4.3. In this case, Lemma 7 suggests an improvement of $h^{3/2}$ in the term associated to $\mathbf{j}_{\mathrm{s}}^{\mathrm{nc}}$, whereas the term associated to $j_{\mathrm{d}}^{\mathrm{nc}}$ vanishes. Thus, the *semi-aligned* variant of Corollary 2 is established as follows.

Corollary 3. Let us consider the same assumptions as in Corollary 2. If the discrete interfaces are *semi-aligned*, then

$$\big(\|\varepsilon^{\mathbf{u}_{\mathrm{s}}}\|_{\Omega_h^{\mathrm{s}}}^2+\|\varepsilon^{p_{\mathrm{d}}}\|_{\Omega_h^{\mathrm{d}}}^2\big)^{1/2}\lesssim h^{k+1}\big(h+C_{\mathrm{nd}}^{1/2}h+C_{\mathrm{g}}^{1/2}h^{\frac{\gamma-1}{2}}+C_{\mathrm{nd}}^{1/2}C_{\mathrm{g}}h^{\gamma+\frac{\beta-3}{2}}\big),$$

$$\|\mathbf{u}_{\mathrm{s}}-\mathbf{u}_{\mathrm{s},h}\|_{\Omega_h^{\mathrm{s}}}+\|p_{\mathrm{d}}-p_{\mathrm{d},h}\|_{\Omega_h^{\mathrm{d}}}\lesssim h^{k+1}\big(1+C_{\mathrm{nd}}^{1/2}h+C_{\mathrm{g}}^{1/2}h^{\frac{\gamma-1}{2}}+C_{\mathrm{nd}}^{1/2}C_{\mathrm{g}}h^{\gamma+\frac{\beta-3}{2}}\big).$$

Let us comment on the consequences of this result.

(D.1) *No-gap and hanging nodes.* Here, $C_\mathrm{g} = C_\mathrm{ns} = 0$, but $C_\mathrm{nd} \neq 0$. Therefore, optimal order of convergence of h^{k+1} for all the variables and order h^{k+2} for the projection of the errors $\varepsilon^{\mathbf{u}_\mathrm{s}}$ and $\varepsilon^{p_\mathrm{d}}$, which improves the power result in **(C.2)**.

(D.2) *Gap $\delta = h^2$ and hanging nodes.* Here, $\gamma = 1$ and $\beta = 1 - \epsilon$ for all $\epsilon > 0$, but now $C_\mathrm{ns} = 0$ and $C_\mathrm{nd} \neq 0$. Therefore, we improve the order of convergence stated in **(C.4)** since now $h^{k+1-\epsilon}$ for all $\epsilon > 0$ is attained for the projection of the errors $\varepsilon^{\mathbf{u}_\mathrm{s}}$ and $\varepsilon^{p_\mathrm{d}}$ and also for the errors in $\mathbf{u}_\mathrm{s}$ and p_d.

(D.3) *Gap $\delta = h^{7/4}$ and hanging nodes.* In this case, there is no improvement in the order of convergence compared to case **(C.6)**.

3.6 Numerical results

We consider four numerical results we the aim of illustrating the convergence of our HDG method presented in Section 3.3 for the two dimensional case. In all of them, we consider the computational domain $\Omega = \Omega_\mathrm{s} \cup \Omega_\mathrm{d} \cup \Sigma$, where $\Omega_\mathrm{s} = (0,1)\times(1/2,1)$, $\Omega_\mathrm{d} = (0,1)\times(0,1/2)$, and $\Sigma = (0,1)\times\{1/2\}$. In turn, we approach our numerical examples by two computational subdomains $\Omega_h^\mathrm{s} = (0,1)\times(1/2+\delta,1)$, $\Omega_h^\mathrm{d} = (0,1)\times(0,1/2-\delta)$, i.e., two rectangular meshed subdomains separated by a flat interface centered at $y = 1/2$. In addition, we define the manufactured exact solution:

$$P_\mathrm{s} = \mathrm{e}^{-x-y} - 2\mathrm{e}^{-2}\left(\sqrt{\mathrm{e}}-1\right)^2\left(\sqrt{\mathrm{e}}+1\right), \quad \mathbf{u}_\mathrm{s} = \begin{pmatrix} \pi\cos(\pi x)\sin(\pi y) \\ -\pi\cos(\pi y)\sin(\pi x) \end{pmatrix},$$
$$p_\mathrm{d} = \cos(\pi x)\cos(\pi y), \quad \text{and} \quad \mathbf{u}_\mathrm{d} = \begin{pmatrix} \pi\cos(\pi y)\sin(\pi x) \\ \pi\cos(\pi x)\sin(\pi y) \end{pmatrix}.$$

Also, hereafter we take $\kappa = \mathbb{I}$, $\nu = 1$, $\omega_1 = 1$ and the stabilization parameter $\tau \equiv 1$. Subsequently, we define the errors:

$$e(\mathrm{L}) = \|\mathrm{L}_\mathrm{s} - \mathrm{L}_{\mathrm{s},h}\|_{\Omega_\mathrm{s}}, \qquad e(\mathbf{u}) = \left(\|\mathbf{u}_\mathrm{s} - \mathbf{u}_{\mathrm{s},h}\|^2_{0,\Omega_\mathrm{s}} + \|\mathbf{u}_\mathrm{d} - \mathbf{u}_{\mathrm{d},h}\|^2_{\Omega_\mathrm{d}}\right)^{1/2},$$
$$e(p) = \left(\|P_\mathrm{s} - P_{\mathrm{s},h}\|^2_{\Omega_\mathrm{s}} + \|p_\mathrm{d} - p_{\mathrm{d},h}\|^2_{\Omega_\mathrm{d}}\right)^{1/2}, \quad \widehat{e} = \left(\|\boldsymbol{\mathcal{P}}^\mathrm{s}\mathbf{u}_\mathrm{s} - \widehat{\mathbf{u}}_{\mathrm{s},h}\|^2_{\partial\Omega_\mathrm{s}} + \left\|\mathcal{P}^\mathrm{d}p_\mathrm{d} - \widehat{p}_{\mathrm{d},h}\right\|^2_{\partial\Omega_\mathrm{d}}\right)^{1/2},$$

$$P_{\mathrm{s},h} = p_{\mathrm{s},h} - \frac{1}{|\Omega_\mathrm{s}|}\int_{\Omega_\mathrm{s}\setminus\Omega_h^\mathrm{s}} \boldsymbol{E}_{p_{\mathrm{s},h}},$$

where $\boldsymbol{E}$ denotes the local extrapolation defined in Section 3.2 and $p_{\mathrm{s},h}$ is the discrete pressure of our HDG scheme that satisfies (3.7e). Next, the experimental convergence rates are set as

$$r = -2\frac{\log(\widetilde{e}/e)}{\log(\widetilde{N}/N)},$$

where e and $\widetilde{e}$ denote errors computed on two consecutive meshes with N and $\widetilde{N}$ elements, respectively.

6.1. No gap. In our first numerical experiment, we take $\delta = 0$ and consider two different scenarios: one free of hanging nodes and one containing hanging nodes on the discrete interfaces. For the first scenario (case **(C.1)** above), the results in Table 3.1, confirm the theoretical rate of convergence for all variables provided by Corollary 2 (for $k = 4$, the error $\widehat{e}$ calculated in the last two rows is affected by round-off errors). For the second scenario, we take coarser meshes for Ω_{d} such that each interface edge corresponds to two interface edges on the meshes for Ω_{s}, effectively introducing one hanging node per side. This corresponds to case **(D.1)**. Table 3.2 shows optimal order of convergence for all variables in this case, observing superconvergence h^{k+2} in the numerical trace, which is the theoretical order of convergence provided by Corollary 3.

k	N	#d.o.f.	$e(\mathrm{L})$	r	$e(\mathbf{u})$	r	$e(p)$	r	$\widehat{e}$	$\widehat{r}$
	32	162	4.32e-01	$*$	3.06e-01	$*$	1.83e-01	$*$	3.11e-02	$*$
	128	642	1.06e-01	2.03	7.49e-02	2.03	4.30e-02	2.09	4.96e-03	2.65
1	492	2462	2.76e-02	1.99	2.00e-02	1.96	1.11e-02	2.01	7.23e-04	2.86
	1978	9896	7.06e-03	1.96	4.99e-03	1.99	2.71e-03	2.02	7.25e-05	3.30
	7834	39176	1.78e-03	2.00	1.27e-03	1.99	6.74e-04	2.02	9.32e-06	2.98
	32	234	6.16e-02	$*$	3.49e-02	$*$	2.42e-02	$*$	2.10e-03	$*$
	128	930	7.87e-03	2.97	4.67e-03	2.90	2.72e-03	3.15	8.07e-05	4.70
2	492	3569	1.13e-03	2.88	6.61e-04	2.90	3.64e-04	2.99	4.61e-06	4.25
	1978	14348	1.47e-04	2.93	8.35e-05	2.97	4.59e-05	2.98	3.14e-07	3.86
	7834	56804	1.76e-05	3.08	1.03e-05	3.04	5.55e-06	3.07	1.85e-08	4.12
	32	306	9.50e-03	$*$	4.67e-03	$*$	2.55e-03	$*$	7.12e-05	$*$
	128	1218	5.27e-04	4.17	2.67e-04	4.13	1.36e-04	4.23	2.01e-06	5.14
3	492	4676	3.68e-05	3.95	1.92e-05	3.91	9.82e-06	3.90	8.06e-08	4.78
	1978	18800	2.53e-06	3.85	1.27e-06	3.91	6.48e-07	3.91	2.66e-09	4.90
	7834	74432	1.62e-07	3.99	7.98e-08	4.02	4.07e-08	4.02	8.06e-11	5.08
	32	378	9.45e-04	$*$	4.66e-04	$*$	2.63e-04	$*$	3.08e-06	$*$
	128	1506	2.94e-05	5.01	1.49e-05	4.97	7.66e-06	5.10	4.89e-08	5.98
4	492	5783	1.25e-06	4.69	6.04e-07	4.76	3.05e-07	4.79	1.03e-09	5.73
	1978	23252	4.37e-08	4.82	2.00e-08	4.90	1.06e-08	4.83	2.22e-11	5.52
	7834	92060	1.25e-09	5.17	6.00e-10	5.10	3.06e-10	5.15	5.95e-13	5.26

Table 3.1: History of convergence of the HDG method for $\delta = 0$ and without hanging nodes

6.2. Gap of order $h^{7/4}$. According to Corollary 2, γ must be larger than $3/4$. In this experiment, we want to observe the behavior of the errors when γ is equal to $3/4$, which means δ of order $h^{7/4}$. Similarly to the previous example, we divide this experiment in two different scenarios. First, we suppose again that the meshes are free of "hanging nodes" (case **(C.5)**), i.e., there is a one-to-one face bijection between the two interfaces, which means that $C_{\mathrm{ns}} = C_{\mathrm{nd}} = 0$. The behavior of the errors reported in Table 3.3 is better than the prediction of Corollary 2. In fact, we observe optimal rates for all the variables and superconvergence in $\widehat{e}$. For the second scenario, we add hanging nodes on the bottom mesh as before, introducing one per interface edge. This corresponds to case **(D.3)**. In Table 3.4 we show the results for this case. We again observe optimal and superconvergent rates, which is better than what the theory predicted.

k	N	#d.o.f.	$e(\mathrm{L})$	r	$e(\mathbf{u})$	r	$e(p)$	r	$\widehat{e}$	$\widehat{r}$
	20	118	4.31e-01	$*$	5.53e-01	$*$	2.76e-01	$*$	4.93e-02	$*$
	80	486	1.06e-01	2.03	1.33e-01	2.06	7.25e-02	1.93	6.10e-03	3.01
1	310	1892	2.76e-02	1.98	3.22e-02	2.09	1.88e-02	1.99	8.44e-04	2.92
	1236	7618	7.06e-03	1.97	8.32e-03	1.96	4.91e-03	1.95	9.93e-05	3.10
	4906	30292	1.78e-03	2.00	2.10e-03	2.00	1.22e-03	2.01	1.31e-05	2.94
	20	168	6.16e-02	$*$	2.42e-01	$*$	5.90e-02	$*$	1.47e-02	$*$
	80	696	7.87e-03	2.97	1.55e-02	3.96	7.59e-03	2.96	2.94e-04	5.65
2	310	2714	1.13e-03	2.87	1.98e-03	3.04	1.02e-03	2.96	1.89e-05	4.05
	1236	10931	1.47e-04	2.95	2.77e-04	2.84	1.43e-04	2.84	1.38e-06	3.79
	4906	43478	1.76e-05	3.07	3.50e-05	3.00	1.77e-05	3.03	9.04e-08	3.95
	20	218	9.50e-03	$*$	4.47e-02	$*$	1.38e-02	$*$	9.59e-04	$*$
	80	906	5.27e-04	4.17	2.23e-03	4.32	9.23e-04	3.90	2.07e-05	5.54
3	310	3536	3.68e-05	3.93	1.24e-04	4.26	5.41e-05	4.19	5.64e-07	5.32
	1236	14244	2.53e-06	3.87	8.67e-06	3.85	3.90e-06	3.80	2.24e-08	4.66
	4906	56664	1.62e-07	3.99	5.92e-07	3.89	2.53e-07	3.97	7.91e-10	4.85
	20	268	9.60e-04	$*$	1.38e-02	$*$	3.25e-03	$*$	2.35e-04	$*$
	80	1116	2.94e-05	5.03	2.22e-04	5.96	9.25e-05	5.13	1.05e-06	7.80
4	310	4358	1.25e-06	4.66	6.86e-06	5.13	3.00e-06	5.06	1.72e-08	6.07
	1236	17557	4.37e-08	4.85	2.89e-07	4.58	1.20e-07	4.65	3.69e-10	5.56
	4906	69850	1.25e-09	5.16	9.30e-09	4.99	3.87e-09	4.99	7.01e-12	5.75

Table 3.2: History of convergence of the HDG method for $\delta = 0$ and with hanging nodes

6.3. Gap of order h. We now consider the last numerical example taking a gap $\delta = h$ and that the meshes are free of “hanging nodes". Since $\gamma = 0$, this case is not covered by the analysis but we observe that the approximations of all the variables converge with optimal order according to Table 3.5. Superconvergence of the numerical trace variables is also achieved, except for the last mesh in the case $k = 4$, probably due to round-off errors.

k	N	#d.o.f.	$e(\mathrm{L})$	r	$e(\mathbf{u})$	r	$e(p)$	r	$\widehat{e}$	$\widehat{r}$
	32	162	4.32e-01	$*$	3.06e-01	$*$	1.83e-01	$*$	3.20e-02	$*$
	128	642	1.06e-01	2.03	7.48e-02	2.03	4.30e-02	2.09	5.07e-03	2.66
1	492	2462	2.95e-02	1.90	2.06e-02	1.92	1.20e-02	1.89	7.10e-04	2.92
	1976	9882	7.11e-03	2.04	5.01e-03	2.03	2.72e-03	2.14	7.89e-05	3.16
	7876	39398	1.77e-03	2.02	1.26e-03	1.99	6.64e-04	2.04	9.55e-06	3.06
	32	234	6.16e-02	$*$	3.49e-02	$*$	2.41e-02	$*$	2.15e-03	$*$
	128	930	7.87e-03	2.97	4.67e-03	2.90	2.71e-03	3.15	8.25e-05	4.71
2	492	3569	1.11e-03	2.91	6.58e-04	2.91	3.67e-04	2.97	4.87e-06	4.20
	1976	14328	1.43e-04	2.94	8.32e-05	2.97	4.47e-05	3.03	3.00e-07	4.01
	7876	57125	1.72e-05	3.06	1.02e-05	3.03	5.44e-06	3.05	1.78e-08	4.08
	32	306	9.50e-03	$*$	4.67e-03	$*$	2.55e-03	$*$	9.03e-05	$*$
	128	1218	5.27e-04	4.17	2.67e-04	4.13	1.36e-04	4.23	2.28e-06	5.31
3	492	4676	4.44e-05	3.67	2.14e-05	3.75	1.17e-05	3.65	1.05e-07	4.57
	1976	18774	2.55e-06	4.11	1.26e-06	4.07	6.46e-07	4.16	2.79e-09	5.22
	7876	74852	1.60e-07	4.01	7.88e-08	4.01	4.01e-08	4.02	8.46e-11	5.06
	32	378	9.45e-04	$*$	4.66e-04	$*$	2.63e-04	$*$	3.28e-06	$*$
	128	1506	2.94e-05	5.01	1.49e-05	4.97	7.66e-06	5.10	4.95e-08	6.05
4	492	5783	1.19e-06	4.77	6.14e-07	4.74	3.05e-07	4.79	1.11e-09	5.64
	1976	23220	4.03e-08	4.87	1.96e-08	4.96	9.77e-09	4.95	1.96e-11	5.80
	7876	92579	1.22e-09	5.06	6.02e-10	5.04	2.99e-10	5.04	3.87e-13	5.67

Table 3.3: History of convergence of the HDG method for $\delta = h^{7/4}$ and without hanging nodes

k	N	#d.o.f.	$e(\mathrm{L})$	r	$e(\mathbf{u})$	r	$e(p)$	r	$\widehat{e}$	$\widehat{r}$
	20	118	4.31e-01	$*$	5.53e-01	$*$	2.76e-01	$*$	5.01e-02	$*$
	80	486	1.06e-01	2.03	1.33e-01	2.06	7.25e-02	1.93	6.19e-03	3.02
1	310	1892	2.95e-02	1.88	3.25e-02	2.08	1.93e-02	1.95	8.35e-04	2.96
	1234	7604	7.11e-03	2.06	8.69e-03	1.91	5.05e-03	1.95	1.10e-04	2.94
	4932	30466	1.77e-03	2.01	2.09e-03	2.06	1.22e-03	2.05	1.32e-05	3.05
	20	168	6.16e-02	$*$	2.42e-01	$*$	5.89e-02	$*$	1.48e-02	$*$
	80	696	7.87e-03	2.97	1.55e-02	3.96	7.59e-03	2.96	2.91e-04	5.66
2	310	2714	1.11e-03	2.90	1.98e-03	3.04	1.02e-03	2.96	1.89e-05	4.04
	1234	10911	1.43e-04	2.96	2.72e-04	2.87	1.43e-04	2.84	1.36e-06	3.81
	4932	43727	1.72e-05	3.05	3.58e-05	2.93	1.78e-05	3.01	9.51e-08	3.84
	20	218	9.50e-03	$*$	4.46e-02	$*$	1.38e-02	$*$	9.60e-04	$*$
	80	906	5.27e-04	4.17	2.23e-03	4.32	9.23e-04	3.90	2.10e-05	5.52
3	310	3536	4.44e-05	3.65	1.24e-04	4.26	5.45e-05	4.18	5.73e-07	5.32
	1234	14218	2.55e-06	4.13	1.04e-05	3.60	4.26e-06	3.69	2.84e-08	4.35
	4932	56988	1.60e-07	4.00	5.87e-07	4.15	2.55e-07	4.06	7.90e-10	5.17
	20	268	9.60e-04	$*$	1.38e-02	$*$	3.25e-03	$*$	2.35e-04	$*$
	80	1116	2.94e-05	5.03	2.22e-04	5.96	9.25e-05	5.13	1.13e-06	7.70
4	310	4358	1.19e-06	4.74	6.86e-06	5.13	3.00e-06	5.06	1.74e-08	6.17
	1234	17525	4.03e-08	4.90	2.76e-07	4.65	1.25e-07	4.60	3.64e-10	5.59
	4932	70249	1.22e-09	5.05	1.01e-08	4.78	3.99e-09	4.97	7.30e-12	5.64

Table 3.4: History of convergence of the HDG method for $\delta = h^{7/4}$ and with hanging nodes

k	N	#d.o.f.	$e(\mathrm{L})$	r	$e(\mathbf{u})$	r	$e(p)$	r	$\widehat{e}$	$\widehat{r}$
	32	162	4.32e-01	$*$	3.06e-01	$*$	1.83e-01	$*$	3.33e-02	$*$
	128	642	1.06e-01	2.03	7.48e-02	2.03	4.30e-02	2.09	5.38e-03	2.63
1	492	2462	2.73e-02	2.01	1.99e-02	1.97	1.11e-02	2.01	8.91e-04	2.67
	1978	9896	7.06e-03	1.94	4.99e-03	1.99	2.71e-03	2.03	1.02e-04	3.11
	7840	39290	1.77e-03	2.01	1.26e-03	1.99	6.67e-04	2.04	1.55e-05	2.74
	32	234	6.16e-02	$*$	3.49e-02	$*$	2.41e-02	$*$	2.23e-03	$*$
	128	930	7.87e-03	2.97	4.67e-03	2.90	2.71e-03	3.15	8.83e-05	4.66
2	492	3569	1.16e-03	2.84	6.75e-04	2.87	3.65e-04	2.98	5.46e-06	4.13
	1978	14348	1.47e-04	2.97	8.35e-05	3.00	4.59e-05	2.98	3.47e-07	3.96
	7840	56963	1.73e-05	3.10	1.02e-05	3.05	5.46e-06	3.09	2.05e-08	4.11
	32	306	9.49e-03	$*$	4.66e-03	$*$	2.56e-03	$*$	1.27e-04	$*$
	128	1218	5.26e-04	4.17	2.67e-04	4.13	1.36e-04	4.23	3.57e-06	5.16
3	492	4676	3.64e-05	3.97	1.92e-05	3.91	9.80e-06	3.91	2.47e-07	3.97
	1978	18800	2.53e-06	3.83	1.27e-06	3.91	6.49e-07	3.90	9.61e-09	4.66
	7840	74636	1.59e-07	4.01	7.94e-08	4.03	4.01e-08	4.04	5.09e-10	4.27
	32	378	9.45e-04	$*$	4.66e-04	$*$	2.63e-04	$*$	4.03e-06	$*$
	128	1506	2.94e-05	5.00	1.49e-05	4.97	7.67e-06	5.10	6.07e-08	6.05
4	492	5783	1.31e-06	4.63	6.24e-07	4.71	3.10e-07	4.76	1.77e-09	5.25
	1978	23252	4.37e-08	4.88	2.00e-08	4.94	1.06e-08	4.86	2.99e-11	5.87
	7840	92309	1.20e-09	5.22	5.92e-10	5.11	2.94e-10	5.20	3.24e-12	3.23

Table 3.5: History of convergence of the HDG method for $\delta = h$ and without hanging nodes

CHAPTER 4

Conclusions and future work

4.1 Conclusions

We summarize the main contributions and conclusions of the thesis.

- Chapter 1. We have developed and analyzed a mixed finite element method for the coupled Navier–Stokes and transport equations with nonlinear transmission conditions. We proved well-posedness of both, the continuous and discrete formulations, specified finite element subspaces and show the convergence properties of the proposed numerical scheme. This work is a contribution that provides a mathematical framework to handle nonlinear transmission conditions in domains with mixed boundary conditions. This is achieved by introducing Lagrange multipliers associated to the trace of salt concentration. The proposed method provides the theoretical foundations and numerical framework for modeling different configurations inspired by reverse osmosis processes that we explored in Chapter 2. In fact, all of these perspectives can also be adapted with minor modifications to the model presented here.
- Chapter 2. A new numerical model based on two-dimensional mixed finite element method has been used to study the fluid flow patterns, concentration of salt, pressure losses and permeate flow in desalination channels, inspired by reverse osmosis processes. The simulations are performed in a Reynolds number range for laminar flow less than 170, typical of sea water membrane module operation. They are based on two different perspectives, the first using the Navier–Stokes coupled to transport equations for the case of empty channels, and also for different configurations of explicit spacers. The second perspective circumvents the high computational cost of including the spacers and instead handles them as a homogeneous porous medium in the entire domain by means of the Brinkman–Forchheimer equation, also coupled to transport equation. The former perspective, shows similar results in terms of relevant values such as permeate flux, pressure behaviour and velocity, compared to previous works. The latter alternative provides comparative results to those cases where explicit spacers also reduce the salt concentration compared to case of empty channels. In our simulations, the case with explicit submerged spacers is emulated more closely, showing that the deviation is only 0.86%. Furthermore, our work suggests that under same parameters, different positions of the spacers in the channel configuration lead to different fluid patterns, which in turn generate a local increment or reduction in the concentration of salt.

Also, a higher local concentration on the membrane, leads in a lower permeate velocity.

- Chapter 3. We have proposed a novel high-order HDG method to handle complex mesh discretizations arising from coupled interface problems, where each subdomain is governed by different equations. More precisely, we extended the analysis proposed in [87, 101] in the context of a single PDE in the entire domain. Our approach handles non-matching and dissimilar meshes with flat interfaces, allowing the presence of hanging nodes. The HDG discretizations associated with each subdomain are tied together by appropriate transmission conditions, allowing the method to maintain high-order accuracy for sufficiently smooth solutions. In particular, the cases covered by our theory consider δ of order $h^{1+\gamma}$, with $\gamma \in (3/4, 3]$. The best scenario allowing the presence of hanging nodes considers *semi-aligned* matching interfaces, yielding an optimal order of convergence of h^{k+1} for all variables. However, if we have *semi-aligned* discrete interfaces and a gap $\delta = h^2$, we obtain an order of convergence of $h^{k+1-\epsilon}$ for all $\epsilon > 0$. Finally, we have provided a variety of numerical experiments illustrating optimality even in cases not completely covered by our theory. The experiments suggest that the assumption $\delta = h^{1+\gamma}$, for all $\gamma \in (3/4, 3]$, could be relaxed, and this is the subject of future work.

4.2 Future work

The methods developed and the results obtained in this thesis have motivated several and ongoing/future projects. Descriptions of some of these projects are given below:

1. As a natural continuation and in order to improve their robustness in cases involving complex geometries or solutions with high gradients, we are interested in performing an *a posteriori* analysis for two contexts:
   - The HDG method for Stokes/Darcy coupling on dissimilar meshes.
   - The mixed-FEM for the coupled Navier–Stokes/transport system modeling reverse osmosis processes.
2. To extend the analysis and results to the unsteady state case of the model studied in Chapter 1, as well as to address an unsteady state version of Chapter 2. The primary motivation is to obtain a more realistic and comprehensive understanding of the models, which is crucial for predicting the behavior of fluid flow patterns, salt concentration, pressure losses, and permeate flow in desalination channels in the context of reverse osmosis.
3. To address the realistic case where $\mathit{\Delta P}$ is not assumed constant.
4. To analyze the unsteady state coupled Brinkman–Forchheimer/transport system with traction boundary conditions modeling RO processes. More precisely, let $\star \in \{\mathrm{f}, \mathrm{p}\}$. Given a suitable initial data $\mathbf{u}_{0,\star}$ and a final time T, the system of equations given by (1.7), can now be expressed

as

$$\rho\frac{\partial}{\partial t}\left(\frac{\mathbf{u}_\star}{\varepsilon_\star}\right) - \nu\triangle\frac{\mathbf{u}_\star}{\varepsilon_\star} + \rho\,\mathbf{div}\left(\frac{\mathbf{u}_\star}{\varepsilon_\star}\otimes\frac{\mathbf{u}_\star}{\varepsilon_\star}\right) + \nabla p_\star = -\mathtt{D}_\star\mathbf{u}_\star - \mathtt{F}_\star|\mathbf{u}_\star|\mathbf{u}_\star \quad \text{in} \quad \Omega_\star\times(0,T],$$
$$\mathrm{div}\left(\frac{\mathbf{u}_\star}{\varepsilon_\star}\right) = 0 \quad \text{in} \quad \Omega_\star\times(0,T], \quad \mathbf{u}_\star = \mathbf{u}_{0,\star} \quad \text{in} \quad \Omega_\star, \quad \frac{\mathbf{u}_\star}{\varepsilon_\star} = \mathbf{u}_{\mathrm{in},\star} \quad \text{on} \quad \Gamma_{\mathrm{in},\star}\times(0,T],$$
$$\mathbf{u}_\star = \mathbf{0} \quad \text{on} \quad \Gamma_{\mathrm{w},\star}\times(0,T], \quad (2\nu\,\mathbf{e}(\mathbf{u}_\star) - \varepsilon_\star\,p_\star\mathbb{I})\,\mathbf{n}_\star = \mathbf{0} \quad \text{on} \quad \Gamma_{\mathrm{out},\star}\times(0,T],$$
$$\frac{\partial}{\partial t}\phi_\star - \kappa\,\triangle\widetilde{\phi}_\star + \frac{\mathbf{u}_\star}{\varepsilon_\star}\cdot\nabla\widetilde{\phi}_\star = 0 \quad \text{in} \quad \Omega_\star\times(0,T],$$
$$\widetilde{\phi}_\star = \phi_{\mathrm{in},\star} \quad \text{on} \quad \Gamma_{\mathrm{in},\star}\times(0,T], \quad \kappa\,\nabla\widetilde{\phi}_\star\cdot\mathbf{n}_\star = 0 \quad \text{on} \quad \Gamma_{\mathrm{w},\star}\cup\Gamma_{\mathrm{out},\star}\times(0,T],$$

where, $\mathbf{e}(\mathbf{u}_\star) := \frac{1}{2}(\nabla\mathbf{u}_\star + (\nabla\mathbf{u}_\star)^{\mathtt{t}})$ is the symmetric part of $\nabla\mathbf{u}_\star$, also named strain rate tensor, ν is the fluid dynamic viscosity, ρ is the fluid density and κ is the solute diffusivity through the solvent, $\mathtt{D}_\star > 0$ and $\mathtt{F}_\star > 0$ are the Darcy and Forchheimer coefficients, respectively, and $\varepsilon_\star$ is the porosity of the medium. In turn, the corresponding transmission conditions are given by

$$\mathbf{u}_\star\cdot\boldsymbol{m}_\Sigma = 0, \quad \mathbf{u}_{\mathrm{f}}\cdot\mathbf{n}_{\mathrm{f}} = -\mathbf{u}_{\mathrm{p}}\cdot\mathbf{n}_{\mathrm{p}}, \quad \frac{\mathbf{u}_{\mathrm{f}}}{\varepsilon_{\mathrm{f}}}\cdot\mathbf{n}_{\mathrm{f}} = A\Delta P - AiRT(\widetilde{\phi}_{\mathrm{f}} - \widetilde{\phi}_{\mathrm{p}}) \quad \text{on} \quad \Sigma\times(0,T],$$
$$\left(\widetilde{\phi}_{\mathrm{f}}\frac{\mathbf{u}_{\mathrm{f}}}{\varepsilon_{\mathrm{f}}} - \kappa\,\nabla\widetilde{\phi}_{\mathrm{f}}\right)\cdot\mathbf{n}_{\mathrm{f}} = -\left(\widetilde{\phi}_{\mathrm{p}}\frac{\mathbf{u}_{\mathrm{p}}}{\varepsilon_{\mathrm{p}}} - \kappa\,\nabla\widetilde{\phi}_{\mathrm{p}}\right)\cdot\mathbf{n}_{\mathrm{p}} \quad \text{on} \quad \Sigma\times(0,T], \quad \text{and}$$
$$\left(\widetilde{\phi}_{\mathrm{f}}\frac{\mathbf{u}_{\mathrm{f}}}{\varepsilon_{\mathrm{f}}} - \kappa\,\nabla\widetilde{\phi}_{\mathrm{f}}\right)\cdot\mathbf{n}_{\mathrm{f}} = B(\widetilde{\phi}_{\mathrm{f}} - \widetilde{\phi}_{\mathrm{p}}) \quad \text{on} \quad \Sigma\times(0,T].$$

This approach will allow us to consider other finite element spaces for the Navier–Stokes variables, such as Arnold–Falk–Winther (AFW) or the plane elasticity element with reduced symmetry (PEERS).

5. To propose an HDG method for the coupling of Linear Elasticity and Stokes flow on dissimilar meshes via appropriate transmission conditions across an interface. This approach is motivated by the fact that it is often desirable to have a finer mesh in the region occupied by the fluid compared to the mesh size used for discretizing the solid.

6. Finally, another future goal is to extend the results of dissimilar meshes to the coupled interfaces problems in the context of mixed finite element methods.

Conclusiones y trabajos futuros

4.3 Conclusiones

Resumimos las principales aportaciones y conclusiones de la tesis.

- Capítulo 1. Hemos desarrollado y analizado un método de elementos finitos mixto para las ecuaciones acopladas de Navier–Stokes y de transporte con condiciones de transmisión no lineales. Demostramos el buen planteamiento tanto de las formulaciones continuas como discretas, especificamos subespacios de elementos finitos y mostramos las propiedades de convergencia del esquema numérico propuesto. Este trabajo es una contribución que proporciona un marco matemático para manejar condiciones de transmisión no lineales en dominios con condiciones de contorno mixtas. Esto se consigue introduciendo multiplicadores de Lagrange asociados a la traza de la concentración de sal. El método propuesto proporciona los fundamentos teóricos y el marco numérico para modelar diferentes configuraciones inspiradas en los procesos de ósmosis inversa que exploramos en el capítulo 2. De hecho, todas estas perspectivas también pueden adaptarse con pequeñas modificaciones al modelo aquí presentado.
- Capítulo 2. Se ha utilizado un nuevo modelo numérico basado en el método de elementos finitos mixtos bidimensionales para estudiar los patrones de flujo de fluidos, concentraciones de sal, pérdidas de presión y flujo de permeado en canales de desalinización, inspirados en procesos de ósmosis inversa. Las simulaciones se realizan en un rango de números de Reynolds para flujo laminar inferior a 170, típico en la operación de módulos de membranas para agua de mar. Las simulaciones se basan en dos perspectivas diferentes, la primera utiliza las ecuaciones de Navier–Stokes acopladas a las de transporte para el caso de canales vacíos, y también para diferentes configuraciones de espaciadores explícitos. La segunda perspectiva evita el elevado coste computacional de incluir los espaciadores y, en su lugar, los trata como un medio poroso homogéneo en todo el dominio mediante la ecuación de Brinkman–Forchheimer, también acoplada a la ecuación de transporte. La primera perspectiva, muestra resultados similares en términos de valores relevantes como el flujo de permeado, el comportamiento de la presión y la velocidad, en comparación con trabajos previos. La segunda alternativa proporciona resultados comparativos con aquellos casos en los que los espaciadores explícitos también reducen la concentración de sales en comparación con el caso de canales vacíos. En nuestras simulaciones, el caso que se emula más cercanamente es con espaciadores explícitos sumergidos, mostrando que la desviación es de sólo $0,86\%$. Además, nuestro trabajo sugiere que bajo los mismos parámetros, diferentes posiciones de los espaciadores en la configuración del canal conducen a diferentes patrones de fluido, que a su vez generan un incremento o reducción local de la concentración de sal. Asimismo, una mayor

concentración local en la membrana conduce a una menor velocidad de permeado.

- Capítulo 3. Hemos propuesto un novedoso método HDG de alto orden para manejar discretizaciones de mallas complejas derivadas de problemas de interfaces acopladas, donde cada subdominio está gobernado por diferentes ecuaciones. Más concretamente, ampliamos el análisis propuesto en [87, 101], en el contexto de una única EDP en todo el dominio. Nuestro enfoque maneja mallas no coincidentes y disimilares con interfaces planas, permitiendo la presencia de nodos colgantes. Las discretizaciones HDG asociadas a cada subdominio están unidas por condiciones de transmisión apropiadas, lo que permite al método mantener una precisión de alto orden para soluciones suficientemente suaves. En particular, los casos cubiertos por nuestra teoría consideran δ de orden $h^{1+\gamma}$, con $\gamma \in (3/4, 3]$. El mejor escenario que permite la presencia de nodos colgantes considera interfaces coincidentes *semi-alineadas*, produciendo un orden óptimo de convergencia de h^{k+1} para todas las variables. Sin embargo, si tenemos interfaces discretas *semialineadas* y un gap $\delta = h^2$, obtenemos un orden de convergencia de $h^{k+1-\epsilon}$ para todo $\epsilon > 0$. Por último, hemos proporcionado una serie de experimentos numéricos que ilustran la óptimidad incluso en casos no cubiertos completamente por nuestra teoría. Los experimentos sugieren que el supuesto $\delta = h^{1+\gamma}$, para todo $\gamma \in (3/4, 3]$, podría relajarse, y este es el tema de futuros trabajos.

4.4 Trabajo futuro

Los métodos desarrollados y los resultados obtenidos en esta tesis han motivado varios proyectos en curso/futuros. A continuación, las descripciones de algunos de estos proyectos:

1. Como continuación natural y con el fin de mejorar sus robusteces en casos de geometrías complejas o soluciones con gradientes elevados, estamos interesados en realizar un análisis *a posteriori* para dos contextos:
   - El método HDG para el acoplamiento Stokes/Darcy en mallas disimilares.
   - El método de elementos finitos mixtos para el sistema acoplado Navier-Stokes/transporte que modela procesos de ósmosis inversa.
2. Extender el análisis y los resultados al caso de estado no estacionario del modelo estudiado en el capítulo 1, así como abordar una versión en estado no estacionario del capítulo 2. La motivación principal es obtener una comprensión más realista y completa de los modelos, lo cual es crucial para predecir el comportamiento de los patrones de flujo de fluidos, las concentraciones de sal, las pérdidas de presión y el flujo de permeado en los canales de desalinización en el contexto de la ósmosis inversa.
3. Abordar el caso realista en el que ΔP no se supone constante.
4. Analizar el sistema acoplado de Brinkman–Forchheimer/transporte en estado no estacionario con condiciones de contorno de tracción modelando procesos de OI. Más precisamente, sea $\star \in \{\mathrm{f}, \mathrm{p}\}$. Dados unos datos iniciales adecuados $\mathbf{u}_{0,\star}$ y un tiempo final T, el sistema de ecuaciones dado por

(1.7), puede ahora expresarse como

$$
\begin{gathered}
\rho\frac{\partial}{\partial t}\left(\frac{\mathbf{u}_\star}{\varepsilon_\star}\right) - \nu\triangle\frac{\mathbf{u}_\star}{\varepsilon_\star} + \rho\,\mathbf{div}\left(\frac{\mathbf{u}_\star}{\varepsilon_\star}\otimes\frac{\mathbf{u}_\star}{\varepsilon_\star}\right) + \nabla p_\star = -\mathtt{D}_\star\mathbf{u}_\star - \mathtt{F}_\star|\mathbf{u}_\star|\mathbf{u}_\star \;\text{ en }\; \mathit{\Omega}_\star\times(0,T],\\
\operatorname{div}\left(\frac{\mathbf{u}_\star}{\varepsilon_\star}\right) = 0 \;\text{ en }\; \mathit{\Omega}_\star\times(0,T], \quad \mathbf{u}_\star = \mathbf{u}_{0,\star} \;\text{ en }\; \mathit{\Omega}_\star, \quad \frac{\mathbf{u}_\star}{\varepsilon_\star} = \mathbf{u}_{\mathrm{in},\star} \;\text{ en }\; \mathit{\Gamma}_{\mathrm{in},\star}\times(0,T],\\
\mathbf{u}_\star = \mathbf{0} \;\text{ en }\; \mathit{\Gamma}_{\mathrm{w},\star}\times(0,T], \quad (2\nu\,\mathbf{e}\,(\mathbf{u}_\star) - \varepsilon_\star\,p_\star\mathbb{I})\,\mathbf{n}_\star = \mathbf{0} \;\text{ en }\; \mathit{\Gamma}_{\mathrm{out},\star}\times(0,T],\\
\frac{\partial}{\partial t}\phi_\star - \kappa\,\triangle\widetilde{\phi}_\star + \frac{\mathbf{u}_\star}{\varepsilon_\star}\cdot\nabla\widetilde{\phi}_\star = 0 \;\text{ en }\; \mathit{\Omega}_\star\times(0,T],\\
\widetilde{\phi}_\star = \phi_{\mathrm{in},\star} \;\text{ en }\; \mathit{\Gamma}_{\mathrm{in},\star}\times(0,T], \quad \kappa\,\nabla\widetilde{\phi}_\star\cdot\mathbf{n}_\star = 0 \;\text{ en }\; \mathit{\Gamma}_{\mathrm{w},\star}\cup\mathit{\Gamma}_{\mathrm{out},\star}\times(0,T],
\end{gathered}
$$

donde, $\mathbf{e}(\mathbf{u}_\star) := \dfrac{1}{2}(\nabla\mathbf{u}_\star + (\nabla\mathbf{u}_\star)^{\mathtt{t}})$ es la parte simétrica de $\nabla\mathbf{u}_\star$, también llamado tensor de deformación, ν es la viscosidad dinámica del fluido, ρ es la densidad del fluido y κ es la difusividad del soluto a través del solvente, $\mathtt{D}_\star > 0$ y $\mathtt{F}_\star > 0$ son los coeficientes de Darcy y Forchheimer, respectivamente, y $\varepsilon_\star$ es la porosidad del medio. A su vez, las condiciones de transmisión correspondientes vienen dadas por

$$
\begin{gathered}
\mathbf{u}_\star\cdot\boldsymbol{m}_\Sigma = 0, \quad \mathbf{u}_\mathrm{f}\cdot\mathbf{n}_\mathrm{f} = -\mathbf{u}_\mathrm{p}\cdot\mathbf{n}_\mathrm{p}, \quad \frac{\mathbf{u}_\mathrm{f}}{\varepsilon_\mathrm{f}}\cdot\mathbf{n}_\mathrm{f} = A\mathit{\Delta}P - AiRT(\widetilde{\phi}_\mathrm{f} - \widetilde{\phi}_\mathrm{p}) \;\text{ en }\; \mathit{\Sigma}\times(0,T],\\
\left(\widetilde{\phi}_\mathrm{f}\frac{\mathbf{u}_\mathrm{f}}{\varepsilon_\mathrm{f}} - \kappa\,\nabla\widetilde{\phi}_\mathrm{f}\right)\cdot\mathbf{n}_\mathrm{f} = -\left(\widetilde{\phi}_\mathrm{p}\frac{\mathbf{u}_\mathrm{p}}{\varepsilon_\mathrm{p}} - \kappa\,\nabla\widetilde{\phi}_\mathrm{p}\right)\cdot\mathbf{n}_\mathrm{p} \;\text{ en }\; \mathit{\Sigma}\times(0,T], \;\text{ y}\\
\left(\widetilde{\phi}_\mathrm{f}\frac{\mathbf{u}_\mathrm{f}}{\varepsilon_\mathrm{f}} - \kappa\,\nabla\widetilde{\phi}_\mathrm{f}\right)\cdot\mathbf{n}_\mathrm{f} = B(\widetilde{\phi}_\mathrm{f} - \widetilde{\phi}_\mathrm{p}) \;\text{ en }\; \mathit{\Sigma}\times(0,T].
\end{gathered}
$$

Este enfoque nos permitirá considerar otros espacios de elementos finitos para las variables de Navier–Stokes, como Arnold–Falk–Winther (AFW) o el elemento de elasticidad plana con simetría reducida (PEERS).

5. Proponer un método HDG para el acoplamiento de la Elasticidad Lineal y el flujo de Stokes en mallas disimilares mediante condiciones de transmisión apropiadas a través de una interfaz. Este enfoque está motivado por el hecho de que a menudo es deseable tener una malla más fina en la región ocupada por el fluido en comparación con el tamaño de malla utilizado para discretizar el sólido.

6. Finalmente, otro objetivo futuro es extender los resultados de mallas disimilares a los problemas de interfaces acopladas en el contexto de métodos de elementos finitos mixtos.

References

[1] R. A. Adams and J. J. F. Fournier, *Sobolev spaces*, vol. 140 of Pure and Applied Mathematics (Amsterdam), Elsevier/Academic Press, Amsterdam, second ed., 2003.

[2] A. L. Ahmad, K. K. Lau, and M. Z. Abu Bakar, *Impact of different spacer filament geometries on concentration polarization control in narrow membrane channel*, J. Membr. Sci., 262 (2005), pp. 138–152.

[3] F. E. Ahmed, A. Khalil, and N. Hilal, *Emerging desalination technologies: Current status, challenges and future trends*, Desalination, 517 (2021), p. 115183.

[4] M. Alvarez, G. N. Gatica, and R. Ruiz-Baier, *An augmented mixed-primal finite element method for a coupled flow-transport problem*, ESAIM Math. Model. Numer. Anal., 49 (2015), pp. 1399–1427.

[5] A. Amiri and K. Vafai, *Transient analysis of incompressible flow through a packed bed*, Int. J. Heat Mass Transfer, 41 (1998), pp. 4259–4279.

[6] M. Amokrane, D. Sadaoui, C. Koutsou, A. Karabelas, and M. Dudeck, *A study of flow field and concentration polarization evolution in membrane channels with two-dimensional spacers during water desalination*, J. Membr. Sci., 477 (2015), pp. 139–150.

[7] N. M. Atallah, C. Canuto, and G. Scovazzi, *The high-order Shifted Boundary Method and its analysis*, Comput. Methods Appl. Mech. Engrg., 394 (2022), pp. Paper No. 114885, 30.

[8] M. Atasoy, I. Owusu-Agyeman, E. Plaza, and Z. Cetecioglu, *Bio-based volatile fatty acid production and recovery from waste streams: Current status and future challenges*, Bioresour. Technol., 268 (2018), pp. 773–786.

[9] U. Ayachit, *The ParaView Guide: A Parallel Visualization Application*, Kitware, Inc., Clifton Park, NY, USA, 2015.

[10] I. Babuška and G. N. Gatica, *On the mixed finite element method with Lagrange multipliers*, Numer. Methods Partial Differential Equations, 19 (2003), pp. 192–210.

[11] L. Badea, M. Discacciati, and A. Quarteroni, *Numerical analysis of the Navier-Stokes/Darcy coupling*, Numer. Math., 115 (2010), pp. 195–227.

[12] F. Ben Belgacem, *The mortar finite element method with Lagrange multipliers*, Numer. Math., 84 (1999), pp. 173–197.

[13] A. S. Berman, *Laminar flow in channels with porous walls*, J. Appl. Phys., 24 (1953), pp. 1232–1235.

[14] I. Bermúdez, V. Burgos, J. Camaño, F. Gajardo, R. Oyarzúa, and M. Solano, *Mixed finite element methods for coupled fluid flow problems arising from reverse osmosis modeling.* Preprint 2024-15, Centro de Investigación en Ingeniería Matemática (CI^{2}MA), Universidad de Concepción, 2024.

[15] I. Bermúdez, J. Camaño, R. Oyarzúa, and M. Solano, *A conforming mixed finite element method for a coupled Navier–Stokes/transport system modeling reverse osmosis processes*, Comput. Methods Appl. Mech. Engrg., 433 (2025), p. Paper No. 117527.

[16] I. Bermúdez, C. I. Correa, G. N. Gatica, and J. P. Silva, *A perturbed twofold saddle point-based mixed finite element method for the Navier-Stokes equations with variable viscosity*, Appl. Numer. Math., 201 (2024), pp. 465–487.

[17] I. Bermúdez, J. Manríquez, and M. Solano, *A hybridizable discontinuous Galerkin method for Stokes/Darcy coupling on dissimilar meshes.* Preprint 2024-5, Centro de Investigación en Ingeniería Matemática (CI^{2}MA), Universidad de Concepción, 2024.

[18] B. Bernales, P. Haldenwang, P. Guichardon, and N. Ibaseta, *Prandtl model for concentration polarization and osmotic counter-effects in a 2-d membrane channel*, Desalination, 404 (2017), pp. 341–359.

[19] C. Bernardi, Y. Maday, and A. T. Patera, *A new nonconforming approach to domain decomposition: the mortar element method*, in Nonlinear partial differential equations and their applications. Collège de France Seminar, Vol. XI (Paris, 1989–1991), vol. 299 of Pitman Res. Notes Math. Ser., Longman Sci. Tech., Harlow, 1994, pp. 13–51.

[20] C. Bernardi, Y. Maday, and F. Rapetti, *Basics and some applications of the mortar element method*, GAMM-Mitt., 28 (2005), pp. 97–123.

[21] M. Braack and P. B. Mucha, *Directional do-nothing condition for the Navier-Stokes equations*, J. Comput. Math., 32 (2014), pp. 507–521.

[22] P. V. Bulat and K. N. Volkov, *Simulation of incompressible flows in channels containing fluid and porous regions*, Int. J. Ind. Syst. Eng., 34 (2020), pp. 283–300.

[23] E. Burman, S. Claus, P. Hansbo, M. G. Larson, and A. Massing, *CutFEM: discretizing geometry and partial differential equations*, Internat. J. Numer. Methods Engrg., 104 (2015), pp. 472–501.

[24] Z. Cai, C. He, and S. Zhang, *Discontinuous finite element methods for interface problems: robust a priori and a posteriori error estimates*, SIAM J. Numer. Anal., 55 (2017), pp. 400–418.

[25] J. Camaño, C. García, and R. Oyarzúa, *Analysis of a momentum conservative mixed-FEM for the stationary Navier–Stokes problem*, Numer. Methods Partial Differential Equations, 37 (2021), pp. 2895–2923.

[26] J. Camaño, C. Muñoz, and R. Oyarzúa, *Numerical analysis of a dual-mixed problem in non-standard Banach spaces*, Electron. Trans. Numer. Anal., 48 (2018), pp. 114–130.

[27] J. Camaño and R. Oyarzúa, *A conforming and mass conservative pseudostress-based mixed finite element method for Stokes*, Preprint 2023-15, Centro de Investigación en Ingeniería Matemática (CI^2MA), Universidad de Concepción, (2023).

[28] J. Camaño, R. Oyarzúa, R. Ruiz-Baier, and G. Tierra, *Error analysis of an augmented mixed method for the Navier–Stokes problem with mixed boundary conditions*, IMA J. Numer. Anal., 38 (2018), pp. 1452–1484.

[29] J. Camaño, R. Oyarzúa, and G. Tierra, *Analysis of an augmented mixed-FEM for the Navier-Stokes problem*, Math. Comp., 86 (2017), pp. 589–615.

[30] A. Cangiani, E. H. Georgoulis, and M. Jensen, *Discontinuous Galerkin methods for mass transfer through semipermeable membranes*, SIAM J. Numer. Anal., 51 (2013), pp. 2911–2934.

[31] ——, *Discontinuous Galerkin methods for fast reactive mass transfer through semi-permeable membranes*, Appl. Numer. Math., 104 (2016), pp. 3–14.

[32] S. Carrasco, S. Caucao, and G. N. Gatica, *New Mixed Finite Element Methods for the Coupled Convective Brinkman-Forchheimer and Double-Diffusion Equations*, J. Sci. Comput., 97 (2023), p. Paper No. 61.

[33] N. Carro, D. Mora, and J. Vellojin, *A finite element model for concentration polarization and osmotic effects in a membrane channel*, Internat. J. Numer. Methods Fluids, 96 (2024), pp. 601–625.

[34] S. Caucao, R. Oyarzúa, and S. Villa-Fuentes, *A new mixed-FEM for steady-state natural convection models allowing conservation of momentum and thermal energy*, Calcolo, 57 (2020), pp. Paper No. 36, 39.

[35] A. Cesmelioglu, J. J. Lee, and S. Rhebergen, *A strongly conservative hybridizable discontinuous Galerkin method for the coupled time-dependent Navier-Stokes and Darcy problem*, ESAIM Math. Model. Numer. Anal., 58 (2024), pp. 273–302.

[36] A. Cesmelioglu, D. D. Pham, and S. Rhebergen, *A hybridizable discontinuous Galerkin method for the fully coupled time-dependent Stokes/Darcy-transport problem*, ESAIM Math. Model. Numer. Anal., 57 (2023), pp. 1257–1296.

[37] A. Cesmelioglu, S. Rhebergen, and G. N. Wells, *An embedded-hybridized discontinuous Galerkin method for the coupled Stokes-Darcy system*, J. Comput. Appl. Math., 367 (2020), pp. 112476, 16.

[38] Y. Chen and B. Cockburn, *Analysis of variable-degree HDG methods for convection-diffusion equations. Part I: general nonconforming meshes*, IMA J. Numer. Anal., 32 (2012), pp. 1267–1293.

[39] ——, *Analysis of variable-degree HDG methods for convection-diffusion equations. Part II: Semimatching nonconforming meshes*, Math. Comp., 83 (2014), pp. 87–111.

[40] P. G. Ciarlet, *Linear and nonlinear functional analysis with applications*, Society for Industrial and Applied Mathematics, Philadelphia, PA, 2013.

[41] B. Cockburn, J. Gopalakrishnan, and R. Lazarov, *Unified hybridization of discontinuous Galerkin, mixed, and continuous Galerkin methods for second order elliptic problems*, SIAM J. Numer. Anal., 47 (2009), pp. 1319–1365.

[42] B. Cockburn, J. Gopalakrishnan, N. C. Nguyen, J. Peraire, and F.-J. Sayas, *Analysis of HDG methods for Stokes flow*, Math. Comp., 80 (2011), pp. 723–760.

[43] B. Cockburn, J. Gopalakrishnan, and F.-J. Sayas, *A projection-based error analysis of HDG methods*, Math. Comp., 79 (2010), pp. 1351–1367.

[44] B. Cockburn, D. Gupta, and F. Reitich, *Boundary-conforming discontinuous Galerkin methods via extensions from subdomains*, J. Sci. Comput., 42 (2010), pp. 144–184.

[45] B. Cockburn, W. Qiu, and M. Solano, *A priori error analysis for HDG methods using extensions from subdomains to achieve boundary conformity*, Math. Comp., 83 (2014), pp. 665–699.

[46] B. Cockburn, F.-J. Sayas, and M. Solano, *Coupling at a distance HDG and BEM*, SIAM J. Sci. Comput., 34 (2012), pp. A28–A47.

[47] B. Cockburn and M. Solano, *Solving Dirichlet boundary-value problems on curved domains by extensions from subdomains*, SIAM J. Sci. Comput., 34 (2012), pp. A497–A519.

[48] E. Colmenares, G. N. Gatica, and S. Moraga, *A Banach spaces-based analysis of a new fully-mixed finite element method for the Boussinesq problem*, ESAIM Math. Model. Numer. Anal., 54 (2020), pp. 1525–1568.

[49] E. Colmenares, G. N. Gatica, and R. Oyarzúa, *Analysis of an augmented mixed-primal formulation for the stationary Boussinesq problem*, Numer. Methods Partial Differential Equations, 32 (2016), pp. 445–478.

[50] C. I. Correa and G. N. Gatica, *On the continuous and discrete well-posedness of perturbed saddle-point formulations in Banach spaces*, Comput. Math. Appl., 117 (2022), pp. 14–23.

[51] T. A. Davis, *Algorithm 832: UMFPACK V4.3—an unsymmetric-pattern multifrontal method*, ACM Trans. Math. Software, 30 (2004), pp. 196–199.

[52] S. Deparis, D. Forti, P. Gervasio, and A. Quarteroni, *INTERNODES: an accurate interpolation-based method for coupling the Galerkin solutions of PDEs on subdomains featuring non-conforming interfaces*, Comput. & Fluids, 141 (2016), pp. 22–41.

[53] E. Di Nezza, G. Palatucci, and E. Valdinoci, *Hitchhiker's guide to the fractional Sobolev spaces*, Bull. Sci. Math., 136 (2012), pp. 521–573.

[54] D. A. Di Pietro and A. Ern, *Mathematical aspects of discontinuous Galerkin methods*, vol. 69 of Mathématiques & Applications (Berlin) [Mathematics & Applications], Springer, Heidelberg, 2012.

[55] M. Discacciati and R. Oyarzúa, *A conforming mixed finite element method for the Navier–Stokes/Darcy coupled problem*, Numer. Math., 135 (2017), pp. 571–606.

[56] M. Duprez, V. Lleras, and A. Lozinski, *A new ϕ-FEM approach for problems with natural boundary conditions*, Numer. Methods Partial Differential Equations, 39 (2023), pp. 281–303.

[57] ——, *ϕ-FEM: an optimally convergent and easily implementable immersed boundary method for particulate flows and Stokes equations*, ESAIM Math. Model. Numer. Anal., 57 (2023), pp. 1111–1142.

[58] M. Duprez and A. Lozinski, *ϕ-FEM: a finite element method on domains defined by level-sets*, SIAM J. Numer. Anal., 58 (2020), pp. 1008–1028.

[59] J. Eke, A. Yusuf, A. Giwa, and A. Sodiq, *The global status of desalination: An assessment of current desalination technologies, plants and capacity*, Desalination, 495 (2020), p. 114633.

[60] A. Ern and J.-L. Guermond, *Theory and practice of finite elements*, vol. 159 of Applied Mathematical Sciences, Springer-Verlag, New York, 2004.

[61] C. Farhat and F.-X. Roux, *A method of finite element tearing and interconnecting and its parallel solution algorithm*, Internat. J. Numer. Methods Engrg., 32 (1991), pp. 1205–1227.

[62] T. Frachon, E. Nilsson, and S. Zahedi, *Divergence-free cut finite element methods for Stokes flow*, BIT, 64 (2024), p. Paper No. 39.

[63] G. Fu and C. Lehrenfeld, *A strongly conservative hybrid DG/mixed FEM for the coupling of Stokes and Darcy flow*, J. Sci. Comput., 77 (2018), pp. 1605–1620.

[64] J. Galvis and M. Sarkis, *Non-matching mortar discretization analysis for the coupling Stokes-Darcy equations*, Electron. Trans. Numer. Anal., 26 (2007), pp. 350–384.

[65] M. Ganesh and O. Steinbach, *Boundary element methods for potential problems with non-linear boundary conditions*, Math. Comp., 70 (2001), pp. 1031–1042.

[66] G. N. Gatica, *Analysis of a new augmented mixed finite element method for linear elasticity allowing $\mathbb{RT}_0$-$\mathbb{P}_1$-$\mathbb{P}_0$ approximations*, M2AN Math. Model. Numer. Anal., 40 (2006), pp. 1–28.

[67] ——, *A simple introduction to the mixed finite element method*, SpringerBriefs in Mathematics, Springer, Cham, 2014. Theory and applications.

[68] G. N. Gatica, R. Oyarzúa, R. Ruiz-Baier, and Y. D. Sobral, *Banach spaces-based analysis of a fully-mixed finite element method for the steady-state model of fluidized beds*, Comput. Math. Appl., 84 (2021), pp. 244–276.

[69] G. N. Gatica, R. Oyarzúa, and F.-J. Sayas, *Analysis of fully-mixed finite element methods for the Stokes-Darcy coupled problem*, Math. Comp., 80 (2011), pp. 1911–1948.

[70] G. N. Gatica, R. Oyarzúa, and F.-J. Sayas, *A twofold saddle point approach for the coupling of fluid flow with nonlinear porous media flow*, IMA J. Numer. Anal., 32 (2012), pp. 845–887.

[71] G. N. Gatica and F. A. Sequeira, *Analysis of the HDG method for the Stokes-Darcy coupling*, Numer. Methods Partial Differential Equations, 33 (2017), pp. 885–917.

[72] P. H. Gleick, *Water in crisis*, Pacific Institute for Studies in Dev., Environment & Security. Stockholm Env. Institute, Oxford Univ. Press. 473p, 9 (1993), pp. 1051–0761.

[73] F. Hecht, *New development in freefem++*, J. Numer. Math., 20 (2012), pp. 251–265.

[74] L. Huang and M. T. Morrissey, *Finite element analysis as a tool for crossflow membrane filter simulation*, J. Membr. Sci., 155 (1999), pp. 19–30.

[75] T. M. Inc., *Matlab version: 9.13.0 (r2022b)*, 2022.

[76] K. Jeong, M. Park, S. Oh, and J. H. Kim, *Impacts of flow channel geometry, hydrodynamic and membrane properties on osmotic backwash of RO membranes—CFD modeling and simulation*, Desalination, 476 (2020), p. 114229.

[77] J. Johnston, S. M. Dischinger, M. Nassr, J. Y. Lee, P. Bigdelou, B. D. Freeman, K. L. Gleason, D. Martinand, D. J. Miller, S. Molins, N. Spycher, W. T. Stringfellow, and N. Tilton, *A reduced-order model of concentration polarization in reverse osmosis systems with feed spacers*, J. Membr. Sci., 675 (2023), p. 121508.

[78] J. Johnston, J. Lou, and N. Tilton, *Application of projection methods to simulating mass transport in reverse osmosis systems*, Comput. & Fluids, 232 (2022), p. 105189.

[79] C. Kleffner, G. Braun, and S. Antonyuk, *Influence of membrane intrusion on permeate-sided pressure drop during high-pressure reverse osmosis*, Chemie Ingenieur Technik, 91 (2019), pp. 443–454.

[80] J. Kucera, *Reverse Osmosis: Design, Processes, and Applications for Engineers*, Wiley, Mar. 2010.

[81] M. G. Larson and S. Zahedi, *Conservative cut finite element methods using macroelements*, Comput. Methods Appl. Mech. Engrg., 414 (2023), pp. Paper No. 116141, 27.

[82] A. Lenci, F. Zeighami, and V. Di Federico, *Effective Forchheimer coefficient for layered porous media*, Transp. Porous Media, 144 (2022), pp. 459–480.

[83] J. Liu, *Open and traction boundary conditions for the incompressible Navier-Stokes equations*, J. Comput. Phys., 228 (2009), pp. 7250–7267.

[84] S. Ma and L. Song, *Numerical study on permeate flux enhancement by spacers in a crossflow reverse osmosis channel*, J. Membr. Sci., 284 (2006), p. 102–109.

[85] S. Ma, L. Song, S. L. Ong, and W. J. Ng, *A 2-D streamline upwind Petrov/Galerkin finite element model for concentration polarization in spiral wound reverse osmosis modules*, J. Membr. Sci., 244 (2004), pp. 129–139.

[86] A. Main and G. Scovazzi, *The shifted boundary method for embedded domain computations. Part I: Poisson and Stokes problems*, J. Comput. Phys., 372 (2018), pp. 972–995.

[87] J. Manríquez, N.-C. Nguyen, and M. Solano, *A dissimilar non-matching HDG discretization for Stokes flows*, Comput. Methods Appl. Mech. Engrg., 399 (2022), pp. Paper No. 115292, 30.

[88] W. McLean, *Strongly elliptic systems and boundary integral equations*, Cambridge University Press, Cambridge, 2000.

[89] K. G. Nayar, M. H. Sharqawy, L. D. Banchik, and J. H. Lienhard V, *Thermophysical properties of seawater: A review and new correlations that include pressure dependence*, Desalination, 390 (2016), pp. 1–24.

[90] S. Oh, S. Wang, M. Park, and J. Ha Kim, *Novel spacer design using topology optimization in a reverse osmosis channel*, J. Fluids Eng., 136 (2013).

[91] R. Oyarzúa, M. Solano, and P. Zúñiga, *A high order mixed-FEM for diffusion problems on curved domains*, J. Sci. Comput., 79 (2019), pp. 49–78.

[92] V. Perfilov, A. Ali, and V. Fila, *A general predictive model for direct contact membrane distillation*, Desalination, 445 (2018), pp. 181–196.

[93] V. Perfilov, V. Fila, and J. Sanchez Marcano, *A general predictive model for sweeping gas membrane distillation*, Desalination, 443 (2018), pp. 285–306.

[94] W. Qiu, M. Solano, and P. Vega, *A high order HDG method for curved-interface problems via approximations from straight triangulations*, J. Sci. Comput., 69 (2016), pp. 1384–1407.

[95] A. Quarteroni and A. Valli, *Domain decomposition methods for partial differential equations*, Numerical Mathematics and Scientific Computation, The Clarendon Press, Oxford University Press, New York, 1999. Oxford Science Publications.

[96] A. Radu, J. Vrouwenvelder, M. van Loosdrecht, and C. Picioreanu, *Modeling the effect of biofilm formation on reverse osmosis performance: Flux, feed channel pressure drop and solute passage*, J. Membr. Sci., 365 (2010), pp. 1–15.

[97] R. Schulz, N. Ray, S. Zech, A. Rupp, and P. Knabner, *Beyond Kozeny-Carman: predicting the permeability in porous media*, Transp. Porous Media, 130 (2019), pp. 487–512.

[98] C. Skuse, A. Gallego-Schmid, A. Azapagic, and P. Gorgojo, *Can emerging membrane-based desalination technologies replace reverse osmosis?*, Desalination, 500 (2021), p. 114844.

[99] M. Slodička and S. Durand, *Fully discrete finite element scheme for Maxwell's equations with non-linear boundary condition*, J. Math. Anal. Appl., 375 (2011), pp. 230–244.

[100] B. Smith, P. E. Bjørstad, and W. Gropp, *Domain decomposition : parallel multilevel methods for elliptic partial differential equations*, Cambridge University Press, 2004.

[101] M. Solano, S. Terrana, N.-C. Nguyen, and J. Peraire, *An HDG method for dissimilar meshes*, IMA J. Numer. Anal., 42 (2022), pp. 1665–1699.

[102] M. Solano and F. Vargas, *A high order HDG method for Stokes flow in curved domains*, J. Sci. Comput., 79 (2019), pp. 1505–1533.

[103] G. Srivathsan, E. M. Sparrow, and J. M. Gorman, *Reverse osmosis issues relating to pressure drop, mass transfer, turbulence, and unsteadiness*, Desalination, 341 (2014), pp. 83–86.

[104] A. Subramani, S. Kim, and E. M. Hoek, *Pressure, flow, and concentration profiles in open and spacer-filled membrane channels*, J. Membr. Sci., 277 (2006), pp. 7–17.

[105] B. I. Wohlmuth, *A mortar finite element method using dual spaces for the Lagrange multiplier*, SIAM J. Numer. Anal., 38 (2000), pp. 989–1012.

[106] G. Womeldorff, J. Peterson, M. Gunzburger, and T. Ringler, *Unified matching grids for multidomain multiphysics simulations*, SIAM J. Sci. Comput., 35 (2013), pp. A2781–A2806.

[107] L. Xu, S. Xu, X. Wu, P. Wang, D. Jin, J. Hu, L. Li, L. Chen, Q. Leng, and D. Wu, *Heat and mass transfer evaluation of air-gap diffusion distillation by ε-NTU method*, Desalination, 478 (2020), p. 114281.